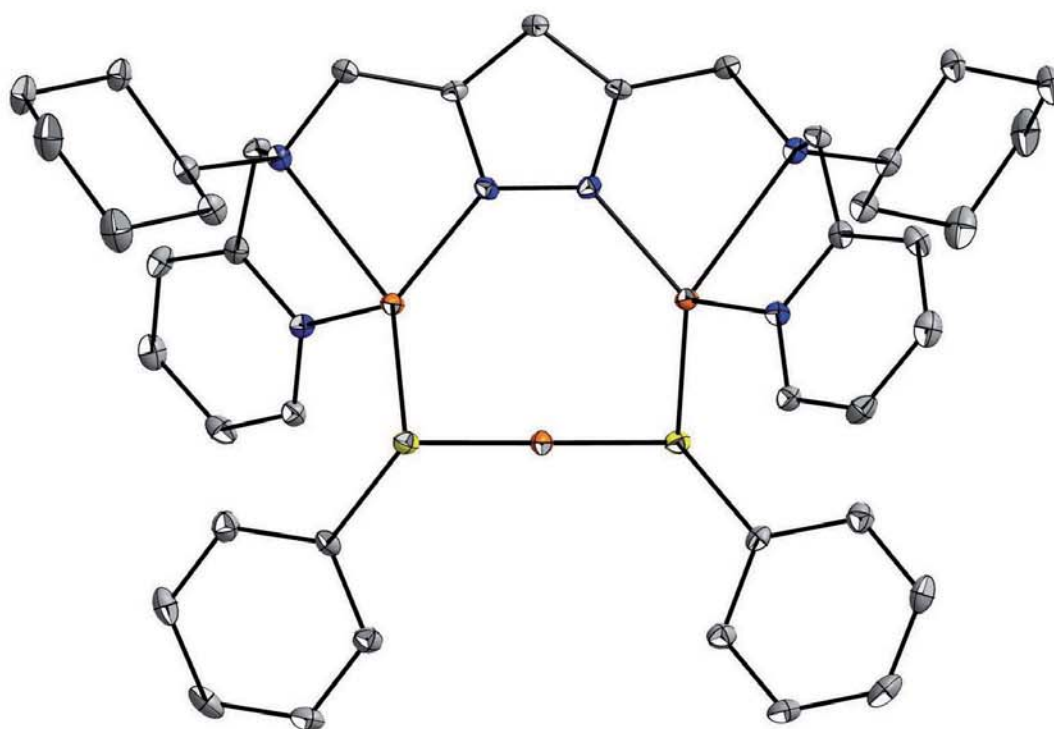


Multinuclear Pyrazolate-Based Copper Complexes

Inspired by the Cu_Z -Site of N_2O -Reductase



Cuvillier Verlag Göttingen
Internationaler wissenschaftlicher Fachverlag







Multinuclear Pyrazolate-Based
Copper Complexes
Inspired by the Cu_Z-Site of N₂O-Reductase

Dissertation

zur Erlangung des mathematisch-naturwissenschaftlichen Doktorgrades

"Doctor rerum naturalium"

der Georg-August-Universität Göttingen



vorgelegt von

Diplomchemikerin

Vera Konstanzer, geb. Kruse

aus Lippstadt

Göttingen 2011



Bibliografische Information der Deutschen Nationalbibliothek

Die Deutsche Nationalbibliothek verzeichnet diese Publikation in der Deutschen Nationalbibliografie; detaillierte bibliografische Daten sind im Internet über <http://dnb.d-nb.de> abrufbar.

1. Aufl. - Göttingen : Cuvillier, 2011

Zugl.: Göttingen, Univ., Diss., 2011

978-3-86955-978-0

Referent: Prof. Dr. Franc Meyer

Coreferent: Prof. Dr. Ulf Diederichsen

Tag der mündlichen Prüfung: 24.10.2011

© CUVILLIER VERLAG, Göttingen 2011

Nonnenstieg 8, 37075 Göttingen

Telefon: 0551-54724-0

Telefax: 0551-54724-21

www.cuvillier.de

Alle Rechte vorbehalten. Ohne ausdrückliche Genehmigung des Verlages ist es nicht gestattet, das Buch oder Teile daraus auf fotomechanischem Weg (Fotokopie, Mikrokopie) zu vervielfältigen.

1. Auflage, 2011

Gedruckt auf säurefreiem Papier

978-3-86955-978-0







Table of contents

1. Introduction	1
2. Current state of research	3
2.1. Metalloenzymes with a copper containing active site.....	3
2.2. The N ₂ O-reductase (N ₂ OR).....	5
2.3. Low-molecular weight models in bioinorganic chemistry.....	9
2.4. Copper-sulfur complexes with N-donor supporting ligands	10
2.5. Copper clusters with thiolate ligands	22
2.6. Pyrazolate-based ligand systems in multimetallic complexes	26
3. Objective.....	31
4. Results and discussion	33
4.1. Ligand synthesis	33
4.2. Copper(II) halide complexes of the type LCu ₂ X ₃ with ligands HL ¹ –HL ⁴	38
4.2.1. Introduction.....	38
4.2.2. Synthesis and Structures	39
4.2.3. Magnetic Properties	43
4.2.4. DFT calculations	49
4.2.5. Summary	52
4.3. Copper(II) halide complexes with ligand HL ⁹	53
4.3.1. Introduction.....	53
4.3.2. Synthesis and Structures	54
4.3.3. Magnetic Properties	60
4.3.4. Summary and outlook	63
4.4. Synthesis of multinuclear μ-SO ₄ -Cu(II) compounds.....	64
4.4.1. Introduction.....	64

4.4.2.	Synthesis and Structures	66
4.4.3.	Magnetic properties	77
4.4.4.	Summary and outlook	81
4.5.	Reactivity of binuclear pyrazolate based copper complexes towards sulfur-transfer reagents	82
4.6.	Copper(I) bromide complexes	87
4.6.1.	Introduction.....	87
4.6.2.	Synthesis of the complexes	88
4.6.3.	Summary and outlook	93
4.7.	Synthesis of Cu(I) thioether complexes as potential precursors for heteroleptic Cu-S compounds	94
4.7.1.	Introduction.....	94
4.7.2.	Synthesis of the ligands	95
4.7.3.	Complex-synthesis of the type $[\text{Cu}(\text{L}^{\text{S1,2}})_2]^+$	96
4.7.4.	Redox properties	101
4.7.5.	Summary	103
4.8.	Synthesis of multinuclear Cu(I) thiolate compounds	104
4.8.1.	Introduction.....	104
4.8.2.	Complex synthesis and structural characterization.....	105
4.8.3.	Characterization in solution and redox properties	109
4.8.4.	Summary and Outlook	114
5.	Summary.....	116
6.	Experimental Section.....	121
6.1.	Ligand synthesis	124
6.1.1.	Preparation of <i>N</i> -(2-picolyl)-cyclohexylamine (LVII)	124
6.1.2.	Preparation of <i>N</i> -(pyridine-2-ylmethyl)- ^t butylamine (LVIX).....	125
6.1.3.	Preparation of HL ⁴	125
6.1.4.	Preparation of HL ⁵	127

6.1.5.	Preparation of HL ⁶	128
6.1.6.	Preparation of HL ⁷	129
6.1.7.	Preparation of HL ⁸	130
6.1.8.	Synthesis of L ^{S1}	131
6.2.	Synthesis of complexes	132
6.2.1.	Preparation of L ² Cu ₂ Cl ₃ (3)	132
6.2.2.	Preparation of L ² Cu ₂ Br ₃ (4)	133
6.2.3.	Preparation of L ³ Cu ₂ Cl ₃ (5)	134
6.2.4.	Preparation of L ³ Cu ₂ Br ₃ (6)	135
6.2.5.	Preparation of L ⁴ Cu ₂ Br ₃ (7)	136
6.2.6.	Preparation of L ⁴ Cu ₂ Br ₃ (8)	137
6.2.7.	Preparation of L ⁹ Cu ₂ Cl ₃ (9)	137
6.2.8.	Preparation of L ⁹ Cu ₂ Br ₃ (10)	138
6.2.9.	Preparation of L ₂ ⁹ Cu ₄ Cl ₂ (SO ₃ CF ₃) ₄ (11)	139
6.2.10.	Preparation of L ^{9'} Cu ₂ (SO ₃ CF ₃) ₂ (12)	140
6.2.11.	Preparation of [L ¹ Cu ₂ (SO ₄)](SO ₃ CF ₃) (13)	141
6.2.12.	Preparation of [L ¹ Cu ₂ (SO ₄)(MeCN)(H ₂ O)](BF ₄) (14)	141
6.2.13.	Preparation of [L ³ Cu ₂ (SO ₄)](SO ₃ CF ₃) (15)	142
6.2.14.	Preparation of [L ³ Cu ₄ (SO ₄)](SO ₃ CF ₃) ₄ (16)	142
6.2.15.	Preparation of [(L ³) ₂ Cu ₄ (SO ₄)(Et ₂ O)(BF ₄) ₃](BF ₄) (17)	143
6.2.16.	Preparation of L ⁵ _x Cu _y Br _z	144
6.2.17.	Preparation of L ₃ ⁶ Cu ₉ Br ₆ (18)	145
6.2.18.	Preparation of [L ^{S,1} ₂ Cu] ⁺ SO ₃ CF ₃ ⁻ (19)	146
6.2.19.	Preparation of [L ^{S,2} ₂ Cu] ⁺ PF ₆ ⁻ (20)	147
6.2.20.	Preparation of L ⁴ Cu ₃ (SPh) ₂ (21)	148
6.2.21.	Preparation of [L ⁴ ₂ Cu ₅ (SPh) ₂] ⁺ BF ₄ ⁻ (22)	149
7.	Crystallography	152



TABLE OF CONTENTS

Appendix A.....	158
Appendix B.....	168
8. Bibliography.....	170
Structures of ligand precursors and ligands.....	180
Structures of complexes.....	181
List of Abbreviations.....	184
Acknowledgements.....	186
List of scientific contributions.....	188
CURRICULUM VITAE.....	190







1. Introduction

Copper plays an important role in various biological processes occurring in higher plants and animals. In its cupric form it is an important constituent of active sites in metalloenzymes and proteins. Most of these copper-containing enzymes are involved in redox processes like electron-transfer, dioxygen chemistry, reduction of nitrogen oxides, including nitrite and nitrous oxide. By performing this kind of redox processes, copper proteins take over similar functions as iron containing metalloenzymes, i.e. hemocyanines are blood O₂-carriers in arthropods and mollusks, and hemoglobin, an iron containing heme-enzyme, is the blood O₂-carrier in the human body. However, copper and iron enzymes feature some differences such as the molecular structure of the active sites or the redox potentials.^[1]

For humans copper is an essential element, too, and with approximately 3 mg per kg body weight the third most abundant trace element in the human body.^[2] Serious diseases can occur when the human copper metabolism is perturbed. Wilson's disease describes the incapability of copper release.^[3] Without medical treatment Wilson's disease leads to an accumulation of copper in the liver and the brain which finally leads to death. Menke's syndrome describes the insufficient copper storage in cells.^[4-6] This hereditary syndrome leads to anemia and the degeneration of the nervous system which can be lethal if the syndrome stays untreated.

The most common oxidation states of copper ions which are involved in biological processes are +1 and +2. According to the PEARSON concept copper(I) ions show soft lewis acid behavior whereas copper(II) ions can be classified as relatively hard acids. This results in different preferences of the coordinated donor atom in coordination compounds. The oxidation state and the resulting electronic configuration of the ion also effects the coordination geometries.^[7]

The electronic configuration of copper(I) ions is d¹⁰. In this closed shell system all electrons are paired. The preferred coordination numbers of copper(I) ions and the corresponding geometries are 2 (linear), 3 (trigonal-planar) and 4 (tetrahedral).^[7] The soft copper(I) ions prefer sulfur ligands and softer N-donor ligands such as pyridines, imidazoles or nitriles in coordination compounds.

Cupric ions feature an electronic d^9 -configuration. The preferred coordination numbers and polyhedra are 4 in a square planar arrangement, 5 in either square pyramidal or trigonal bipyramidal configuration or 6 in a Jahn-Teller distorted octahedral coordination sphere.^[8] Copper(II) ions prefer aliphatic amines and anions as donor sets, i. e. carboxylate or deprotonated amidine units, in coordination compounds.

According to the electronic properties of the copper ions, the resulting complexes show different spectroscopic features. Copper(I) ions are spectroscopically silent because of their closed shell d^{10} -configuration, whereas copper(II) ions possess one single electron and show interesting spectroscopic and magnetic features.

The behavior of metal ions in proteins cannot be completely separated from the fundamental chemistry of the particular metal. Therefore the synthesis and characterization of bioinspired copper complexes represents an interesting field in synthetic copper coordination chemistry.



2. Current state of research

2.1. Metalloenzymes with a copper containing active site

In nature metalloenzymes with a copper containing active site play a crucial role in metabolic and cellular processes of eucaryotes and procaryotes. They take over a wide range of functions, such as electron transfer, oxygen transport, the oxidation of organic substrates or the reduction of small inorganic molecules.^[2]

Historically, copper proteins have been divided into three different subclasses, according to their structural and spectroscopic features. The first class are the so called *type I* copper proteins. These proteins employ one copper ion in their active site which is coordinated by two histidine residues and one cysteinato residue. The strongly distorted tetrahedral coordination sphere is usually completed by a weakly bound methionine residue (Figure 2.1). *Type I* proteins are also called blue copper proteins due to their characteristic blue color in the cupric state. This color originates from a LMCT (ligand to metal charge transfer) of the cysteinato-residue to the copper(II) ion. In nature, *type I* copper proteins are responsible for electron transfer, e.g. in herbal or bacterial photosynthesis.^[9]

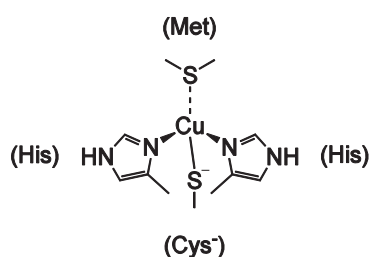


Figure 2.1: Structural constitution of *type I* copper proteins.

Type II copper active sites describe mononuclear copper proteins with an N or N/O ligand sphere (Figure 2.2). They exhibit an EPR-signal that is typical for copper(II) ions in coordination compounds. A weak d-d electronic transition of the cupric ion leads to the characteristic light blue color of these enzymes in the oxidized state. The enzyme class plays an important role in the activation of dioxygen in the presence of organic coenzymes.^[9]

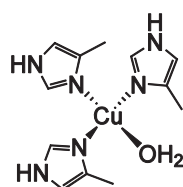
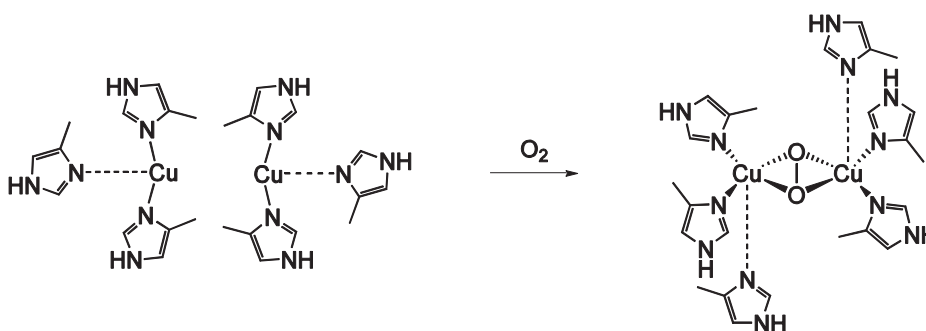


Figure 2.2: Structural constitution of *type II* copper proteins.

Type III copper enzymes exhibit a binuclear copper core. Each copper atom is coordinated by two strongly bound and one weakly coordinated histidine residue (Scheme 2.1). The vacant coordination site of the copper ions is utilized to incorporate oxygen and substrates between the metal centers, which is accompanied by an oxidation of the copper ions. *Type III* copper proteins are either involved in oxygen transport (e.g. hemocyanine) or in the oxidation and oxygenation of organic substrates (e.g. catechol oxidase or tyrosinase).^[2, 9-10]



Scheme 2.1: Structural constitution of *type III* copper proteins (hemocyanine as the example). Left: desoxy form, right: oxy form.^[2]

In the last decades further copper containing enzymes have been identified, for example the mixed-valent Cu_A -site, the Cu_B -heme_A center of cytochrome *c* oxidase, the Cu_Z -center of nitrous oxide reductase and the multinuclear centers of metallothioneines, to mention the most important.

The Cu_A -center is a binuclear mixed-valent copper-cluster that is bridged by two cysteinato residues. The Cu_A -cluster was first identified in cytochrome *c* oxidase. Cu_A is responsible for electron delivery in the catalytic process of the reduction of molecular dioxygen to water.^[10]

The second site of cytochrome *c* oxidase, the Cu_B -center, exhibits a single copper ion, which is coordinated by either two or three histidine residues. The Cu_B -center interacts

with a heme_A-iron-center in the catalytic process. Cytochrome *c* oxidases are involved in the eucariotic respiratory process.^[10]

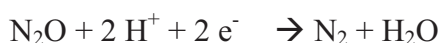
Metallothioneines (MT) are low molecular weight proteins that are characterized by their high percentage of cysteine; they bind up to eight cysteinato-bridged copper ions. MTs are responsible for copper transport and copper storage in humans and animals. Additionally it is assumed that they have a detoxifying protection function towards divalent metal ions like cadmium, copper and mercury.^[2, 11]

Recently a further novel copper containing enzyme was described. Nitrous oxide reductase (N₂OR) is involved in the nitrogen cycle, it decomposes nitrous oxide (N₂O). The enzyme employs two different copper-containing active sites, the already mentioned Cu_A-center^[12] and the Cu_Z-center. The Cu_Z-center contains a unique structure with four copper ions and two inorganic sulfido ligands.^[13]

Due to the exceptional structure of the Cu_Z-site and the biological role of the enzyme N₂OR stands in the spotlight of modern biological and bioinorganic research.

2.2. The N₂O-reductase (N₂OR)

Nitrous oxide (N₂O) is an important component of earth's atmosphere. It is part of the natural denitrification cycle^[14] and one of the most important greenhouse gases.^[15] Although its percentage is much lower than that of methane or carbon dioxide, the warming potential of N₂O is 310 times higher than the one of CO₂.^[15] Furthermore it has been identified as one of the most important ozone depleting substances recently.^[16-17] Although the decomposition of N₂O to yield dinitrogen and dioxygen (Scheme 2.2) is thermodynamically favorable, the molecule is kinetically inert due to the high activation barrier of 250 kJ·mol⁻¹ because the process is spin-forbidden. In nature the enzyme N₂OR performs the two electron reduction of N₂O to yield dinitrogen and water (Scheme 2.2).



Scheme 2.2: Decomposition pathways of N_2O , top: thermal decomposition, bottom: catalyzed decomposition.

N_2OR was isolated in 1982^[18] for the first time and it was proposed that the enzyme contains two distinct copper sites, the Cu_A -center and the Cu_Z -center. The Cu_A -center delivers the electrons for the reduction process and the reaction proceeds at the Cu_Z -center.

In 1991 FARRAR *et al.* suggested two different coexisting forms of the Cu_Z -site in the enzyme, namely the redox-active form Cu_Z and the inactive form Cu_Z^* .^[19] The corresponding percentage of each form depends on the purification method.^[20] In case of an anaerobic purification method the Cu_Z -form is enriched while aerobic purification methods lead to a higher percentage of the Cu_Z^* -form. The two forms are often distinguished according to their spectroscopic features into the purple, anaerobic form and the pink, aerobic form.^[21]

The first N_2OR enzyme that was crystallized and analyzed by single crystal X-ray diffraction methods was extracted from *Pseudomonas nautica* and purified under aerobic conditions in 2000.^[22] The results of the measurement revealed the structure of the two different copper-containing active sites.

The structure of the Cu_A -center is almost similar to the one from cytochrome *c* oxidase.^[23-24] The binuclear copper site is bridged by two cysteinato residues which leads to a very efficient electron delocalization in the oxidized $\text{Cu}^{1.5+}\text{Cu}^{1.5+}$ -state. The coordination sphere of the copper ions is completed by one histidine residue and a methionine residue for the first copper ion and a tryptophane residue for the second copper ion, respectively (Figure 2.3).

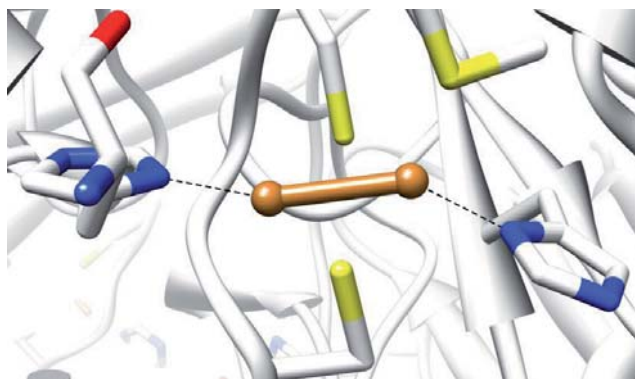


Figure 2.3: Cu_A-center of N₂OR from *Pseudomonas nautica*.^[25]

Cu_A is a highly efficient electron transfer unit.^[26] The distance of 2.5 Å between the two copper ions implied a copper-copper bond, which was proved *via* EXAFS spectroscopy.^[27-28]

The Cu_Z^{*}-center comprises a μ₄-sulfido bridged tetranuclear copper cluster in the inactive, pink form (Figure 2.4).^[25]

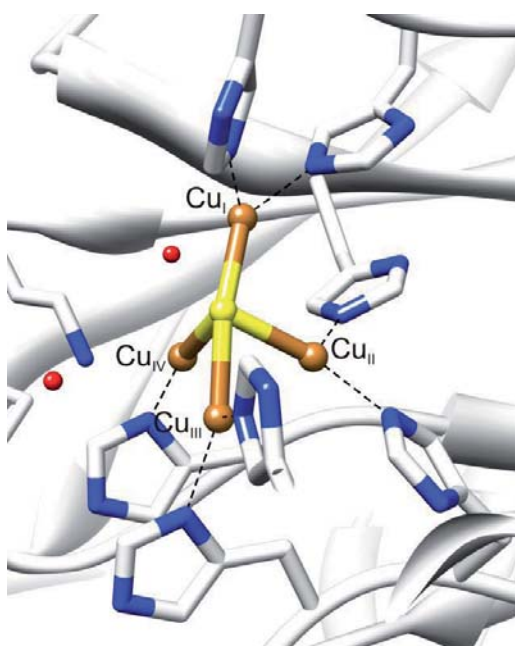


Figure 2.4: Cu_Z-center of N₂OR from *Pseudomonas nautica*.^[25]

The Cu₄S moiety is coordinated by seven histidine residues as depicted in Figure 2.4. The nature of the molecule between the Cu_I and the Cu_{IV} ion could not be clearly identified^[22, 25, 29] and was finally assigned as hydroxide or water molecule.^[30]

The pink aerobic form of the enzyme has been studied over the last years to elucidate the catalytic cycle of N₂O reduction,^[29, 31-33] but the detailed mechanism of the decomposition

of N_2O at the active site is not yet clarified. Theoretical studies suggested an initial μ -1,3-coordination of N_2O between the Cu_I and the Cu_{IV} ion of the cluster.^[32] The redox-state of the active form was assumed to be all-cuprous and the bridging sulfido ligand was expected to facilitate electron delocalization over the whole unit after the two electron reduction process.^[34]

The active purple form of N_2OR ^[35-36] is exclusively available under strict anaerobic conditions.^[20, 37] Recently, the appendent crystal structure was published.^[13] The structure exhibits a slightly different binding motif of the Cu_Z -site. An additional sulfide ligand has been incorporated between the Cu_I and the Cu_{IV} ions yielding a Cu_4S_2 -motif (Figure 2.5). As in the previously reported structure of the pink N_2OR the copper ions are coordinated by seven histidine residues.

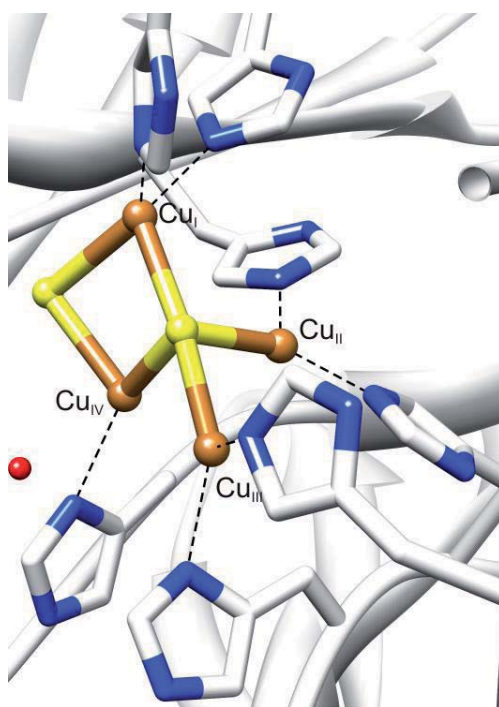


Figure 2.5: Structure of the recently discovered anaerobic Cu_Z -site of *Pseudomonas stutzeri*.^[13]

The second bridging sulfido ligand seems to disappear in the oxic form. Presumably under aerobic conditions dioxygen can enter the inner sphere of the enzyme and might remove the coordinated sulfido ligand irreversibly. This is corroborated by the low activities of aerobically purified N_2OR .^[34]

Additionally EINSLE *et al.* were able to obtain crystals suitable for X-ray diffraction of an enzyme-substrate adduct (Figure 2.6). In contrast to previous studies, they showed that N_2O is bound *side-on* above the Cu_{II} and Cu_{IV} ions and the central sulfido ligand.

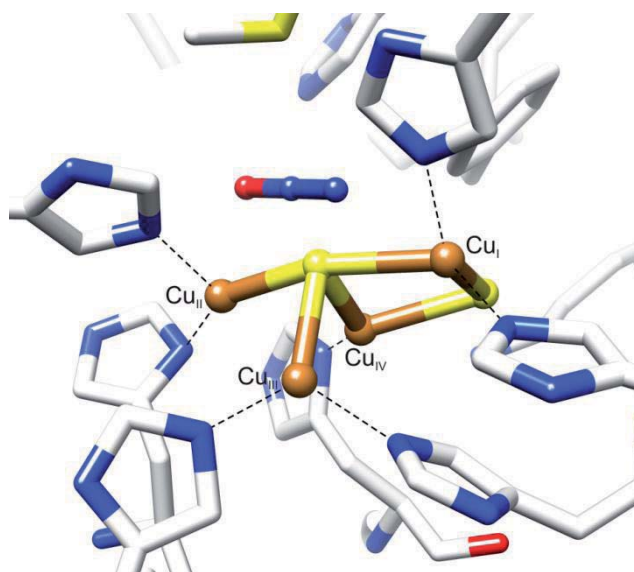


Figure 2.6: Substrate binding in N_2OR .^[13]

These recent results push the investigations of N_2OR into a different direction. Spectroscopic data have to be re-evaluated under the new aspects.

2.3. Low-molecular weight models in bioinorganic chemistry

Metalloenzymes are involved in numerous processes that impact life and the environment. These enzymes are able to perform catalytic reactions with high selectivity and efficiency. Up to now the relationship between function and structure is not yet fully understood for most metalloenzymes.

In nature, the active site of proteins is surrounded by the protein cavity. Therefore spectroscopic investigations and studies about the fundamental steps of the reaction at the active center are very difficult. One possibility to get a deeper insight into these processes, is the synthesis of low molecular weight complexes that somehow mimic the active site of the targeted metalloenzyme. Detailed characterization and reactivity studies



of these molecules are much easier and can provide functional insight transferable to the biological system. REEDIJK *et al.* classified low molecular weight complexes into three different types.^[38]

The first group are the so-called “speculative models”. This kind of model complexes can be useful, when the structure of the enzyme is not yet known. The complexes are designed based on the gained knowledge from spectroscopic data of the enzyme. The comparison of the spectroscopic data of the model complex with the ones of the enzyme can help to get some information about the structure of the active center.

The second group are the so-called “corroborative models”. Such model complexes are designed based on the knowledge of the structure of the active site of the enzyme. The evaluation of the effect of ligand constraints on spectroscopic and catalytic properties of the metal ion can help to give an insight into the structure activity relationship.

The third group of metal complexes are the “functional models”. These models are designed with the full knowledge about the structure and the mode of action of the enzyme. Functional model complexes perform the same reactions as the enzyme and thus may be used in industrial and medical applications.

Despite extensive research of such model complexes, the structure function relationship at the molecular level is not yet fully understood for most metalloenzymes. Therefore the synthesis and intensive study of low molecular weight models still seems to be worthwhile.

2.4. Copper-sulfur complexes with N-donor supporting ligands

The mode of action of the Cu_Z-center is not yet well understood. In order to get further insight about the structure of the active center and about the structure activity relationship, some model complexes have been synthesized and characterized. Some speculative and some corroborative model complexes with multinuclear copper-sulfur cores have been developed to date, though complexes with a Cu₄S or Cu₄S₂ core could not yet be prepared. Only one of those complexes is able to decompose N₂O to yield N₂.

Synthesis of binuclear Cu₂S₂ species

The most frequently reported copper-sulfur complexes feature a Cu₂S₂-core with a disulfido bridge (S₂²⁻). There are mainly three possible binding modes for a disulfido moiety in binuclear metal complexes (Figure 2.7).^[39] The bidentate ligand is able to bind either μ - η^2 : η^2 -*side-on*, *trans* μ -1,2-*end-on* or *cis* μ -1,2-*end-on*. The *cis* μ -1,2-*end-on* binding mode has not been observed in copper complexes until now.

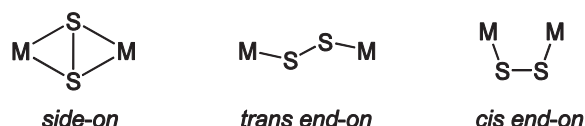
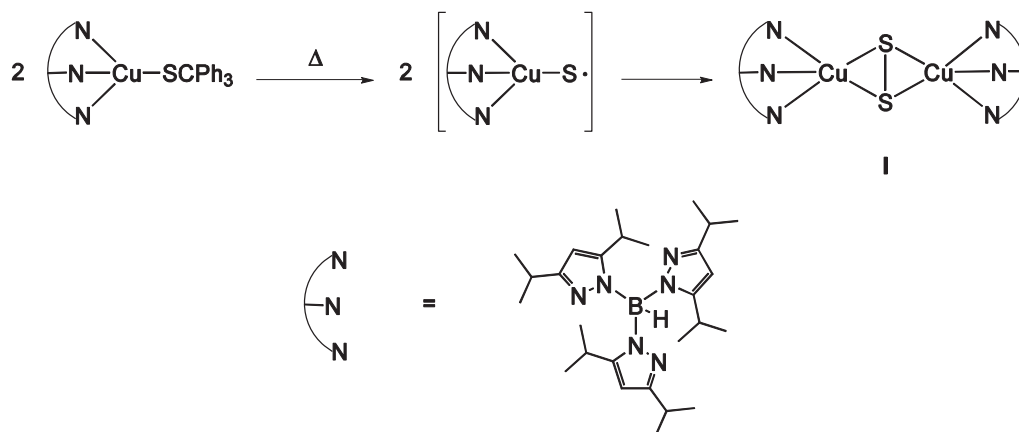


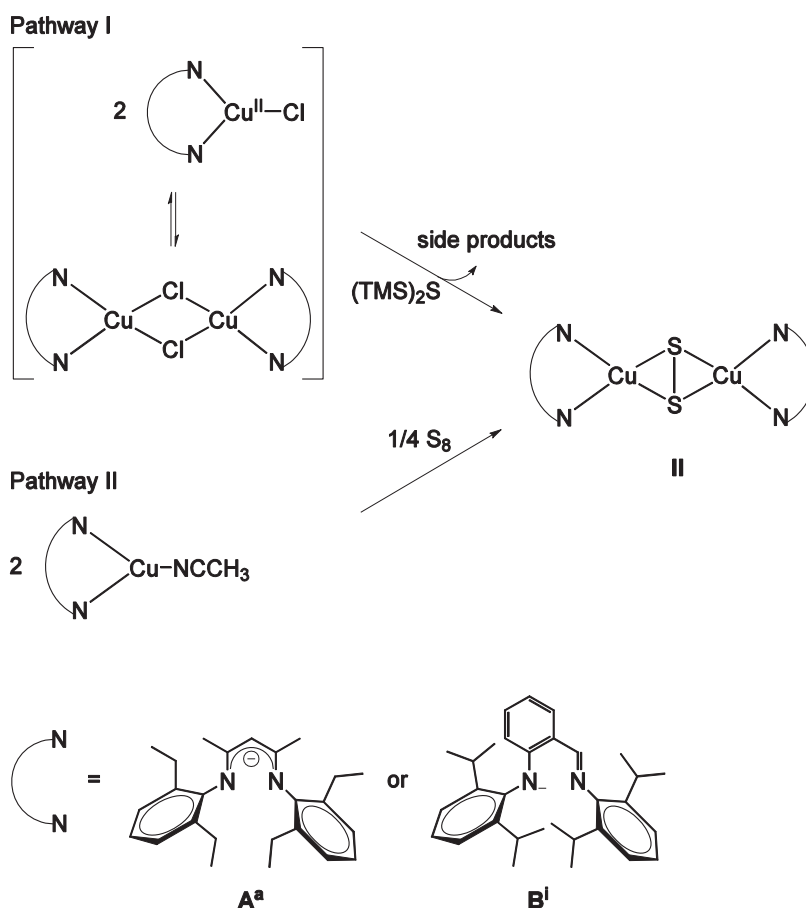
Figure 2.7: Possible binding modes of the disulfido ligand between two metal ions.

The first binuclear copper complex with a μ - η^2 : η^2 -*side-on* disulfido bridge was described by KITAJIMA *et al.* in 1994 (Scheme 2.3).^[40] This *side-on*-complex was obtained *via* thermal decomposition of Cu(SCPh₃)(HB(3,5-*i*Pr₂pz)₃).^[41] Presumably this decomposition process proceeds *via* the formation of the radical intermediate [(HB(3,5-*i*Pr₂pz)₃Cu-S·] (Scheme 2.3).



Scheme 2.3: Synthetic route to the first *side-on* disulfido complex with N-donor ligands.

Two different synthetic routes have been presented to obtain μ - η^2 : η^2 -*side-on*-Cu₂S₂-species by TOLMAN *et al.* in 2004.^[42] On the one hand copper(II) chloride complexes are treated with (TMS)₂S (pathway I) and on the other hand copper(I) complexes are treated with stoichiometric amounts of elemental sulfur (pathway II). In both cases either a β -diketiminato-ligand **A**^a or an anilido-imine-ligand **B**ⁱ was employed (Scheme 2.4).



Scheme 2.4: Synthetic routes to *side-on* copper-disulfido complexes.

The first route leads to the formation of the desired $\mu\text{-}\eta^2\text{:}\eta^2\text{-side-on-Cu}_2\text{S}_2$ moiety in very low yields because several byproducts are formed (ligand **A^a**: 17 %, ligand **Bⁱ**: 29 %). Employing ligand **Bⁱ** the byproduct **BⁱCu^I(MeCN)** could be characterized and utilizing ligand **A^a** the tetramer **III** is formed (Figure 2.8). Additionally, since the sulfide forms a disulfido bond in the reaction, some further oxidized products must be formed.

The synthesis was modified to avoid these side reactions (pathway II in Scheme 2.4). The copper(I) complexes **A^aCu(MeCN)** and **BⁱCu(MeCN)** were oxidized *in situ* with one equivalent of elemental sulfur. This suppressed the undesired side reactions and the yield was raised to 54 % (**A^a**) and 59 % (**Bⁱ**), respectively. With this improved synthesis a whole series of complexes has been synthesized by TOLMAN *et al.* (Figure 2.9).^[43]

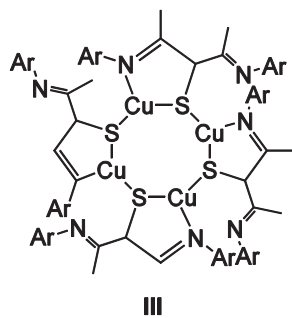
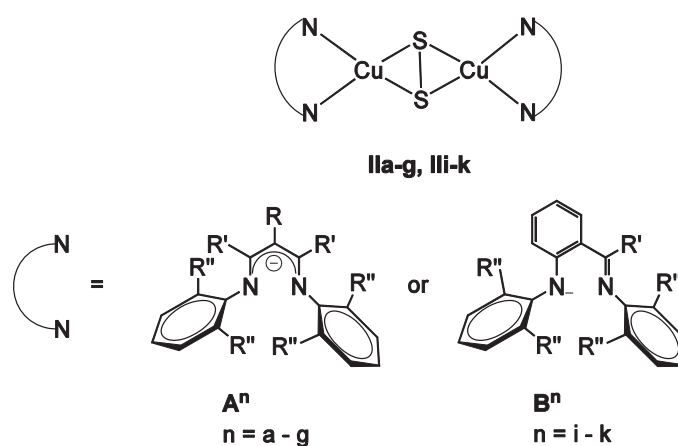


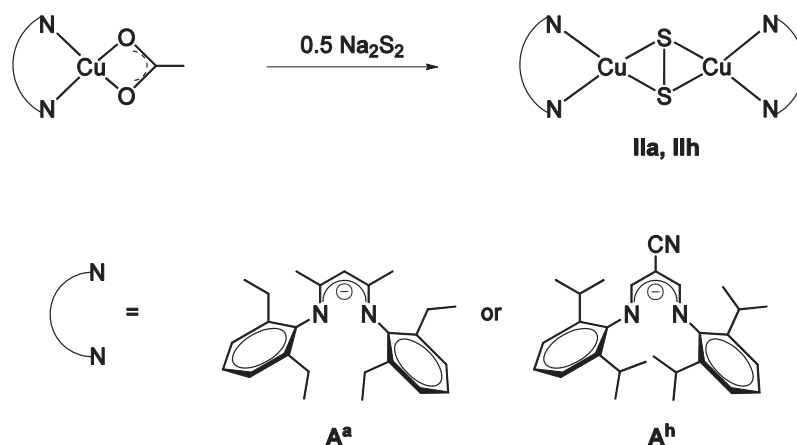
Figure 2.8: Byproduct III of the synthesis of $\mu\text{-}\eta^2\text{:}\eta^2\text{-side-on-Cu}_2\text{S}_2$ species.



ligand	a - g			i - k		
	R	R'	R''	ligand	R'	R''
a	H	Me	Et	i	H	<i>i</i> Pr
b	H	Me	Me	j	H	Me
c	H	<i>t</i> Bu	<i>i</i> Pr	k	Me	<i>i</i> Pr
d	Ph	H	Et			
e	Ph	H	<i>i</i> Pr			
f	3,5-(CF ₃) ₂ C ₆ H ₃	H	Me			
g	3,5-(CF ₃) ₂ C ₆ H ₃	H	<i>i</i> Pr			

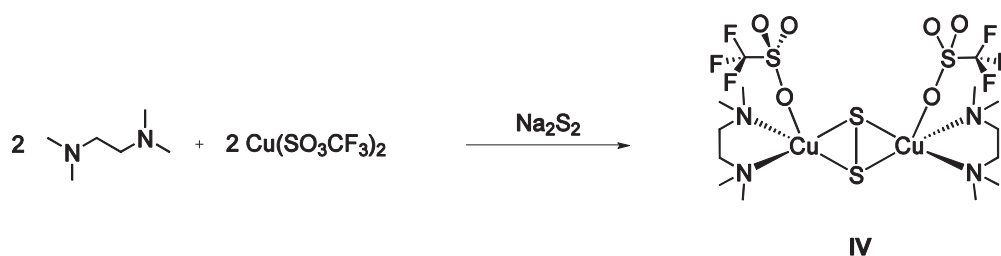
Figure 2.9: Synthesized $\mu\text{-}\eta^2\text{:}\eta^2\text{-side-on-Cu}_2\text{S}_2$ complexes (IIa – g and IIi - k) by TOLMAN *et al.*.

In 2007 ITOH *et al.* published a different route to synthesize $\mu\text{-}\eta^2\text{:}\eta^2\text{-side-on}$ Cu_2S_2 -complexes.^[44] Na_2S was added to a solution of copper(II) acetate precursor to yield complexes with the desired Cu_2S_2 moiety (Scheme 2.5). As ligands, the well known β -diketiminato compounds A^{a} and A^{h} were employed. Employing A^{a} the product was formed in moderate yields, while the yield increased significantly when an electron withdrawing group was introduced in α -position of the β -diketiminato ligand (A^{h}).



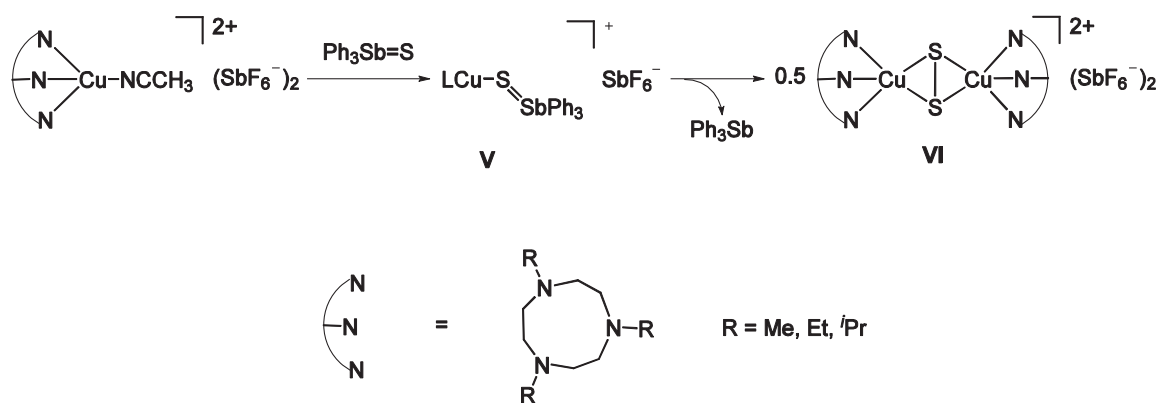
Scheme 2.5: Modified synthesis of complexes **IIa** and **IIIh**.

The reaction of N,N,N',N' -tetramethylethylenediamine (tmeda) and copper(II) triflate with Na_2S yields a Cu_2S_2 species, too (Scheme 2.6).^[45] In **IV** the copper ions of the Cu_2S_2 moiety are coordinated additionally by the triflate anions.



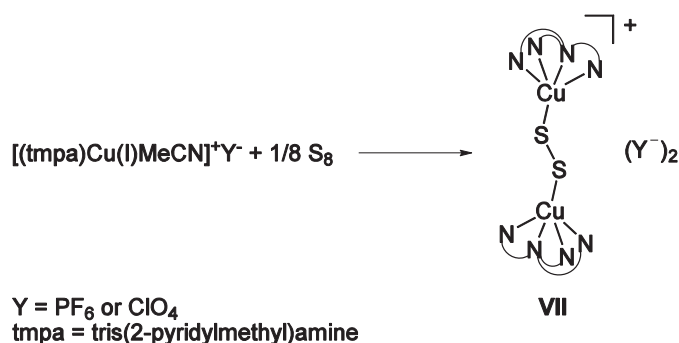
Scheme 2.6: *Side-on* Cu_2S_2 complex with tmeda as employed ligand.

The most recent synthetic route to obtain a $\mu\text{-}\eta^2\text{:}\eta^2\text{-side-on-Cu}_2\text{S}_2$ complex was presented by TOLMAN *et al.*^[46] They reacted $[(\text{tacn})\text{Cu}(\text{MeCN})]^+[\text{SbF}_6]^-$ (tacn = 1,4,7-trialkyltriazacyclononane) with Ph_3SbS (Scheme 2.7). Detailed mechanistic investigation of the reaction showed the formation of **V** in the first step, which slowly decomposes to yield the desired complex **VI**.



Scheme 2.7: Synthesis of complexes V and VI.

Employing the tetradentate ligand tris(2-pyridylmethyl)amine (tropa) in the reaction the formation of complexes with a μ - $\eta^2\eta^2$ -disulfido-binding mode was observed in contrast to the otherwise μ - $\eta^2:\eta^2$ -*side-on*- Cu_2S_2 binding mode as observed in Scheme 2.8.^[47] **VII** was synthesized *via* oxidation of the corresponding acetonitrile copper(I) complex with elemental sulfur. This indicates that the binding mode of the disulfido ligand depends on the steric demand and the denticity of the employed ligand.

Scheme 2.8: Synthesis of the first μ -1,2-*end-on* Cu_2S_2 moiety.

Synthesis of multinuclear copper sulfur complexes

The reaction of $[(\text{tmeda})\text{Cu}^{\text{I}}(\text{MeCN})]^+$ with an excess of elemental sulfur yielded two complexes with different copper sulfur motifs in dependence on the counter ion (Figure 2.10).^[48] On the one hand in the presence of SbF_6^- or PF_6^- as anions the trinuclear copper complex **VIII** is formed which exhibits two bridging sulfido units.^[49] On the other hand, when triflate is employed as counterion, complex **IX** with a $\text{Cu}_2(\text{S}_2)_2$ -core is formed as

depicted in Figure 2.10. This result indicates that the formation of the product is not only sensitive to the ligand but also to the counterion.

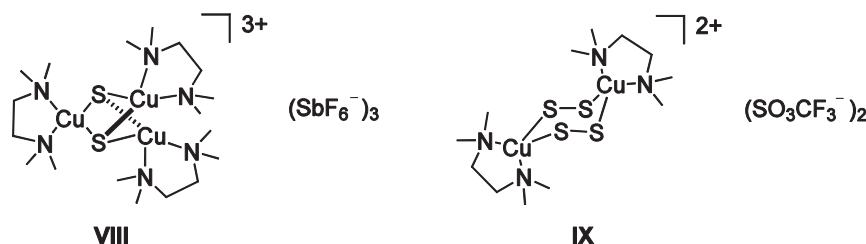
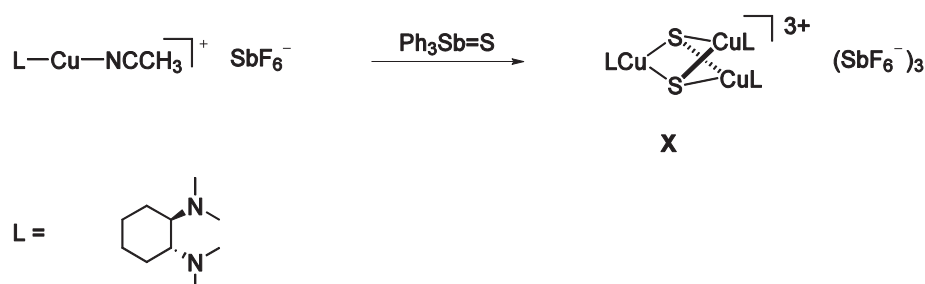


Figure 2.10: Copper sulfur compounds from the reaction of copper(I) complexes with elemental sulfur.

The oxidation state for the disulfido unit in complex **IX**, i. e. $[(S_2)^{2-}]$ or $[(S_2)^{1-}]$, was identified by a combination of EXAFS spectroscopy and DFT calculations.^[50] The results of the measurement revealed the dicopper(II)-bis-disulfide($\cdot 1-$) nature of the core motif.

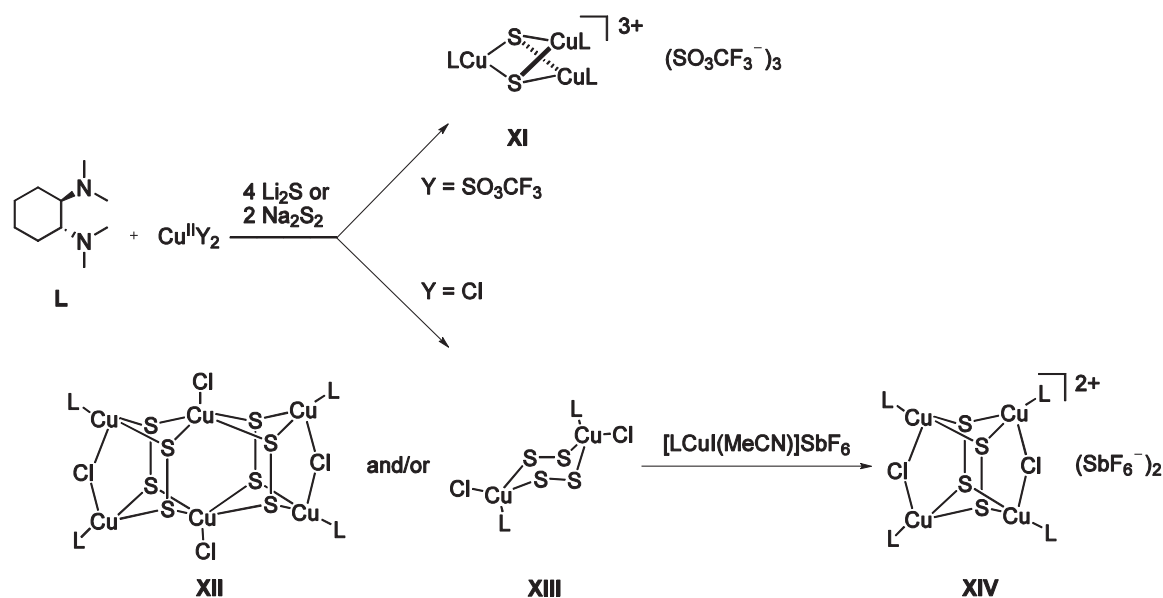
Up to now trinuclear complexes such as **VIII**, with an $L_3Cu_3S_2$ core motif, are only available if bidentate ligands are employed, but various sulfur sources can be used in the synthesis. In Scheme 2.9 a second reaction pathway to a $L_3Cu_3S_2$ species is depicted: TOLMAN *et al.* reacted $[LCu(MeCN)]^+$ ($L = N,N,N',N'$ -tetramethyl-*trans*-(1R,2R)-diaminocyclohexane (Me₄chd)) with Ph₃SbS to yield complex **X**.^[46]



Scheme 2.9: Synthesis of complex **IX**.

A third possibility to synthesize multinuclear copper-sulfur complexes is the reaction of Me₄chd, a copper(II) salt and either Li₂S or Na₂S₂.^[51] The formation of the product is highly sensitive to the utilized counterion of the copper salt. Employing copper(II) triflate on the one hand the already described $L_3Cu_3S_2$ species (complex **XI**, $L = Me_4chd$) was obtained (Scheme 2.10). On the other hand the hexanuclear complex **XII** is accessible in the reaction of copper(II) chloride, Me₄chd and Li₂S. Employing Na₂S₂ instead of Li₂S complex **XIII** is isolated. TOLMAN *et al.* reported that the purification and isolation of the products **XII** and **XIII** is difficult. Hence they assume a coexistence of the two species in

the reaction mixture. Anyway, they treated this solution with $[\text{LCu}^{\text{I}}\text{MeCN}]\text{SbF}_6$ and obtained the pure product **XIV**.



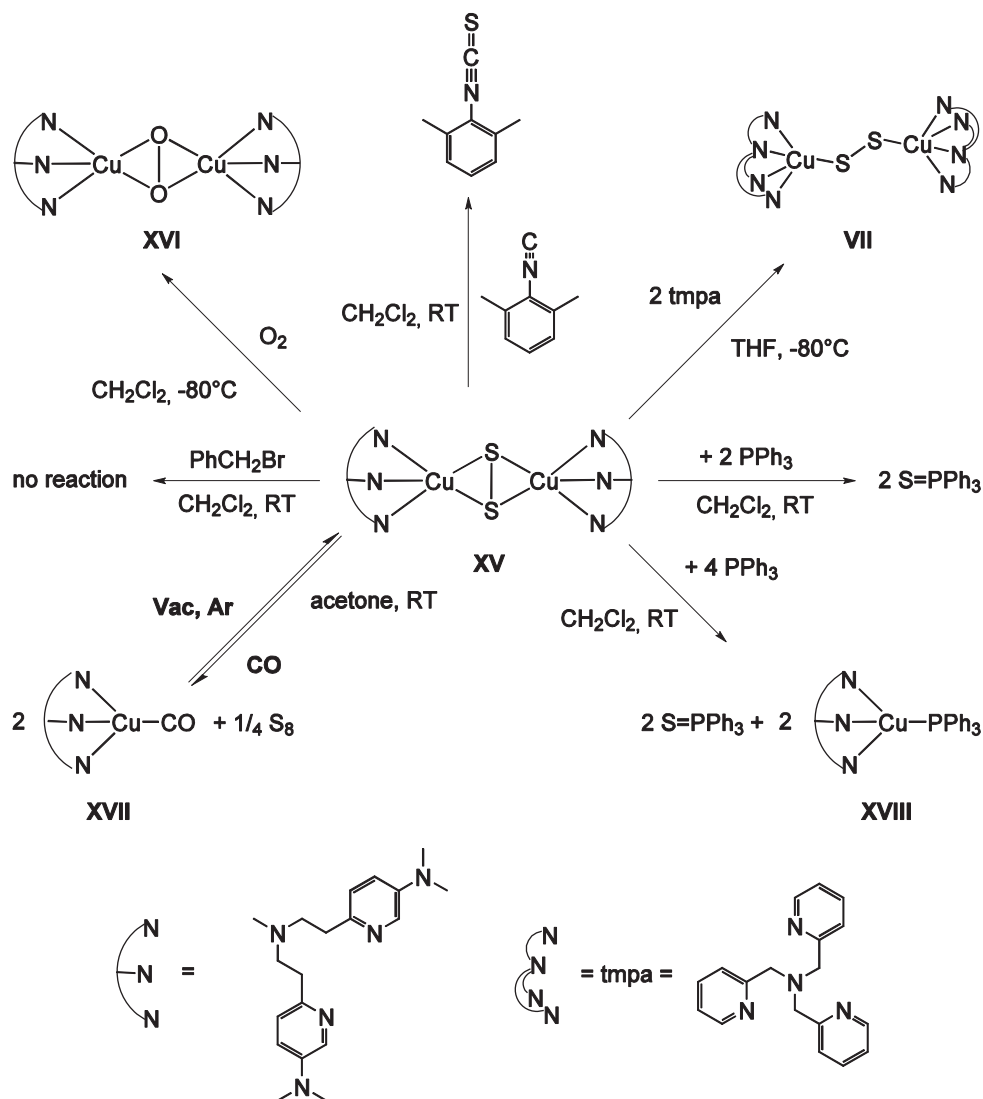
Scheme 2.10: Synthesis of multinuclear copper sulfur compounds.

Reactivity studies of copper sulfur complexes towards different substrates

In 2003 the bonding and spectroscopic features of the *side-on* and the *end-on* Cu_2S_2 complexes have been investigated and compared with their well examined oxygen analogues.^[52] The results of different spectroscopic investigations led to the conclusion, that disulfido ligands are better electron donors than peroxido ligands and that *side-on* and *end-on* copper(II) disulfido interactions have more covalent character than the *side-on* and *end-on* copper(II) peroxido interactions. DFT calculations revealed, that the ground state of the *side-on* Cu_2S_2 -species is more covalent than the ground state of the *end-on* Cu_2S_2 -species. To confirm these results both complex types have been investigated chemically by KARLIN *et al.*,^[53-54] i. e. they studied the reactivity of copper disulfido complexes towards various substrates.

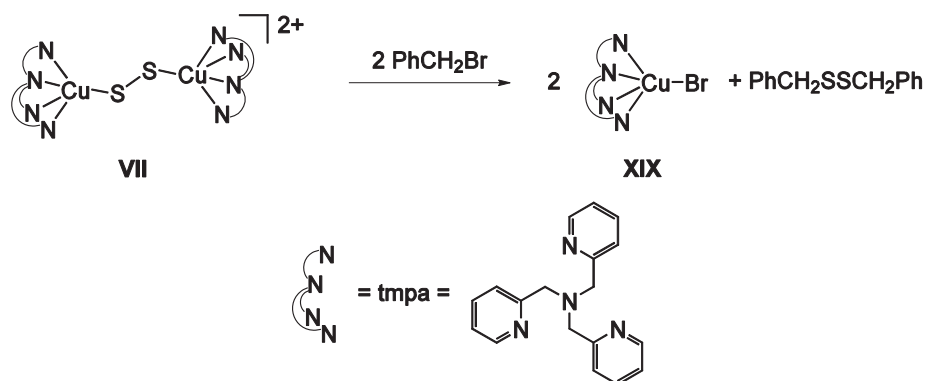
The $\mu\text{-}\eta^2\text{:}\eta^2\text{-side-on-Cu}_2\text{S}_2$ -species **XV** shows a wide range of reactivity as summarized in Scheme 2.11.^[53] **XV** is able to transfer sulfur to PPh_3 and isocyanide. The disulfido ligand is replaced by dioxygen or the original used tridentate ligand $\text{HB}(3,5\text{-}i\text{Pr}_2\text{pz})_3$ can be exchanged with *tmpa* forming the *end-on* species **VII**. In presence of carbon monoxide

an equilibrium between **XV** and **XVII** under formation of elemental sulfur is observed, while no reactivity was observed towards PhCH_2Br .



Scheme 2.11: Reactivity pattern of **XV** towards various substrates.

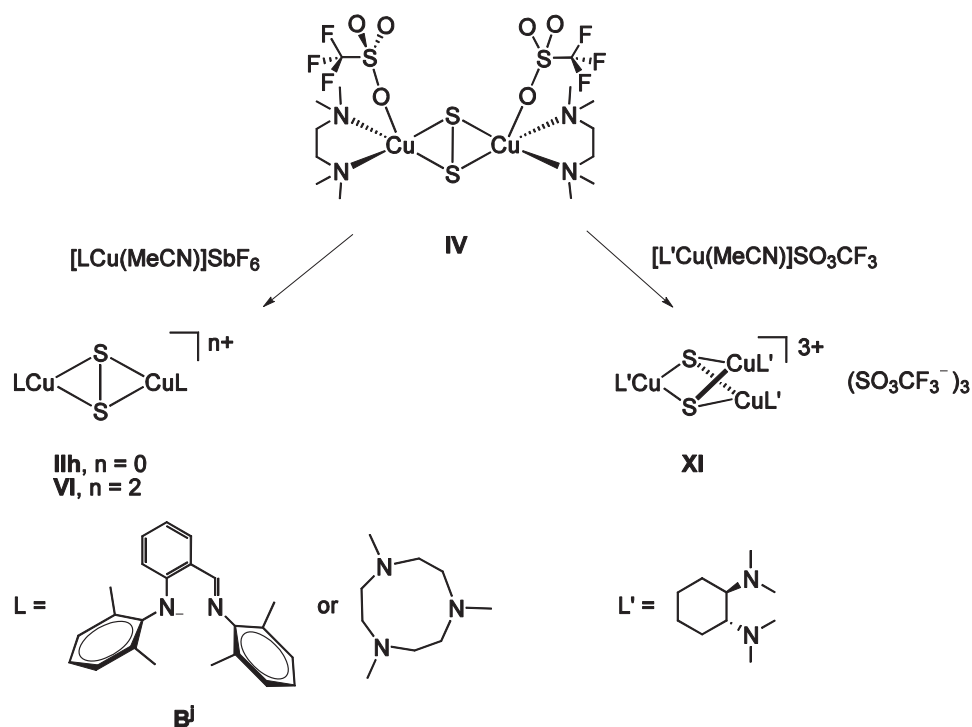
The chemical features of the *end-on* copper disulfido complex **VII** have also been investigated by KARLIN *et al.*^[54] They chose the same substrates as for complex **XV**. The observed reactivity of **VII** is similar to the one of **XV** and includes sulfur transfer of **VII** to PPh_3 and isocyanide as well as the $(\text{S}_2)^{2-}$ exchange reaction with carbon monoxide or dioxygen. In contrast to **XV**, however, **VII** reacts with PhCH_2Br to yield **XIX** and $\text{PhCH}_2\text{SSCH}_2\text{Ph}$ (Scheme 2.12).



Scheme 2.12: Reactivity of **VII** towards PhCH_2Br .

The investigated complexes **XV** and **VII** are able to perform similar reactions towards the same substrates. Anyway KARLIN *et al.* suggest that the different binding modes of the disulfido ligand show different electronic character.^[54] They propose that the *side-on* bound Cu_2S_2 species possesses an electrophilic disulfido moiety and the *end-on* Cu_2S_2 species possesses a nucleophilic one. These assumptions are in agreement with the related peroxido copper chemistry, where the *side-on* bound O_2 species shows electrophilic behavior towards substrates, while the *end-on* bound O_2 species shows nucleophilic behavior.^[55-56] However, **VII** and **XV** undergo almost the same reactions, so the electronic structure of the disulfido ligand seems to be more complicated than in the peroxido analoga. To clarify this issue more experimental data and further mechanistic investigations are necessary.

Complex **IV** was investigated in various reactions, too (Scheme 2.13).^[45] In a conversion reaction the N-donor-ligand in **IV** can be exchanged to either the tridentate ligand tacn or an anionic anilido-imine ligand yielding the same Cu_2S_2 motif.

Scheme 2.13: Conversion reactions of complex **IV**.

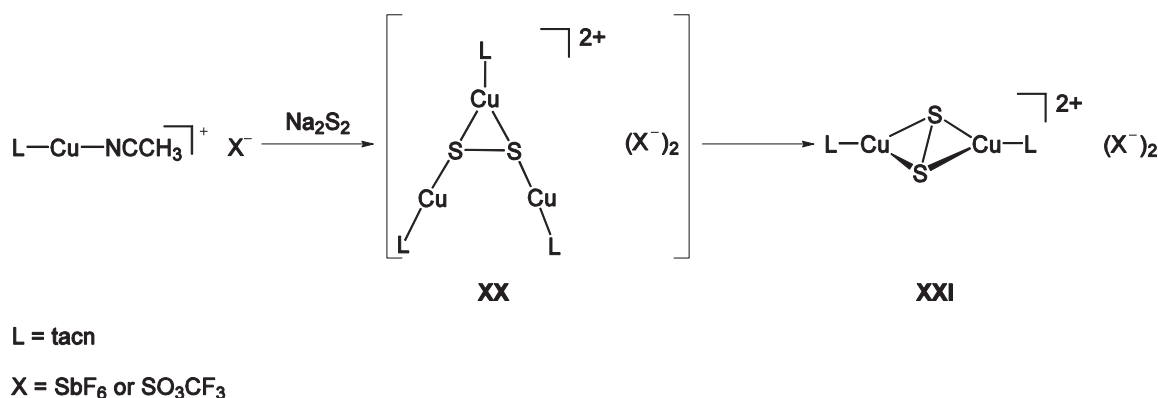
Additionally, compound **IV** was investigated with respect to its capability to oxidize organic substrates, and, indeed, **IV** is able to oxidize phenols. Selected examples of phenols and the corresponding products are summarized in Figure 2.11. The oxidation of biphenols to the corresponding quinone and C-C coupling products of phenols are the main products. In case of 2,4-*tert*-butylphenol as substrate, the C-C-coupling is accompanied by sulfur insertion into the generated C-C-bond. Hence **IV** is able to act as a two-electron oxidizing agent.

substrate	product	substrate	product

Figure 2.11: Substrates and products of the oxidation reactions performed by **IV**.

Decomposition of N₂O

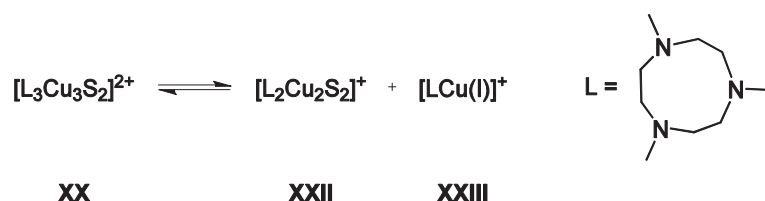
Until now there is only one complex known that reacts with N₂O and is able to decompose N₂O to yield N₂ (Scheme 2.14).^[57] Complex **XX** features a L₃Cu₃S₂ motif (L = tacn) and is stable only at -80°C.



Scheme 2.14: Synthesis of a L₃Cu₃S₂ complex, which is active towards N₂O.

XX features a bridged disulfido (S₂²⁻) ligand and three copper ions in two different oxidation states. The five coordinated copper ion shows presumably the oxidation state of +2 and the four coordinated copper ions have an oxidation state of +1. Warming up **XX** to room temperature leads to decomposition of the complex to a binuclear copper complex **XXI** with a bridged *side-on* disulfido ligand as depicted in Scheme 2.14.

Warming up a solution of **XX** to ambient temperature in the presence of N₂O leads to the formation of [L₂Cu₂(OH)₂](SbF₆)₂ and N₂. [L₂Cu₂(OH)₂](SbF₆)⁺ was detected by mass spectrometry. Detailed mechanistic studies revealed that the active species seems to be the mixed-valent binuclear copper complex [LCu₂S₂]⁺ (**XXII**). Presumably **XX** is present in an equilibrium (Scheme 2.15) with the active binuclear species **XXII**, which converts N₂O to N₂ quantitatively (based on **XX**).



Scheme 2.15: Equilibrium of **XX**.



DFT-calculations suggest that the N₂O substrate coordinates *via* its oxygen atom between the two copper ions of [LCu₂S₂]⁺ (XXII) as the initial step. This is different from the proposed binding mode in the enzyme (μ -1,3-bridged species).^[34]

The presented reactions and model complexes show that the formation of complexes with a copper sulfur core is highly sensitive to the employed sulfur transfer reagents, the counterion of the copper source and the coupling ligand. Only one complex has been developed that is able to decompose N₂O to N₂ until now. A Cu₄S-cluster could not be isolated yet, but some progress towards a synthetic model of the Cu_z-center has been already made.

2.5. Copper clusters with thiolate ligands

In nature copper enzymes like metallothioneines, *type I* copper proteins and the Cu_A-center feature sulfur-rich coordination surroundings due to their cysteinato ligands. In order to emulate the structures of the active centers and to elucidate structure activity relationships, low molecular weight models have been synthesized and characterized for these proteins. As mimic for the cysteine-rich surrounding, organothiolate ligands have been employed during the synthesis.

Organothiolates (RS⁻) have been used as ligands for metal centers since the beginning of coordination chemistry.^[58-60] According to the PEARSON concept thiolate ligands (RS⁻) are soft bases. The organic residue R can be adapted to the steric and electronic demands of the coordinated metal ions. Additionally the ligand is very flexible and labile in the resulting binding motif, due to the ability to bind either as monodentate ligand, or as bridging ligand between two or three metal ions.

Multinuclear copper-thiolate complexes without N-donor supporting ligands

Copper-thiolate complexes without N-donor supporting ligands are well investigated compounds. Until now there are either mononuclear compounds known or clusters with

2 – 12 copper ions in a discrete unit. These compounds are usually synthesized by deprotonating the corresponding organothiols with a base and subsequently reacting this mixture with a copper(I) or a copper(II) salt. If copper(II) salts are employed, the copper ions are often reduced to the cupric state since organothiolates are able to transfer electrons to copper(II) ions. The prediction of the structures of the resulting copper thiolate compounds is difficult because the thiolate ligand can bridge either in a μ_2 - or in a μ_3 -mode.

Mononuclear homoleptic copper(I) thiolate complexes can be obtained with either two or three thiolate ligands (Figure 2.12). Complexes with the stoichiometric composition $(\text{Cu}(\text{RS})_2)^-$ are exclusively obtained when thiolate ligands with bulky residues like the aliphatic adamantyl-residue or the 2,3,5,6-tetramethylbenzene are employed.^[61-62] With smaller residues like thiophenolate or *o*-pivaloylaminobenzenethiolate the $[\text{Cu}(\text{SR})_3]^{2-}$ species are preferred.^[63-65]

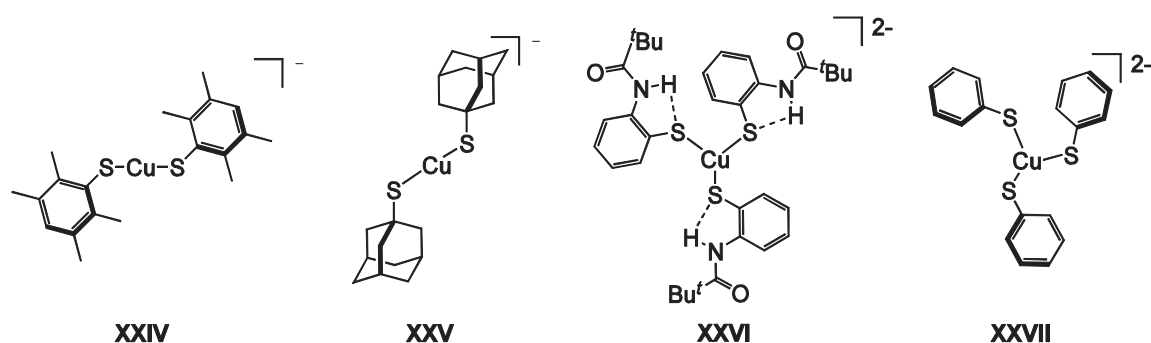


Figure 2.12: Mononuclear homoleptic copper thiolate complexes.

Copper thiolate clusters with 2 – 12 copper ions have been described more frequently than the already discussed mononuclear copper thiolate compounds. These clusters usually feature a thiolate to copper ratio of 1 or higher. In detail the following copper thiolate ratios could be obtained: $\text{Cu}_2(\text{SPh})_2(\text{PPh}_3)_2$,^[66] $\text{Cu}_3(\text{SPh})_3(\text{PPh}_3)_4$,^[67] $\text{Cu}_4(\text{SR})_4$ (SR = 2,6-(bistrimethylsilyl)-benzenethiolate)^[68] $\text{Cu}_4(\text{SR})_6$, (R = Me, Et, Ph)^[64, 69-72], $\text{Cu}_5(\text{S}^t\text{Bu})_6$ ^[73-74], $\text{Cu}_5(\text{SAd})_6$ (Ad = adamantyl = $\text{C}_{10}\text{H}_{15}$),^[61] $\text{Cu}_5(\text{SPh})_7$,^[69, 75] $\text{Cu}_7(\text{SEt})_8$ ^[72] and $\text{Cu}_{12}(\text{SR})_{12}$ (SR = 2-trimethyl-silylbenzenethiolate).^[76] The most common motif is the $\text{Cu}_4(\text{SR})_6$ (R = Me, Et, Ph) cluster. The corresponding structure of the complexes is similar to the structure of adamantane ($\text{C}_{10}\text{H}_{16}$) and therefore builds a very stable coordination framework (Figure 2.13).

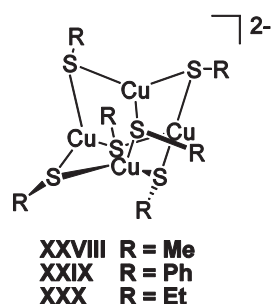


Figure 2.13: Structure motif of $[\text{Cu}_4(\text{SR})_6]^{2-}$ clusters (R = Me, Et, Ph).

Complexes **XXVIII** – **XXX** feature exclusively μ_2 -coordinated thiolato ligands. As an example for a compound where the thiolato ligand binds in a μ_2 - and in a μ_3 -fashion, the $\text{Cu}_{12}(\text{SR})_{12}$ (**XXXI**) complex is depicted in Figure 2.14.

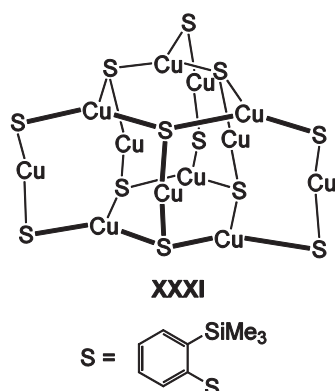


Figure 2.14: $\text{Cu}_{12}(\text{SR})_{12}$ complex (SR = 2-trimethylsilylbenzenethiolate) with μ_3 -thiolate units.

As already mentioned, the thiolate to copper ratio is usually one or higher. Therefore complexes with a ratio that is smaller than one are stabilized by coligands. The copper thiolate cluster $\text{Cu}_6(\text{SPh})_4\text{X}_6$ (X = Cl, Br)^[54] which employs either chloride ions or bromide ions as coligands is depicted in Figure 2.15.

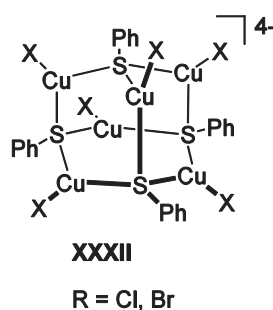


Figure 2.15: $\text{Cu}_6(\text{SPh})_4\text{X}_6$ (X = Cl, Br).

Copper(I) thiolate complexes with N-donor-supporting ligands

In principle, there are two synthetic routes known to synthesize complexes that feature a thiolate function and are coordinated by N-donor atoms at the same time. First, it is possible to synthesize complexes in which the copper ions are coordinated by two different ligands, one ligand which exhibits N-donor atoms and one ligand which exhibits thiolate functions. Second, one ligand can contain both, N-donor atoms and thiolate functions at the same time. Examples for both classes will be presented.

Copper complexes which exhibit two different ligands usually feature besides the anionic thiolate ligand a neutral N-donor ligand like phenantroline or bipyridine.^[77-81] Selected complexes are depicted in Figure 2.16. The general synthetic route is to add the neutral N-donor ligand to the corresponding copper(I) thiolate. Although complexes **XXXIII** - **XXXVI** feature the same copper to thiophenolate to phenantroline ratio (1:1:1) the complexes possess different nuclearities. This indicates that the nuclearity of the resulting complexes can be tuned *via* the steric demand of the ligand.

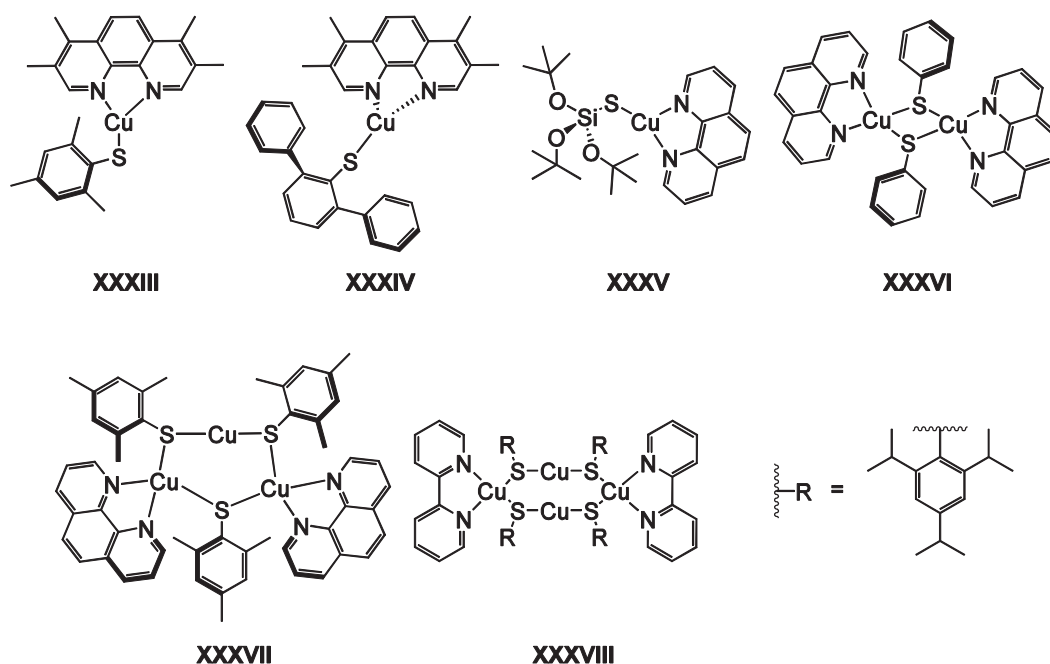


Figure 2.16: Copper thiolate complexes with phenantroline or bipyridine as N-donor ligand.

The second synthetic route to synthesize copper(I) thiolate complexes with N-donor supporting ligands is to employ ligands that feature already a donor set of both atoms. In Figure 2.17 two complexes which feature ligands with S- and N-donor atoms are depicted.^[82-83] Complex **XXXIX** is synthesized *via* deprotonation of the ligand and

subsequent addition of copper(I) iodide. The resulting tetranuclear complex features a ligand with two thiolate functions and two neutral N-donor atoms. The four copper ions are set in two different coordination spheres. In complex **XL** the ligand exhibits one neutral N-donor atom and one thiolate function. The tetranuclear complex is synthesized *via* electrochemical methods. All copper atoms feature the same trigonal coordination sphere. Although different coordination numbers (2, 3 and 4) are observed for the copper atoms, the S atom of the thiolate function bridges two copper ions in both cases.

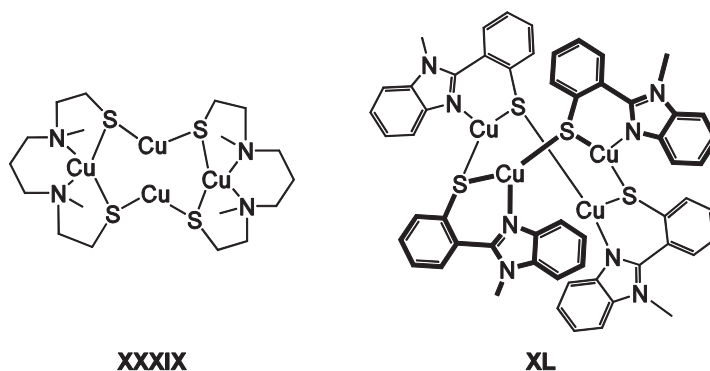


Figure 2.17: Complexes with thiolate-functionalized ligands.

It is possible to synthesize complexes that feature higher nuclearities with these ligand systems, but these will not be discussed here.^[84-86]

2.6. Pyrazolate-based ligand systems in multimetallic complexes

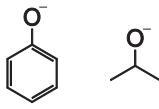
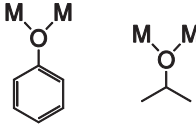
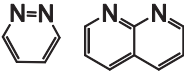
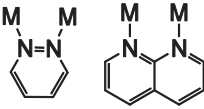


The cooperation of two metal ions in close proximity could lead to interesting magnetic and electronic features. For example, the reducing power of a binuclear complex is expected to cover a wider range simply because each metal ion can contribute electrons within its normally accessible oxidation states. Thus, multielectron redox processes are performed more easily.^[87]

Various ligand systems with two adjacent binding sites have been designed during the last decades. They are commonly classified by the bridging group that is used to assemble

two metal ions in close proximity. Selected bridging units and the corresponding metal binding mode are depicted in Table 2.1.^[88]

The bridging units can be equipped with manifold substituents that vary in number and kind of donor atoms. The chelating substituents are usually introduced at the ortho-positions of the phenolate-function, the 1 and 3 position of the alkoxide, the 2 and 6 position of the pyridazine, the 2 and 7 position of the naphthyridine and the 3 and 5 position of the pyrazole and the triazole unit, respectively.^[88] With this add-on system the ligand precursor can be modified according to the characteristics of the desired metal ion.

Table 2.1: Selected established bridging units for binucleating ligand systems.

bridging unit name	bridging unit	metal binding mode
phenolate, alkoxide		
pyridazine 1,8-naphthyridine		
pyrazolate triazolate		

To mimic the nitrogen-rich surrounding of active sites in enzymes, often tertiary amines or nitrogen containing heterocycles are attached.^[88] Alcohol or acid functions are introduced to mimic the natural aspartate, glutamate or tryptophane environment. Selected well established ligands which contain one of the presented bridging units, are depicted in Figure 2.18. This kind of ligands and some derivatives have already been shown to coordinate two metal ions in close proximity.^[89-99]

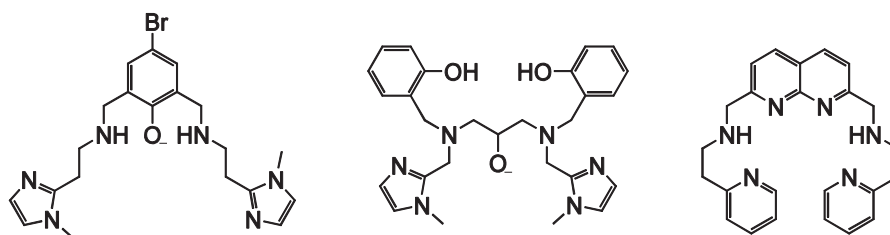


Figure 2.18: Selected ligands that are able to bind two metal ions in close proximity.^[93, 95, 98]

Employing 3,5-substituted pyrazoles as bridging unit, MEYER *et al.* were able to synthesize an extensive ligand-portfolio. Various chelating units in 3- and 5-positions were introduced such as amine functions, N-heterocycles or thioether units. In Figure 2.19 selected ligand precursors are depicted that have been prepared in the MEYER group.^[100-104]

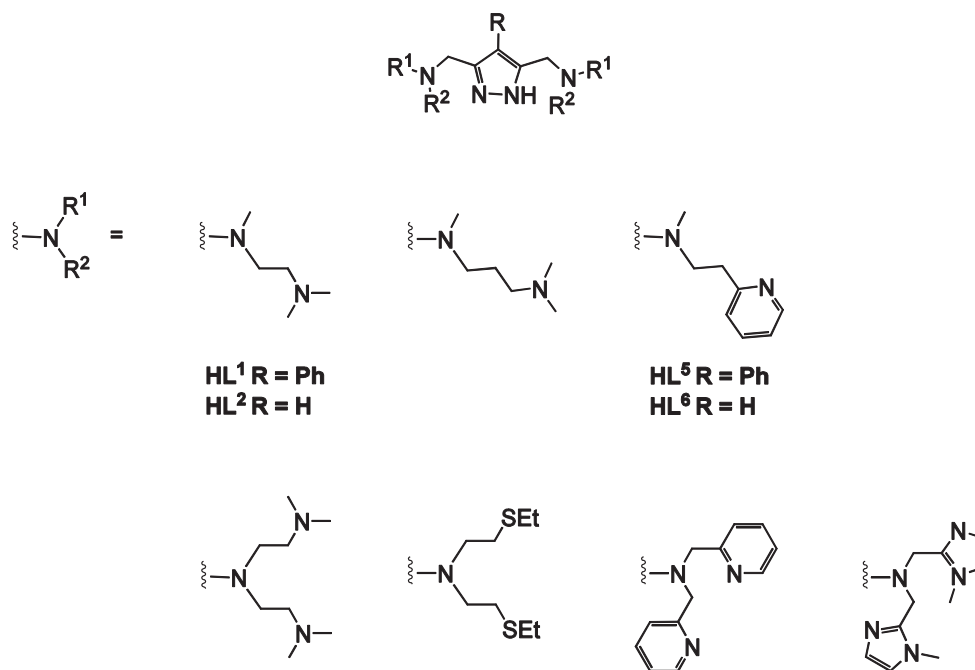


Figure 2.19: Selected pyrazolate based ligands designed by MEYER *et al.*.

The depicted ligand precursors differ in number and kind of donor atoms in the chelating sidearm and in the sidearm length. The length of the sidearm has a direct influence on the distance between the coordinated metal ions. The longer the sidechain the higher the ability to push the ions together leading to a shorter metal-metal distance.^[100] Hence it is possible to tune the distance between the metal ions in pyrazolate-bridged complexes in a range of 3.4 to 4.5 Å.^[100, 105-106]

Based on such pyrazolate ligands, various homonuclear bimetallic zinc,^[107] cobalt,^[108] nickel^[106] and copper^[103] complexes or organometallic compounds^[109] were synthesized. Employing zinc^[110] and copper^[111] salts tetranuclear complexes were observed, too. Some of these complexes have been investigated with respect to their ability to activate small molecules, and, indeed, the complexes show cooperative effects.^[106, 112]

The variety of the pyrazolate based ligand system is not limited to tertiary amines as sidearms. It is also possible to introduce imine functions to design a new ligand subclass that combines the properties of pyrazolate and imine systems (Figure 2.20).^[113] Bulky aryl substituents are employed to prevent the formation of grid complexes^[114-115] and unreactive L₂M₂-species.^[116-117] The designed ligation scaffold enforces a square planar or square pyramidal coordination sphere on the targeted metal ions. Binuclear nickel- and palladium-complexes based on this ligand type have been successfully investigated with respect to their catalytic activity in ethylene polymerization reactions.^[113]

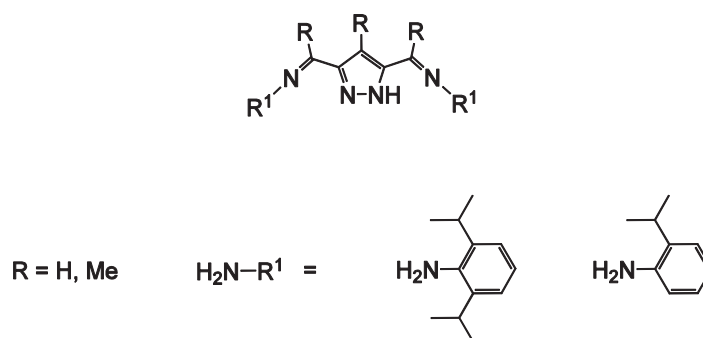


Figure 2.20: Pyrazolate based ligands with imine-sidearms.

The presented pyrazolate based ligand class represents a very flexible construction kit which can be perfectly tuned to the desired binding motif of various metal ions. The presented ligands have already been utilized to synthesize bioinspired copper complexes, i.e. complexes **XLI** and **XLII** (Figure 2.21).^[100, 111-112] **XLI** has been successfully applied in the oxidation of 3,5-di-*tert*-butylcatechol and **XLII** in the oxidative C-C coupling of 2,4,6-trimethylphenol.

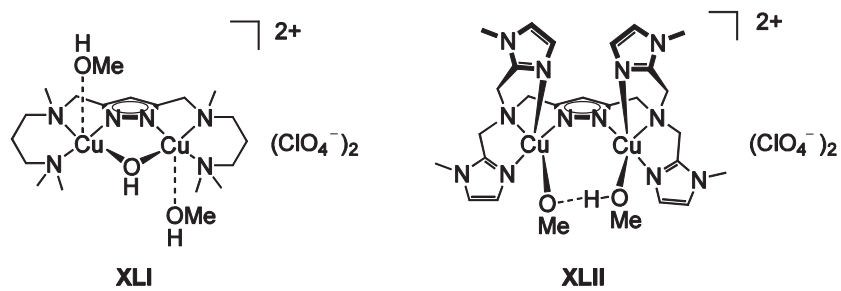


Figure 2.21: Bioinspired pyrazolate-based copper-complexes.



3. Objective

Building upon the established 3,5-disubstituted pyrazolate ligand platform, the objective of this work is to synthesize multinuclear copper complexes with a sulfur-rich environment.

Therefore, first of all several ligands were to be synthesized that bear only N-donor atoms in the chelating sidearms to mimic the biological nitrogen rich surrounding of the respective copper sites in enzymes. The sidechains of the ligands should be modified in the length of the alkyl chain, the number of donor atoms and the nature of the coordinating moiety (aromatic N-donor atoms and aliphatic N-donor atoms).

Since the reactivity of copper pyrazolate systems towards sulfur-containing ligands is not yet investigated, new approaches should be explored in order to obtain multinuclear copper sulfur compounds. Keeping in mind that the biological active sites of proteins usually contain N-donor and S-donor ligands, two different synthetic pathways were developed and explored.

One approach was to explore the reactivity of binuclear pyrazolate based copper halide complexes towards sulfur-transfer reagents in order to obtain copper sulfur complexes supported by N-donor ligands. Since binuclear copper halide complexes with pyrazolate-based ligands had not been described yet, these should be synthesized first. The synthesis should be performed with copper(I) halide and copper(II) halide salts. Furthermore, the resulting copper(II) halide complexes should be investigated with respect to the influence of structural parameters on the magnetic exchange of pyrazolate-based copper(II) complexes in order to gain further insight into this relationship.

In a complementary approach, copper containing building blocks which already feature a sulfur-rich environment should be utilized as starting material, and subsequently the pyrazolate ligand should be introduced. As starting material novel dithioether copper complexes and organothiolate complexes were to be utilized and thus had to be synthesized and characterized first. To obtain the desired copper(II) complexes which feature N-donor and S-donor ligands, the novel dithioether building blocks and the

commercially available copper(I) thiophenolate are reacted with the N-donor-rich pyrazolate ligands.

4. Results and discussion

4.1. Ligand synthesis

As already described in chapter 2.6, 3,5-disubstituted pyrazolate ligands were successfully applied to synthesize bioinspired binuclear metal complexes.^[100, 110, 112] The general architecture of this ligand class allows the broad variation of N-rich ligand precursors that emulate the protein surrounding of the targeted active site. The ligand precursors which were employed during this work are shown in Figure 4.1 below. **HL**¹⁻³, **HL**⁶ and **HL**⁹ have been reported previously.^[101, 105, 118-120]

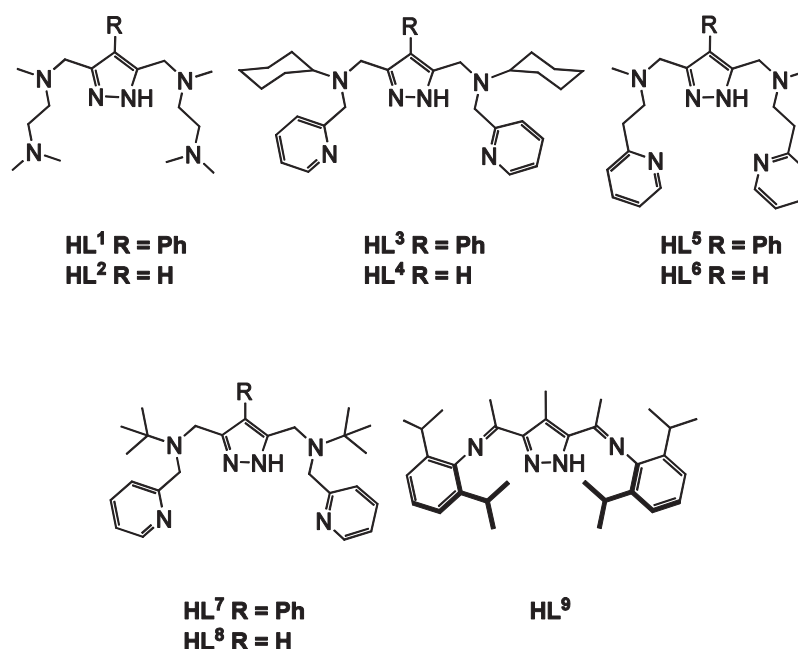


Figure 4.1: Pyrazole-based ligands **HL**¹ – **HL**⁹.

All ligand precursors have a central pyrazole unit with different sidearms at the 3 and 5 position and either a proton, a phenyl or a methyl substituent in the 4 position of the pyrazole. All ligands used here are symmetric, and except **HL**⁹ all of them feature two N-donors per sidearm to coordinate various metal ions. In the sidechain one CH₂-group is employed between the hinge amine function and the pyrazole unit.

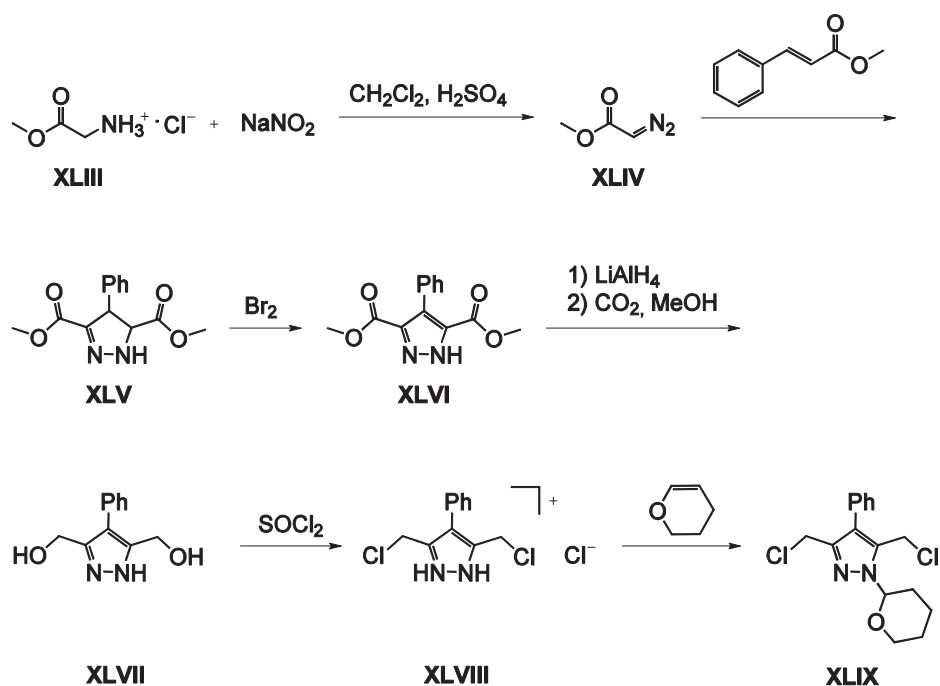
Considering the sidearms that are attached at 3- and 5-positions of the pyrazole unit different binding features are accessible. Regarding ligands **HL**¹ – **HL**⁸ all sidearms provide two nitrogen atoms as donor functions, which are either incorporated in an

aromatic (**HL**³⁻⁸) or an aliphatic (**HL**^{1,2}) scaffold. Taking the PEARSON concept into account the ligand precursors with aliphatic sidearms should be preferred by copper(II) ions and the aromatic sidearms are able to stabilize copper(I) ions.^[121] **HL**¹⁻⁴ and **HL**^{7,8} provide C₂-units between the amine functions at the sidearms whereas C₃-units are present in the ligand precursors **HL**⁵ and **HL**⁶. As already mentioned in chapter 2.6 this leads to a shorter metal-metal distance in the corresponding complexes.^[100] The variation of the residue at the amine function nearer to the pyrazole unit, i.e. *tert*-butyl, cyclohexyl or methyl groups, should increase the stability of the complexes as well as the crystallization ability.

HL⁹ provides only an imine-function in the sidearm. Thus [**L**⁹]⁺ was expected to be an appropriate ligand to coordinate copper(II) ions.

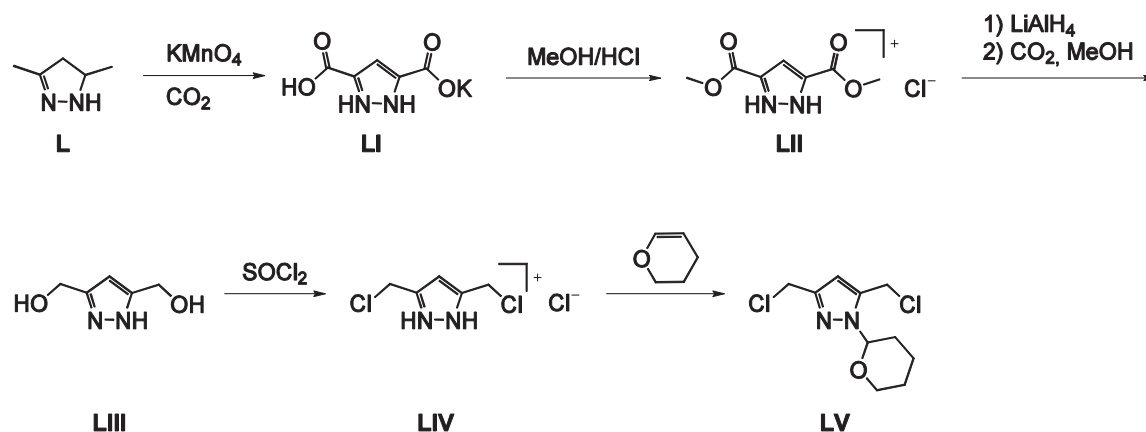
Synthesis of the central pyrazole building blocks

A six step synthesis was followed to obtain building block **XLIX**.^[119-120] Glycine methylester hydrochloride (**XLIII**) was treated with sodium nitrite in the presence of sulfuric acid to yield diazoacetic acid methylester (**XLIV**) as an orange oil. In the next step, **XLIV** was reacted with methylcinnamate to obtain the methyl ester of 4-phenylpyrazoline dicarboxic acid (**XLV**). **XLV** was first oxidized with bromine to get 4-phenyl-pyrazole dicarboxic acid methylester (**XLVI**), subsequently reduced with lithium aluminium hydride to obtain 3,5-bis(hydroxymethyl)-pyrazole (**XLVII**) and then chlorinated with thionyl chloride to yield 3,5-bis(chloromethyl)-4-phenyl-pyrazole (**XLVIII**). The last step of the synthesis, the protection of the NH-group of the pyrazole with 3,4-dihydro-2H-pyran (DHP), leads to the desired product 3,5-bis(chloromethyl)-4-phenyl-1-(tetrahydropyran-2-yl)-pyrazole (**XLIX**).



Scheme 4.1: Synthesis of 3,5-bis(chloromethyl)-4-phenyl-1-(tetrahydropyran-2-yl)-pyrazole (**XLIX**).

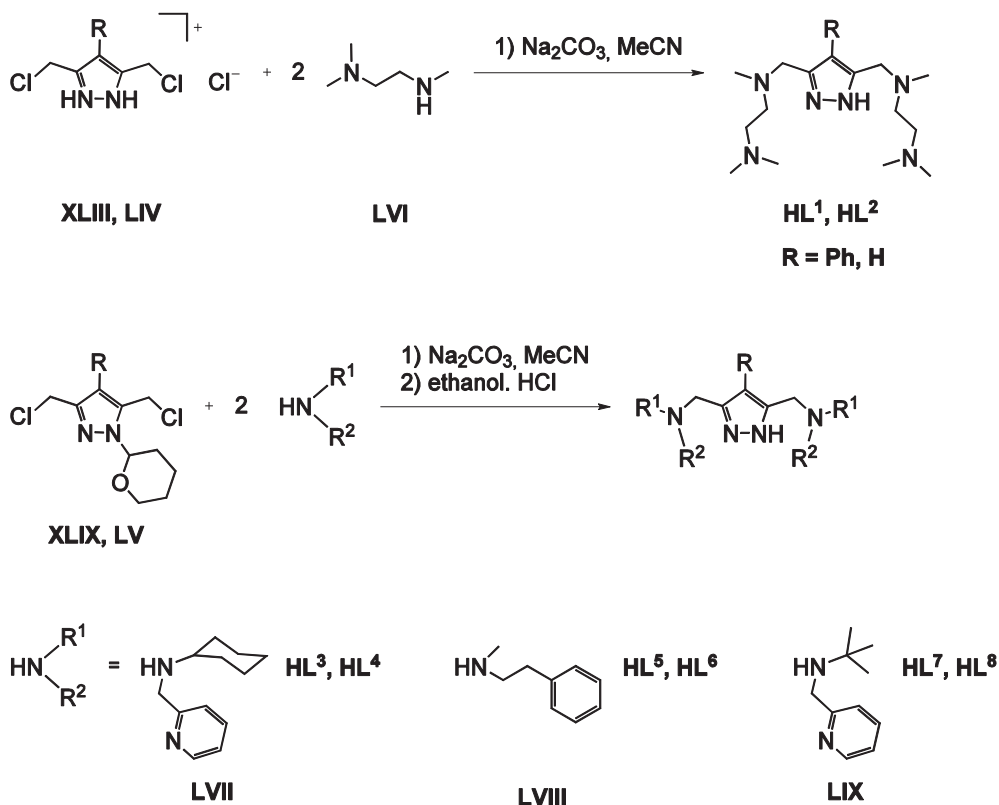
Building block **LV** was synthesized *via* a five step synthesis as reported previously in literature (Scheme 4.2).^[109, 122] 3,5-dimethyl-pyrazole (**L**) was oxidized with potassium permanganate to obtain the mono potassium salt of 3,5-pyrazole dicarboxonic acid (**LI**). The esterification was performed under acetic conditions in methanol leading to 3,5-pyrazole dicarboxonic acid methyl ester (**LII**). Subsequently **LII** was reduced with lithium aluminium hydride to get 3,5-bis(hydroxymethyl)-pyrazole (**LIII**) which was then chlorinated with thionyl chloride to yield 3,5-bis(chloromethyl)-pyrazole hydrochloride (**LIV**). The last step of the synthesis, the protection of the NH-group of the pyrazole with 3,4-dihydro-2H-pyran (DHP), leads to the desired product 3,5-bis(chloromethyl)-1-(tetrahydropyran-2-yl)-pyrazole (**LV**).



Scheme 4.2: 3,5-bis(chloromethyl)-1-(tetrahydropyran-2-yl)-pyrazole (LV).

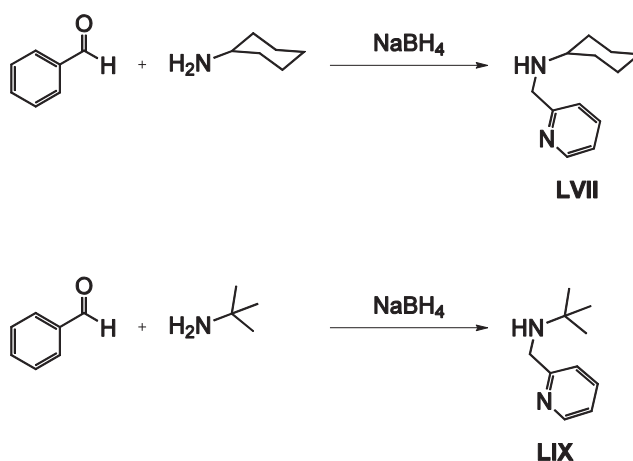
Synthesis of the ligand precursors $\text{HL}^1 - \text{HL}^8$

The final step in the synthesis of the desired ligand precursors was performed according to standard literature procedures (Scheme 4.3).^[123] Secondary amines were coupled with the pyrazole building block in the presence of sodium carbonate under standard conditions (acetonitrile, reflux) *via* nucleophilic substitution reactions. In the case of HL^1 and HL^2 3,5-bis(chloromethyl)-pyrazole (XLVIII, LIV) can be used directly. In order to get the ligands $\text{HL}^3 - \text{HL}^8$ the THP-protected derivatives (XLIX, LV) were employed to prevent a polymerization of the pyrazole building block.



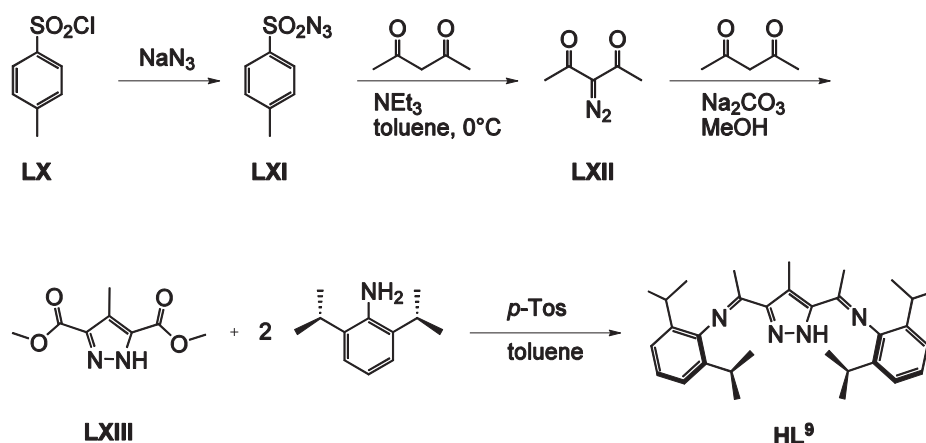
Scheme 4.3: Final step of the ligand synthesis.

Diamines **LVI** and **LVIII** (Scheme 4.3) are commercially available. *N*-(2-picolyl)cyclohexylamine (**LVII**) and *N*-(pyridin-2-ylmethyl)⁴butylamine (**LIX**) were synthesized by reductive amination of 2-pyridylcarboxaldehyde with either cyclohexylamine or *tert*-butylamine in the presence of NaBH₄ (Scheme 4.4) in order to obtain **LVII** and **LIX**, respectively.

Scheme 4.4: Synthesis of the sidearms **LVII** and **LIX**.

Synthesis of HL⁹

HL⁹ was synthesized *via* a different route.^[119] *para*-Toluene sulfonic acid chloride (**LX**) was treated with sodium azide to yield *para*-toluene sulfonic azide (**LXI**). Adding one equivalent of acetyl acetone under basic conditions results in the formation of compound **LXII**. The subsequent ring closure reaction is performed by adding a second equivalent of acetyl acetone yielding 3,5-bis(acetyl)-4-methylpyrazole (**LXIII**). Finally, **HL⁹** was obtained in a condensation reaction of **LXIII** with 2,6-diisopropyl-aniline.



Scheme 4.5: Synthesis of **HL⁹**.

4.2. Copper(II) halide complexes of the type LCu_2X_3 with ligands HL^1 – HL^4

4.2.1. Introduction

Recently the coordination chemistry of compartmental pyrazolate ligands towards transition metals has been reviewed.^[104] The formation of binuclear copper complexes that are coordinated by compartmental pyrazolate ligands is well known. Most of the discussed complexes bear the coordination motif $Cu_2(\mu\text{-pz})_2$ where two copper ions are bridged by two pyrazolato ligands.

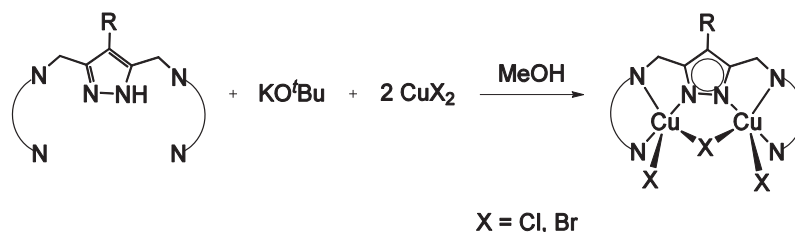
Copper complexes that feature only one pyrazole bridge and are additionally coordinated by an exogenous bridging ligand like chloride, bromide or azide, have been described

less frequently. Additionally, these complexes have been barely investigated with respect to their magnetic behavior.

In this chapter, the coordination chemistry of ligands $\text{HL}^1 - \text{HL}^4$ towards copper(II) halides is described and the magnetic interaction within the resulting complexes is determined and evaluated with respect to structural parameters. Halides are chosen since they are able to bridge two metal ions in close proximity and communicate magnetic interactions.^[124] Furthermore halide coligands are expected to undergo ligand exchange reactions. Therefore the resulting complexes might be utilized as starting material for the synthesis of copper sulfur complexes.

4.2.2. Synthesis and Structures

The general route for preparing complexes of the type $\text{L}^{1-4}\text{Cu}_2\text{X}_3$ ($\text{X} = \text{Cl}, \text{Br}$) is shown in Scheme 4.6. To obtain the desired complexes, the ligand is treated with 1 eq. potassium-*tert*-butanolate (KO^tBu) and 2 eq. of the corresponding copper(II) halide.



Scheme 4.6: General synthesis of binuclear copper halides.

In previous work complexes **1** and **2** were already successfully synthesized and fully characterized (Figure 4.2).^[118]

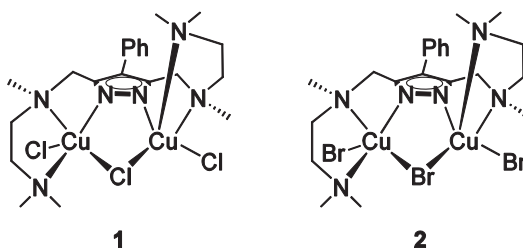


Figure 4.2: Complexes **1** and **2** that have been synthesized in previous work.

With the ligands $\mathbf{HL}^2 - \mathbf{HL}^4$ it was also possible to synthesize and fully characterize complexes with the constitution $\mathbf{L}^{2-4}\text{Cu}_2\text{X}_3$ ($\text{X} = \text{Cl}, \text{Br}$). The corresponding molecular structures of complexes **3** – **8** and the empirical formula are shown in Figure 4.3. The corresponding crystal system, the space group and selected structural parameters are summarized in Table 4.1. Selected interatomic distances and angles are summarized in the appendix in tables A.1 – A.6.

The metal ions in all complexes exhibit fivefold coordination sphere. The coordination polyhedron of five coordinate metal ions can either be described as square pyramidal or as trigonal bipyramidal. The degree of trigonality within the continuum of both geometries can be described by the geometric parameter τ .^[125] This parameter is defined by the following equation: $\tau = (\beta - \alpha)/60^\circ$, where β and α are the two largest bond angles at the metal ion and $\beta > \alpha$. This leads to a value of $\tau = (180^\circ - 120^\circ)/60^\circ = 1$ for the perfectly trigonal bipyramidal geometry and to $\tau = (180^\circ - 180^\circ)/60^\circ = 0$ for the perfectly square pyramidal geometry. The corresponding τ -values for all copper complexes have been determined and are included in Table 4.1. All copper atoms are found in a distorted square pyramidal coordination sphere (τ in the range of 0.07 – 0.23).

In all cases the copper ions are coordinated in the basal plane by one pyrazole nitrogen atom (N1 for Cu1 and N2 for Cu2), the nitrogen atom which is next to the central pyrazolato unit (N3 and N5, respectively), and two halide anions, the bridging halide ion X1 and one terminal halide anion (X2 in case of Cu1 and X3 in case of Cu2). The axial position is occupied in all complexes by the remaining peripheral nitrogen atom of the sidechain of the ligand (N4 in the case of Cu1 and N6 in the case of Cu2).

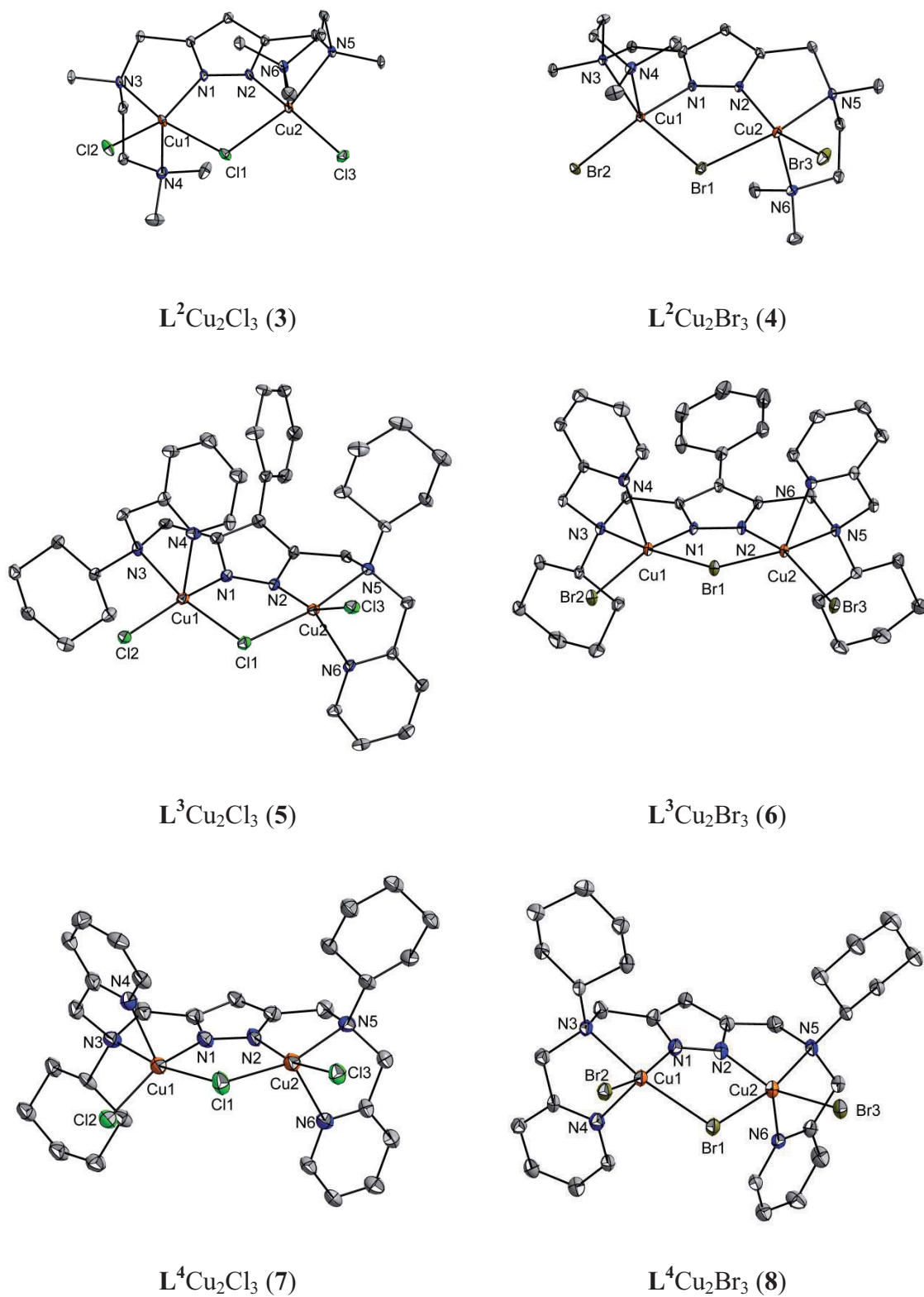


Figure 4.3: Molecular structures of 3 - 8. ADPs: 30% probability thermal ellipsoids, hydrogen atoms are omitted for clarity.

Table 4.1: Selected structural parameters for compounds **1 – 8**. Distances are given in [Å] and angles in [°].

compound	crystal system	space group	Z	$d(\text{Cu1-Cu2})$	$\tau(\text{Cu1})$	$\tau(\text{Cu2})$	$d(\text{Cu-}\mu\text{-X1})$	$\angle(\text{Cu1-X1-Cu2})$
1	monoclinic	<i>Cc</i>	4	3.7706(5)	0.35	0.17	2.3928(8), 2.3821(8)	104.31(3)
2	monoclinic	<i>Cc</i>	4	3.859(1)	0.40	0.22	2.5080(11), 2.4988(11)	100.84(4)
3	monoclinic	<i>P2₁/c</i>	4	3.7927(13)	0.15	0.10	2.3912(9); 2.3812(9)	105.23(3)
4	monoclinic	<i>P2₁/c</i>	4	3.8766(2)	0.11	0.21	2.4996(9), 2.5168(10)	101.21(3)
5	monoclinic	<i>P2₁/c</i>	4	3.6894(6)	0.09	0.23	2.2071(19); 2.3513(19)	103.43(7)
6	triclinic	<i>P$\bar{1}$</i>	2	3.8258(6)	0.14	0.21	2.4652(5); 2.4884(5)	101.125(18)
7	triclinic	<i>P$\bar{1}$</i>	2	3.7734(14)	0.13	0.07	2.3444(19); 2.330(2)	107.66(8)
8	triclinic	<i>P$\bar{1}$</i>	2	3.8718(18)	0.13	0.17	2.4947(15); 2.5319(15)	100.75(5)

There are two possible isomers for **1** - **8**, which differ in the coordination of the axial nitrogen donors. The sidechains can either coordinate both from the same side (*cis*-configuration) or from opposite sides (*trans*-configuration, see Figure 4.4).

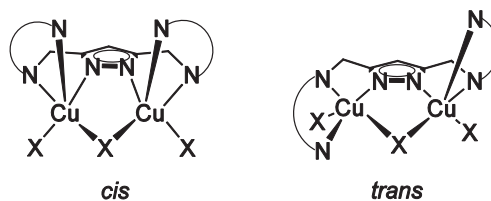


Figure 4.4: Schematic picture of the *cis*- and *trans*-configuration in complexes **1** – **8**.

Comparing the coordination pattern of the complexes **1** - **8**, only complexes **6** and **8** feature the *cis*-configuration (Figure 4.4). **6** and **8** contain the ligand $[L^3]^-$ and $[L^4]^-$, respectively. The reason for the different coordination mode might be the steric demand of the cyclohexyl group in the sidearm of the ligand, though the *trans*-configuration is formed in **5** and **7**.

Since copper(II) ions feature one unpaired electron ($S = \frac{1}{2}$), all complexes have been investigated by SQUID measurements.

4.2.3. Magnetic Properties

Magnetic susceptibility measurements were carried out on complexes **2** – **8** at a magnetic field of 5000 Oe and at 2000 Oe for complex **1**. The temperature dependence of the product $\chi_M T$ is shown in Figure 4.5 for all eight complexes. Experimental data were modelled by using a fitting procedure to the appropriate Heisenberg-Dirac-van-Vleck (HDvV) spin Hamiltonian for isotropic exchange coupling and Zeeman splitting, equation (1).

$$\hat{H} = -2J\hat{S}_1 \cdot \hat{S}_2 + g\mu_B(\hat{S}_1 + \hat{S}_2)B \quad (1)$$

Temperature-independent paramagnetism (*TIP*) and a Curie-behaved paramagnetic impurity (*PI*) with spin $S = \frac{1}{2}$ were included according to $\chi_{\text{calc}} = (1 - PI) \cdot \chi + PI \cdot \chi_{\text{mono}} + TIP$. The calculated curve fits are shown as solid line.

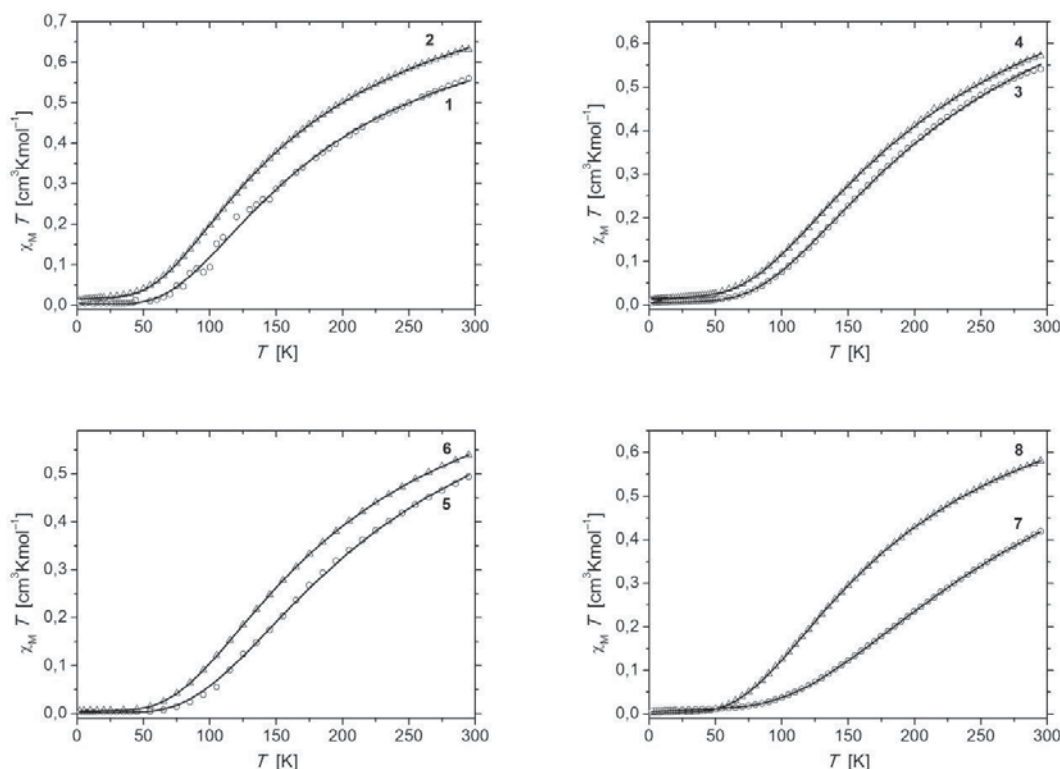


Figure 4.5: Plots of $\chi_M T$ vs. T for complexes **1** – **8**.

In all complexes $\chi_M T$ decreases and finally trends to zero when lowering the temperature, indicating antiferromagnetic coupling. The best fit parameters for the $L^{1-4}Cu_2Cl_3$ complexes **1**, **3**, **5** and **7** are summarized in Table 4.2 and for the L^{1-4} bridged complexes **2**, **4**, **6** and **8** in Table 4.3.

Table 4.2: Best fit parameters of magnetic data analyses for complexes **1**, **3**, **5** and **7**.

	1	3	5	7
g	2.11	2.19	2.16	2.10
J [cm^{-1}]	-113	-137	-142	-177
PI [%]	1.0	1.3	0.8	1.7
$TIP/10^{-6}$ [$cm^3 \cdot mol^{-1}$]	180	100	0	120

Magnetic properties of transition metal complexes are mainly explained by the orbital interactions.^[126-128] Antiferromagnetic systems require magnetic orbitals which feature the same symmetry and are able to overlap with each other. This overlap is usually not

observed directly, but can be communicated by suitable bridging ligands like pyrazolate, azide, hydroxide, halide or cyanide *via* superexchange.^[114, 129-130]

Table 4.3: Best fit parameters of magnetic data analyses for complexes **2**, **4**, **6** and **8**.

	2	4	6	8
g	2.07	2.09	2.09	2.09
J [cm ⁻¹]	-97	-124	-119	-114
PI [%]	4.0	3.3	1.5	0.2
$TIP/10^{-6} \cdot [\text{cm}^3 \cdot \text{mol}^{-1}]$	220	220	50	130

Usually four structure factors are discussed to have a main influence on the overlap of the orbitals and therefore the magnetic interaction in pyrazolato- and halide-bridged complexes. These are the τ -parameter, the angle Cu-X-Cu (X = Cl, Br) unit, the torsion angle Cu1-N1-N2-Cu2 and the angle α between the basal planes of the copper ions.

As already described before, the τ -parameter is an indicator for the geometry of the coordination polyhedron around the fivefold coordinated copper ions. The coordination polyhedra of complex **7** are depicted in Figure 4.6 left. The influence of the distortion of the copper(II) coordination geometry between square pyramidal ($\tau = 0$) and trigonal bipyramidal ($\tau = 1$) on the magnetic coupling constant in binuclear pyrazolate-bridged copper complexes has been described by MATSUSHIMA *et al.*^[131] The magnetic interaction is expected to increase when the geometry approaches square pyramidal, and, indeed, MATSUSHIMA *et al.* observed an increasing coupling with a decreasing τ -value.

The influence of the angle α at the bridging atom X at a Cu-X-Cu motif was described for the first time by CRAWFORD *et al.*^[132] They investigated binuclear μ -hydroxo copper(II) complexes. It turned out that the magnitude and nature of the interaction in Cu(μ -OH)₂Cu complexes depends on the Cu-O-Cu angle α (for $\alpha > 97.5^\circ$ the coupling is antiferromagnetic and becomes stronger as the α value increases) or the copper-copper distance. Therefore the magnetic interaction is expected to increase with an increasing α -value in binuclear copper complexes.

The degree of distortion of the CuNNCu unit is determined by the torsion angle and the two CuNN angles, respectively. All these angles have to be low for a small distortion. HANOT *et al.* stated that J decreases significantly with increasing distortion.^[133] Here only the torsion angle of the complexes will be discussed.

Since the magnetic orbital of copper(II) ions in a square-pyramidal environment is the $d_{x^2-y^2}$ orbital, the magnetic exchange depends on the angle between the basal planes (β). The exchange constant J should increase if the magnetic orbitals are coplanar, i. e. with a smaller angle.^[134] The corresponding planes in the case of **7** are visualized in Figure 4.6, right.

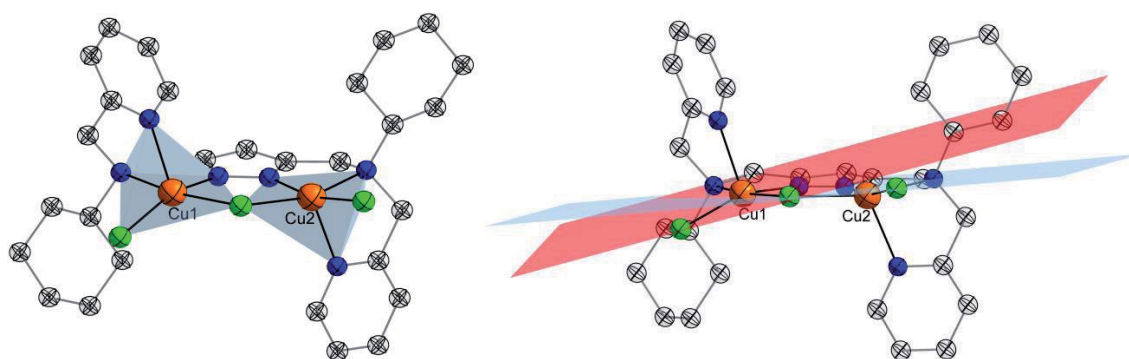


Figure 4.6: left: coordination polyhedra of the copper ions in the case of complex **7**. Right: visualization of the planes spanned by the basal atoms of the copper coordination sphere in complex **7**. Hydrogen atoms are omitted for clarity.

The angles and the sum of the two τ -values of each complex are summarized for the copper chloride complexes in Table 4.4 and for the bromide complexes in Table 4.5. The requirements for strong antiferromagnetic coupling are a small τ -value, a small torsion angle, a large angle Cu1-X1-Cu2 and a small β .

Table 4.4: Selected geometric parameters for complexes **1**, **3**, **5** and **7**.

	1	3	5	7
τ -values ($\tau_1 + \tau_2$)	0.52	0.25	0.32	0.19
α_{tors} (Cu1-N1-N2-Cu2)	16.94	19.81	15.22	0.48
α Cu1-Cl1-Cu2	104.3	105.2	103.5	107.6
$\beta = \alpha$ between basal planes of the copper ions	28.74	19.90	34.94	15.02
J [cm^{-1}]	-113	-137	-142	-177

Table 4.5: Selected geometric parameters for complexes **2**, **4**, **6** and **8**.

	2	4	6	8
τ -values ($\tau_1 + \tau_2$)	0.62	0.32	0.35	0.3
α_{tors} (Cu1-N1-N2-Cu2)	17.55	20.09	4.84	0.40
α Cu1-Br1-Cu2	100.8	101.2	101.1	100.8
$\beta = \alpha$ between basal planes of the copper ions	28.18	20.09	32.18	32.98
J [cm^{-1}]	-96.5	-124	-119	-114

Comparing the J -values of the chloride complexes with those of the bromide complexes of the same ligand, the data show that the $\text{L}^{1-4}\text{Cu}_2\text{Cl}_3$ complexes exhibit a stronger antiferromagnetic interaction than the corresponding $\text{L}^{1-4}\text{Cu}_2\text{Br}_3$ complexes.

$$\mathbf{1} (J = -113 \text{ cm}^{-1}) > \mathbf{2} (J = -97 \text{ cm}^{-1})$$

$$\mathbf{3} (J = -137 \text{ cm}^{-1}) > \mathbf{4} (J = -124 \text{ cm}^{-1})$$

$$\mathbf{5} (J = -142 \text{ cm}^{-1}) > \mathbf{6} (J = -119 \text{ cm}^{-1})$$

$$\mathbf{7} (J = -177 \text{ cm}^{-1}) > \mathbf{8} (J = -114 \text{ cm}^{-1})$$

The Cu-X-Cu-angle in the $\text{L}^{1-4}\text{Cu}_2\text{Br}_3$ complexes is found in the range $100.8^\circ - 101.2^\circ$ while in the $\text{L}^{1-4}\text{Cu}_2\text{Cl}_3$ complexes it is in the range $103.5^\circ - 107.6^\circ$ and, indeed, the coupling constant seems to increase with an increasing angle.

Having a closer look at the four chloride complexes now, the coupling constants can be ranked as follows:

$$J(1) < J(3) \approx J(5) < J(7)$$

This observation is consistent with the expected trend of the τ -values:

$$\tau(1) > \tau(3) \approx \tau(5) > \tau(7)$$

Concerning the torsion angle, the angle Cu1-C11-Cu2 and the angle β between the basal planes the expected trend is perturbed by the values for complex **3** in case of the torsion angle and by the values for **5** in case of the angle between the atoms Cu1, C11 and Cu2 and β .

$$\alpha_{\text{tors}}(3) > \alpha_{\text{tors}}(1) > \alpha_{\text{tors}}(5) > \alpha_{\text{tors}}(7)$$

$$\alpha(\text{Cu1-C11-Cu2})(5) < \alpha(\text{Cu1-C11-Cu2})(1) < \alpha(\text{Cu1-C11-Cu2})(3) < \alpha(\text{Cu1-C11-Cu2})(7)$$

$$\beta(5) > \beta(1) \approx \beta(3) > \beta(7)$$

Deviation from the expected trend of the structural parameters indicates that the discussed factors are able to partially compensate each other. Therefore it is possible that some parameters do not follow the usual trend in some cases.

The $\text{L}^{1-4}\text{Cu}_2\text{Br}_3$ complexes show a different behavior compared to the $\text{L}^{1-4}\text{Cu}_2\text{Cl}_3$ complexes and a trend of the J -values is not apparent since it is influenced by various structural parameters. The coupling constants in this case can be ranked as follows:

$$J(2) < J(8) \approx J(6) \approx J(4)$$

This can be correlated with the τ -value and the angle Cu1-Br1-Cu2:

$$\tau(2) > \tau(6) \approx \tau(4) \approx \tau(8)$$

$$\alpha(\text{Cu1-Br1-Cu2})(2) = \alpha(\text{Cu1-Br1-Cu2})(8) < \alpha(\text{Cu1-Br1-Cu2})(6) < \alpha(\text{Cu1-Br1-Cu2})(4)$$

The trend of the torsion angle of the pyrazole unit is perturbed by complex **6** in case of the torsion angle and the expected trend of β by the value for complex **2**.

$$\alpha_{\text{tors}}(4) > \alpha_{\text{tors}}(2) > \alpha_{\text{tors}}(6) > \alpha_{\text{tors}}(8)$$

$$\beta(8) \approx \beta(6) > \beta(2) > \beta(4)$$

The observed trend of the τ -value and the angle between the atoms Cu1, Br1 and Cu2 can be correlated to the trend of the J -value. The deviation of the trend of the torsion angle by **6** and of β by **2** confirms the previous assumption that some structural parameters are able to compensate each other.

4.2.4. DFT calculations

To gain more insight into the identity and shape of the magnetic orbitals, theoretical calculations have been carried out.^[135] To have a system that is as near to the structural data as possible, only the hydrogen atoms have been optimized in the first step. For the optimization run the functional BP with the basis set SVP^[136] was utilized in the triplet state of the molecule. The RI method was employed during the optimization run to shorten the calculation time.^[137]

For the magnetic coupling information the broken symmetry solution was calculated with the hybrid functional B3LYP^[138-139] and the basis set TZVP^[140] for all atoms. B3LYP was chosen because previous DFT investigations on binuclear systems carried out that this hybrid functional provided good quantitative results for coupling constants.^[141]

The J -value has been calculated according to the following equation:

$$J = -\frac{E_{HS} - E_{BS}}{S_{max}(S_{max} + 1)} \quad (2)$$

In equation (2) J stands for the calculated magnetic coupling constant, E_{HS} and E_{BS} for the energy values calculated for the high spin state and the broken symmetry solution and S_{max} for the maximum spin of the system. Equation (2) can be employed when the overlap of the magnetic orbitals is sufficiently large,^[142] as in the complexes **1** – **8**. The equation was already employed previously to provide good results in the calculation of magnetic interactions of binuclear copper complexes.^[143-144] The calculated J -values and the experimental J -values are summarized in Table 4.6 for $L^{1-4}Cu_2Cl_3$ and in Table 4.7 for $L^{1-4}Cu_2Br_3$.

Table 4.6: Calculated and experimental J -values [cm^{-1}] for complexes **1**, **3**, **5** and **7**.

	1	3	5	7
$J_{\text{calc}} [\text{cm}^{-1}]$	-107	-126	-103	-144
$J_{\text{exp}} [\text{cm}^{-1}]$	-112	-137	-142	-177

Table 4.7: Calculated and experimental J -values [cm^{-1}] for complexes **2**, **4**, **6** and **8**.

	2	4	6	8
$J_{\text{calc}} [\text{cm}^{-1}]$	-99	-132	-114	-107
$J_{\text{exp}} [\text{cm}^{-1}]$	-96	-124	-119	-114

A comparison of both values reveals a good match for $\text{L}^{1-4}\text{Cu}_2\text{Br}_3$. The values of the chloro complexes **5** and **7** are too low, while the ones for **1** and **3** match experimental values well. Since the chosen model fits for six out of eight values quantitatively, it is assumed that the model is suitable for further discussion.

The calculated and experimental J -values can be ranked as follows:

$$J_{\text{exp}}(\mathbf{1}) < J_{\text{exp}}(\mathbf{3}) < J_{\text{exp}}(\mathbf{5}) < J_{\text{exp}}(\mathbf{7})$$

$$J_{\text{calc}}(\mathbf{5}) < J_{\text{calc}}(\mathbf{1}) < J_{\text{calc}}(\mathbf{3}) < J_{\text{calc}}(\mathbf{7})$$

$$J_{\text{exp}}(\mathbf{2}) < J_{\text{exp}}(\mathbf{8}) < J_{\text{exp}}(\mathbf{6}) < J_{\text{exp}}(\mathbf{4})$$

$$J_{\text{calc}}(\mathbf{2}) < J_{\text{calc}}(\mathbf{8}) < J_{\text{calc}}(\mathbf{6}) < J_{\text{calc}}(\mathbf{4})$$

The strong antiferromagnetic coupling can be specified by further investigations by observing the orbitals involved. The corresponding SOMOs (Single Occupied Molecular Orbital) of complex **1** are depicted in Figure 4.7. The SOMOs of complexes **2** – **7** are similar and are depicted in the appendix in Figures A.1, A.4, A.7, A.10, A.13, A.16 and A.19.

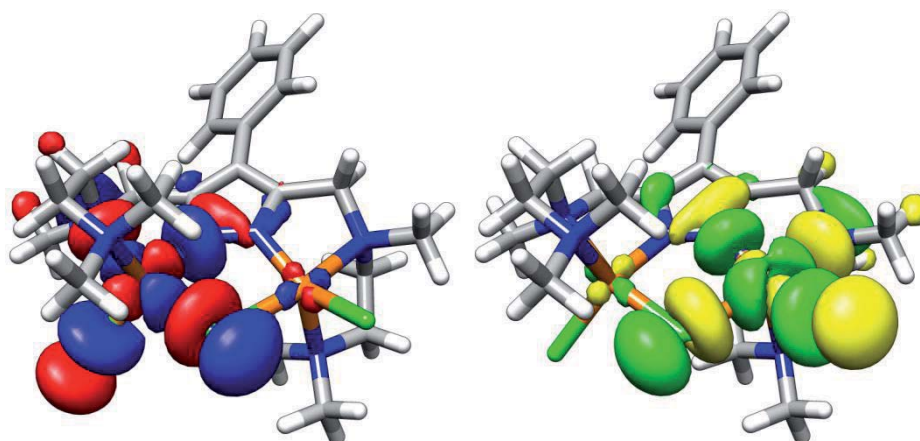


Figure 4.7: SOMOs of complex **1** (0.02 a.u. level), left: spin up orbital (alpha), right: spin-down orbital (beta). The blue and green colored parts represent the positive part of the wave function, the red and yellow colored parts represent the negative part of the wave function.

Visualization of the SOMOs confirms the previous assumption that the unpaired electrons are localized in the two metal-centered $d_{x^2-y^2}$ -orbitals. Both orbitals have the same symmetry.

The overlap of the two orbitals is depicted in Figure 4.8. Both bridging units – the chloride anion and the pyrazolate unit - feature parts of the two SOMOs thus both contribute to the strong magnetic interaction. The same is true for complexes **2** – **8**. The corresponding pictures are shown in the appendix in Figures A.2, A.5, A.8, A.11, A.14, A.17 and A.20.

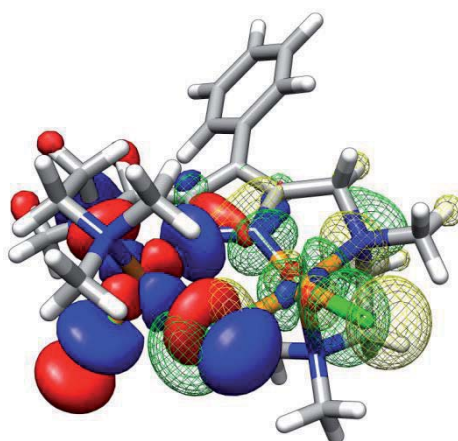


Figure 4.8: Magnetic molecular orbitals of complex **1** (0.02 a.u. level). Solid: spin up part, dashed: spin-down part.

The contribution of both bridging units is confirmed by the spin density distribution of the complexes. As an example, the plot for **1** is depicted in Figure 4.9, the ones for the other complexes can be found in appendix A in Figures A.3, A.6, A.9, A.12, A.15, A.18 and A.21. The spin density is spread over the metal ion and the corresponding coordinating donor atoms. Therefore it confirms the results of the first calculation that both bridging moieties are responsible for the magnetic interaction.

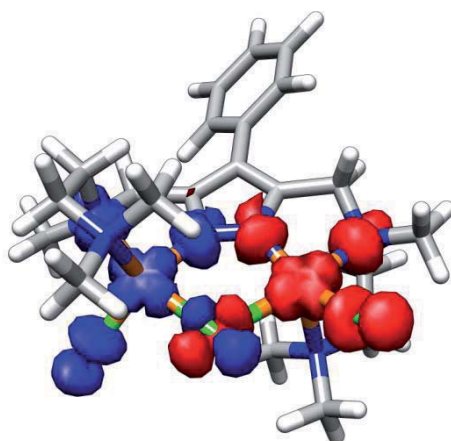


Figure 4.9: Spin density plot of complex **1** (0.002 a.u. level), blue: spin-up part, red: spin-down part.

4.2.5. Summary

It was possible to synthesize and fully characterize six different complexes with the binding motif $L^{2-4}Cu_2X_3$ ($X = Cl, Br$).

Magnetic interactions in these complexes $L^{2-4}Cu_2X_3$ (**3 - 8**) have been examined *via* SQUID measurements and compared with the previously synthesized complexes **1** and **2**. Analyses of the experimental data revealed strong antiferromagnetic coupling for all complexes. It is shown, that the magnetic interactions cannot be correlated to only one particular structural parameter but depend on multiple factors.

Furthermore the identity of the SOMOs and the spin density distribution were examined by DFT methods. The employed methods represent a good model for the present

complexes. This investigation showed that the coupling is communicated by both bridging units, the chloride and the pyrazole.

4.3. Copper(II) halide complexes with ligand HL⁹

4.3.1. Introduction

A particular subclass of compartmental pyrazolate-based ligands feature imine groups with bulky aryl substituents in the sidechains.^[119] The coordination chemistry of this ligand class towards several late transition metal ions like palladium(II), nickel(II) or cobalt(II) has been already studied and reported.^[113, 145-147] The corresponding ligands are depicted in Figure 4.10.

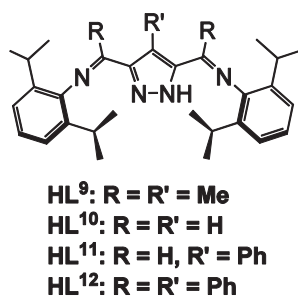
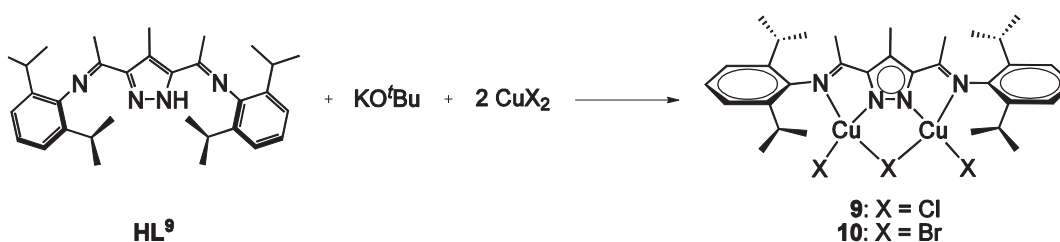


Figure 4.10: Pyrazolate-based ligands with imine substituents in the sidechain.

While the reaction of the protonated potential ligand with base and palladium(II) chloride leads to the compounds $L^{9-12}Pd_2Cl_3$,^[113, 145] the reaction with nickel(II) bromide results in aggregates of the type $L^9Ni_4Br_6$,^[145] $L^{10}Ni_4Cl_6$,^[148] and $L^{10}Ni_6Br_9$.^[113] Using cobalt(II) chloride the resulting complex depends on the substituents in the backbone of the ligand: Binuclear ($L^9Co_2Cl_3$) and tetranuclear species ($L^{11,12}Co_4Cl_6$) were obtained.^[146] The reactivity of $[L^9]^-$ towards copper halides has not been investigated yet. The synthesis of these complexes is of high interest since tetranuclear copper(II) complexes might be obtained. These complexes could be utilized in ligand exchange reactions with sulfur transfer reagents in order to pave the access to a Cu_4S motif.

4.3.2. Synthesis and Structures

In order to obtain copper(II) halide complexes with the ligand $[L^9]^-$ the ligand precursor **HL**⁹ was deprotonated in THF with one equivalent of KO^tBu, and subsequently, two equivalents of the corresponding copper(II) halide were added. After workup, in both experiments complexes of the type $L^9Cu_2X_3$ (X = Cl, Br) (Scheme 4.7) could be isolated and fully characterized. Pentane diffusion into solutions of the complexes in DCM yielded crystals of **9** and **10**, respectively, which were suitable for X-ray analysis.



Scheme 4.7: Synthetic route to complexes **9** and **10**.

Both complexes **9** and **10** crystallize in the space group *Pbca* with eight molecules per unit cell. As depicted in Figure 4.11, each copper ion is coordinated by two nitrogen atoms of the ligand, one terminal halide and one bridging halide ion.

The copper ions are set in a nearly ideal square-planar coordination sphere. The sum of the angles between the *cis* donor atoms of the copper ions in **9** is 360.08 ° (Cu1) and 359.98 ° (Cu2). In **10** the values have been determined to 359.99 ° (Cu1) atom and 359.97 ° (Cu2). The deviation from the ideal angle of 360 ° is therefore insignificant. The separation of the copper ions was determined to be 3.79 Å in **9** and 3.86 Å in **10**, respectively. Selected bond lengths and angles are summarized in Table 4.8 for complex **9** and in Table 4.9 for complex **10**.

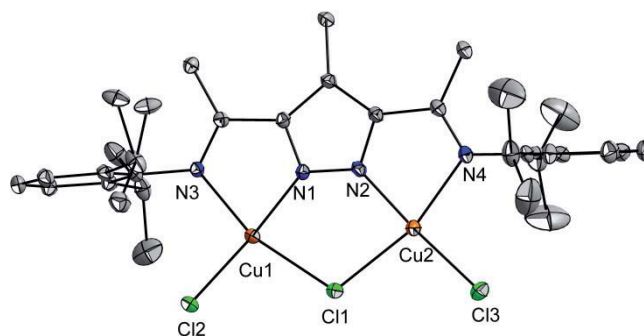
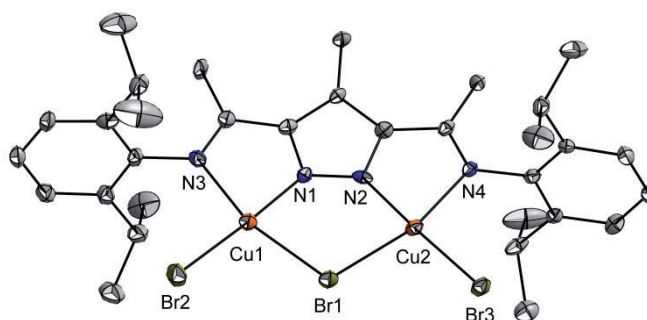
 $L^9Cu_2Cl_3$ (9) $L^9Cu_2Br_3$ (10)

Figure 4.11: Molecular structures of **9** and **10**. ADPs: 30% probability thermal ellipsoids, hydrogen atoms are omitted for clarity.

Table 4.8: Selected interatomic distances [\AA] and angles [$^\circ$] for **9**.

distances			
Cu1-N1	1.901(2)	Cu2-N2	1.898(3)
Cu1-N3	2.079(2)	Cu2-N4	2.110(2)
Cu1-Cl1	2.3476(9)	Cu2-Cl1	2.3444(9)
Cu1-Cl2	2.1590(8)	Cu2-Cl3	2.1565(10)
Cu1-Cu2	3.7879(7)		
angles			
N1-Cu1-N3	77.95(9)	N2-Cu2-N4	77.46(10)
N1-Cu1-Cl1	85.55(7)	N2-Cu2-Cl1	85.80(7)
N1-Cu1-Cl2	175.60(8)	N2-Cu2-Cl3	176.23(8)
N3-Cu1-Cl1	163.23(6)	N4-Cu2-Cl1	163.05(7)
N3-Cu1-Cl2	98.02(7)	N4-Cu2-Cl3	98.81(8)
Cl1-Cu1-Cl2	98.56(3)	Cl1-Cu2-Cl3	97.91(4)
Cu1-Cl1-Cu2	107.67(3)		

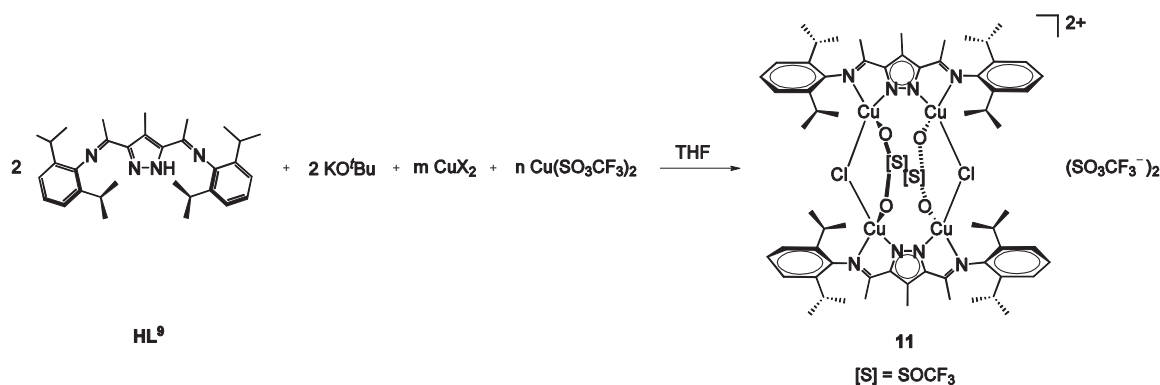
The experiments showed that the reaction of one equivalent of the potential ligand with two equivalents of the corresponding metal salt yields only binuclear complexes, whereas with cobalt(II) halide salts and nickel(II) halide salts oligonuclear complexes were formed.^[145-146]

Table 4.9: Selected interatomic distances [Å] and angles [°] for **10**.

distances			
Cu1-N1	1.901(7)	Cu2-N2	1.897(6)
Cu1-N3	2.095(6)	Cu2-N4	2.057(7)
Cu1-Br1	2.4563(13)	Cu2-Br1	2.4588(15)
Cu1-Br2	2.3014(16)	Cu2-Br3	2.2975(13)
Cu1-Cu2	3.8636(16)		
angles			
N1-Cu1-N3	77.9(3)	N2-Cu2-N4	78.3(3)
N1-Cu1-Br1	86.75(19)	N2-Cu2-Br1	86.4(2)
N1-Cu1-Br2	177.2(2)	N2-Cu2-Br3	177.1(2)
N3-Cu1-Br1	164.5(2)	N4-Cu2-Br1	164.66(18)
N3-Cu1-Br2	99.5(2)	N4-Cu2-Br3	98.82(19)
Br1-Cu1-Br2	95.84(5)	Br1-Cu2-Br3	96.45(5)
Cu1-Br1-Cu2	103.64(5)		

In order to obtain copper(II) complexes that exhibit higher nuclearities than two, the ligand to chloride ratio was lowered while maintaining the ligand to metal ratio. Therefore reactions with different ratios of [**L**⁹]⁻, copper(II) chloride and copper(II) triflate were explored.

According to Scheme 4.8, the ligand was first deprotonated and subsequently the corresponding amounts of copper(II) chloride and copper(II) triflate were added. The employed ratios are shown in Table 4.10. All reactions yielded to the same product, namely a tetranuclear Cu₄(μ-Cl)₂(μ-SO₃CF₃)₂(μ-pz)₂ species. All reactions yielded crystals *via* pentane diffusion into a complex solution in acetone; these were crystallographically characterized.

Scheme 4.8: Synthesis of complex **11**.Table 4.10: Equivalents which were employed in the synthesis of compound **11**.

Experiment No	m	N
1	1 equivalent	3 equivalents
2	1.5 equivalents	2.5 equivalents
3	2 equivalents	2 equivalents

Complex **11** crystallizes in the triclinic space group $P\bar{1}$ with four molecules per unit cell. Since the molecule is highly symmetric, only one half molecule is found in the asymmetric unit. The cation of the resulting tetranuclear complex is shown in Figure 4.12. Each copper ion is coordinated by two nitrogen atoms of one ligand. The two resulting L^9Cu_2 -units are bridged by two chloride atoms that are located on the short edges of the Cu_4 arrangement.

The inner sphere of the complex is mostly occupied by two strongly disordered triflate molecules. The disorder of the triflate anions affects at least two positions of the triflate itself. Additionally it is possible that a third position of the disorder is occupied with a chloride anion instead of a triflate anion. Hence, it was not possible to exactly refine the structure. Therefore the shown picture represents an educated guess and the interatomic distances and angles are not further discussed.

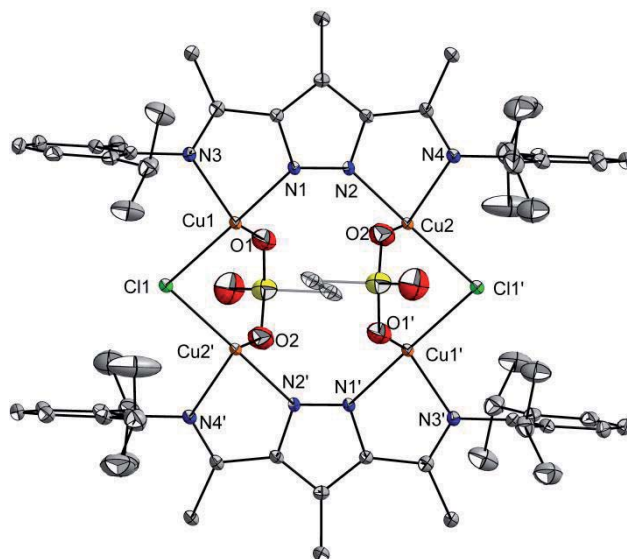
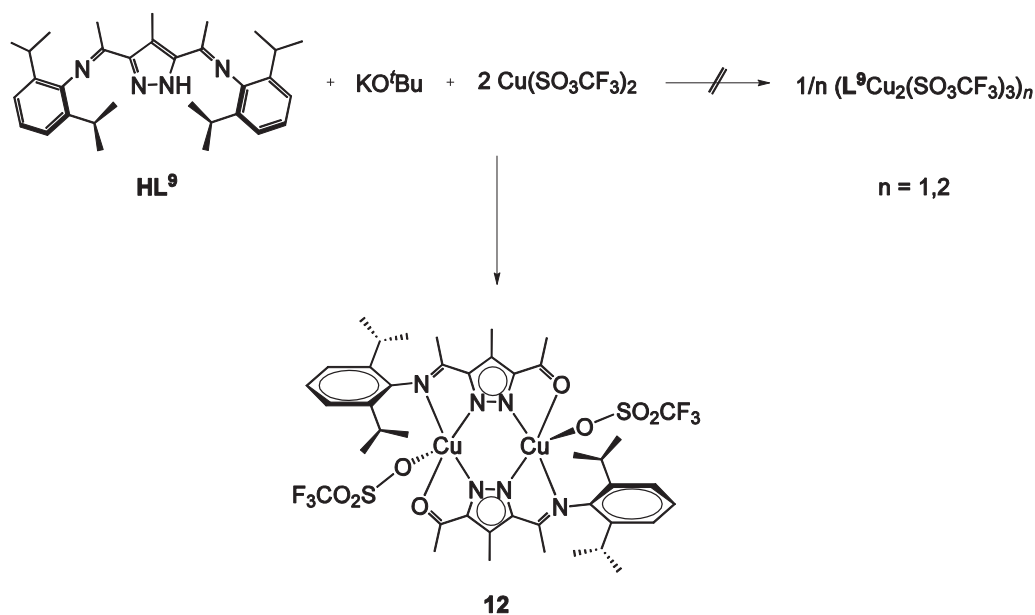


Figure 4.12: Educated guess of the structure of the cation of compound **11**. ADPs: 30% probability thermal ellipsoids. Hydrogen atoms, counterions and the CF₃-group of the coordinating triflate anion are omitted for clarity. Symmetry operation used to generate equivalent atoms (*): -x, -y, -z.

To gain further insight into the binding mode of the triflate anion to the $[\mathbf{L}^9\text{Cu}_2]_n^{3+}$ moiety ($n = 2$) in **11** the reaction of \mathbf{HL}^9 with KO^tBu and two equivalents of anhydrous copper(II) triflate was investigated in order to obtain di- or tetranuclear copper complexes with the composition $[\mathbf{L}^9\text{Cu}_2(\text{SO}_3\text{CF}_3)_2]_n$ ($n = 1, 2$) (Scheme 4.9). Pentane diffusion into a solution of the complex in THF yielded crystals which were suitable for X-ray analysis. The measurement revealed the formation of **12** that contains a partially hydrolyzed ligand instead of complexes with the desired composition as shown in Scheme 4.9 right hand side.



Scheme 4.9: Synthetic strategy to obtain **12**.

Compound **12** crystallizes in the orthorhombic space group *Pbca* with four molecules per unit cell. Only one half of the molecule is found in the asymmetric unit (Figure 4.13). The measurement revealed that one imine function of the coordinating ligands was hydrolyzed and thus the bis(pyrazolato) bridged complex $\text{L}^9\text{Cu}_2(\text{SO}_3\text{CF}_3)_2$ was formed. The hydrolysis reaction occurred presumably during the crystallization process since p.A. quality solvents have been employed.

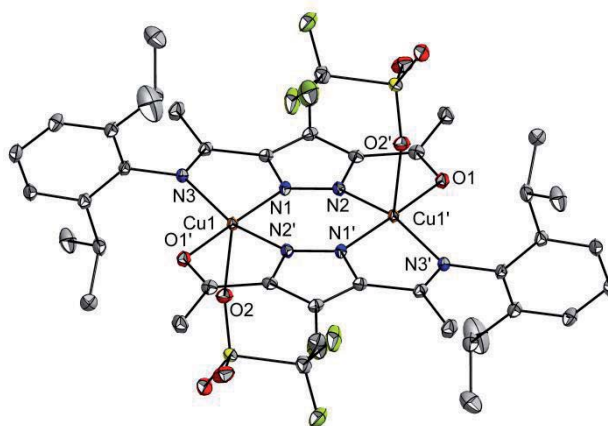


Figure 4.13: Molecular structure of complex **12**. ADPs: 30% probability thermal ellipsoids, hydrogen atoms and counter ions are omitted for clarity. Symmetry operation used to generate equivalent atoms: (') - $x, -y, -z$.

The copper ions in **12** exhibit a fivefold coordination which is defined by the nitrogen atoms N1 and N3 of one sidechain of one ligand and the nitrogen atom N2 and the

oxygen atom O1 of the carbonyl group of the sidechain of the second ligand. The axial position is occupied at relatively long distance by one oxygen atom of the triflate anion. The τ -value of the copper ions is 0.13. The copper-copper distance is 3.92 Å and therefore typical for bis(pyrazolato) bridged binuclear copper complexes.^[116-117] Selected interatomic distances and angles are summarized in Table 4.11.

Table 4.11: Selected interatomic distances [Å] and angles [°] for **12**.

distances			
Cu1-N1	1.921(2)	Cu1-N3	2.0141(19)
Cu1-N2'	1.9251(19)	Cu1-O1'	2.0389(17)
Cu1-O2	2.2384(17)	Cu1-Cu1'	3.9205(8)
angles			
N1-Cu1-N2'	94.20(8)	N2'-Cu1-O1'	79.121(71)
N1-Cu1-N3	79.74(8)	N2'-Cu1-O2	100.98(7)
N1-Cu1-O1'	172.03(7)	N3-Cu1-O1'	105.57(7)
N1-Cu1-O2	92.44(8)	N3-Cu1-O2	94.001(69)
N2'-Cu1-N3	164.10(8)	O1'-Cu1-O2	93.090(69)

4.3.3. Magnetic Properties

Magnetic susceptibility measurements were carried out on complexes **9**, **10** and **12** at a magnetic field of 5000 Oe. Experimental data were modeled with $S = \frac{1}{2}$ according to the procedure that was described in chapter 4.2.3. The temperature dependence of the product $\chi_M T$ is shown in Figure 4.14 for all three complexes.

The rapid decrease of $\chi_M T$ upon lowering the temperature and the close to zero $\chi_M T$ values below 150 K indicate strong antiferromagnetic coupling. The best fit parameters for all three complexes are summarized in Table 4.12. The simulation of the experimental data showed that all three complexes exhibit very strong antiferromagnetic coupling.

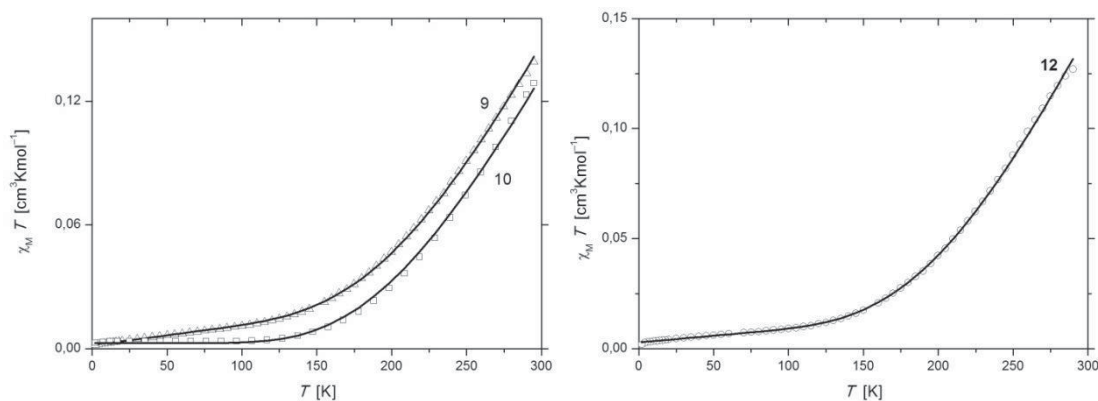


Figure 4.14: Plots of $\chi_{\text{M}}T$ vs. T for complexes **9**, **10** and **12**.

Table 4.12: Best fit parameters of magnetic data analyses for complexes **9**, **10** and **12**.

	9	10	12
g	2.10	2.10	2.10
J [cm^{-1}]	-336	-324	-330
PI [%]	0.5	0.7	0.8
$TIP/10^{-6} \cdot [\text{cm}^3 \cdot \text{mol}^{-1}]$	96	0	60

The chloro bridged complex **9** shows an identical antiferromagnetic coupling constant as the bromo bridged complex **10**.

$$\mathbf{9} (J = -336 \text{ cm}^{-1}) \approx \mathbf{10} (J = -324 \text{ cm}^{-1})$$

Compounds **9** and **10** feature a slightly distorted square-planar coordination sphere. According to the ligand field theory, the magnetic orbital of the d^9 copper ion in a square planar coordination sphere is the $d_{x^2-y^2}$ -orbital. Structural parameters that might influence the overlap between the magnetic orbitals of **9** and **10** *via* superexchange are summarized in Table 4.13.

Table 4.13: Structural parameters that influence the magnetic exchange for complexes **9** and **10**. Interatomic distances are given in Å, angles in °.

complex	$d(\text{Cu1-Cu2})$	$d(\text{Cu1-}\mu\text{-X})$	$d(\text{Cu2-}\mu\text{-X})$	$(\text{Cu1-}\mu\text{-X-Cu2})$
9	3.7879(7)	2.3476(9)	2.3444(9)	107.67(3)
10	3.8636(16)	2.4563(13)	2.4588(15)	103.64(5)

A comparison of the J -values of **9** and **10** with the ones of **1 – 8** (-96 cm^{-1} - -180 cm^{-1}) shows that the magnetic coupling seems to be much stronger in complexes **9** and **10**. The rigid ligand scaffold in complexes **9** and **10** enforces a nearly ideal square planar coordination sphere on the coordinated copper ions, whereas all copper ions of complexes **1 – 8** feature a distorted square pyramidal coordination sphere. And as already mentioned in chapter 4.2.3, the less distorted the coordination polyhedron and the better the ligand-mediated overlap of the magnetic $d_{x^2-y^2}$ orbitals the stronger the antiferromagnetic coupling. However, the already observed trend that chloro complexes exhibit a stronger magnetic coupling than bromo complexes is confirmed (see complexes **1 – 8** chapter 4.2.3).

In complex **12** the two copper ions are bridged by two pyrazolate units. Previously described coupling constants for $\text{Cu}(\mu\text{-pz})_2\text{Cu}$ -complexes lie within the range of $-252 \text{ cm}^{-1} \leq J \leq -70 \text{ cm}^{-1}$.^[116-117, 131, 133-134, 149-150] **12** features a much stronger antiferromagnetic coupling than the reported complexes. According to AJO *et al.* the coupling constant J is dependent on the deviation from coplanarity of the pyrazolate planes and the equatorial planes.^[134] In **12** all atoms of the pyrazolate moiety and the donor atoms in the equatorial planes are located in the same plane. Therefore the magnetic exchange in **12** is very efficient and leads to the unusually strong antiferromagnetic coupling.

The magnetic coupling of all three complexes can be ranked as follows:

$$\mathbf{9} (J = -336 \text{ cm}^{-1}) \approx \mathbf{12} (J = -330 \text{ cm}^{-1}) \approx \mathbf{10} (J = -324 \text{ cm}^{-1})$$

In chapter 4.2 it was proved that both bridging moieties, the pyrazolato and the halide ligand, are responsible for the magnetic superexchange between the copper ions. Since

the three complexes **9**, **10** and **12** feature an identical coupling constant but different bridging units (either $(\mu\text{-pz})_2$ or $(\mu\text{-pz}, \mu\text{-X})$ with $X = \text{Cl}, \text{Br}$) the contribution of the two bridging ligands to the magnetic coupling seems to be the same.

4.3.4. Summary and outlook

The coordination chemistry of **HL**⁹ towards different copper(II) salts was explored. It turned out that the reaction of **HL**⁹ with two equivalents of copper(II) bromide or copper(II) chloride leads to complexes with the already familiar motif $\text{L}^9\text{Cu}_2\text{X}_3$ ($X = \text{Cl}, \text{Br}$).

Employing triflate in the reaction, **12**, a $\text{Cu}_2(\mu\text{-pz})_2$ -complex, is obtained after partial hydrolysis of the ligand during the crystallization process.

To obtain higher nuclearities than two, **HL**⁹ was successfully reacted with a mixture of copper(II) chloride and copper(II) triflate. Due to the strongly disordered triflate anion the exact structure in the solid state could not be clarified. Further investigations should focus on a modified reaction pathway to **11**, in which different anions than triflate, like perchlorate or tetrafluoroborate, are employed. It is possible that the coordination motif of $\text{Cu}_4(\mu\text{-Cl})_2(\mu\text{-pz})_2$ is still observable and other counterions might help to solve the structure and clarify the binding mode of the core motif.

The investigation of the magnetic exchange in complexes **9**, **10** and **12** revealed unusually strong magnetic interactions. **12** even exhibits the strongest antiferromagnetic coupling that has been observed in $\text{Cu}_2(\mu\text{-pz})_2$ -complexes until now.



4.4. Synthesis of multinuclear μ -SO₄-Cu(II) compounds

4.4.1. Introduction

The interest in the synthesis and characterization of copper compounds is not limited to biological factors. Since copper(II) ions feature one unpaired electron they usually possess interesting magnetic features.^[151-153] The magnitude of magnetic interactions between two metal ions is usually directly influenced by the bridging ligand between these two ions.^[154] Anions such as hydroxide, chloride or bromide are often employed as bridging units. Diatomic bridges like pyrazolate, or triatomic bridges like azide or carboxylate are also able to communicate magnetic interactions. All of these bridges are able to bind two metal ions. Another very flexible bridging ligand is the sulfate anion (SO₄²⁻). This anion possesses the capability to bind up to four metal ions in coordination compounds. Since it acts as triatomic bridge, the anion should be able to be involved in magnetic interactions.

The observed different binding modes of copper-sulfate complexes which have been reported until now are depicted in Figure 4.15. The $[(\mu_2\text{-SO}_4)_2\text{Cu}_2]_n$ motif is the most frequent one.^[155-158] In these cases the sulfate anions are usually bridging two independent mononuclear copper complexes to form infinite chains throughout the crystal in the solid state (Figure 4.15, f).

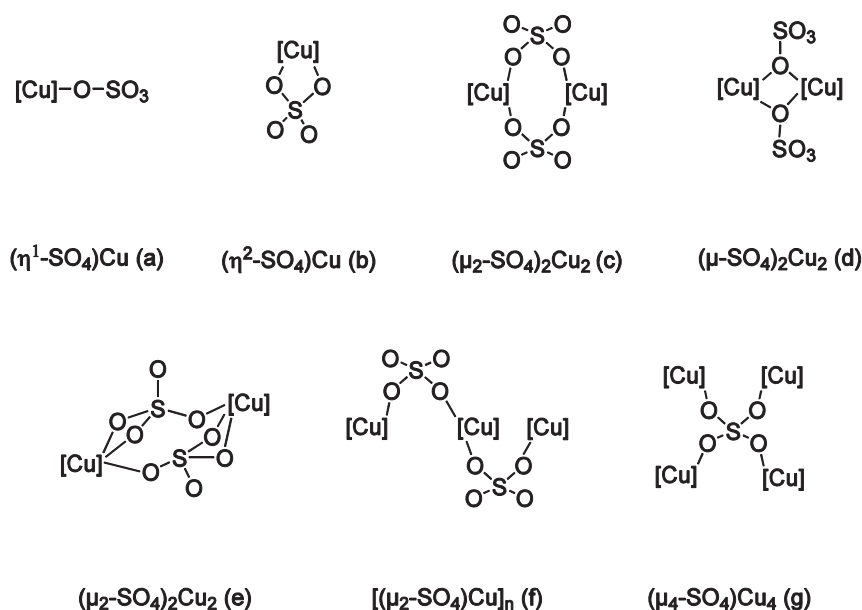


Figure 4.15: Reported sulfate binding modes of copper complexes.

Until now only one complex has been reported with a μ_4 -SO₄-binding moiety between four adjacent copper ions (Figure 4.15, g).^[159] In this particular case two copper dimers are connected *via* the sulfate moiety with the desired μ_4 -SO₄-binding mode where each oxygen atom of the sulfate moiety coordinates a different copper ion. Further described copper-sulfate complexes feature a η^1 -SO₄-coordination (Figure 4.15, a) or a η^2 -SO₄-coordination (Figure 4.15, b) in mononuclear complexes.^[160] Various (μ_2 -SO₄)₂Cu₂-cores have also been described (Figure 4.15, c, d, e).^[161-162] Up to now only little information is available about the magnetic properties of such species.

Keeping this in mind, two different aspects of copper coordination chemistry are investigated in this chapter. First the ligand exchange reaction of pyrazolate-ligated copper halide complexes with silver salts is explored and second the magnetic properties of the resulting complexes are examined.

Complexes **1** and **6** have been chosen as starting material because these complexes provide ligands with different electronic (aromatic N-donor *vs.* aliphatic N-donor) and steric (cyclohexyl *vs.* methyl group) characteristics.

For the anion exchange reaction AgBF₄ and AgSO₃CF₃ have been chosen as source because this should lead to the formation of the thermodynamically favored byproduct AgCl and AgBr, respectively, and hence complexes of the type [L^{1,3}Cu₂X](BF₄) and [L^{1,3}Cu₂X](SO₃CF₃) (X = Cl, Br). The reaction with one equivalent or one half equivalent Ag₂SO₄ might lead to the formation of either binuclear complexes of the type [L^{1,3}Cu₂SO₄]⁺[Y]⁻ or tetranuclear complexes of the type [L^{1,3}₂Cu₄(SO₄)]⁴⁺[Y]⁻₄ (Y = BF₄, SO₃CF₃). The formation of the product might be influenced by the ratio of reactants leading to either a μ_2 -SO₄-coordination (Figure 4.16 left) or to a μ_4 -SO₄-coordination (Figure 4.16 right).

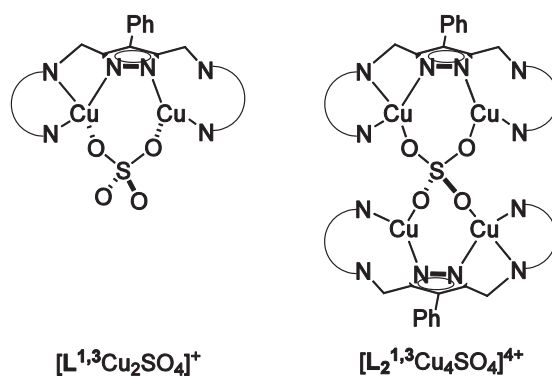
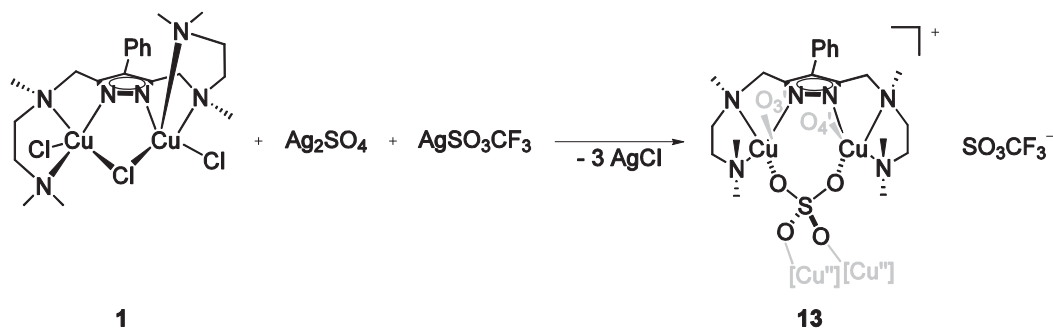


Figure 4.16: Targeted binding modes of the salt methathesis reaction, left: μ_2 -coordination of the sulfate, right: μ_4 -coordination of the sulfate.

4.4.2. Synthesis and Structures

In the general procedure, the starting material **1** or **6** was dissolved in MeCN under inert conditions and subsequently the silver salts were added. To investigate whether complexes of different nuclearity may be formed, the ratio of **1** or **6** to $AgSO_4$ has been varied.

At first **1** was reacted with 1 eq. of Ag_2SO_4 and 1 eq. of $AgSO_3CF_3$ to obtain **13** (Scheme 4.10). Diffusion of Et_2O into the filtered reaction solution yielded blue crystals suitable for X-ray analysis. **13** is a binuclear copper complex with the composition $[L^1Cu_2SO_4]^+[SO_3CF_3]^-$.



Scheme 4.10: Synthesis of **13**.

Complex **13** crystallizes in the tetragonal space group $I4_1$ with sixteen molecules per unit cell. One molecule of the asymmetric unit is depicted in Figure 4.17. The central unit of **13** is the desired $[\text{L}^1\text{Cu}_2\text{SO}_4]$ core where the sulfate anion binds with the atoms O1 and O2. Additionally the atoms O3 and O4 of the sulfate moiety are coordinating the adjacent $[\text{L}^1\text{Cu}_2\text{SO}_4]^+$ unit leading to a μ_4 -coordination of all sulfate anions and a fivefold coordination of all copper ions. Hence **13** forms infinite chains throughout the crystal as shown in Figure 4.18.

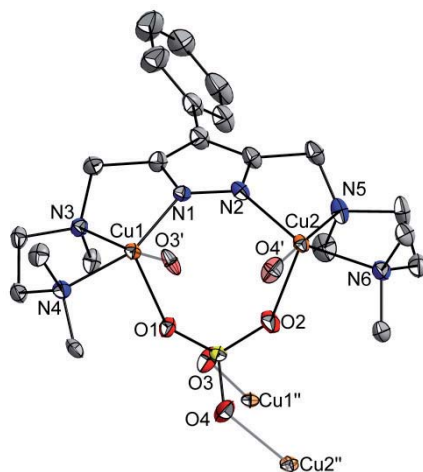
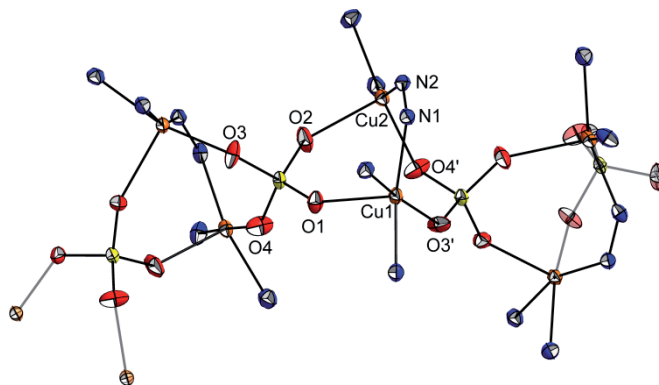


Figure 4.17: Molecular structure of the cation of **13**. ADPs: 30 % probability, hydrogen atoms omitted for clarity.

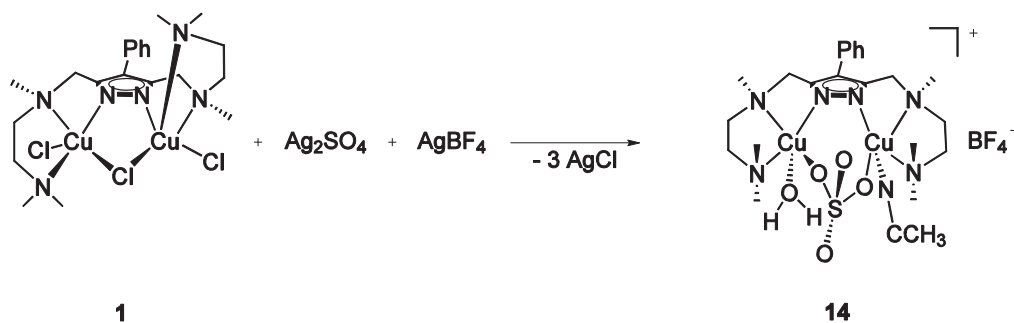
The τ -values have been determined to $\tau_1(\text{Cu1}) = 0.10$ and $\tau_2(\text{Cu2}) = 0.25$. This represents a slightly distorted square pyramidal coordination sphere of the copper ions. Three positions of the equatorial plane of the copper ions are occupied by the N-donor atoms of the pyrazolate ligand. Additionally the oxygen atoms O3' in case of the Cu1 atom and O4' in case of the Cu2 atom are completing the coordination in the equatorial plane. The axial positions are occupied by the oxygen atoms O1 and O2 of the sulfate anion. The copper-copper distance between the copper ions that are coordinated by the same pyrazolate ligand is $d(\text{Cu1-Cu2}) = 3.9469(9) \text{ \AA}$. The copper ions of the two adjacent $[\text{L}^1_2\text{Cu}_2\text{SO}_4]^+$ units are separated between $5.1612(11) \text{ \AA}$ and $6.2315(10) \text{ \AA}$. Selected interatomic distances and bond angles are summarized in Table 4.14.

Table 4.14: Selected interatomic distances [Å] and angles [°] for **13**.

distances			
Cu1-N1	1.957(5)	Cu2-N2	1.947(5)
Cu1-N3	2.088(5)	Cu2-N5	2.066(5)
Cu1-N4	2.026(5)	Cu2-N6	2.028(5)
Cu1-O1	2.180(4)	Cu2-O2	2.153(4)
Cu1-O3 [⋄]	1.953(4)	Cu2-O4 [⋄]	1.947(4)
Cu1-Cu2	3.9469(9)	Cu1-Cu1 [⋄]	
Cu1 [⋄] -Cu2 [⋄]		Cu2-Cu2 [⋄]	
angles			
N1-Cu1-N3	80.89(19)	N2-Cu2-N5	81.9(2)
N1-Cu1-N4	160.5(2)	N2-Cu2-N6	158.4(2)
N1-Cu1-O1	98.71(18)	N2-Cu2-O2	100.3(2)
N1-Cu1-O3 [⋄]	101.14(18)	N2-Cu2-O4 [⋄]	100.90(19)
N3-Cu1-N4	85.71(19)	N5-Cu2-N6	85.0(2)
N3-Cu1-O1	95.58(17)	N5-Cu2-O2	96.5(2)
N3-Cu1-O3 [⋄]	166.7(2)	N5-Cu2-O4 [⋄]	173.4(2)
N4-Cu1-O1	96.59(18)	N6-Cu2-O2	98.2(2)
N4-Cu1-O3 [⋄]	88.81(18)	N6-Cu2-N4 [⋄]	90.5(2)
O1-Cu1-O3 [⋄]	97.09(19)	O2-Cu2-O4 [⋄]	88.9(2)

**Figure 4.18:** Molecular packing of **13** in the solid state. ADPs: 30 % probability, hydrogen and carbon atoms omitted for clarity.

In a similar reaction **1** was reacted with 1 eq. of Ag_2SO_4 and 1 eq. of AgBF_4 under inert conditions (Scheme 4.11). Diffusion of Et_2O into a MeCN-solution of the reaction mixture (p.A. solvents) leads to crystals suitable for X-ray analysis. The measurement revealed the formation of **14**, a solvent coordinated copper(II) species.



Scheme 4.11: Synthesis of complex **14**.

Complex **14** crystallizes in the monoclinic space group $P2_1/c$ with four molecules per unit cell. Both copper ions are five coordinated, the Cu1 ion is found in a nearly ideal square pyramidal coordination sphere ($\tau_1(\text{Cu1}) = 0.02$) and the Cu2 ion exhibits a slightly distorted square pyramidal coordination polyhedron ($\tau_2(\text{Cu2}) = 0.28$). The basal plane of both copper ions is occupied by the N-donor atoms of the pyrazolate ligand and one oxygen atom of the bridging sulfate anion. An additional water in case of Cu1 and a MeCN molecule in case of Cu2, respectively, completes the coordination sphere.

The copper-copper distance is $d(\text{Cu1-Cu2}) = 4.1166(7) \text{ \AA}$, which is consistent with previously reported complexes coordinated by pyrazolate-based ligands.^[104] Selected interatomic distances and angles are summarized in Table 4.15.

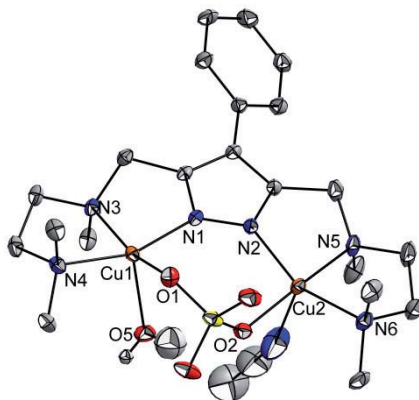
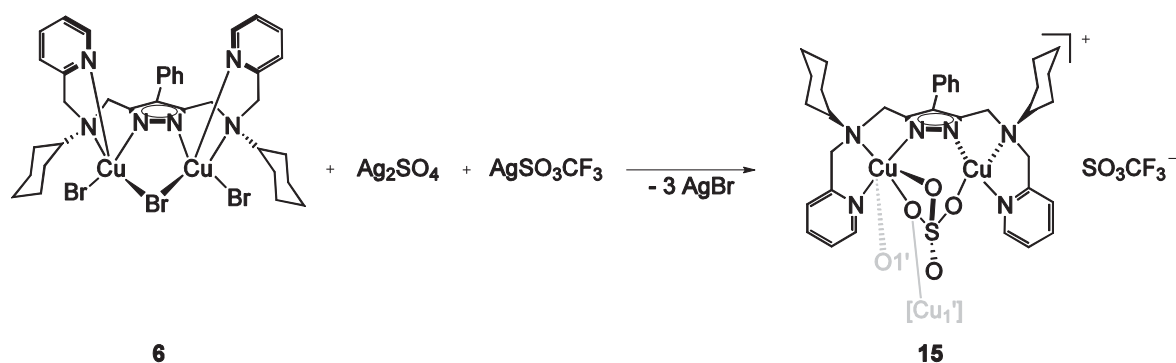


Figure 4.19: Molecular structure of the cation of **14**. ADPs: 30 % probability. Most hydrogen atoms are omitted for clarity.

Table 4.15: Selected interatomic distances [Å] and angles [°] for **14**.

distances			
Cu1-N1	1.955(3)	Cu2-N2	1.941(3)
Cu1-N4	2.022(3)	Cu2-N6	2.009(5)
Cu1-N3	2.055(3)	Cu2-N5	2.071(6)
Cu1-O1	1.979(3)	Cu2-O1	1.978(3)
Cu1-O5	2.230(3)	Cu2-N7	2.319(6)
Cu1-Cu2	4.1166(7)		
angles			
N1-Cu1-N3	80.85(12)	N5A-Cu2-N6A	86.8(2)
N1-Cu1-N4	160.76(14)	N5A-Cu2-N6B	82.4(7)
N1-Cu1-O1	97.03(12)	N5A-Cu2-N7	89.1(3)
N1-Cu1-O5	94.68(15)	N5A-Cu2-O2	172.2(2)
N3-Cu1-N4	85.83(14)	N5B-Cu2-N6A	78.6(5)
N3-Cu1-O1	162.14(13)	N5B-Cu2-N6B	80.9(9)
N3-Cu1-O5	102.37(14)	N5B-Cu2-N7	108.9(8)
N4-Cu1-O1	91.39(13)	N5B-Cu2-O2	167.8(8)
N4-Cu1-O5	101.73(15)	N6A-Cu2-N7	106.0(3)
O1-Cu1-O5	95.47(14)	N6A-Cu2-O2	96.13(18)
N2-Cu2-N5A	81.66(19)	N6B-Cu2-N7	86.7(8)
N2-Cu2-N5B	83.4(5)	O2-Cu2-N6B	98.0(7)
N2-Cu2-N6A	155.6(2)	O2-Cu2-N7	83.1(2)
N2-Cu2-N6B	163.9(7)		
N2-Cu2-N7	95.3(2)		
N2-Cu2-O2	98.14(13)		

Compound **15** was synthesized *via* the same procedure as complex **13**, but complex **6** was used instead of **1** as starting material (Scheme 4.12). Et₂O diffusion into the filtered complex solution resulted in the formation of purple crystals suitable for X-ray analysis.

**Scheme 4.12:** Synthesis of complex **15**.

Complex **15** crystallizes in the triclinic space group $P\bar{1}$ with two molecules per unit cell. The cation found in the asymmetric unit is depicted in Figure 4.20. The basic unit of **15** is

the desired $[\text{L}^3\text{Cu}_2\text{SO}_4]^+$ core where the sulfate anion binds with the atoms O1, O2 and O4. Additionally, the O1 atom of the sulfate anion binds the Cu1' ion and the Cu1 atom is coordinated by the O1' atom.

The copper ions in the central core feature different coordination patterns. Cu1 is sixfold coordinated in a slightly distorted octahedral coordination polyhedron. The basal plane of the Cu1 ion is occupied by three N-donor atoms of the ligand and the oxygen atom O1 of the bridging SO_4^{2-} ligand. The coordination sphere is completed by the weakly bound oxygen atom O4 of the same sulfate anion and the oxygen atom O1 of the adjacent sulfate moiety. The atom Cu2 is four coordinated. The sum of the angles between the donor atoms has been determined to 362° . Therefore the Cu2 ion is set in a slightly distorted square planar fashion and is coordinated by the three N-donor atoms of the second binding pocket of the ligand and an O2 atom of the sulfate moiety. The copper-copper distance is $d(\text{Cu1}-\text{Cu2}) = 4.2023 \text{ \AA}$, which is in the typical range for binuclear pyrazolate-bridged complexes.^[104] Selected interatomic distances and angles are summarized in Table 4.16.

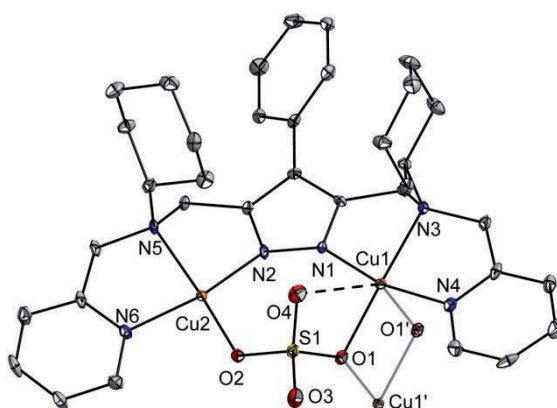
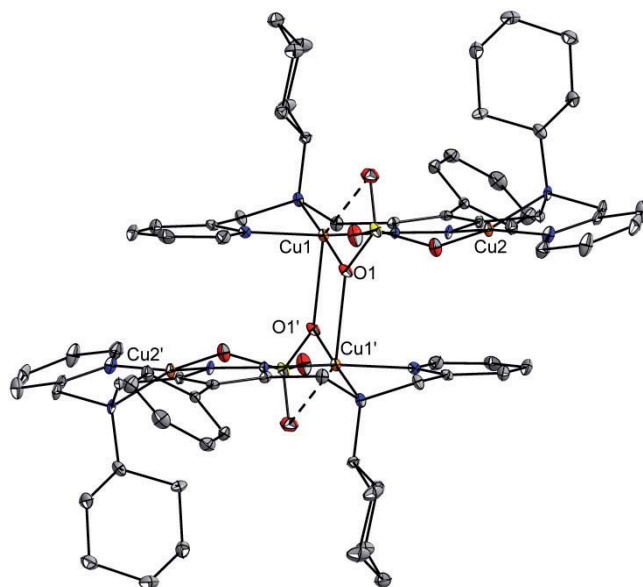


Figure 4.20: Molecular structure of the cation of **15**. ADPs: 30 % probability, hydrogen atoms omitted for clarity.

The sideview of the dimer (Figure 4.21) shows that the pyrazolate- and the pyridine units of one ligand are located roughly in the same plane. The copper ions which are located in these planes are connected by oxygen atom O1 of the sulfate anion. Hence the cyclohexyl groups of the two coordinating ligands are pointing up and down the plane defined by the ligands, blocking all other coordination sites of the molecule. Therefore the formation of a chain as observed for **13** is prevented.

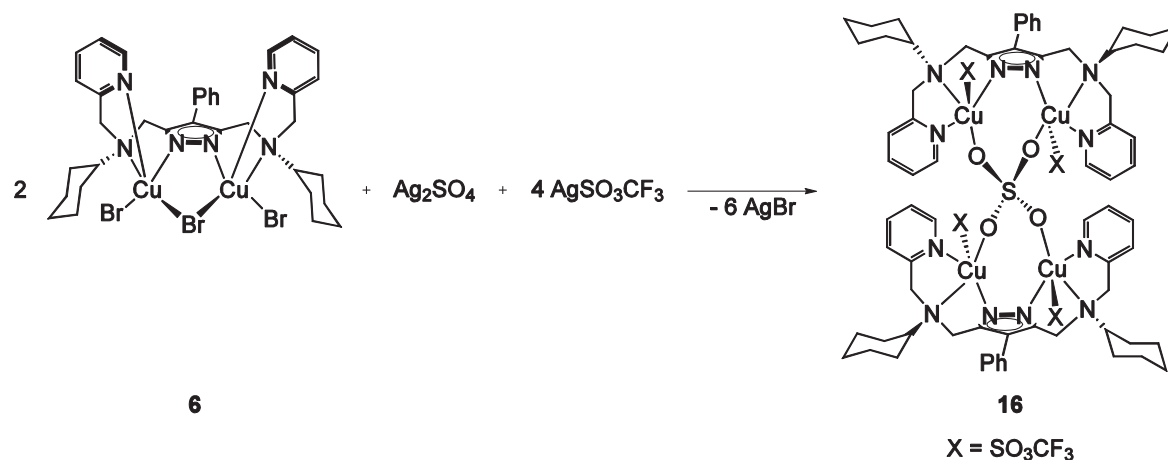
Table 4.16: Selected interatomic distances [Å] and angles [°] for **15**.

distances			
N1-Cu1	1.941(4)	N2-Cu2	1.947(4)
N3-Cu1	2.054(4)	N5-Cu2	2.050(4)
N4-Cu1	1.965(4)	N6-Cu2	1.975(4)
O1-Cu1	1.962(3)	O2-Cu2	1.913(3)
O1 [′] -Cu1	2.430(3)	Cu1-Cu2	4.2023(13)
O4-Cu1	2.7123(4)		
angles			
N1-Cu1-O1	98.09(15)	N2-Cu2-O2	105.43(15)
N1-Cu1-N3	83.01(16)	N2-Cu2-N5	82.54(16)
N1-Cu1-N4	166.67(16)	N2-Cu2-N6	161.01(17)
N1-Cu1-O1 [′]	88.81(15)	N5-Cu2-O2	165.97(16)
N3-Cu1-O1	178.50(15)	N5-Cu2-N6	83.56(16)
N3-Cu1-N4	83.73(16)	N6-Cu2-O2	90.92(16)
N3-Cu1-O1 [′]	94.85(14)	S1-O2-Cu2	126.3(2)
N4-Cu1-O1	95.14(15)	O1-S1-O2	105.836(18)
N4-Cu1-O1 [′]	91.00(15)	O1-S1-O3	108.788(24)
O1-Cu1-O1 [′]	84.17(13)	O1-S2-S4	107.799(23)
S1-O1-Cu1	110.72(19)	O2-S1-S3	108.415(23)
S1-O1-Cu1 [′]	148.5(2)	O2-S1-S4	110.070(24)
Cu1-O1-Cu1 [′]	95.83(12)	O3-S1-O4	115.496(21)

**Figure 4.21:** Sideview of the dimeric form of **15**. ADPs: 30% probability thermal ellipsoids, hydrogen atoms omitted for clarity. Symmetry operation used to generate equivalent atoms: (') 1-x, 1-y, 2-z.

In a further experiment, 2 eq. of **6** were treated with 1 eq. Ag_2SO_4 and 4 eq. AgSO_3CF_3 in order to get a tetranuclear copper complex Scheme 4.13. Et_2O diffusion into a MeCN

solution of the reaction mixture yielded green crystals that were suitable for X-ray analysis. The obtained complex **16** exhibits the desired $[\text{L}_2^3\text{Cu}_4(\mu^4\text{-SO}_4)]^{4+}$ core structure.



Scheme 4.13: Synthesis of complex **16**.

Compound **16** crystallizes in the monoclinic space group Cc with four molecules per unit cell. Although the obvious disorder of the phenyl group in the backbone of the pyrazolate-ligand could not be refined satisfyingly, Figure 4.22 shows a reasonable solution of the structure ($R1 = 0.1044$, $wR2 = 0.1600$ over all data). Hence the τ -values, interatomic distances and angles discussed below should be considered with caution.

The tetranuclear copper core shows the targeted arrangement of the copper-sulfate moiety. All copper ions are five coordinated by the three N-donor atoms of the pyrazole-ligands, one oxygen atom of the sulfate anion and one oxygen atom of the triflate anion.

Interatomic distances of the copper ions that are fixed in the two adjacent pyrazolate binding pockets of the same ligand are $d(\text{Cu1-Cu2}) = 4.0914(19) \text{ \AA}$ and $d(\text{Cu3-Cu4}) = 4.1087(18) \text{ \AA}$. All other copper-copper distances are formed in a range between $5.5893(18) \text{ \AA}$ and $5.6805(18) \text{ \AA}$. Therefore the values are in line with previously reported structures.^[104, 159] Selected interatomic distances and angles of **16** are summarized in Table 4.17 and Table 4.18.

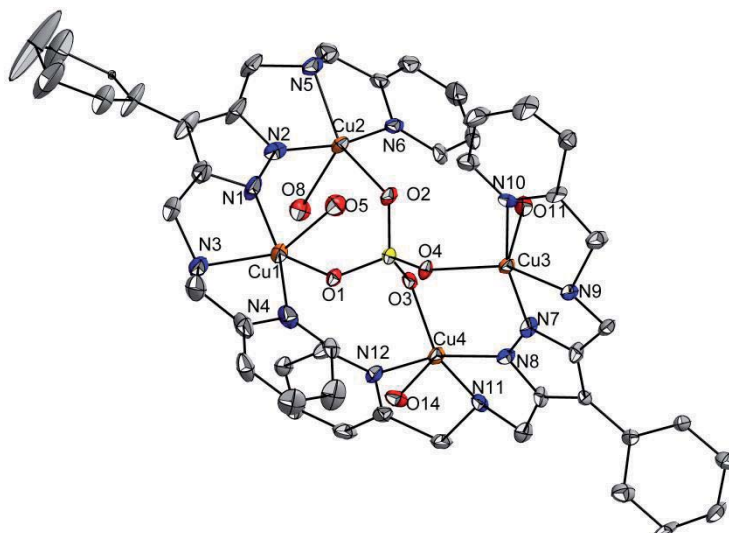


Figure 4.22: Molecular structure of **16**. ADPs: 30% probability thermal ellipsoids. For clarity reasons hydrogen atoms and cyclohexyl groups of the sidearms are omitted and the coordinating triflates are indicated with the coordinating oxygen atom.

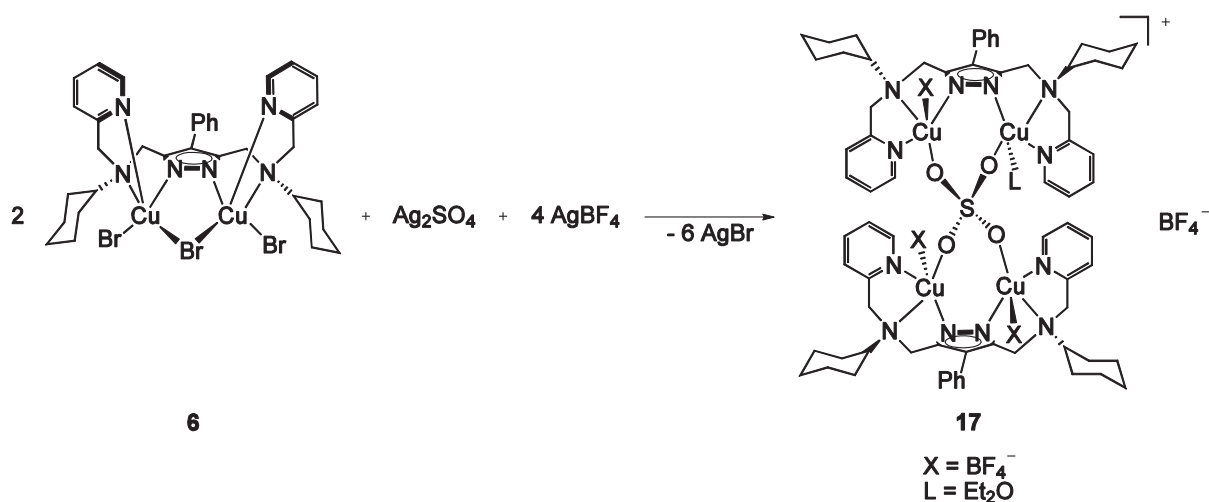
Table 4.17: Selected interatomic distances [\AA] for **16**.

distances			
N1-Cu1	1.923(8)	N7-Cu3	1.910(8)
N3-Cu1	2.042(9)	N9-Cu3	2.075(7)
N4-Cu1	1.990(8)	N10-Cu3	1.948(9)
O1-Cu1	1.980(6)	O4-Cu3	1.995(6)
O5-Cu1	2.257(8)	O11-Cu3	2.381(7)
N2-Cu2	1.897(9)	N8-Cu4	1.932(7)
N5-Cu2	2.058(8)	N11-Cu4	2.068(8)
N6-Cu2	1.963(9)	N12-Cu4	1.972(8)
O2-Cu2	1.987(5)	O3-Cu4	1.993(6)
O8-Cu2	2.380(8)	O14-Cu4	2.283(7)
Cu1-Cu2	4.0914(19)	Cu2-Cu3	5.5893(18)
Cu1-Cu3	5.5641(20)	Cu2-Cu4	5.6805(18)
Cu1-Cu4	5.6477(20)	Cu3-Cu4	4.1087(18)

Table 4.18: Selected interatomic angles [°] for **16**.

angles			
N1-Cu1-N3	84.3(3)	N7-Cu3-N9	82.9(3)
N1-Cu1-N4	163.6(4)	N7-Cu3-N10	163.0(3)
N1-Cu1-O1	99.6(3)	N7-Cu3-O4	100.7(3)
N1-Cu1-O5	92.5(4)	N7-Cu3-O11	90.3(3)
N3-Cu1-N4	81.7(3)	N9-Cu3-N10	84.2(3)
N3-Cu1-O1	137.9(3)	N9-Cu3-O4	141.0(3)
N3-Cu1-O5	123.2(4)	N9-Cu3-O11	121.7(3)
N4-Cu1-O5	88.1(3)	N10-Cu3-O4	96.4(3)
N4-Cu1-O1	96.6(3)	N10-Cu3-O11	87.0(3)
O1-Cu1-O5	98.7(3)	O4-Cu3-O11	97.2(2)
N2-Cu2-N5	83.4(4)	N8-Cu4-N11	82.0(3)
N2-Cu2-N6	164.1(3)	N8-Cu4-N12	163.7(3)
N2-Cu2-O2	100.5(3)	N8-Cu4-O3	100.7(3)
N2-Cu2-O8	86.9(3)	N8-Cu4-O14	89.8(3)
N5-Cu2-N6	83.6(3)	N11-Cu4-N12	82.9(3)
N5-Cu2-O2	149.5(3)	N11-Cu4-O3	145.5(3)
N5-Cu2-O8	112.9(3)	N11-Cu4-O14	118.4(3)
N6-Cu2-O2	95.3(3)	N12-Cu4-O3	95.3(3)
N6-Cu2-O8	89.7(3)	N12-Cu4-O14	92.0(3)
O2-Cu2-O8	97.6(2)	O3-Cu4-O14	96.0(3)

A slightly different coordination motif is observed when AgBF_4 is employed instead of AgSO_3CF_3 in the synthesis Scheme 4.14. Et_2O diffusion into a MeCN solution of the reaction mixture led to the formation of single crystals suitable for X-ray analysis. The obtained complex **17** again exhibits the desired $[\text{L}^3_2\text{Cu}_4(\mu^4\text{-SO}_4)]^{4+}$ core structure.

**Scheme 4.14:** Synthesis of complex **17**.



Complex **17** crystallizes in the orthorhombic space group $Fdd2$ with sixteen molecules per unit cell. The Et_2O molecule which is coordinating to the Cu_2 ion could not be refined properly, still the depicted structure in Figure 4.23 represents a good solution ($R_1 = 0.0739$, $wR_2 = 0.1477$ over all data). The discussed structural parameters might deviate slightly from the correct values but represent a good approximation.

The tetranuclear copper core of **17** shows the expected arrangement with a central $\mu_4\text{-SO}_4$ anion. All copper ions are five coordinated and set in a distorted square-pyramidal coordination sphere ($\tau_1(\text{Cu}_1) = 0.22$, $\tau_2(\text{Cu}_2) = 0.04$, $\tau_3(\text{Cu}_3) = 0.19$, $\tau_4(\text{Cu}_4) = 0.44$). The equatorial plane is coordinated by three N-donor atoms of the ligand and one oxygen atom of the sulfate anion. The axial position is occupied by a fluorine atom of the BF_4^- counterion in case of the atoms Cu_1 , Cu_3 and Cu_4 and the O_5 atom of the coordinating Et_2O molecule for the Cu_2 atom, respectively.

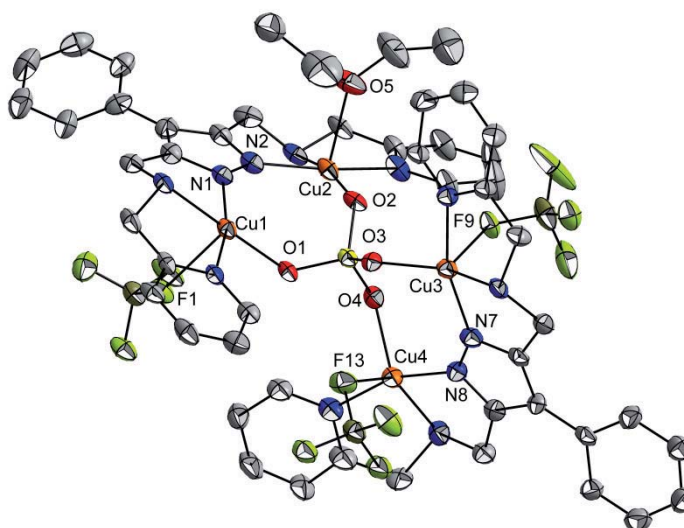


Figure 4.23: Molecular structure of the cation of complex **17**. ADPs: 30% probability thermal ellipsoids, hydrogen atoms and the cyclohexylegroups of the ligand are omitted for clarity.

The copper-copper distances of the adjacent ions within one compartmental ligand are $d(\text{Cu}_1\text{-Cu}_2) = 4.1138(12) \text{ \AA}$ and $d(\text{Cu}_3\text{-Cu}_4) = 4.0348(12) \text{ \AA}$. The distances between the atoms Cu_1 and Cu_3 and the atoms Cu_2 and Cu_4 , respectively, are $d(\text{Cu}_1\text{-Cu}_3) = 5.6058(15) \text{ \AA}$ and $d(\text{Cu}_2\text{-Cu}_4) = 5.5219(15) \text{ \AA}$. All distances are approximately the same as already observed in complex **17**. Selected interatomic distances and angles are summarized in Table 4.19.

Table 4.19: Selected interatomic distances [Å] and angles [°] for **17**.

distances			
Cu1-N1	1.889(6)	Cu3-N7	1.906(6)
Cu1-N3	2.045(5)	Cu3-N9	2.042(6)
Cu1-N4	1.977(6)	Cu3-N10	1.932(5)
Cu1-O1	1.938(5)	Cu3-O3	1.984(5)
Cu1-F1	2.4638(41)	Cu3-F9	2.399(4)
Cu2-N2	1.913(6)	Cu4-N8	1.890(6)
Cu2-N5	2.067(6)	Cu4-N11	2.043(6)
Cu2-N6	1.952(6)	Cu4-N12	1.931(6)
Cu2-O2	1.985(5)	Cu4-O4	2.018(5)
Cu2-O5	2.351(6)	Cu4-F13	2.295(4)
Cu1-Cu2	4.1138(12)	Cu2-Cu3	5.7064(17)
Cu1-Cu3	5.6058(15)	Cu2-Cu4	5.5219(15)
Cu1-Cu4	5.5991(14)	Cu3-Cu4	4.0348(12)
angles			
N1-Cu1-O1	99.0(2)	N7-Cu3-N10	161.5(2)
N1-Cu1-N4	165.3(2)	N7-Cu3-N9	83.1(2)
N1-Cu1-N3	81.2(2)	N7-Cu3-O3	103.0(2)
N1-Cu1-F1	94.573(182)	N7-Cu3-F9	88.5(2)
N3-Cu1-N4	84.1(2)	N9-Cu3-N10	84.5(2)
N3-Cu1-O1	178.6(2)	N9-Cu3-O3	150.4(2)
N3-Cu1-F1	90.761(72)	N9-Cu3-F9	115.46(18)
N4-Cu1-O1	95.7(2)	N10-Cu3-O3	94.5(2)
N4-Cu1-F1	84.828(174)	N10-Cu3-F9	84.5(2)
O1-Cu1-F1	90.570(162)	O3-Cu3-F9	93.80(16)
N2-Cu2-N5	81.2(2)	N8-Cu4-N11	82.0(2)
N2-Cu2-N6	164.7(3)	N8-Cu4-N12	160.5(3)
N2-Cu2-O2	97.9(2)	N8-Cu4-O4	100.7(2)
N2-Cu2-O5	92.6(2)	N8-Cu4-F13	88.1(2)
N5-Cu2-N6	83.8(2)	N11-Cu4-N12	85.6(2)
N5-Cu2-O2	167.10(19)	N11-Cu4-O4	134.4(2)
N5-Cu2-O5	105.3(2)	N11-Cu4-F13	132.5(2)
N6-Cu2-O2	97.4(2)	N12-Cu4-O4	98.6(2)
N6-Cu2-O5	88.5(2)	N12-Cu4-F13	89.3(2)
O2-Cu2-O5	87.6(2)	O4-Cu4-F13	93.07(16)

4.4.3. Magnetic properties

Magnetic susceptibility measurements were carried out on complexes **14**, **15** and **17** at a magnetic field of 5000 Oe. The corresponding experimental data for the complexes were simulated by using the appropriate Heisenberg-Dirac-van-Vleck (HDvV) spin

Hamiltonian for two or four, respectively, $S = \frac{1}{2}$ copper centers with isotropic exchange coupling and Zeeman splitting (Complex **14**: Equation (1), complexes **15** and **17**: equation (3)).

$$\hat{H} = -2J\hat{S}_1 \cdot \hat{S}_2 + g\mu_B(\hat{S}_1 + \hat{S}_2)B \quad (1)$$

$$\hat{H} = -2J(\hat{S}_1 \cdot \hat{S}_2 + \hat{S}_3 \cdot \hat{S}_4) + g\mu_B B \sum_i \hat{S}_{z,i} \quad (3)$$

Temperature-independent paramagnetism (*TIP*) and a Curie-behaved paramagnetic impurity (*PI*) with spin $S = \frac{1}{2}$ were included according to $\chi_{\text{calc}} = (1 - PI)\chi + PI\chi_{\text{mono}} + TIP$. The plots of $\chi_M T$ vs. T are shown in Figure 4.24. The calculated curve fits are shown as solid lines.

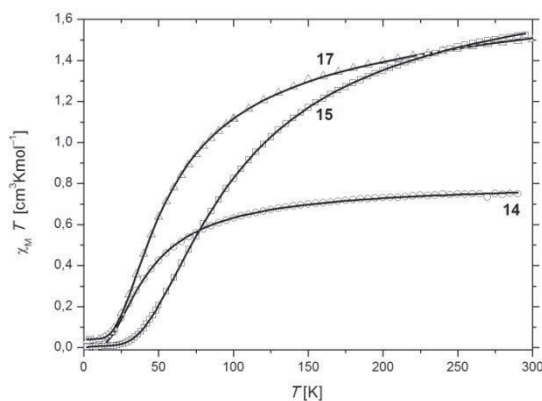


Figure 4.24: Plots of $\chi_M T$ vs. T for complexes **14**, **15** and **17**.

The data of all complexes indicate an antiferromagnetic coupling between the copper ions. The best fit parameters of the compounds according to equations (1) and (3) are summarized in Table 4.20.

Table 4.20: Best fit parameters of the magnetic data analyses for complexes **14**, **15** and **17**.

	14	15	17
g	2.09	2.21	2.09
J [cm^{-1}]	-25.1	-61.6	-34.2
PI [%]	0.8	2.7	10.3
$TIP/10^{-6} \cdot [\text{cm}^3 \cdot \text{mol}^{-1}]$	711	160	441

Due to the inversion center that generates the dimeric structure of **15**, the coupling constants J_{12} and J_{34} are ($J_{12} = J_{34} = J$). Coupling between the dinuclear subunits is considered negligible in this simplified scheme similarly the coupling constants J_{12} and J_{34} of complex **17** are assumed to be identical, and any coupling between the dinuclear subunits is neglected ($J_{12} = J_{34} = J$, see below).

The J -value of **14** ($J = -25.09 \text{ cm}^{-1}$) is much lower than the observed values for the halide-bridged copper complexes in chapter 4.2. Magnetic interactions can be very strong between two metal ions if they are bridged by either aromatic bridges like pyrazolate or single atoms like halides. Since in the sulfate moiety the bridging unit is O1-S1-O2 or O3-S1-O4, respectively, the magnetic exchange through this bridge is usually much weaker.

Since the binuclear complex **15** forms a dimer in the solid state (see Figure 4.21), two independent couplings have been anticipated: J_{12} between Cu1 and Cu2 (or J_{23} between Cu1' and Cu2') and J_{23} between Cu1 and Cu1' (Figure 4.25). Surprisingly, the fitting of the data leads only to one coupling between the copper ions, namely J_{12} between the Cu1 and the Cu2 atom and J_{34} between the Cu1' and the Cu2' atom, respectively, but no magnetic interactions could be observed between the Cu1 and Cu1' ion although the two copper ions Cu1 and Cu1' are bridged by the oxygen atom O1 of the sulfate moiety ($J_{23} = 0$).

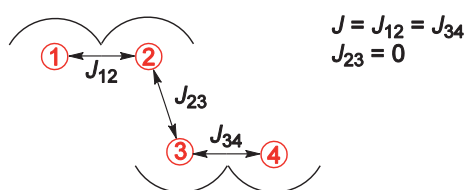


Figure 4.25: Pattern of the possible magnetic interactions of **15**.

Inspection of the coordination polyhedra of the Cu1 and Cu1' atoms is instructive. Since the octahedral coordination sphere is completed by the weakly bound O4 (O4') atom, the coordination of that atom is neglected and the coordination polyhedron is considered to be square pyramidal. According to the ligand field theory the single unpaired electron is localized in the $d_{x^2-y^2}$ -orbital in square pyramidal metal ions as in **15** (Figure 4.26). The $d_{x^2-y^2}$ -orbitals of the Cu1 and the Cu1' atoms are localized in the plane defined by the

atoms N1, N3, N4 and O1 and N1', N3', N4' and O1', respectively, and these basal planes are parallel to each other. Hence the orbitals are parallel and do not overlap with each other. Therefore no magnetic exchange can be observed between Cu1 and Cu1'.

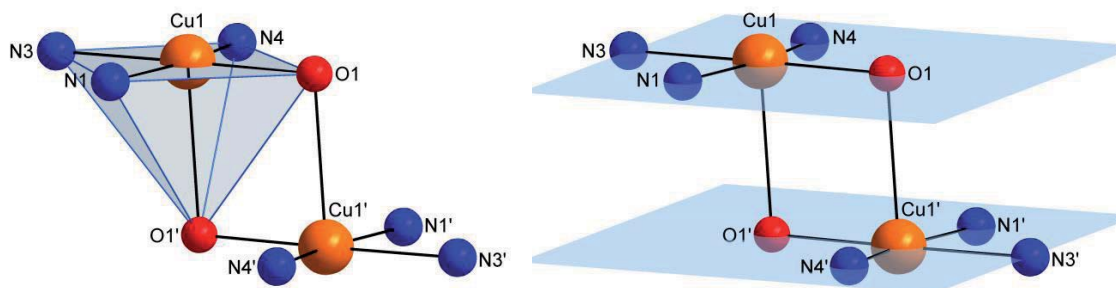


Figure 4.26: Coordination polyhedra of the Cu1 and the Cu1' atom of complex **15** (left) and the parallel planes of the Cu1 and Cu1' atoms.

The tetranuclear complex **17** features antiferromagnetic coupling with a J -value of $J = J_{12} = J_{34} = -34.2 \text{ cm}^{-1}$. Due to the already discussed minor magnetic communication mediated by the sulfate moiety, any interactions *via* the sulfate bridged were ignored ($J_{13} = J_{14} = J_{23} = J_{24} = 0$).

Since the absolute value of the magnetic coupling is directly dependent on the geometric features of the complexes (see chapter 4.2 and 4.3), selected geometric parameters have been summarized in Table 4.21.

The J -values of the three complexes can be ranked as follows:

$$\mathbf{15} (J = |-61.6| \text{ cm}^{-1}) > \mathbf{17} (J = |-34.2| \text{ cm}^{-1}) > \mathbf{14} (J = |-25.1| \text{ cm}^{-1})$$

Out of the three complexes, **15** shows the strongest antiferromagnetic coupling and **14** the weakest.

Complex **14** features a different ligand and is a binuclear complex instead of tetranuclear like the other two, but since **15** and **17** exhibit only one coupling constant, these complexes can be compared with each other. Considering the structural parameters, **15** features the lowest torsion angle between Cu1-N1-N2-Cu2, but **14** features the smallest τ -value. Usually a high coupling constant requires a small torsion angle and a small τ -value. Hence the deviation of the trend of the two parameters confirms the previous

assumption that some structural parameters are able to compensate each other (see chapter 4.2).

Table 4.21: Selected structural parameters for **14**, **15** and **17**.

	τ_1	τ_2	τ_3	τ_4	$\Delta \tau$	χ_{tors} Cu1-N1-N2-Cu2 (χ_{tors} Cu3-N7-N8-Cu4)
14	0.02	0.28	-	-	0.15	12.18
15	0.20	-	-	-	-	4.82
17	0.22	0.04	0.19	0.44	0.22	31.26 (17.76)

4.4.4. Summary and outlook

In summary it was possible to synthesize five different pyrazolate-ligated copper-sulfate complexes containing either two or four copper ions. The four observed different binding modes of the sulfate anion and the corresponding copper complexes are summarized in Figure 4.27.

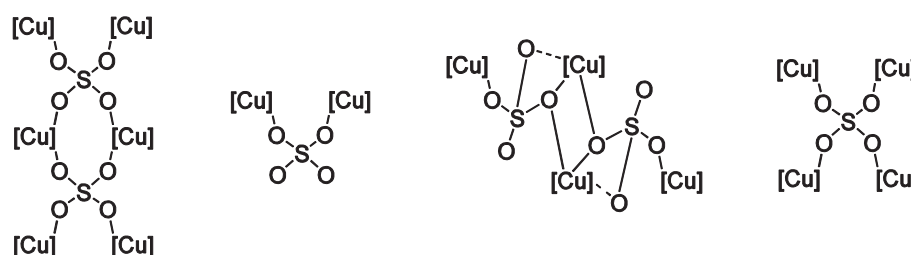


Figure 4.27: Observed binding modes of the sulfate anion in complex **13** – **17**.

Three complexes, **14**, **15** and **17**, were investigated with respect to their magnetic behavior. All of them show antiferromagnetic coupling, and coupling *via* the sulfate bridge seems to be negligible compared to pyrazolate.

The formation of the resulting complexes is sensitive to multiple factors. Considering complexes **13** and **15**, the crystal packing is sensitive to the substituents attached to the nitrogen-donor of the sidearms.

The next steps to understand the formation of the pyrazolate-ligated copper sulfate compounds is to synthesize the complete complex series. Especially the effect of solvents has to be investigated since it is possible that **14** might also form, as compound **13**, an interesting molecular packing in the solid state in the absence of water. An influence of the counter ion on the resulting complexes is also possible and should be investigated.

Another future prospect should be the full investigation of the magnetic properties by collecting and analyzing the magnetic data of all complexes.

4.5. Reactivity of binuclear pyrazolate based copper complexes towards sulfur-transfer reagents

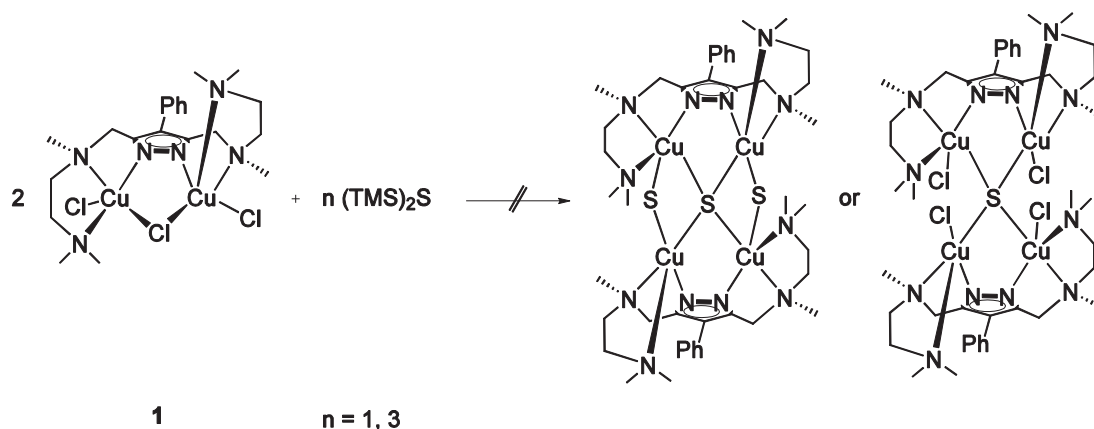
In chapter 2.5 copper-sulfur complexes have been introduced as corroborative and structural models for the Cu_Z -site of N_2O -reductase. Although there has been extensive research, the structure function relationship of the Cu_Z -center is not yet fully understood. In particular, a complex that exhibits a Cu_4S core or a Cu_2S_2 core reminiscent of the Cu_Z -site has not been synthesized yet.

Since pyrazolate-based ligands have already shown the ability to form tetranuclear complexes,^[110-111] different synthetic pathways towards a $\text{L}_2\text{Cu}_4\text{S}$ species (L represents a pyrazolate ligand) are explored.

First, the ligand exchange reaction of complex **1** towards different sulfur-transfer reagents has been investigated. TOLMAN *et al.* showed that it is possible to obtain *side-on* Cu_2S_2 -complexes by use of a ligand exchange reaction in which the chloro ligand of a copper(II) complex is replaced by a disulfido ligand. They employed $(\text{TMS})_2\text{S}$ as sulfur source to get the desired product (see chapter 2.4, Scheme 2.4).^[42]

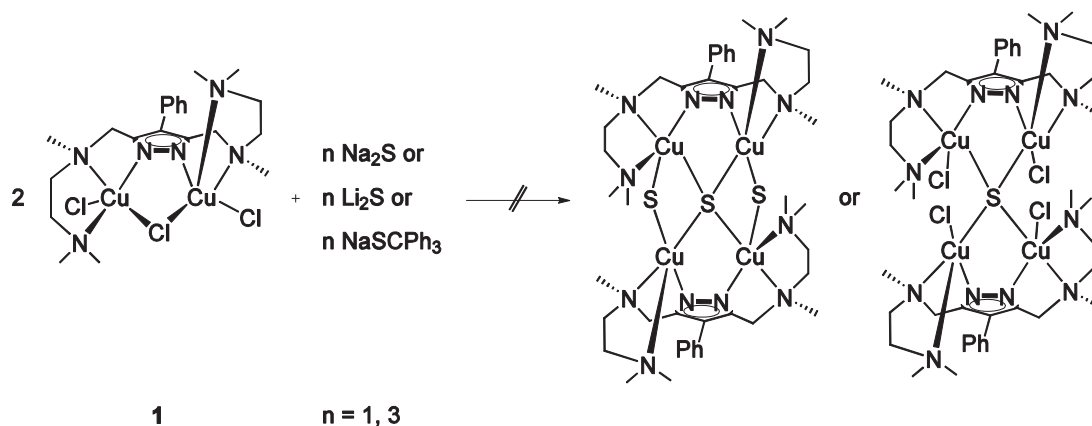
In accordance with this, **1** was treated with varying amounts of $(\text{TMS})_2\text{S}$ to obtain either a tetranuclear species $\text{L}^1_2\text{Cu}_4\text{SCl}_x$ where the chloride anions are still bound as coligands or the neutral species $\text{L}^1_2\text{Cu}_4\text{S}_3$. The reaction pathway and the desired products are depicted in Scheme 4.15.

At first, **1** was dissolved in MeCN yielding a brown solution. Subsequently $(\text{TMS})_2\text{S}$ is added and the color of the reaction mixture immediately turns dark brown forming a brownish precipitate. When the solution is exposed to air the color turns slowly to green and the precipitate dissolves again. Due to the color changes it can be assumed that a reaction takes place, but no products could be identified until now.



Scheme 4.15: Reaction pathway I to synthesize tetranuclear pyrazolate based copper-sulfur complexes.

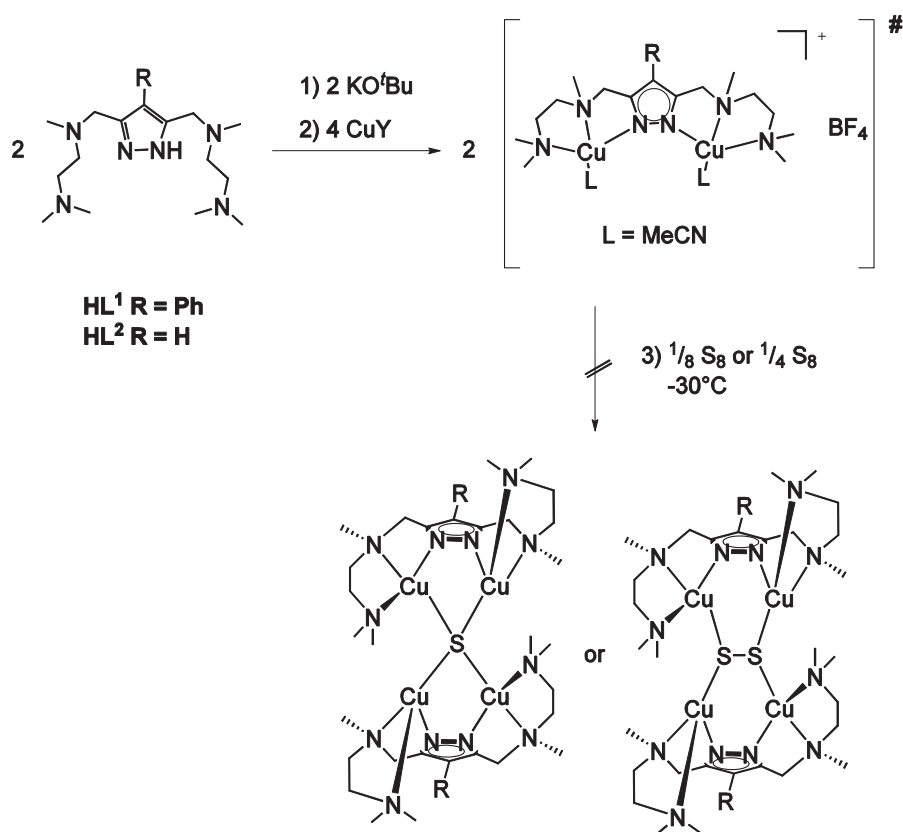
Similar reactions were carried out with Na_2S , Li_2S and NaSCPh_3 as sulfur source, employing the same conditions as described above. First, **1** was dissolved in MeCN and then Na_2S , Li_2S or NaSCPh_3 , have been added to the solution Scheme 4.16. In all three cases the color of the solution turned from brown to green. After workup, it was not possible to isolate or crystallize any product. Further analysis like mass spectrometry did not clarify the chemical composition of the products either. Anyway it can be assumed that a reaction takes place. Furthermore the reaction seems to be sensitive towards the employed sulfur-transfer reagent since the reaction mixture in case of pathway I with $(\text{TMS})_2\text{S}$ as reagent changes to a different color than in case of the other three reactions.



Scheme 4.16: Reaction pathway II to synthesize tetranuclear pyrazolate based copper-sulfur complexes.

Another possible strategy to obtain copper sulfur complexes is the oxidation of copper(I) complexes with elemental sulfur. This synthetic route has been described before by TOLMAN^[42-43] and KARLIN *et al.*^[47] Therefore the potential ligands **HL**¹ or **HL**², have been deprotonated with KO^tBu and treated with [Cu(I)(MeCN)₄]⁺ salts to form a [L^{1,2}Cu₂]⁺ intermediate (Scheme 4.17). In the second step the intermediate has been oxidized with either one equivalent of elemental sulfur, anticipating the formation of a μ₄-sulfido bridged tetranuclear copper species, or with two equivalents of elemental sulfur which might potentially give rise to a disulfide species bridging four copper ions.

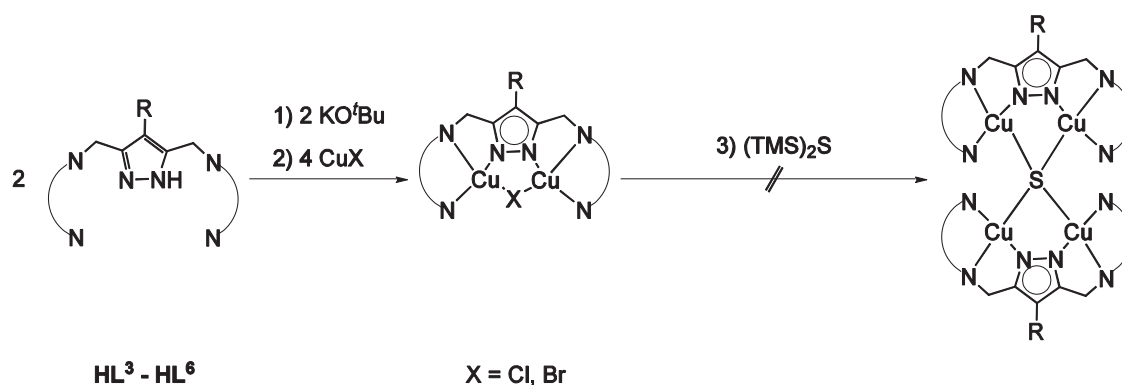
In this synthetic strategy the ligand is first deprotonated with KO^tBu and the corresponding [Cu(I)(MeCN)₄]⁺ salt is added to form the intermediate [L^{1,2}Cu₂]⁺. Subsequently elemental sulfur is added to the reaction mixture. It can be assumed that the cuprous ions have been oxidized to the cupric state since the light yellow color of the intermediate [L^{1,2}Cu₂]⁺ turns to green after the addition of elemental sulfur. The green color is typical for copper(II) ions in solution. Whether the sulfido- or disulfido ligands are bound to the copper ions in the product could not be clarified until now. Furthermore the resulting oxidation state of the copper ions could not be identified since it is possible that more than two copper ions have been oxidized to the cupric state.



Scheme 4.17: Reaction pathway III to synthesize tetranuclear pyrazolate based copper-sulfur complexes.

In order to avoid redox reactions between the copper ions and the sulfur reagent, copper(I) salts have been reacted directly with $(\text{TMS})_2\text{S}$. In this synthetic strategy, copper(I) bromide and copper(I) chloride have been employed since the formation of the thermodynamically favored byproducts TMSCl and TMSBr is considered to be a good driving force. Since the oxidation state of all copper ions is supposed to stay cuprous throughout the reaction, only ligands with pyridine substituents in the sidechains of the pyrazolate ligands have been employed. These ligands are expected to stabilize copper(I) ions better than ligands, that solely bear aliphatic N-donor functions in the sidearm.

First, the potential ligand is deprotonated with KO^tBu and then treated with copper(I) bromide or copper(I) chloride to yield the neutral intermediates $\text{L}^{3-6}\text{Cu}_2\text{X}$ ($\text{X} = \text{Br}, \text{Cl}$). Subsequently, the intermediates are reacted with $(\text{TMS})_2\text{S}$ to yield the desired $\text{L}_2^{3-6}\text{Cu}_4\text{S}$ species *via* ligand exchange Scheme 4.18. In this case it can be assumed that a ligand exchange reaction took place since the color of the solution (yellow in case of chloride as coligand and orange in case of bromide as coligand) turned to dark red after the addition of the $(\text{TMS})_2\text{S}$. Until now, the products could not be identified.



Scheme 4.18: Reaction pathway IV to synthesize tetranuclear pyrazolate based copper-sulfur complexes.

In summary four different synthetic strategies have been explored to synthesize a pyrazolate-based Cu_4S species. Although a reaction can be expected in all cases it was not possible to identify the respective products until now.

Therefore starting material **1** should be replaced in further reactions by one of the complexes **5** - **8** (see chapter 4.2). It is possible that the pyridine substituent influences the electronic structure of the resulting complexes and therefore increases the stability of the copper(II) sulfur species. Additionally, the cyclohexyl group at the N-donor atom close to the pyrazolate unit might increase the crystallization ability.

Using copper(I) complexes as starting material, the further investigations should focus on the isolation of the intermediates $[\text{L}^{1,2}\text{Cu}_2]^+[\text{Y}]^-$ ($\text{Y} = \text{BF}_4, \text{SO}_3\text{CF}_3, \text{PF}_6$) and $\text{L}^{3-6}\text{Cu}_2\text{X}$ ($\text{X} = \text{Br, Cl}$). First, it should be confirmed that the intermediate is a binuclear complex as anticipated, second, the pure intermediates can be utilized as starting materials and thus directly reacted with $(\text{TMS})_2\text{S}$ to avoid possible side reactions.



4.6. Copper(I) bromide complexes

4.6.1. Introduction

As described in chapters 4.2 and 4.3 it is possible to synthesize neutral binuclear pyrazolate-based copper(II) complexes that feature the coordination motif $L^{1-4}Cu_2X_3$ ($X = Cl, Br$). Up to date no neutral binuclear copper(I) compound of the type LCu_2X has been synthesized that is bridged by a pyrazolate-ligand on the one hand and by a halide ligand on the other hand.

Up to now only few copper(I) complexes with compartmental pyrazolate ligands have been described.^[120, 123, 163] The most frequently reported motif is an octanuclear pyrazolate-based μ_4 -oxo species ($L_2Cu_8OMes_4$, Mes = 2,4,6-trimethyl-phenyl). Only one further neutral complex is known in which a L_4Cu_4 (L represents a compartmental pyrazolate-ligand) is formed^[163] and few examples with N-heterocyclic carbenes in the sidechains.^[164] However, the structural motif $[(\mu\text{-pz})M]_n$ $n = 3, 4$ is a well known motif in pyrazolate-based coinage metal chemistry.^[165-167]

Some binuclear monocationic complexes $[LCu_2^1L_2']^+$ that feature a compartmental pyrazolate ligand L and exogenous ligands L' (such as PMe_3) could be obtained.^[123]

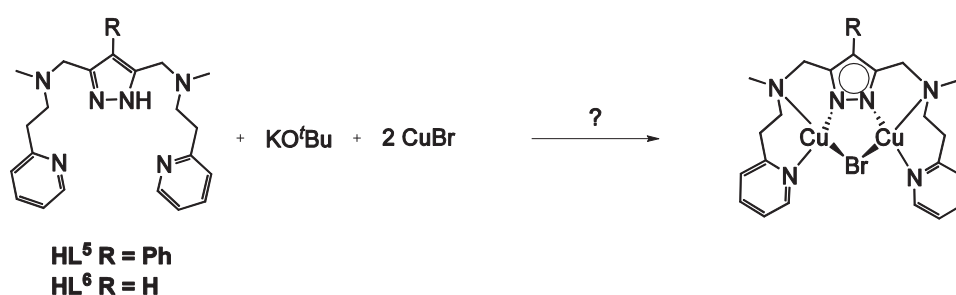
Therefore the synthesis of neutral pyrazolate-based copper(I) halide complexes represents a new substance class in pyrazolate-based copper(I) chemistry and an investigation of the coordination behavior of pyrazolate-based ligands towards copper(I) halides seems worthwhile.

According to the PEARSON concept^[168] Cu^+ -ions are soft acids, Br^- -ions are borderline bases and Cl^- -ions are relatively hard bases. PEARSON stated in his concept that "hard acids prefer to coordinate hard bases and soft acids to soft bases".^[169] Therefore only copper(I) bromide is employed in this synthetic strategy since the copper(I) bromide complexes are supposed to be more stable than the corresponding chloro complexes.

Again, according to the PEARSON concept, the ligands with pyridine-containing sidearms should be more suitable in the coordination of copper(I) ions than these with aliphatic sidearms, since the N-donor atom of pyridine exhibits a softer character than the N-donor

atom of a tertiary aliphatic amine. In view of the preferred tetrahedral coordination sphere of copper(I) the length of the sidearm of the ligand has been considered. The sidearms of **HL**⁵ and **HL**⁶ are one CH₂-group longer than the sidearms of **HL**^{3,4} and **HL**^{7,8} (see chapter 4, Figure 4.1). Therefore they are supposed to be more flexible in providing a tetrahedral coordination sphere for the copper ions.

The synthetic strategy to obtain pyrazolate-based copper(I) bromide complexes is depicted in Scheme 4.19. The appropriate ligand is deprotonated with KO^tBu and is then reacted with two equivalents of copper(I) bromide to yield the desired copper(I) complexes **L**^{5,6}Cu₂Br.



Scheme 4.19: Synthetic strategy for binuclear pyrazolate-based copper(I) bromide complexes.

4.6.2. Synthesis of the complexes

At first the reactivity of the potential ligand [**L**⁵]⁻ towards copper(I) bromide was investigated. Therefore **HL**⁵ and KO^tBu were dissolved in MeCN and copper(I) bromide was added as a solid (Scheme 4.19). The light yellow color of the solution changed immediately to orange. Although no crystals could be obtained that were suitable for X-ray analysis, the colour change of the crude solution indicated the formation of a pyrazolate complex. Thus the complex was investigated *via* ¹H NMR spectroscopy and ESI mass spectrometry.

An overlay of the ¹H NMR spectrum of the crude product (blue line) and the ¹H NMR spectrum of the potential ligand [**L**⁵]⁻ (red line) is depicted in Figure 4.28. The coordinating nitrogen atoms of the ligand are supposed to transfer electron density to the

copper ions and thus the protons that are close to these N-donor atoms are expected to be shifted and, indeed, compared to $[L^5]^-$ the complex spectrum exhibits a shift of the chemical shift of all proton signals to the deep field.

Especially the protons of the methyl group and the protons of the methylene groups that surround the nitrogen atom close to the pyrazole ring feature a shift to lower field. Furthermore, the protons in the 6 and 4 position of the pyridine substituent are shifted to lower field.

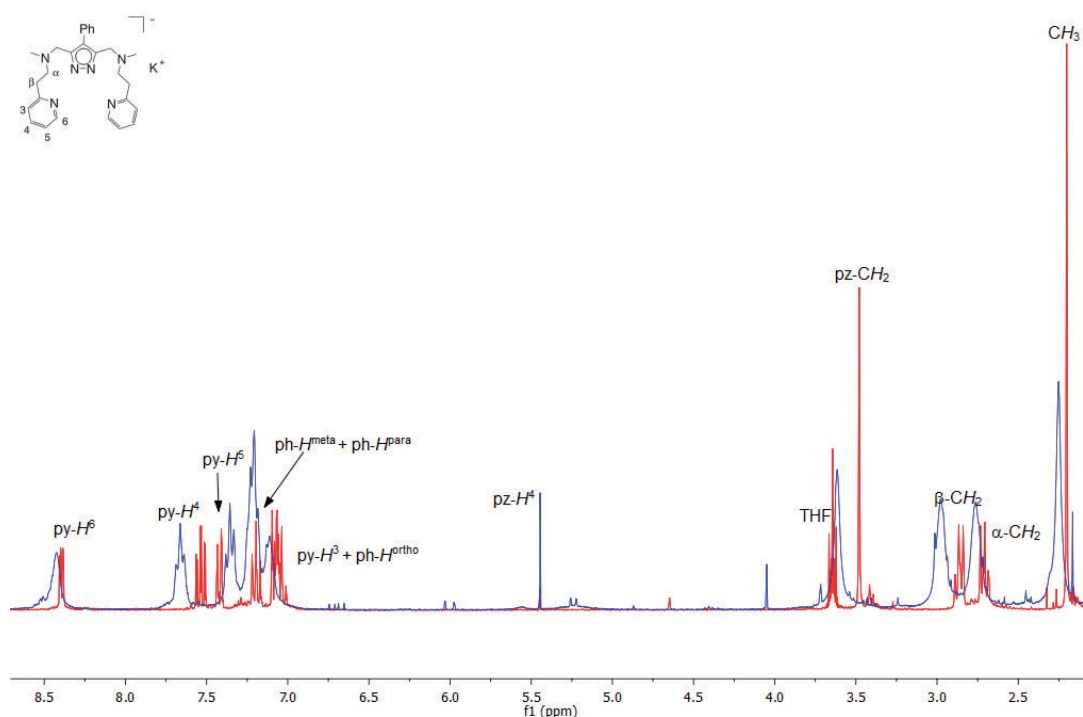


Figure 4.28: NMR spectrum of the crude product (blue line) and $[L^5]^-$ (red line).

To prove the formation of a pyrazolate-based copper(I) complex an ESI mass spectrum of the reaction mixture has been recorded in MeCN under inert conditions. The whole spectrum is depicted in the appendix in Figure B.1. This spectrum exhibits the fragments $[L^5Cu_2]^+$, $[L^5_2Cu_3]^+$, $[L^5_2Cu_3Br]^+$ and $[L^5_2Cu_4Br]^+$, which confirm the formation of a pyrazolate-bridged copper(I) compound, but does not clarify the molecular structure. The multinuclear fragments suggest the formation of a multinuclear compound that is containing at least one bromide ion and the pyrazole ligand. Hence the formation of a pyrazolate-based complex is likely, but no further conclusions can be drawn about its nuclearity or the binding mode of the ligand.

Subsequently the same reaction was repeated with $[\mathbf{L}^6]^-$ instead of $[\mathbf{L}^5]^-$ (Scheme 4.19). After workup the crude reaction mixture has been investigated by $^1\text{H-NMR}$ spectroscopy and ESI mass spectrometry. The $^1\text{H-NMR}$ spectrum of the potential ligand $[\mathbf{L}^6]^-$ (red line) and the crude product (blue line) are depicted in Figure 4.29, and, indeed, all observed signals are shifted to lower field again, which indicates a coordination of the copper(I) ions by the ligand.

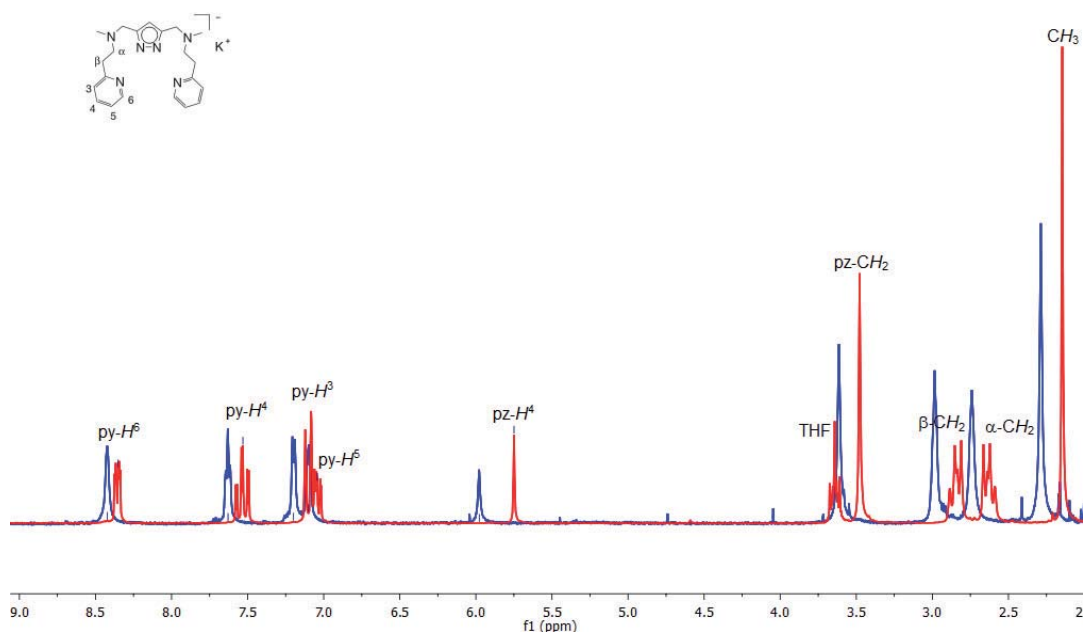


Figure 4.29: NMR spectrum of the crude product (blue line) and the protonated ligand $[\mathbf{L}^6]^-$ (red line).

Especially the protons of the methyl group and the protons of the methylene groups that surround the nitrogen atom close to the pyrazole ring feature a shift to the deep field. Furthermore, all protons of the pyridine substituent are shifted to lower field.

Subsequently the crude reaction mixture has also been investigated by ESI mass spectrometry in MeCN under inert conditions. The fragments $[\mathbf{L}^6\text{Cu}_2]^+$, $[\mathbf{L}^6_2\text{Cu}_3]^+$, $[\mathbf{L}^6_2\text{Cu}_3]^{2+}$, $[\mathbf{L}^6_2\text{Cu}_2\text{Br}]^+$, $[\mathbf{L}^6_2\text{Cu}_3\text{Br}]^+$ and $[\mathbf{L}^6_2\text{Cu}_4\text{Br}]^+$ were observed, which might indicate the formation of a multinuclear pyrazolate copper species, as already observed before. The full spectrum is depicted in appendix B, Figure B.2.

An X-ray measurement of single crystals revealed the formation of **19**, a neutral nonanuclear $\mathbf{L}^6_3\text{Cu}_9\text{Br}_6$ species, instead of the anticipated neutral binuclear complex (Figure 4.30). **19** crystallizes in the triclinic space group $P\bar{1}$ with two molecules per unit cell. Three pyrazole units and three copper ions form a nine-membered metallacycle as

central unit. These three copper ions are set in a slightly bent, but almost linear coordination sphere ($\angle(\text{N1-Cu1-N14}) = 172.2(4)^\circ$, $\angle(\text{N2-Cu2-N7}) = 166.4(4)^\circ$ and $\angle(\text{N8-Cu3-N13}) = 168.6(4)^\circ$). Interatomic distances between the copper ions in the three-membered ring are $d(\text{Cu1-Cu2}) = 3.1815(32) \text{ \AA}$, $d(\text{Cu1-Cu3}) = 3.2277(27) \text{ \AA}$ and $d(\text{Cu2-Cu3}) = 3.0897(25) \text{ \AA}$. These distances and angles are typical for cyclic $\text{Cu}_3(\mu\text{-pz})_3$ complexes.^[170-173]

Each of the six peripheral copper ions is coordinated by the two N-donor atoms of one sidearm of the ligand and two bromide anions. The latter are bridging two copper ions forming $\{\text{Cu}_2\text{Br}_2\}$ -units. The copper ions in these units feature the typical distorted tetrahedral coordination sphere of copper(I). The copper-copper distances in the three $\{\text{Cu}_2\text{Br}_2\}$ -units are shorter than the ones in the previously described three-membered ring [$d(\text{Cu4-Cu9}) = 2.715(2) \text{ \AA}$, $d(\text{Cu5-Cu6}) = 2.653(2) \text{ \AA}$ and $d(\text{Cu7-Cu8}) = 2.929(2) \text{ \AA}$]. These distances are typical for $\{\text{Cu}_2\text{Br}_2\}$ -species.^[174-177] Selected interatomic distances and bond angles are summarized in Table 4.22.

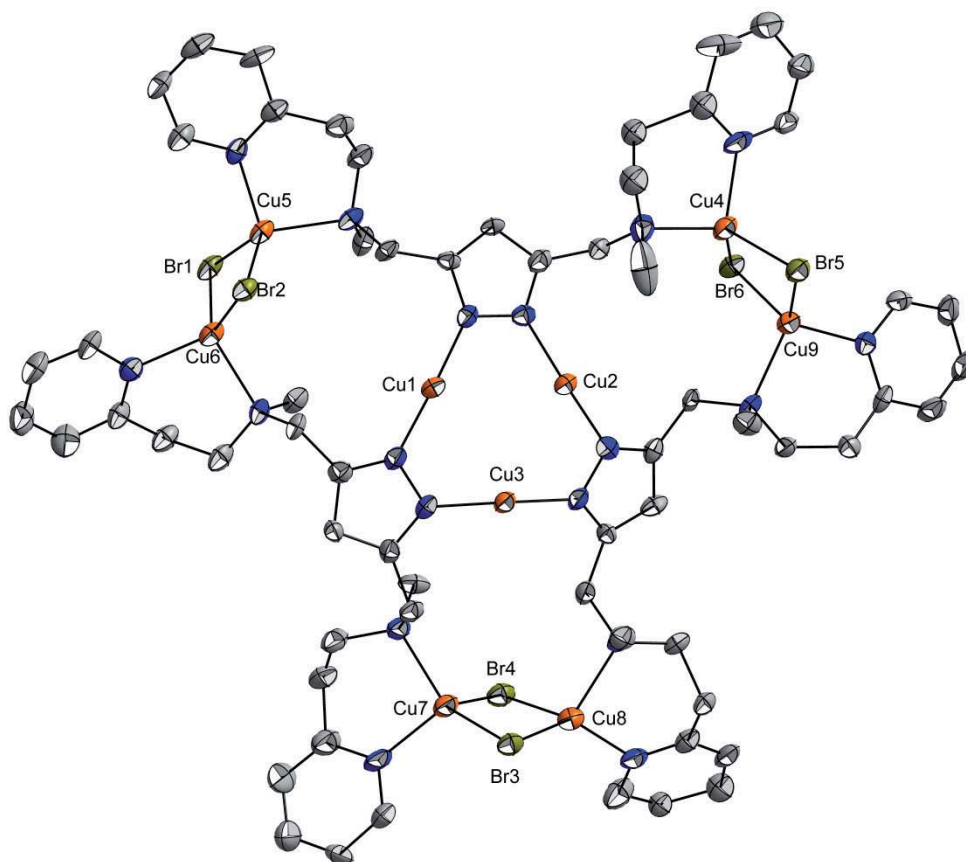


Figure 4.30: Molecular structure of complex **18**. ADPs: 30% probability thermal ellipsoids, hydrogen atoms omitted for clarity.

Table 4.22: Selected interatomic distances [Å] and angles [°] for **18**.

distances			
Cu1-N1	1.852(9)	Cu6-N18	2.046(10)
Cu1-N14	1.866(10)	Cu6-Br1	2.469(2)
Cu2-N2	1.892(9)	Cu6-Br2	2.4850(19)
Cu2-N7	1.892(10)	Cu7-N15	2.155(9)
Cu3-N8	1.876(9)	Cu7-N16	2.035(12)
Cu3-N13	1.875(9)	Cu7-Br3	2.4876(19)
Cu4-N5	2.149(11)	Cu7-Br4	2.439(2)
Cu4-N6	2.027(11)	Cu8-N11	2.190(9)
Cu4-Br5	2.4764(19)	Cu8-N12	2.052(11)
Cu4-Br6	2.465(2)	Cu8-Br3	2.404(2)
Cu5-N3	2.131(10)	Cu8-Br4	2.612(2)
Cu5-N4	2.031(10)	Cu9-N9	2.140(9)
Cu5-Br1	2.488(2)	Cu9-N10	2.053(10)
Cu5-Br2	2.464(2)	Cu9-Br5	2.437(2)
Cu6-N17	2.160(9)	Cu9-Br6	2.5357(18)
angles			
N1-Cu1-N14	172.2(4)	N15-Cu7-N16	98.2(4)
N2-Cu2-N7	166.4(4)	N15-Cu7-Br3	117.2(3)
N8-Cu3-N13	168.6(4)	N15-Cu7-Br4	111.2(3)
N5-Cu4-N6	99.5(5)	N16-Cu7-Br3	108.3(3)
N5-Cu4-Br5	109.9(3)	N16-Cu7-Br4	113.1(4)
N5-Cu4-Br6	117.8(3)	Br3-Cu7-Br4	108.53(8)
N6-Cu4-Br5	109.3(3)	N11-Cu8-N12	98.3(4)
N6-Cu4-Br6	106.5(4)	N11-Cu8-Br3	106.9(3)
Br5-Cu4-Br6	112.69(7)	N11-Cu8-Br4	110.63(19)
N3-Cu5-N4	101.2(4)	N12-Cu8-Br3	135.9(3)
N3-Cu5-Br1	112.6(2)	N12-Cu8-Br4	98.1(3)
N3-Cu5-Br2	111.9(3)	Br3-Cu8-Br4	105.66(8)
N4-Cu5-Br1	104.8(3)	N9-Cu9-N10	99.7(4)
N4-Cu5-Br2	111.4(3)	N9-Cu9-Br5	117.0(3)
Br2-Cu5-Br1	114.06(8)	N9-Cu9-Br6	106.3(2)
N17-Cu6-N18	98.6(4)	N10-Cu9-Br5	114.5(3)
N17-Cu6-Br1	110.4(2)	N10-Cu9-Br6	106.5(3)
N17-Cu6-Br2	112.4(3)	Br5-Cu9-Br6	111.62(7)
N18-Cu6-Br1	114.4(3)	Cu7-Br3-Cu8	73.53(7)
N18-Cu6-Br2	106.1(3)	Cu7-Br4-Cu8	70.78(7)
Br1-Cu6-Br2	113.97(8)	Cu4-Br5-Cu9	67.10(7)
Cu5-Br1-Cu6	64.71(6)	Cu4-Br6-Cu9	65.75(6)
Cu5-Br2-Cu6	64.83(6)		

The central $M_3(\mu\text{-pz})_3$ metallacycle ($M = \text{Cu}$) of **18** represents a well known motif in pyrazolate-based coinage metal chemistry.^[165-167] Most complexes of this type show interesting luminescence properties and exhibit intra- or intermolecular aurophilic,^[178] argentophilic^[179-181] and cuprophilic^[182-183] $d^{10}\text{-}d^{10}$ interactions. The distances within the metallacycle are too long for cuprophilic interactions, but the interatomic copper distances in the $\{\text{Cu}_2\text{Br}_2\}$ -units are shorter than the sum of the van der Waals radii of 2.8 Å,^[184] and therefore $d^{10}\text{-}d^{10}$ interactions might be present.

4.6.3. Summary and outlook

It was possible to synthesize a novel Cu_9 complex that consists of a central three-membered copper(I) pyrazolate ring decorated with sidearms that bind three peripheral $\{\text{Cu}_2\text{Br}_2\}$ -units. This particular assembly is unique for pyrazolate-based copper complexes.

Since most of the previously described three-membered copper complexes show interesting luminescence properties, these should be investigated in case of **19**, too.

Since ESI-MS measurements showed similar product fragments in the spectra of both complexes obtained with ligands $[\text{L}^5]^-$ and $[\text{L}^6]^-$ it can be assumed that the same or at least similar products are formed. Presumably the particular arrangement of the $\{\text{Cu}_2\text{Br}_2\}$ -units depends on the length of the sidearms. Therefore the reaction should also be carried out with ligands that exhibit shorter sidearms, i.e. $[\text{L}^3]^-$, $[\text{L}^4]^-$, $[\text{L}^7]^-$ or $[\text{L}^8]^-$, which might lead to either higher or lower nuclearities.



4.7. Synthesis of Cu(I) thioether complexes as potential precursors for heteroleptic Cu-S compounds

4.7.1. Introduction

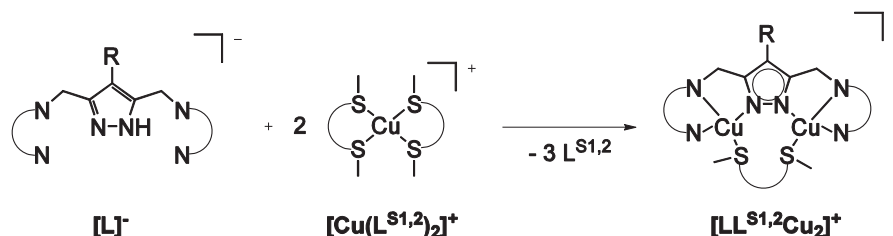
Recently, the synthesis of the first binuclear copper(I) complexes with a pyrazolate-based ligand scaffold bearing the coordination motif $[\text{LCu}_2]^+$ had been reported.^[123] The complexes were stabilized by either two PMe_3 ligands or two isocyanide molecules, respectively. Since thioethers show similar coordination behavior as phosphines^[185-187] the question arose, if such pyrazolate-coordinated binuclear complexes can be synthesized with chelating dithioethers instead of phosphine ligands to obtain the first binuclear copper complexes coordinated by N-donor and thioether ligands.

Homoleptic copper complexes with thioether ligands have been extensively studied over the last decades.^[186] The investigations are often motivated by the apparent parallelism of these ligands to phosphine ligands. Both ligand classes contain large polarizable third row-elements as donor atoms and their soft LEWIS properties enable the ligands to stabilize cations in low oxidation states.^[185-187] However, thioether and phosphine ligands have two major differences: Since sulfur usually features two organic residues and phosphine three the resulting ligands have different steric demand. Secondly, thioether complexes exhibit two lone pairs, thus the electronic structure of the resulting complexes differs due to the remaining lone pair.^[188] These two differences are believed to influence the catalytic activity of the complexes and hence their application.

Often bidentate dithioethers have been employed in thioether copper complexes, leading to a L_2Cu^+ coordination motif.^[188-191] Various structural and NMR-spectroscopic studies have been carried out with such type of homoleptic mononuclear complexes thus far.

Although thioethers are weakly bound ligands because of their low σ -donor and π -acceptor abilities the corresponding complexes have rarely been investigated in ligand exchange reactions.^[192] In principle, the thioether ligands in such complexes should be easily replaced and thus copper(I) dithioether complexes could act as starting material for mono- or multinuclear heteroleptic complexes with N- and S-donor ligands.

The synthetic strategy to obtain such complexes is depicted in Scheme 4.20. Appropriate pyrazolate-ligands $[L]^-$ should be reacted with a dithioether copper complex of the type $[L_2^{S1,2}Cu]^+$ to yield the desired heteroleptic complex $[LL^{S1,2}Cu_2]^+$.



Scheme 4.20: Synthetic strategy towards a thioether bridged pyrazolate-based binuclear Cu(I) complex.

4.7.2. Synthesis of the ligands

To obtain complexes of the type $[Cu(L^{S1,2})_2]^+$, two different potential ligands were employed (Figure 4.31). $L^{S,1}$, an *ortho*-xylyl-derivative, was already successfully employed in the synthesis of a $[L_2^{S,1}Cu]^+$ motif.^[188] The coordination of copper(I) ions leads to two seven-membered metallacycles.

$L^{S,2}$, 1,3-bis(thiomethyl)-propane, exhibits an aliphatic C_3 -unit between the two sulfur atoms; coordination of copper(I) ions should thus lead to a six-membered ring. $L^{S,2}$ is commercially available.

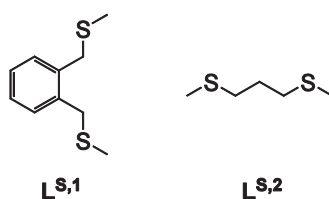
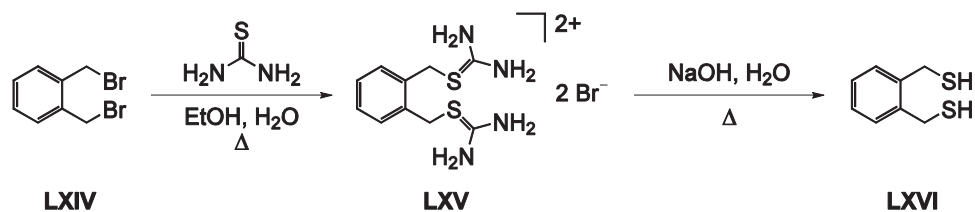


Figure 4.31: Employed potential ligands $L^{S1,2}$.

Synthesis of L^{S1}

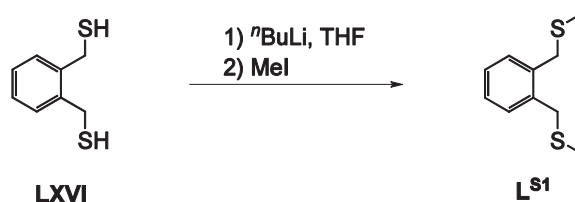
Although the synthesis of L^{S1} is well known^[188] a more convenient synthesis was developed.

In the first step α,α' -dibromo-xylene (**LXIV**) was reacted with thiourea to yield **LXV**. Aqueous workup under basic conditions led to the formation of dithiol **LXVI** (Scheme 4.21).^[193]



Scheme 4.21: Synthesis of **LXVI**.

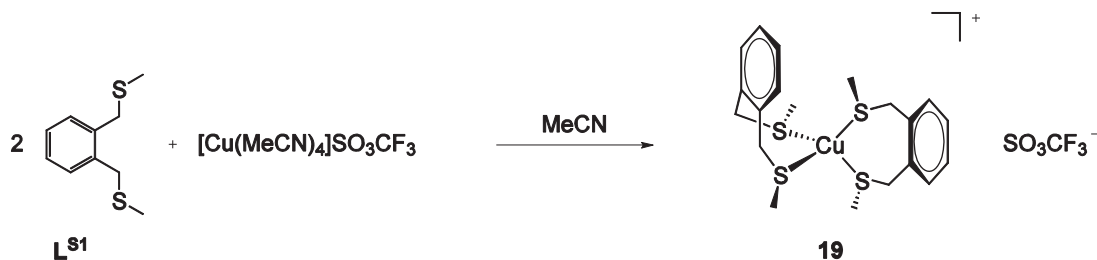
In the final step, **LXVI** was deprotonated with n BuLi and subsequently alkylated with MeI (Scheme 4.22) to obtain L^{S1} .



Scheme 4.22: Synthesis of L^{S1} .

4.7.3. Complex-synthesis of the type $[Cu(L^{S1,2})_2]^+$

To get the desired $[L_2^{S1,2}Cu]$ -motif one equivalent of $[Cu(I)(MeCN)](SO_3CF_3)$ was reacted with two equivalents of L^{S1} in MeCN to yield complex **19** (Scheme 4.23). **19** was isolated and fully characterized. Et₂O diffusion into the reaction mixture led to the formation of airstable colourless crystals suitable for X-ray analysis.



Scheme 4.23: Synthesis of **19**.

The molecular structure of the cation of complex **19** is depicted in Figure 4.32. **19** crystallizes in the triclinic space group $P\bar{1}$ with two molecules per unit cell. The crystallographic data confirmed the expected distorted tetrahedral coordination sphere that is typical for copper(I) ions. The sulfur atoms of two chelating dithioethers coordinate the copper ion, leading to the proposed $[\text{CuL}_2]^+$ -motif. The same motif has already been observed employing BF_4 instead of SO_3CF_3 as counterion.^[188] The copper-sulfur distances of both cations are consistent with each other (Here: $d(\text{Cu-S}) = 2.2875(11) - 2.3239(11)$ Å, Lit.:^[188] $d(\text{Cu-S1}) = 2.2846(9)$ Å and $d(\text{Cu-S2}) = 2.3288(8)$ Å. The observed S-Cu-S angles are also approximately the same. [**19**: $100.94(3)^\circ$ and $121.55(4)^\circ$, Lit.:^[188] $95.29(4) - 120.23(5)^\circ$]. Selected interatomic distances and angles are summarized in Table 4.23.

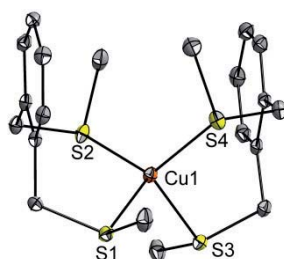


Figure 4.32: Molecular structure of **19**. ADPs: 30% probability thermal ellipsoids, hydrogen atoms omitted for clarity.

Table 4.23: Selected interatomic distances [Å] and angles [°] for **19**.

distances			
Cu1-S1	2.3239(11)	Cu1-S3	2.3237(10)
Cu1-S2	2.2875(11)	Cu1-S4	2.2897(11)
angles			
S1-Cu1-S2	110.01(4)	S2-Cu1-S3	107.40(4)
S1-Cu1-S3	100.94(3)	S2-Cu1-S4	121.55(4)
S1-Cu1-S4	107.68(4)	S3-Cu1-S4	107.29(4)

The crystal packing of **19** in the solid state shows that the cations form infinite chains. The phenyl substituents of the adjacent $[\text{L}_2^{\text{S1}}\text{Cu}]^+$ cations are aligned parallel in a distance of 3.4 Å and 3.5 Å, respectively, which confirms intermolecular π -stacking interactions (Figure 4.33).

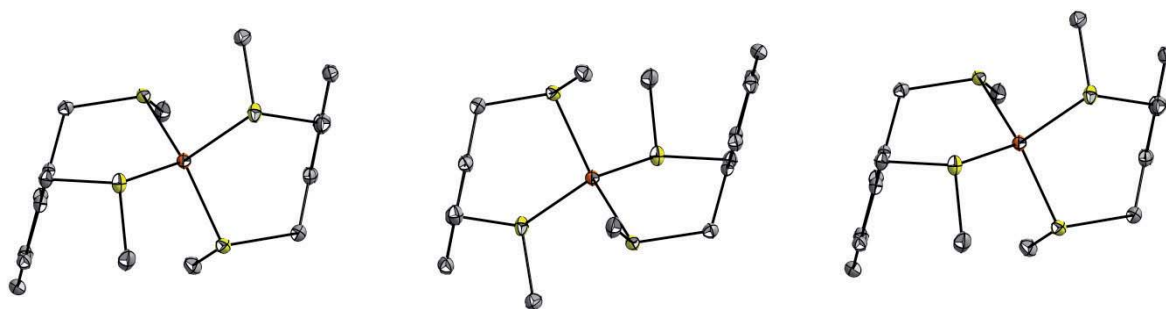
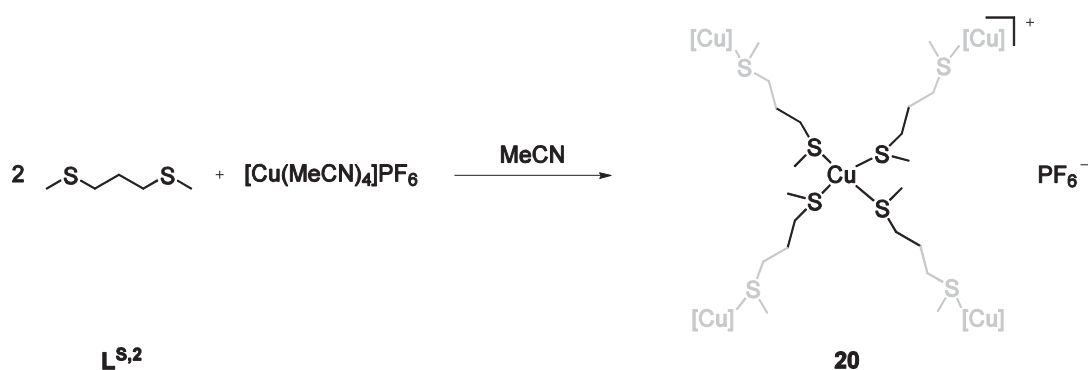


Figure 4.33: Molecular packing of compound **19** in the solid state along the *c* axis, showing the intermolecular π -stacking interactions between the aromatic rings. ADPs: 30% probability thermal ellipsoids, hydrogen atoms omitted for clarity.

Subsequently the same reaction was performed employing $L^{S,2}$ as a ligand (Scheme 4.24). Et_2O diffusion into the reaction mixture in EtCN yielded airstable colourless crystals which were suitable for X-ray diffraction analysis. The results of the measurement revealed the formation of **20**. The resulting complex is of the desired stoichiometric composition, but the ligand does not prefer the chelating coordination of one copper ion. $L^{S,2}$ rather coordinates two copper ions forming an infinite 3D-network.



Scheme 4.24: Synthesis of complex **20**.

The molecular structure of the cation of **20** is depicted in Figure 4.34. **20** crystallizes in the monoclinic space group $C2/c$ with four molecules per unit cell. The molecule is highly symmetric and both the copper(I) ion and the phosphorus atom of the hexafluorophosphate ion are located on a center of symmetry. Therefore only one half of the molecule is observed in the asymmetric unit.

The copper ion is tetrahedrally coordinated by the sulfur atoms of four different dithioether ligands. The second sulfur atom of each ligand coordinates a second copper ion, leading to a 3D-network (Figure 4.35). The copper-sulfur distances [$d(Cu-$

$S2A) = 2.296(4) \text{ \AA}$ and $d(\text{Cu}-S1) = 2.3021(13) \text{ \AA}$] and the S-Cu-S angles [$102.00(6)^\circ$ and $114.40(9)^\circ$] are typical for thioether-coordinated copper(I) ions.^[188-189, 191, 194] In the molecular structure the S2 and C4 atoms as well as the PF_6 counterion are disordered over two positions. Selected interatomic distances and angles are summarized in Table 4.24.

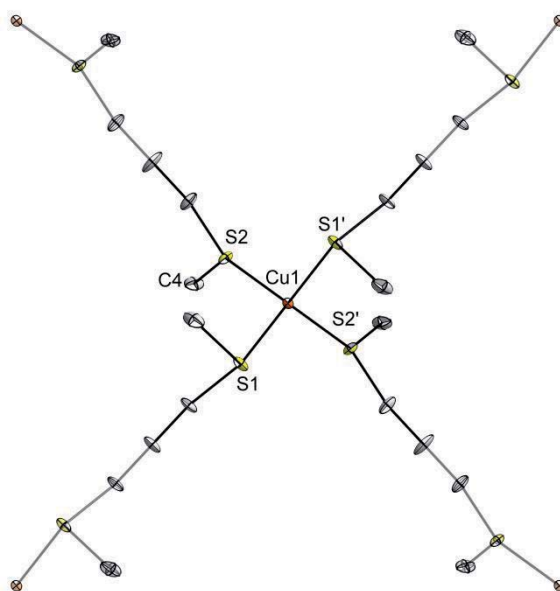


Figure 4.34: Molecular structure of the cation of **23**. ADPs: 30% probability thermal ellipsoids, copper atoms: orange, sulfur atoms: yellow, carbon atoms: grey. Hydrogen atoms omitted for clarity. Symmetry operation used to generate equivalent atoms: (') $2-x, y, 1-z+1/2$.

Table 4.24: Selected interatomic distances [\AA] and angles [$^\circ$] for **23**.

distances			
Cu1-S1	2.3021(13)	Cu1-S2A	2.296(4)
Cu1-S2B	2.312(4)		
angles			
S1-Cu1-S1'	102.00(6)	S1-Cu1-S2A'	114.40(9)
S1-Cu1-SA2	111.94(9)	S2-Cu1-S2A'	102.63(18)
S1-Cu1-S2B	124.24(9)	S2B-Cu1-S2B'	101.43(18)
S1'-Cu1-S2B	103.56(9)		

In principle ligand $\text{L}^{\text{S}2}$ should be able to form a six-membered metallacycle in coordination compounds and the coordination of a “linear” coordination mode seems to be unusual. In $\text{L}^{\text{S}1}$ the two substituents are located in ortho-positions of the phenyl-group and their structure might promote the formation of the seven-membered ring as in **19**.

The possible explanation of the formation of the 3D-network in **20** might be the energy advantage of the packing of the molecules in the solid state compared to the thermodynamic advantage of the chelate effect.

Taking into account that L^{S1} is forming stable seven-membered rings in complex **19**, the coordination pattern of L^{S2} in **20** is even more surprising.

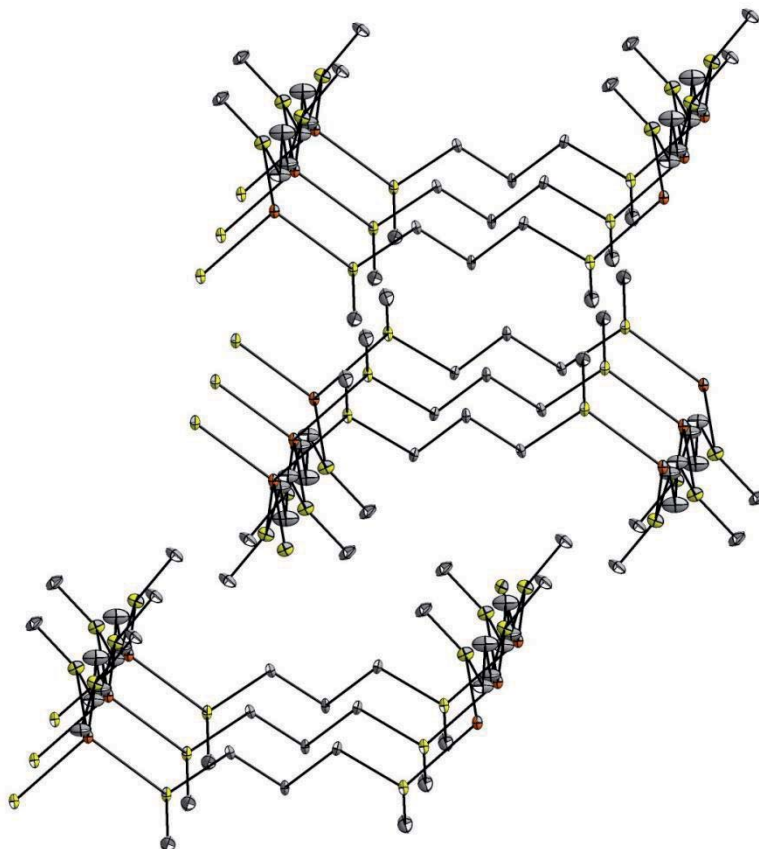


Figure 4.35: Three dimensional view of the polymeric 3D network of **20**. ADPs: 30% probability thermal ellipsoids, copper atoms: orange, sulfur atoms: yellow, carbon atoms: grey. Hydrogen atoms omitted for clarity.

4.7.4. Redox properties

The redox potentials of homoleptic mononuclear copper thioether complexes have not been investigated so far. In principle, **19** and **20** feature five centers that can be involved in redox processes. The first one is the $\text{Cu}^+/\text{Cu}^{2+}$ ion redox process and the others are the thioether functions, which can be oxidized from the neutral thioether R_2S to the radical R_2S^+ . Therefore the redox properties of **19** and **20** have been explored by cyclic voltammetry.

The measurements have been carried out in MeCN/0.1 M NBu_4PF_6 at room temperature. Since both compounds feature cupric ions, the oxidation processes of the complexes have been investigated at first and subsequently the reducing processes were stated. The measurements have been carried out at a scan rate of 100 mV/s and are depicted in Figure 4.36 for complex **19** and in Figure 4.37 for complex **20**. All given potentials were calculated versus the $\text{Cp}_2\text{Fe}/\text{Cp}_2\text{Fe}^+$ redox potential.

Compound **19** exhibits six independent irreversible redox signals, three oxidation processes and three reduction processes. Three oxidation processes have been assigned to the potentials $E_p^{ox} = 1.051$ V, $E_p^{ox} = 1.349$ V and $E_p^{ox} = 1.821$ V.

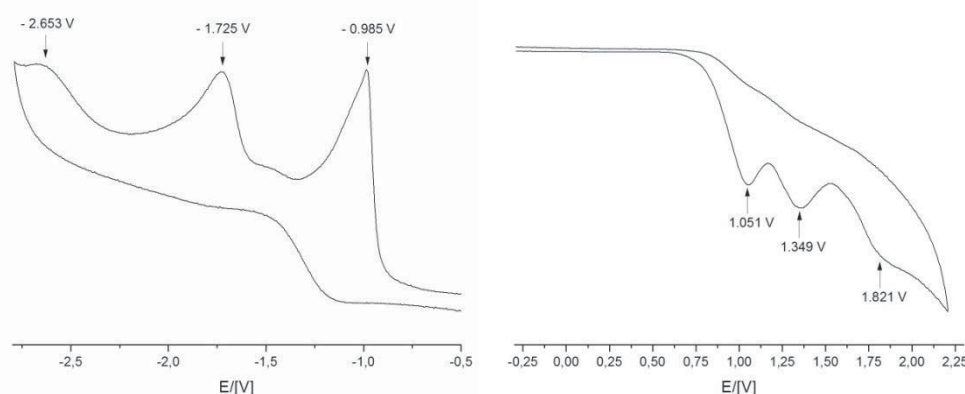


Figure 4.36: Cyclic voltammogram of **19** in MeCN vs. $\text{Cp}_2\text{Fe}/\text{Cp}_2\text{Fe}^+$. Left : range of -2.8 V - -0.5 V, right : range of -0.3 - 2.3 V.

Detailed investigations of the oxidation of different thioethers like methionine^[195] or benzylmethylsulfide^[196] showed that the oxidation process of R_2S to R_2S^+ is always

irreversible and the oxidation of benzylmethylsulfide to the cationic radical in MeCN was determined to $E_p^{ox} = 1.354$ V versus the Cp_2Fe/Cp_2Fe^+ redox potential.^[196]

The redox potential of the free thioether is very close to one of the observed oxidation steps of **19** at $E_p^{ox} = 1.349$ V, the other two oxidation processes cannot be assigned to a certain oxidation in the complex. Possibly the first oxidation step at $E_p^{ox} = 1.051$ V reflects the oxidation of the copper ion and the third step at $E_p^{ox} = 1.821$ V may correspond to the oxidation of the second thioether function.

Examining the reductive part of the cyclic voltammogram, three irreversible reduction processes can be observed at potentials of $E_p^{red} = -0.985$ V, $E_p^{red} = -1.725$ V and $E_p^{red} = -2.653$ V. Since all of these processes are irreversible, too, they have not been assigned to certain reduction step.

The cyclic voltammogram of compound **20** is depicted in Figure 4.37. The measurement revealed two irreversible oxidation processes and three irreversible reduction steps. This indicates a very complex redox behavior of **20**. The first oxidation process is observed at $E_p^{ox} = 1.055$ V and the second one is observed at $E_p^{ox} = 1.623$ V.

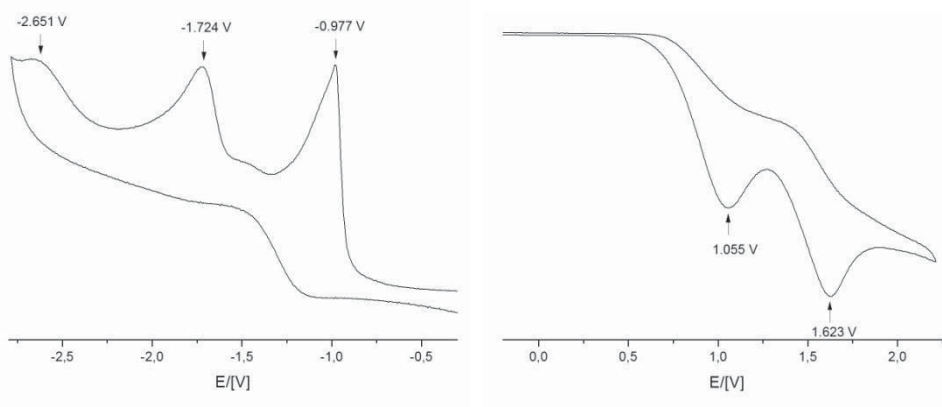


Figure 4.37: Cyclic voltammogram of **20** in MeCN vs. Cp_2Fe/Cp_2Fe^+ . Left : range of -2.8 V - -0.4 V, right : range of -0.2 – 2.3.

The oxidation potential of methionine to the corresponding radical in water at pH = 2.1 was determined to be $E_p^{ox} = 1.04$ V.^[195] In MeCN the potentials of the free thioethers are usually higher.^[196] Thus, the first oxidation step of **19** and **20** can be assigned to the Cu^+/Cu^{2+} oxidation process while the second one likely represents the ligand to form the

corresponding cation radical, but no further investigation of the formed products after the electrochemical oxidations have been carried out so far.

The reductive part of the cyclic voltammogram features three irreversible reduction processes. The first one at $E_p^{red} = -0.977$ V, the second one at $E_p^{red} = -1.724$ V and the third one at $E_p^{red} = -2.651$ V. Since the numbers of oxidation and reduction processes are not equal for **20**, an explanation is very difficult. Further investigation of the products, for example by EPR-spectroscopy, will be needed to clarify the oxidation and reduction products.

4.7.5. Summary

It was possible to synthesize two different potential precursors with the stoichiometric composition $[(L^{S1,2})_2Cu]^+$. Both complexes have been explored with respect to structural and electrochemical properties.

The next step, the reaction of **19** and **20** with pyrazolate-based ligands could not be fully investigated within the time range of this work. Preliminary results showed that it is possible to use complexes **19** and **20** as starting material for complexes of the type $[LCu_2]^+$ (**L** represents a pyrazolate-based ligand). The formation of $[LCu_2]^+$ could be confirmed via 1H NMR spectroscopy. Whether the dithioether is still coordinated to the copper ions could not be elucidated. No analytically pure sample could be obtained to clarify the structure of the coordination motif of the copper ion. Further investigations should focus on this reaction.

4.8. Synthesis of multinuclear Cu(I) thiolate compounds

4.8.1. Introduction

In chapter 4.5 the synthesis of a unique nonanuclear copper(I) complex that is assembled from compartmental pyrazolate ligands (**19**) has been reported (Figure 4.38). **19** features a nine-membered metallacycle as central unit. Additionally, the sidearms of the pyrazolate ligand hold three $\{\text{Cu}_2\text{Br}_2\}$ -units. Hence the question arose if it is possible to exchange the bromide ion with another anion, that is able to bridge two adjacent metal ions.

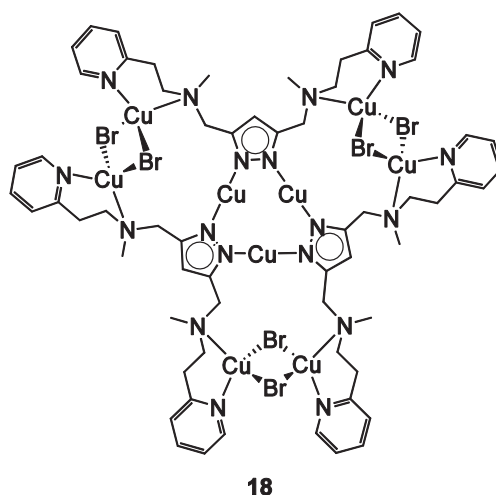


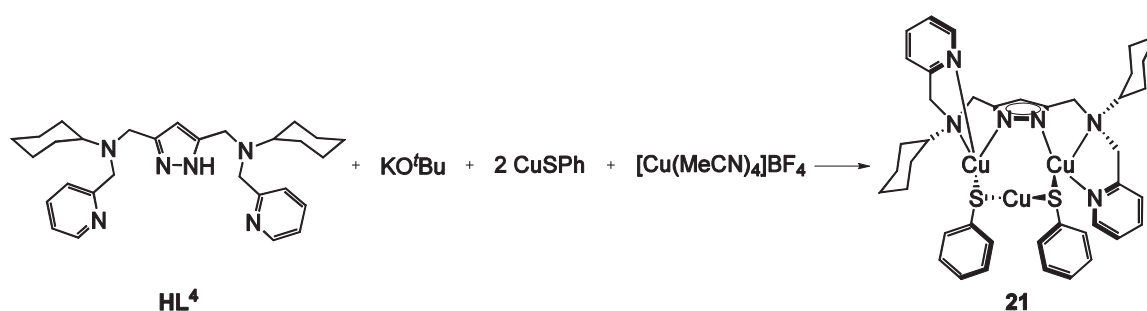
Figure 4.38: Complex 18.

As already presented in chapter 2.5, organothiolates (RS^-) can be classified as soft bases according to the PEARSON concept.^[197] Additionally, they are able to form multinuclear clusters with copper(I) ions in different ratios where the S-donor atom of the thiolate ligand can either bind in a μ_2 - or in a μ_3 -fashion. Therefore copper(I) thiophenolate seems to be suitable to replace copper(I) bromide during the synthesis.

HL^{3-6} have been employed in this synthetic approach. The corresponding reaction behavior towards $[\text{Cu}(\text{MeCN})_4]^+$ salts and copper(I) thiophenolate in different ratios has been investigated. Finally, two discrete copper(I) complexes with $[\text{L}^4]^-$ as ligand and thiophenolate as coligand could be isolated.

4.8.2. Complex synthesis and structural characterization

The synthesis of complex **21** is depicted in Scheme 4.25. **HL**⁴ was deprotonated with KO^tBu and subsequently reacted with 1 eq. of [Cu(MeCN)₄](BF₄) and 2 eq. of copper(I) thiophenolate. Layering a complex solution in benzene with hexane yielded crystals that were suitable for X-ray analysis. It revealed that **21** is a trinuclear copper species with the chemical composition L⁴Cu₃(SPh)₂.



Scheme 4.25: Synthetic strategy to synthesize **21**.

21 crystallizes in the monoclinic space group *Cc* with eight molecules per unit cell. Two independent molecules are observed in the crystal and only one half of each molecule is observed in the asymmetric unit. The two molecules are enantiomers, hence only one of the molecules is depicted in Figure 4.39. Since the two molecules feature slightly different bond lengths and angles the interatomic distances and angles of both molecules are summarized in Table 4.25.

In **21** the Cu1 atom is found in a strongly distorted tetrahedral coordination sphere. The Cu1 ion is coordinated by the three N-donor atoms of the pyrazolate ligand and the sulfur atom of the thiolate anion. The distance Cu1-Cu1' is $d(\text{Cu1-Cu1}') = 3.86772(2) \text{ \AA}$.

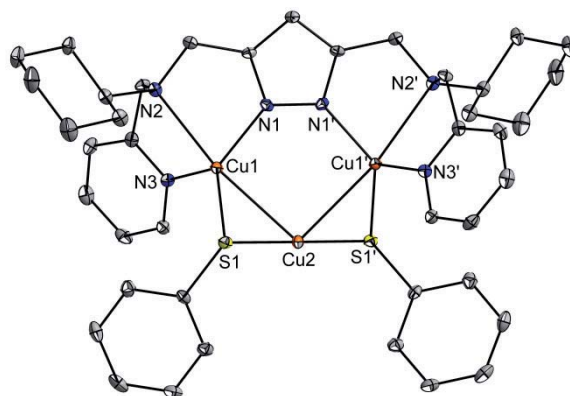


Figure 4.39: Molecular structure of **21**. ADPs: 30% probability thermal ellipsoids, hydrogen atoms omitted for clarity. Symmetry operation to generate equivalent atoms: $-x+2,y,-z+1/2$.

Table 4.25: Selected interatomic distances [Å] and angles [°] for **21**.

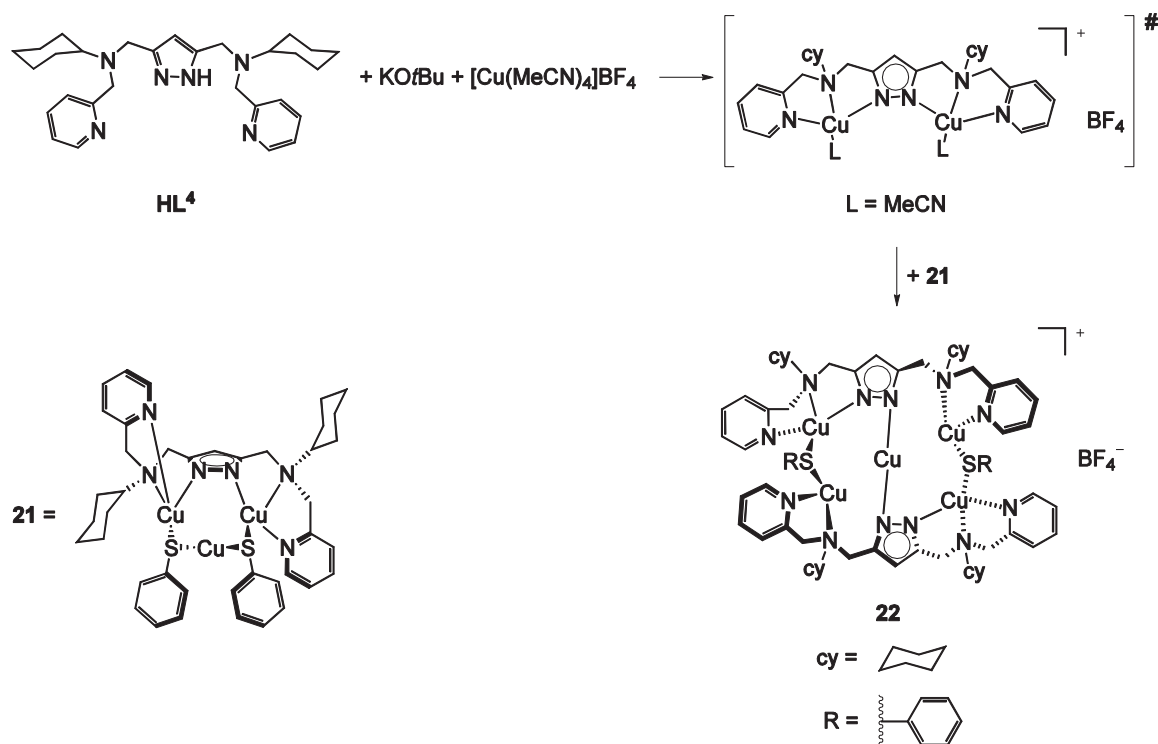
distances			
molecule 1		molecule 2	
Cu1-N1	1.964(2)	Cu3-N4	1.978(2)
Cu1-N2	2.429(3)	Cu3-N5	2.478(3)
Cu1-N3	2.047(3)	Cu3-N6	2.041(3)
Cu1-S1	2.2515(9)	Cu3-S2	2.2475(9)
Cu2-S1	2.1641(8)	Cu4-S2	2.1612(9)
Cu2-S1'	2.1641(8)	Cu4-S2'	2.1613(9)
Cu1-Cu1'	3.86772(2)	Cu3-Cu3'	3.9888(3)
Cu1-Cu2	2.6789(5)	Cu3-Cu4	2.6885(6)
Cu2-Cu1'	2.6789(5)	Cu4-Cu3'	2.6885(6)
angles			
molecule 1		molecule 2	
N1-Cu1-N2	76.65(9)	N4-Cu3-N5	77.10(10)
N1-Cu1-N3	122.09(10)	N4-Cu3-N6	112.61(10)
N1-Cu1-S1	122.20(8)	N4-Cu3-S2	119.25(8)
N3-Cu1-N2	78.98(9)	N6-Cu3-N5	75.93(10)
S1-Cu1-N2	130.69(6)	S2-Cu3-N5	131.09(6)
N3-Cu1-S1	113.60(7)	N6-Cu3-S2	125.10(8)
S1-Cu2-S1'	179.80(5)	S2-Cu4-S2'	175.32(5)
Cu1-S1-Cu2	74.557(3)	Cu3-S2-Cu4	75.117(3)
Cu1-Cu2-Cu1'	92.41(2)	Cu3-Cu4-Cu3'	95.775(3)

Symmetry operation used to generate equivalent atoms: $-x+2,y,-z+1/2$ (molecule 1) and $-x+1,y,-z+1/2$ (molecule 2).

The Cu2 atom features an almost linear coordination between the S-donor atoms of the thiolate ligands with $\angle(\text{S1-Cu2-S1}') = 179.80(5)^\circ$. Since the interatomic distance

$d(\text{Cu1-Cu2}) = 2.6789(5) \text{ \AA}$ is relatively short, presumably cuprophilic $d^{10}\text{-}d^{10}$ interactions are present in this compound.

In order to investigate if complexes with thiophenolate coligands can be obtained in higher nuclearities, a complex solution of **21** was added to a complex solution of the intermediate $[\text{L}^4\text{Cu}_2](\text{BF}_4)$. To yield the intermediate $[\text{L}^4\text{Cu}_2](\text{BF}_4)$, **HL**⁴ was deprotonated with KO^tBu and subsequently reacted with 2 eq. of $[\text{Cu}(\text{MeCN})_4](\text{BF}_4)$. Layering a complex solution in DCM with hexane yielded crystals that were suitable for X-ray analysis. It was later found that the resulting complex **22**, which contains a $[\text{L}^4_2\text{Cu}_5(\text{SPh})_2]^+$ cation, can also be obtained *via* a one pot synthesis using stoichiometric amounts of the copper salts (Scheme 4.26).



Scheme 4.26: Synthesis of **22**.

22 crystallizes in the triclinic space group $P\bar{1}$ with two molecules per unit cell. The complex features two pyrazolate ligands and two thiophenolates as coligands. The five copper ions of the pentanuclear complex exhibit three distinct coordination spheres in the molecular structure (Figure 4.40).

The atoms Cu1 and Cu4 are found in distorted tetrahedral environment. They are coordinated by the three N-donor atoms in a binding pocket of the $[\text{L}^4]$ ligands. In detail

the Cu1 atom is coordinated by the N-donor atoms N2, N3 and N4, and the Cu2 atom is surrounded by the N-donor atoms N8, N11 and N12. The fourfold coordination sphere is completed by the coordination of the S1 atom of the first thiolate in case of the Cu1 atom and the S2-donor atom of the second thiolate in case of the Cu2 atom.

The central copper ion Cu2 features a linear coordination and is set between the two ligands, namely between two N atoms (N1 and N7) of the pyrazolate units. The corresponding angle is \angle (N1-Cu2-N7) = 176.32(13)° and thus is only slightly deviating from 180°.

The copper ions Cu3 and Cu5 are both set in distorted trigonal planar coordination. The Cu3 ion is coordinated by two N-donor atoms of one sidearm of the ligand (N9 and N10) and the S-donor atom (S1) of a thiolate, the Cu5 ion is coordinated by the N-donor atoms of the sidearm of the other ligand (N5 and N6) and by the second bridging thiolate (S2). The sum of angles at Cu3 and Cu5 is 354°, i.e., close to 360°.

The shortest Cu-Cu distances in **22** have been observed between the atoms Cu2 and Cu3 and between the atoms Cu2 and Cu5, respectively [$d(\text{Cu2-Cu3}) = 2.8717(7) \text{ \AA}$ and $d(\text{Cu2-Cu5}) = 2.8767(7) \text{ \AA}$]. Since both values are higher than twice the van der Waals radius of copper,^[184] cuprophilic interactions are likely weak if present at all. Selected interatomic distances and angles are summarized in Table 4.26.

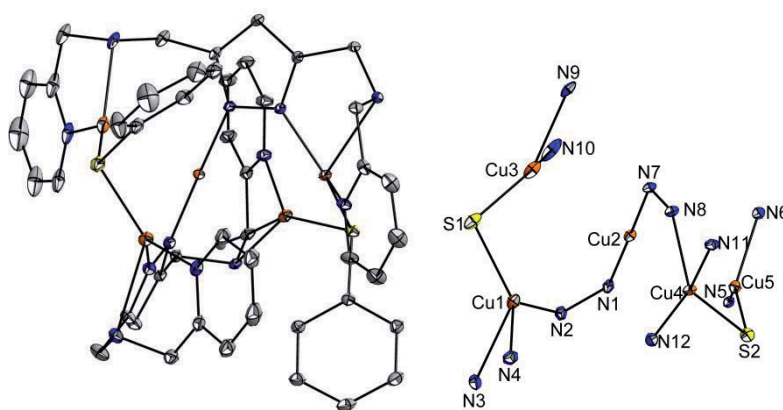


Figure 4.40: Left: Molecular structure of **22**. ADPs: 30% probability thermal ellipsoids. Counterion, hydrogen atoms and cyclohexyl groups omitted for clarity. Right: coordination pattern of the copper ions of **22**. Counterions, all carbon and all hydrogen atoms omitted.

Table 4.26: Selected interatomic distances [Å] and angles [°] of **22**.

distances			
Cu1-N2	1.968(3)	Cu4-N8	1.980(3)
Cu1-N3	2.463(3)	Cu4-N11	2.4871(4)
Cu1-N4	2.016(3)	Cu4-N12	2.038(3)
Cu1-S1	2.2228(12)	Cu4-S2	2.2410(10)
Cu2-N1	1.848(3)	Cu5-N6	1.995(3)
Cu2-N7	1.853(3)	Cu5-N5	2.187(3)
Cu3-N10	1.991(4)	Cu5-S2	2.1562(11)
Cu3-N9	2.185(4)	Cu2-Cu3	2.8717(7)
Cu3-S1	2.1503(14)	Cu2-Cu4	3.3490(8)
Cu3-N9	2.185(4)	Cu2-Cu5	2.8767(7)
Cu1-Cu2	3.3150(9)	Cu3-Cu4	5.5364(12)
Cu1-Cu3	3.2917(9)	Cu3-Cu5	5.7184(8)
Cu1-Cu4	4.7950(12)	Cu4-Cu5	3.3321(4)
Cu1-Cu5	5.5029(13)		
angles			
N2-Cu1-N3	74.44(12)	N10-Cu3-S1	136.86(15)
N2-Cu1-N4	120.49(14)	N10-Cu3-Cu2	86.58(10)
N2-Cu1-S1	121.78(10)	S1-Cu3-Cu2	103.48(4)
N3-Cu1-N4	78.13(13)	N8-Cu4-N11	74.019(15)
N3-Cu1-S1	127.73(9)	N8-Cu4-N12	123.78(12)
N4-Cu1-S1	116.90(11)	N8-Cu4-S2	122.40(9)
N1-Cu2-N7	176.32(13)	N11-Cu4-N12	77.473(17)
N1-Cu2-Cu3	97.59(9)	N11-Cu4-S2	127.372(19)
N1-Cu2-Cu5	82.08(9)	N12-Cu4-S2	113.50(9)
N7-Cu2-Cu3	82.03(9)	N5-Cu5-N6	81.43(12)
N7-Cu2-Cu5	99.04(9)	N5-Cu5-S2	137.19(8)
Cu3-Cu2-Cu5	168.30(2)	N5-Cu5-Cu2	99.13(8)
N9-Cu3-N10	81.83(16)	N6-Cu5-S2	135.82(10)
N9-Cu3-S1	135.30(9)	N6-Cu5-Cu2	85.04(9)
N9-Cu3-Cu2	99.51(8)	S2-Cu5-Cu2	103.68(3)

4.8.3. Characterization in solution and redox properties

In order to verify the stability of **22** in solution, compound **22** in CD₂Cl₂ was investigated via ¹H NMR spectroscopy at room temperature and at -40 °C. The resulting spectra are shown in Figure 4.41. Since the signals are broadened at room temperature, a dynamic behavior is assumed. At -40 °C the spectrum exhibits sharp signals that could be assigned to specific protons as will be discussed below.

The first notable feature of the spectrum at $-40\text{ }^{\circ}\text{C}$ is that for the proton in 4 position of the pyrazolate function only one signal is observed at 5.91 ppm. Therefore the ligands are expected to be chemically equivalent and, hence, **22** might exhibit a center of inversion in solution. This is in contrast to the solid state structure but in that case packing effects might cause the distortion of the symmetry of the complex.

However, eight signals for the protons of the four CH_2 units and eight signals of the eight protons of the two pyridine functions are observed and thus indicate diastereotopic and unsymmetric behavior.

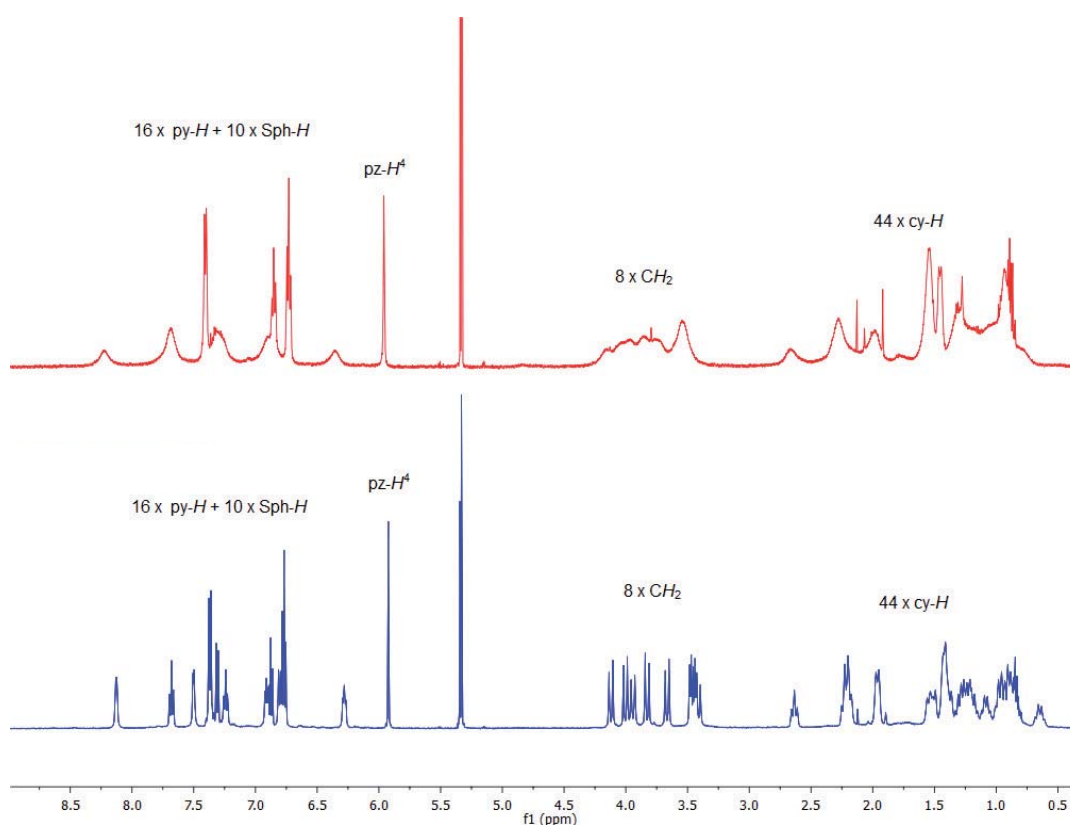


Figure 4.41: ^1H NMR spectra of complex **22** in CD_2Cl_2 at different temperatures, top: room temperature, bottom: $-40\text{ }^{\circ}\text{C}$.

In order to get further insight into the dynamic process of **22**, the aromatic region of the complex was investigated (Figure 4.42). The spectrum at room temperature exhibits four sharp signals which could be assigned to the proton at the 4 position of the pyrazolate unit (pz-H^4 (5.91 ppm)) and the protons of the thiophenolate coligands ($\text{Sph-H}^{\text{ortho}}$ (7.36 ppm), $\text{Sph-H}^{\text{meta}}$ 6.76 ppm and $\text{Sph-H}^{\text{para}}$ 6.87 ppm). These four signals do obviously not take

part in the dynamic process and hence it can be assumed that these coligands do not change their chemical surrounding.

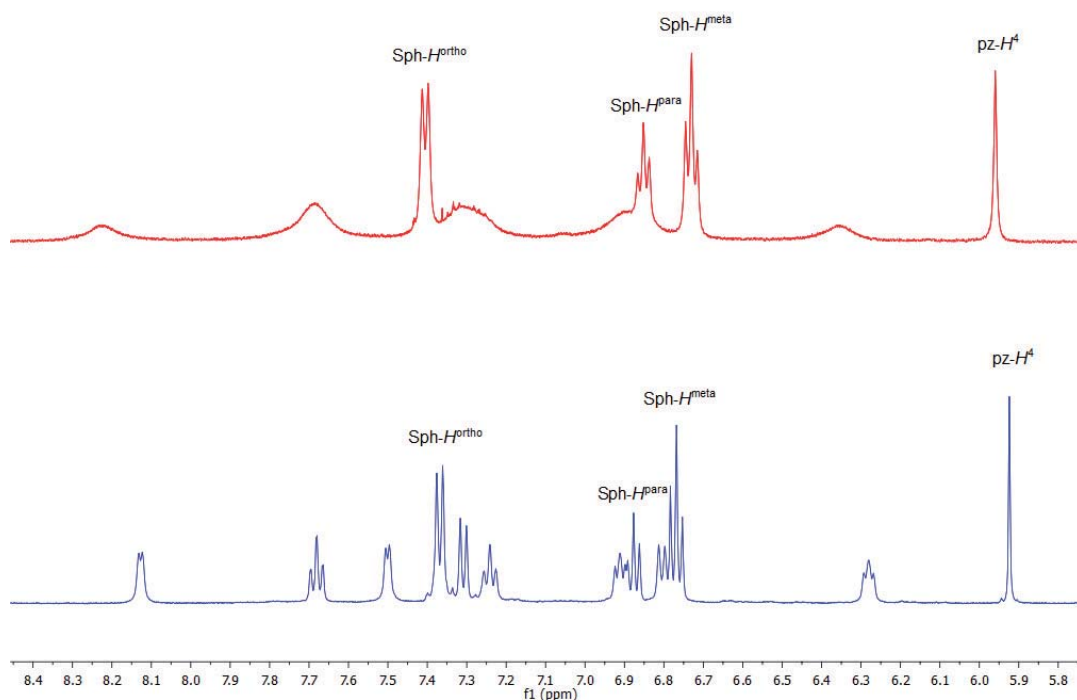


Figure 4.42: Aromatic region of the ^1H NMR spectra of complex **22** in CD_2Cl_2 at different temperatures, top: room temperature, bottom: $-40\text{ }^\circ\text{C}$.

To specify the dynamic process, **22** has been examined by 2D EXSY NMR at $-30\text{ }^\circ\text{C}$. The aromatic region of the resulting spectrum is depicted in Figure 4.43. The evaluation of the data revealed that the observed signals represent exchange peaks between the pyridine protons of the two sidearms. Hence a coordination exchange of the ligand is expected and the suggested equilibrium is depicted in Scheme 4.27.

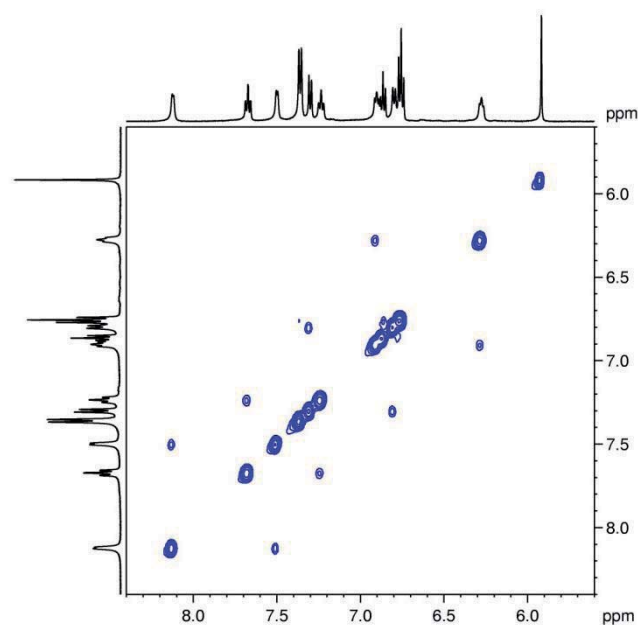
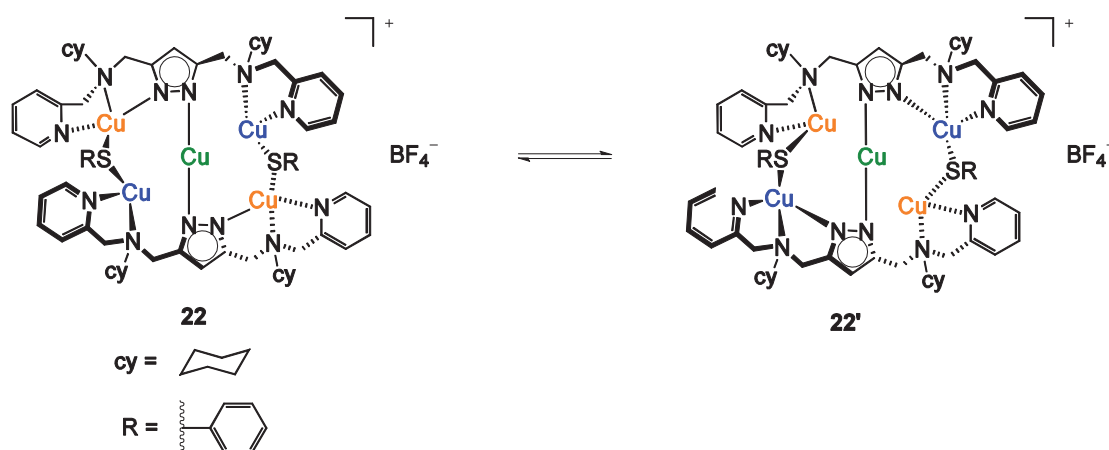


Figure 4.43: Aromatic region of the 2D EXSY NMR spectrum of **22** in CD_2Cl_2 at $-30\text{ }^\circ\text{C}$.



Scheme 4.27: Suggested equilibrium of **22** in solution.

As already described in chapter 4.8.2 the copper atoms in **22** can be divided into three different groups due to their coordination spheres. These different groups are highlighted with different colors (Scheme 4.27). The green colored copper atom is linear coordinated and represents the center of inversion. The blue colored copper atoms are threefold coordinated and the orange colored copper atoms are fourfold coordinated. In **22'** the coordination of the green colored copper atom is switched to the other two N-donor atoms of the central pyrazolate units while the coordinations spheres of the blue and orange colored copper atoms are swapped. Although the exact transition state between the two

isomers could not be clarified, the suggested configurations of **22** and **22'** all are consistent with all present NMR data.

The rate constant of this process could be determined from the EXSY spectrum as $k_{22} = 0.2 \text{ s}^{-1}$ (at $-30 \text{ }^\circ\text{C}$). Hence the free energy barrier ΔG can be determined from the Eyring equation (equation (4)):

$$k_{22} = \frac{kT}{h} \exp\left(-\frac{\Delta G^\ddagger}{RT}\right) \quad (4)$$

In equation (4) k_{22} represents the rate constant of the process, k Boltzmann's constant, h Planck's constant, R the universal gas constant and T the temperature at which the spectrum was recorded.

Solving the equation leads to an energy barrier of $\Delta G = 63 \text{ kJ/mol}$. This corresponds to an energy barrier that typically leads to line broadening in NMR spectra at room temperature.

Further lowering of the temperature results in the complete freezing of the process and may allow the determination of the exact structure of **22** in solution.

Redox properties

21 features five sites that can potentially be involved in redox processes, namely the three cuprous ions that could be oxidized to the cupric state and the two S-atoms of the thiolate functions which could be oxidized to radicals RS^\cdot (perhaps giving disulfide in the end). Complex **22** features even seven potential redox-active sites since the complex has five copper ions and two thiolates. Since both complexes return their integrity in solution, the redox properties of both complexes have been investigated by cyclic voltammetry.

Both **21** and **22** feature ill-behaved responses in their cyclic voltammograms with irreversible redox processes only peak potentials shown in Figure 4.44 and Figure 4.45. Most likely, upon oxidation these complexes undergo major structural rearrangements.

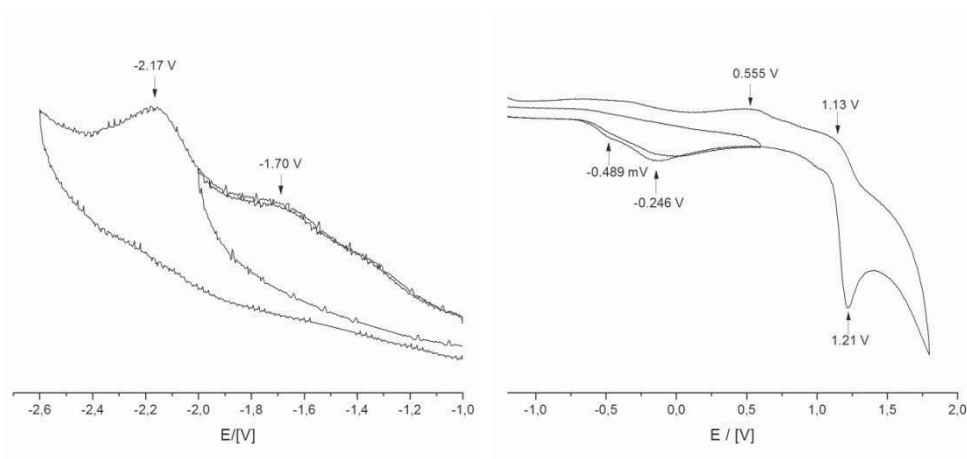


Figure 4.44: Cyclic voltammogram of **21** in MeCN vs. $\text{Cp}_2\text{Fe}/\text{Cp}_2\text{Fe}^+$. Left : range of -2.6 V - -1.0 V, right : range of -1.0 – 2.0 V.

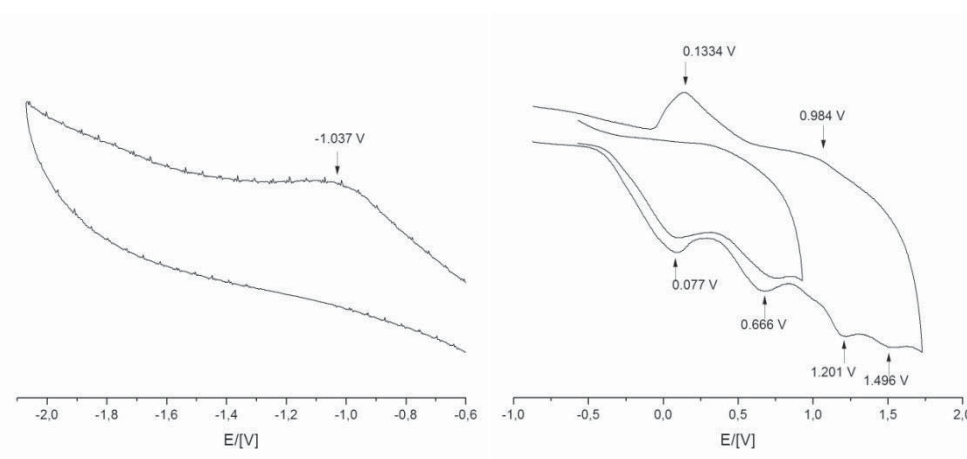


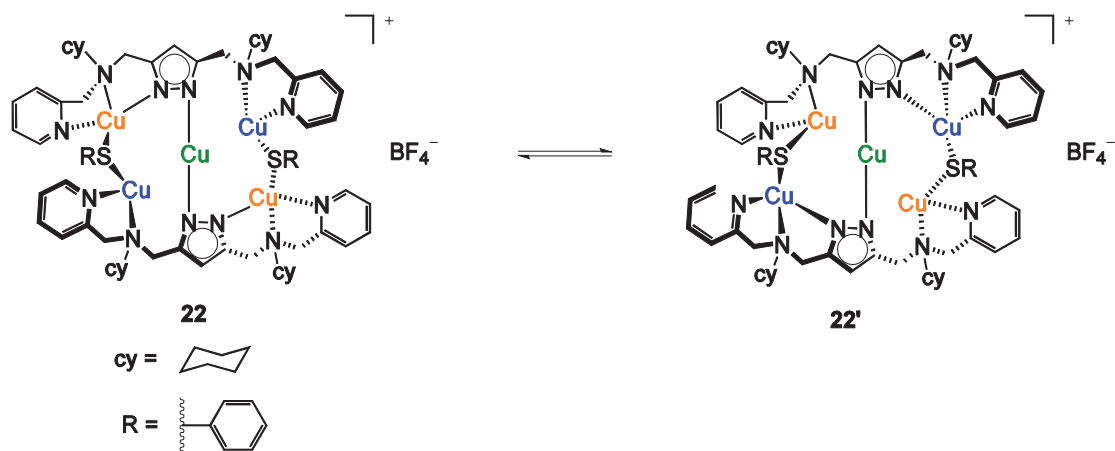
Figure 4.45: Cyclic voltammogram of **22** in MeCN vs. $\text{Cp}_2\text{Fe}/\text{Cp}_2\text{Fe}^+$. Left : range of -2.6 V - -1.0 V, right : range of -1.0 – 2.0 V.

4.8.4. Summary and Outlook

In summary, it was possible to synthesize and fully characterize the first two copper(I) thiolate complexes with compartmental pyrazolate ligands. The structure analysis revealed that **21** is a neutral trinuclear $\text{L}^4\text{Cu}_3(\text{SPh})_2$ species and **22** is a pentanuclear $[\text{L}^4_2\text{Cu}_5(\text{SPh})_2]^+$ species. The trinuclear complex **21** can be transformed into the pentanuclear complex **22** upon reaction with *in situ* generated $[\text{L}^4\text{Cu}_2](\text{BF}_4)$.

The stability of **22** in solution was investigated *via* ^1H NMR spectroscopy and revealed that **22** coexists with **22'** in solution (Scheme 4.28). The energy barrier of the

transformation has been determined to $\Delta G = 63$ kJ/mol and thus giving rise to line broadening in the NMR spectra at room temperature due to the dynamic process.



Scheme 4.28: Equilibrium in solution of 22.

5. Summary

The objective of the work was the synthesis of multinuclear copper complexes that are based on compartmental pyrazolate ligands and have sulfide or thiolate coligands. The work was inspired by the search for model systems for the Cu_Z -center, i.e. Cu_4S or Cu_4S_2 sites of N_2OR .

Therefore nine different compartmental pyrazolate ligands have been synthesized with different N-donor sidechains. The ligand precursors HL^1 ^[118], HL^2 ^[105], HL^3 ^[123] and HL^9 ^[119] have been synthesized according to literature procedures. Additionally it was possible to optimize the purification of the ligand precursors HL^4 ^[123] and HL^6 ^[101] and to design and synthesize the new potential ligands HL^5 , HL^7 and HL^8 (Figure 5.1).

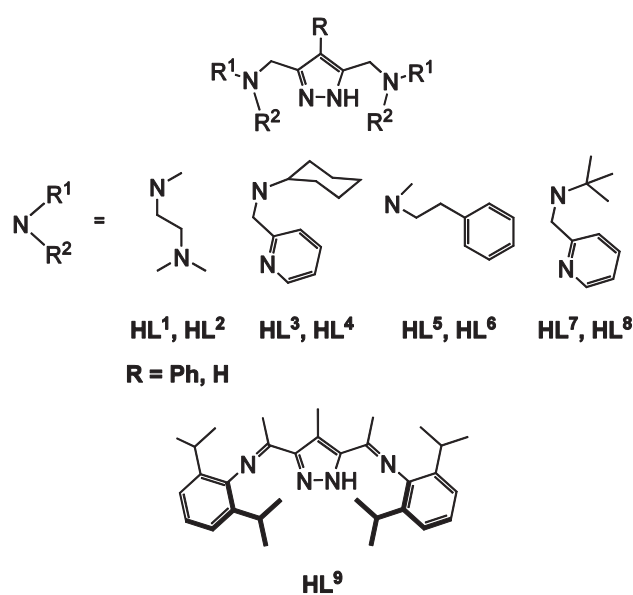


Figure 5.1: Synthesized ligand precursors HL^1 - HL^9 .

Multinuclear copper complexes as precursor complexes for ligand exchange reactions

Employing the ligands $[\text{L}^2]^-$, $[\text{L}^3]^-$, $[\text{L}^4]^-$ and $[\text{L}^9]^-$ it was possible to synthesize and fully characterize eight different binuclear copper(II) halide complexes of the type $\text{L}^{2-4,9}\text{Cu}_2\text{X}_3$ ($\text{X} = \text{Cl, Br}$) (Figure 5.2).

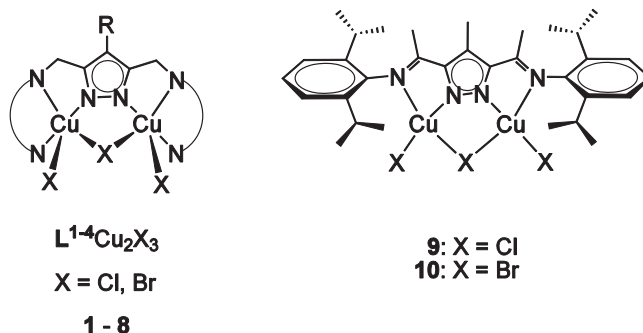


Figure 5.2: Synthesized complexes **1-10**.

Since binuclear copper(II) complexes possess two unpaired electrons, their magnetic interaction in the new complexes has been investigated. The results showed that the magnitude of the antiferromagnetic interaction depends on various structural parameters that are determined by the pyrazolate scaffold and the choice of chloride or bromide as exogenous ligands. Additionally DFT-calculations of the complexes have confirmed that both bridging ligands, the halide ligand and the pyrazolate bridge are involved in the magnetic coupling in complexes **1 - 8**. The complexes $L^9Cu_2X_3$ ($X = Cl, Br$) (**9, 10**) show very strong coupling of around range 330 cm^{-1} which can be explained by the coplanarity of the two $d_{x^2-y^2}$ magnetic orbitals and the central pyrazolate bridge.

To obtain complexes with a higher nuclearity than two, $[L^9]^-$ was successfully reacted with a mixture of copper(II) chloride and copper(II) triflate yielding a tetranuclear copper species with a $Cu_4Cl_2(\mu\text{-pz})_2$ core. The copper ions are additionally coordinated by triflate anions, but due to severe disorder of the triflate anions the exact structure in the solid state could not be clarified. Therefore **11** could not be further characterized and was not employed in ligand exchange reactions either.

The exploration of the coordination behavior of the ligands towards copper(I) bromide focused on the ligands $[L^5]^-$ and $[L^6]^-$. In case of $[L^6]^-$ the unexpected formation of a neutral nonanuclear copper bromide complex **18** was obtained (Figure 5.3). The central $Cu_3(\mu\text{-pz})_3$ core is common in pyrazolate/copper(I) chemistry,^[165-167] but **18** is the first complex in which a pyrazolate ligand with multidentate N-donor sidearms yield this motif that is additionally surrounded by three peripheral $\{Cu_2Br_2\}$ -units.

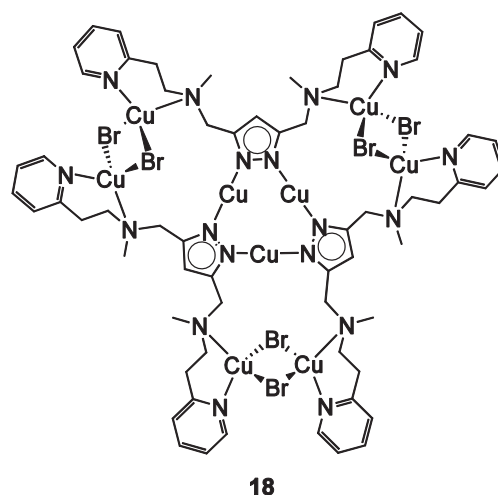


Figure 5.3: Synthesized pyrazolate-based copper(I) bromide complex **18**.

Ligand exchange reactions of complexes LCu_2X_3

In view of the Cu_4S or Cu_4S_2 site of N_2OR numerous attempts were carried out to exchange the halide ligands in LCu_2X_3 by sulfide or (in a somewhat related approach) by sulfate. The reaction of complexes **1** and **6** with silver sulfate led to the formation and isolation of five different pyrazolate-based copper-sulfate complexes. These five complexes reveal four different coordination patterns that are determined by the employed stoichiometric ligand to Ag_2SO_4 ratio (see Figure 5.4). The binding modes of the sulfate in complexes **13** and **15** had not been reported before.

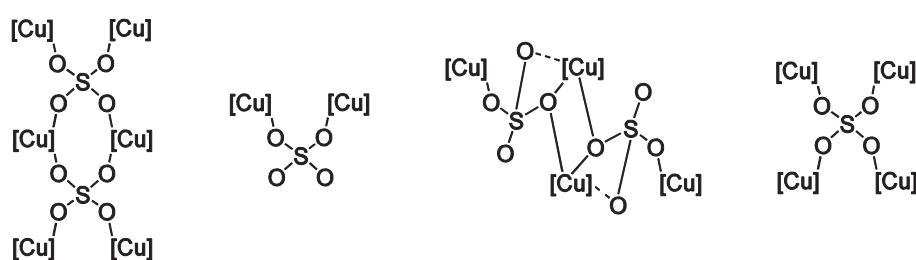


Figure 5.4: Binding modes of the sulfate ligands in complexes **13** – **17**.

Magnetic interactions of the copper(II) ion in complexes **14**, **15** and **17** have been investigated. All three complexes feature antiferromagnetic coupling and the trend could be correlated to structural parameters.

Furthermore the reactivity of **1** towards Na₂S, Li₂S, NaSCPh₃ and (TMS)₂S as sulfur-transfer reagents has been investigated. Although a reaction could be observed in all cases, it was not possible to isolate and identify products.

Further synthetic pathway towards copper-sulfur complexes were the oxidation of the *in situ* formed intermediate [L^{1,2}Cu₂]⁺ with elemental sulfur and the ligand exchange reaction of the *in situ* formed intermediate L³⁻⁶Cu₂X (X = Br, Cl) with (TMS)₂S. In all cases a reaction could be observed, but again it was not possible to isolate and identify any of the products.

Mononuclear copper(I) thioether complexes

Two mononuclear copper(I) complexes [L^{S1,2}Cu]Y (Y = SO₃CF, PF₆) coordinated by dithioether ligands were synthesized and fully characterized. They may become valuable copper(I) sources for the preparation of heteroleptic complexes [LL^{S,1,2}Cu₂]⁺ (L = pyrazolate-based ligand). However, initial experiments in that direction were not successful until now.

Multinuclear pyrazolate-based copper(I) thiolate complexes

The ability of oligonuclear pyrazolate-based copper complexes to bind thiolate coligands has been explored, and, indeed, the first two heteroleptic pyrazolate-based copper(I) thiolate complexes could be isolated: the neutral trinuclear complex L⁴Cu₃(SPh)₂ (**21**) and the pentanuclear complex **22** [L⁴₂Cu₅(SPh)₂](BF₄). Both complexes have been fully characterized. **21** transforms into **22** upon reaction with [L⁴Cu₂](BF₄) that is prepared *in situ*.

The stability of **22** in solution was investigated *via* ¹H NMR spectroscopy and revealed that **22** coexists with **22'** in solution. The energy barrier of the transformation has been determined to ΔG = 63 kJ/mol and thus giving rise to line broadening in the NMR spectra at room temperature due to the dynamic process.

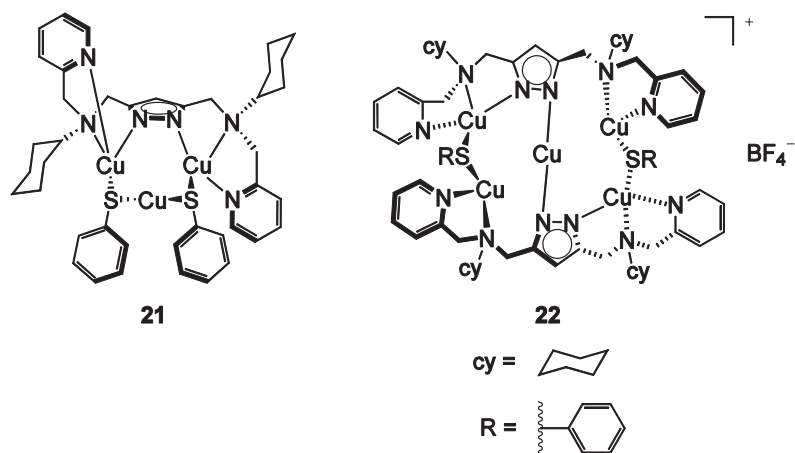


Figure 5.5: Synthesized complexes **21** and **22**.

The stability of **22** in solution was investigated *via* ^1H NMR spectroscopy and revealed that **22** coexists with **22'** in solution. The energy barrier of the transformation has been determined to $\Delta G = 63$ kJ/mol.



6. Experimental Section

General considerations

Equipment: The synthesis of air sensitive materials as carried out under a dry and oxygen-free argon atmosphere using standard Schlenk techniques.

Solvents: Solvents were dried according to established procedures, in particular: acetonitrile (potassium hydride), benzene (sodium), dichloromethane (potassium hydride), diethylether (sodium), ethanol (magnesium), methanol (magnesium), tetrahydrofuran (sodium and potassium). Deuterated solvents were dried and distilled according to the undeuterated analogues. All solvents were degassed and saturated with argon prior to use.

NMR-Spectroscopy: ^1H -NMR and ^{13}C -NMR spectra have been recorded on a Bruker Avance 200 MHz, 300 MHz or 500 MHz spectrometer. ^1H and ^{13}C chemical shifts are reported in ppm relative to residual solvent signals of CDCl_3 (7.26 ppm and 77.0 ppm), CD_3CN (1.94 ppm and 118.3 ppm) or CD_2Cl_2 (5.32 ppm and 53.8 ppm).

UV/vis-Spectroscopy: UV/vis-spectra of solid compounds (diffuse reflectance) were recorded with a CARY 5000 spectrometer (Varian) as a mixture with potassium bromide. UV/vis spectra in solution were recorded either on a Specord S100 (ANALYTIK JENA), on a CARY 50 Spectrometer (Varian) or on a CARY 5000 spectrometer (Varian). All solutions have been measured in (Schlenk) quartz cuvettes.

Mass-Spectrometry: ESI-MS spectra were recorded either on a Bruker HCT Ultra spectrometer or on a Thermo Finnigan Trace LCQ spectrometer. FD-MS spectra were recorded on a AccuTOF spectrometer (Joel). The used voltage for the ionization was 10 kV.

Infrared spectroscopy: Infrared spectra (KBr pellet, sodium chloride windows and solution) were recorded on a Digilab Excalibur FTS 3000 spectrometer.

Elemental Analysis: Microanalyses were performed by the “Analytical Laboratory of the Institute of Inorganic Chemistry at the University of Göttingen”. The determination of

carbon, hydrogen, nitrogen and sulfur percentage was performed on a Vario EL III (Elementar).

Magnetic susceptibility measurements: Temperature dependent magnetic susceptibilities were measured in the temperature range 2 K – 295 K by using a SQUID magnetometer (Quantum Design MPMS XL-5) at 5000 Oe. The powdered samples were contained in a gel bucket and fixed in a non-magnetic sample holder. Simulation of the experimental data with full-matrix diagonalization of exchange coupling and Zeeman splitting was performed with the *julX* program.^[198]

Cyclic voltammetry: Cyclovoltammetric measurements have been performed on a Potentiostat/Galvanostat model 263A (Perkin-Elmer). The measurements were carried out at room temperature using either MeCN or DCM/0.1 M [NBu₄]PF₆ as solvent. A glassy carbon electrode was used as working electrode, platinum as counter electrode and silver as reference electrode. As internal standard either ferrocene or decamethylferrocene was added. All potentials were calculated against ferrocen/ferrocinium couple.

Crystallographie: X-ray data were collected at 133 K on a STOE IPDS II diffractometer with graphite monochromated Mo-K_α-radiation ($\lambda = 0.71073 \text{ \AA}$). In addition to corrections in terms of Lorentz and polarization effects,^[199] absorption corrections of the crystallographic data were performed.^[200]

X-ray chrystallographic data of **11** were measured on a Bruker three circle diffractometer equipped with SMART 6000 CCD detector using Cu-K_α radiation ($\lambda = 1.54178$) at 100 K.

X-ray data of **13** were collected at 100 K on a Bruker D8 Goniometer Platform equipped with an Apex II CCD X-ray detector and an Incoatec microfocus source with mirror optics with Mo-K_α-radiation ($\lambda = 0.71073 \text{ \AA}$). The absorption correction was performed with SADABS.^[201] The crystal structures were solved and refined using the programs SHELXS-97^[202] and SHELXL-97.^[203-204]

X-ray data of complexes **21** and **22** have been measured in cooperation with M. Granitzka.^[205]

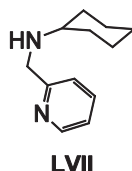
*Chemicals:*

XLVIII,^[119] **XLIX**,^[120] **LIV**,^[122] **LV**,^[109] **HL**¹,^[118] **HL**²,^[105] **HL**³^[123] and **HL**⁹^[119] were prepared according to literature procedures. All other chemicals were used as purchased.



6.1. Ligand synthesis

6.1.1. Preparation of *N*-(2-picolyl)-cyclohexylamine (LVII)



The literature procedure for compound **LVII** was optimized.^[206]

2-Pyridinecarboxaldehyde (16.1 g, 150 mmol, 1.0 eq.) was dissolved in MeOH (100 mL) and cyclohexylamine (15.2 g, 150 mmol, 1.0 eq.) was added dropwise at 0 °C. The mixture was allowed to warm up to room temperature, stirred for one hour and cooled down again to 0 °C. Subsequently sodium borohydride (5.70 g, 150 mmol, 1.0 eq.) was added. The reaction mixture was warmed up and stirred over night at room temperature. For workup the solution was cooled to 0 °C and a pH value of 3 was adjusted with concentrated HCl. The solvent was removed under vacuum and the residue dissolved in water (50 mL). The aqueous phase was extracted with DCM (4 x 50 mL). The pH value was brought to 8 with a saturated Na₂CO₃ solution and the aqueous phase was extracted again with DCM (5 x 50 mL). The combined organic phases were dried with MgSO₄ and the solvent evaporated. The resulting yellow solid was dried under vacuum (21.7 g, 110 mmol, 76 %).

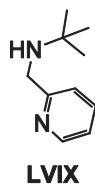
¹H NMR (500 MHz, CDCl₃): δ [ppm] = 1.21 – 1.43 (m, 3 H, cy), 1.74 – 1.77 (m, 2 H, cy), 2.10 (d, ³J_{H,H} = 7.35 Hz, 2 H, cy), 2.74 – 2.80 (m, 1 H, cy), 4.18 (s, 2 H, py-CH₂), 7.19 – 7.22 (m, 1 H, py-H⁵), 7.50 (br, 1 H, NH), 7.57 – 7.59 (m, 1 H, py-H³), 7.66 – 7.69 (m, 1 H, py-H⁴), 8.52-8.53 (m, 1 H, py-H⁶).

¹³C {¹H} NMR (125 MHz, CDCl₃): δ [ppm] = 24.5 (cy-C⁴), 25.1 (2 C, cy-C^{3,5}), 30.3 (cy-C^{2,6}), 49.1 (py-CH₂), 56.3 (cy-C¹), 123 (py-C⁴), 124 (py-C³), 137 (py-C⁵), 149 (py-C⁶), 154 (py-C²).

MS (ESI⁺, MeOH) m/z (%): 191 (92, [M+H]⁺), 109 (100 [py-CH₂-NH₃]⁺), 92 (69, [py-CH₂]⁺).



6.1.2. Preparation of *N*-(pyridine-2-ylmethyl)-^tbutylamine (LVIX)



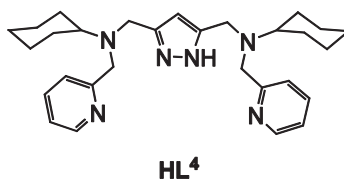
Compound **LVIX** (22.7 g, 138 mmol, 46 %) was synthesized according to the synthesis described for **LVII**.

¹H NMR (500 MHz, CDCl₃): δ [ppm] = 1.33 (s, 9 H, ^tBu-C(CH₃)₃), 4.07 (s, 2 H, py-CH₂), 4.76 (s, 1 H, NH), 7.18-7.24 (m, 1 H, py-H⁵), 7.36 (d, ³J_{H,H} = 6.25 Hz, 1 H, py-H³), 7.68 (td, ³J_{H,H} = 6.25 Hz, ⁴J_{H,H} = 3.13 Hz, 1 H, py-H⁴), 8.53 (d, ³J_{H,H} = 6.25 Hz, 1 H, py-H⁶).

¹³C {¹H} NMR (125 MHz, CDCl₃): δ [ppm] = 26.2 (^tBu-C(CH₃)₃), 45.0 (py-CH₂), 57.6 (^tBu-C(CH₃)₃), 123 (py-C⁴), 124 (py-C⁵), 138 (py-C³), 149 (py-C⁶), 151 (py-C²).

MS (ESI⁺, MeOH) m/z (%): 191 (92, [M+H]⁺), 109 (100 [py-CH₂-NH₃]⁺), 92 (69, [py-CH₂]⁺).

6.1.3. Preparation of HL⁴



A suspension of anhydrous sodium carbonate (5.56 g, 52.5 mmol, 10 eq.), 3,5-bis(chloromethyl)-1-(tetrahydro-2*H*-pyran-2-yl)-1*H*-pyrazol (**LV**) (1.31 g, 5.26 mmol, 1 eq.) and *N*-(2-picolyl)-cyclohexylamine (**LVII**) (2.00 g, 10.5 mmol, 2.2 eq.) in MeCN (200 mL) was heated to reflux for 4 days, cooled to room temperature and filtered. The solvent was evaporated and the residue dried in vacuo. The residue was

dissolved in EtOH (50 mL) and subsequently ethanolic HCl (50 mL) was added. After stirring the solution for one hour Et₂O (300 mL) was added. The solution was stirred for 5 min and filtered. The residue was dried and treated with aqueous NaOH (1.0 g in 200 mL H₂O). The product was extracted with DCM (2 x 50 mL). The aqueous phase was brought to pH 12 with NaOH solution and extracted with DCM (6 x 50 mL) again. The combined organic phases were dried over MgSO₄, filtered and the solvent removed using rotary evaporation. The crude product was purified by column chromatography (neutral alumina, EE, EE:MeOH = 10:1, R_f = 0.55) obtaining a light brown solid (1.17 g, 2.48 mmol, 47 %).

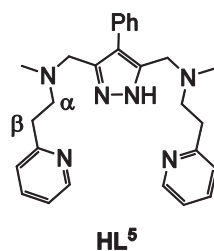
¹H NMR (300 MHz, C₆D₆): δ [ppm] = 0.95 – 1.34 (m, 10 H, cy-H^{2e-6e}), 1.56 (d, ³J_{H,H} = 9.7 Hz, 2 H, cy-H^{4a}), 1.72 (d, ³J_{H,H} = 11.6 Hz, 4 H, cy-H^{3a}, cy-H^{5a}), 1.84 (d, ³J_{H,H} = 12.1 Hz, 4 H, cy-H^{2a}, cy-H^{6a}), 2.54 (ddd, ³J_{H,H} = 11.3 Hz, ³J_{H,H} = 7.4 Hz, ⁴J_{H,H} = 3.3 Hz, 2 H, cy-H¹), 3.73 (s, 4 H, pz-CH₂), 3.80 (s, 4 H, py-CH₂), 6.05 (s, 1 H, pz-H⁴), 7.08 (ddd, ³J_{H,H} = 7.4 Hz, ³J_{H,H} = 4.9 Hz, ⁴J_{H,H} = 1.2 Hz, 2 H, py-H⁵), 7.44 (d, ³J_{H,H} = 7.8 Hz, 2 H, py-H³), 7.57 (td, ³J_{H,H} = 7.6 Hz, ⁴J_{H,H} = 1.8 Hz, 2 H, py-H⁴), 8.49 (ddd, ³J_{H,H} = 4.9 Hz, ⁴J_{H,H} = 1.7 Hz, ⁵J_{H,H} = 0.9 Hz, 2 H, py-H⁶).

¹³C {¹H} NMR (75 MHz, CDCl₃): δ [ppm] = 26.1 (cy-C³, cy-C⁵), 26.4 (cy-C⁴), 29.2 (cy-C², cy-C⁶), 47.2 (pz-CH₂), 56.0 (py-CH₂), 60.1 (cy-C¹), 103 (pz-C⁴), 122 (py-C⁵), 123 (py-C⁴), 137 (py-C²), 148 (pz-C³, pz-C⁵), 149 (py-C⁶), 161 (py-C²).

MS (ESI⁺, MeOH) m/z (%): 473 (100, [M+H]⁺), 495 (41, [M+Na]⁺).

IR (KBr) $\tilde{\nu}$ [cm⁻¹]: 3259 (vs), 3102 (w), 3075 (w), 3043 (w), 3001 (m), 2922 (vs), 2847 (vs), 2708 (w), 2668 (w), 1732 (w), 1588 (s), 1569 (s), 1470 (s), 1438 (s), 1382 (w), 1360 (m), 1344 (w), 1292(w), 1261 (m), 1240 (w), 1222 (w), 1159 (w), 1138 (m), 1108 (s), 1085 (w), 1045 (w), 996 (s), 969 (m), 951 (w), 904 (w), 891 (w), 874 (w), 843 (w), 816 (s), 795 (s), 760 (s), 729 (w), 679 (w), 612 (w), 508 (w), 471 (w).

Elemental analysis: Calcd. (%) for C₂₉H₄₀N₆: C 73.69, H 8.53, N 17.78. Found: C 73.08, H 8.80, N 17.45.

6.1.4. Preparation of HL⁵

A suspension of anhydrous sodium carbonate (25.0 g, 0.24 mol, 10 eq.), 3,5-bis(chloromethyl)-4-phenyl-1-(tetrahydro-2*H*-pyran-2-yl)-1*H*-pyrazol (**XLIX**) (7.81 g, 24 mmol, 1.0 eq.) and 2-[(2-methylamino)ethyl]-pyridine (**LVIII**) (6.54 g, 48 mmol, 2.0 eq.) in MeCN (500 mL) was heated to reflux for two days, cooled to room temperature and filtered. The solvent was evaporated and the residue was dried in vacuo. EtOH (200 mL) and ethanolic HCl (200 mL) were added. After stirring the solution for one hour at room temperature Et₂O (600 mL) was added. The solution was stirred further 5 min and filtered. The residue was dried and treated with aqueous NaOH solution (1.0 g in 200 mL H₂O). The product was extracted with DCM (2 x 100 mL). The aqueous phase was brought to pH 12 with NaOH solution and extracted with DCM (6 x 100 mL) again. The combined organic phases were dried with MgSO₄, filtered and the solvent removed using rotary evaporation. The crude product was purified by column chromatography (neutral alumina, EE:MeOH = 10:1, R_f = 0.83). A brown oil was obtained (6.34 g, 14 mmol, 60 %).

¹H NMR (300 MHz, CDCl₃): δ [ppm] = 2.31 (s, 6 H, 2 x CH₃), 2.90 (d, ³J_{H,H} = 10 Hz, 4 H, 2 x CH₂ (α)), 2.98 (d, ³J_{H,H} = 10 Hz, 4 H, 2 x CH₂ (β)), 3.67 (s, 4 H, pz-CH₂), 7.11 – 7.14 (m, 2 H, py-*H*⁵), 7.27 – 7.35 (m, 2 H, py-*H*³), 7.33 (s, 5 H, ph), 7.57 (td, ³J_{H,H} = 10 Hz, ⁴J_{H,H} = 5 Hz, 2 H, py-*H*⁴), 8.56 - 8.58 (m, 2 H, py-*H*⁶).

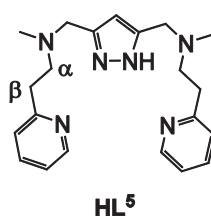
¹³C {¹H} NMR (75 MHz, CDCl₃): δ [ppm] = 35.5 (CH₂ (β)), 42.2 (CH₃), 52.4 (CH₂, pz-CH₂), 56.5 (CH₂ (α)), 119 (py-*C*⁵), 121 (py-*C*³), 123 (ph-*C*^{ipso}), 126 (ph-*C*^{ortho}), 128 (ph-*C*^{para}), 130 (ph-*C*^{meta}), 133 (py-*C*⁴), 136 (pz-*C*⁴), 149 (py-*C*⁶), 160 (py-*C*²), pz-*C*^{3,5} could not be observed.

MS (ESI⁺, MeOH) m/z (%): 903 (18, [2M + Na]⁺), 463 (63, [M + Na]⁺), 441 (100, [M + H]⁺), 327 (25, [-SA+Na]⁺), 305 (41, [-SA]⁺).

IR (MeCN) $\tilde{\nu}$ [cm⁻¹]: 4436 (w), 4363 (w), 3323 (w), 3163 (m), 3000 (m), 2943 (m), 2623 (w), 2409 (w), 2291 (s), 2249 (vs), 1440 (s), 1375 (s), 1039 (s), 918 (m), 750 (m).

Elemental analysis: Calcd. (%) for C₂₇H₃₂N₆·0.5 H₂O: C 72.13, H 7.40, N 18.69. Found: C 72.59, H 7.49, N 18.65.

6.1.5. Preparation of HL⁶



HL⁶ was prepared according to the literature procedure.^[101] The obtained yellow oil (5.69 g, 15.6 mmol, 65 %) was purified by column chromatography (neutral alumina, EE:MeOH = 10:1, R_f = 0.87).

¹H NMR (500 MHz, CDCl₃): δ [ppm] = 2.29 (s, 6 H, 2 x CH₃), 2.81 (t, ³J_{H,H} = 7.5 Hz, 4 H, 2 x CH₂(α)), 2.99 (t, ³J_{H,H} = 7.5 Hz, 4 H, 2 x CH₂(β)), 3.63 (s, 4 H, 2 x pz-CH₂), 6.03 (s, 1 H, pz-H⁴), 7.09 (dd, ³J_{H,H} = 7.4 Hz, 5.0 Hz, 2 H, 2 x py-H⁵), 7.13 (d, ³J_{H,H} = 7.8 Hz, 2 H, 2 x py-H³), 7.56 (td, ³J_{H,H} = 7.7 Hz, 1.8 Hz, 2 H, 2 x py-H⁴), 8.51 (d, ³J_{H,H} = 4.5 Hz, 2 H, 2 x py-H⁶).

¹³C {¹H} NMR (125 MHz, CDCl₃): δ [ppm] = 35.9 (2 CH₂(β)), 42.3 (2 CH₃), 53.6 (2 pzCH₂N), 56.7 (2 CH₂(α)), 105 (pz-C⁴), 121 (2 py-C⁵), 123 (2 py-C³), 137 (2 py-C⁴), 149 (2 py-C⁶), 160 (2 py-C²), pz-C^{3,5} could not be observed.

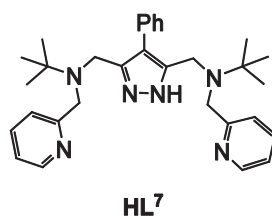
MS (ESI⁺, MeOH) m/z (%): 365 (100 [M + H]⁺).

IR (NaCl-plates) $\tilde{\nu}$ [cm⁻¹]: 3360 (s), 3207 (s), 2949 (s), 1847 (s), 2801 (s), 2217 (w), 1659 (w), 1954 (s), 1571 (m), 1475 (s), 1439 (s), 1358 (m), 1311 (w), 1253 (w), 1225 (w),

1180 (w), 1149 (m), 1122 (m), 1094 (w), 1049 (m), 1001 (m), 871 (w), 766 (w), 633 (w), 609 (w).

Elemental analysis: Calcd. (%) for $C_{21}H_{28}N_6 \cdot 2 H_2O$: C 62.96, H 8.06, N 20.99. Found: C 61.37, H 8.05, N 20.53.

6.1.6. Preparation of HL⁷



A suspension of anhydrous sodium carbonate (2.35 g, 22 mmol, 10 eq.), 3,5-bis(chloromethyl)-4-phenyl-1-(tetrahydro-2*H*-pyran-2-yl)-1*H*-pyrazol (**XLIX**) (716 mg, 2.2 mmol, 1 eq.) and *N*-(pyridine-2-ylmethyl)-*t*-butylamine (**LVIX**) (788 mg, 4.8 mmol, 2.2 eq.) in MeCN (60 mL) was heated to reflux for 4 days, then cooled to room temperature and filtered. The solvent was evaporated and the residue was dried in vacuo. Then EtOH (20 mL) and ethanolic HCl (20 mL) were added. After stirring for one hour Et₂O (60 mL) was added. The solution was stirred for a few more moments and filtered. The residue was dried, treated with aqueous NaOH solution (1.0 g in 200 mL H₂O). The product was extracted with DCM (2 x 50 mL). The aqueous phase was brought to pH 12 with NaOH solution and extracted with DCM (6 x 50 mL) again. The combined organic phases were dried with MgSO₄, filtered and the solvent removed using rotary evaporation. The crude product was purified by column chromatography (neutral alumina, EE, EE:MeOH = 10:1, MeOH, R_f = 0.67). A yellow solid (308 mg, 0.62 mmol, 28 %) was obtained.

¹H NMR (300 MHz, CDCl₃): δ [ppm] = 0.99 (s, 18 H, 2 x ^tBu-C(CH₃)₃), 3.86 (s, 4 H, 2 x pzCH₂N), 3.91 (s, 4 H, 2 x NCH₂-py), 6.98 (t, ³J_{H,H} = 9.38 Hz, 2 H, py-*H*⁵), 7.19 – 7.41 (m, 9 H, ph, py-*H*³, py-*H*⁴), 8.44 (d, ³J_{H,H} = 9.38 Hz, 2 H, py-*H*⁶).

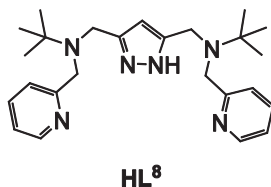
^{13}C $\{^1\text{H}\}$ NMR (75 MHz, CDCl_3): δ [ppm] = 26.9 (3 $^t\text{Bu-C}(\text{CH}_3)_3$), 46.0 (pz- CH_2), 55.1 (py- CH_2), 121 (py- C^5), 123 (py- C^3), 126 (ph- C^{para}), 128 (2 ph- C^{meta}), 130 (2 ph- C^{ortho}), 136 (py- C^4), 148 (py- C^6), $^t\text{Bu-C}(\text{CH}_3)_3$, py- C^2 , pz- $\text{C}^{3,4,5}$, ph- C^{ipso} could not be observed.

MS (ESI $^+$, MeOH) m/z (%): 519 (14 $[\text{M}+\text{Na}]^+$), 497 (100 $[\text{M}+\text{H}]^+$), 333 (72 $[-\text{SA}]^+$), 277 (23).

IR (MeCN) $\tilde{\nu}$ [cm^{-1}]: 4443 (w), 4359 (w), 3626 (m), 3545 (m), 3163 (m), 3005 (m), 2943 (m), 2630 (w), 2291 (m), 2252 (vs), 1631 (m), 1446 (s), 1377 (s), 1037 (m), 918 (m), 752 (m).

Elemental analysis: Calcd. (%) for $\text{C}_{31}\text{H}_{40}\text{N}_6$: C 74.96, H 8.11, N 16.92. Found: C 71.58, H 8.27, N 15.95.

6.1.7. Preparation of HL 8



A suspension of anhydrous sodium carbonate (5.30 g, 50 mmol, 10 eq.), 3,5-bis(chloromethyl)-1-(tetrahydro-2*H*-pyran-2-yl)-1*H*-pyrazol (**LV**) (1.25 g, 5.0 mmol, 1.0 eq.) and *N*-(pyridin-2-ylmethyl)-*t*-butylamin (**LVIX**) (2.46 g, 15 mmol, 3.0 eq.) in MeCN (150 mL) was heated to reflux for 4 days, then cooled to room temperature and filtered. The solvent was evaporated and the residue was dried in vacuo. Then EtOH (50 mL) and ethanolic HCl (50 mL) were added. After stirring for one hour Et $_2$ O (150 mL) was added. The solution was stirred for 5 min and filtered. The residue was dried, treated with aqueous NaOH solution (1.0 g in 200 mL H $_2$ O). The product was extracted with DCM (2 x 50 mL). The aqueous phase was brought to pH 12 with NaOH solution and extracted with DCM (6 x 50 mL) again. The combined organic phases were dried with MgSO $_4$, filtered and dried in vacuo. The crude product was purified by column

chromatography (neutral alumina, EE, EE:MeOH = 10:1, MeOH, $R_f = 0.77$). A yellow solid (488 mg, 1.16 mmol, 23 %) was obtained.

^1H NMR (500 MHz, CDCl_3): δ [ppm] = 1.07 (s, 18 H, $^t\text{Bu-C}(\text{CH}_3)_3$), 3.77 (s, 4 H, pz- CH_2), 3.87 (s, 4 H, py- CH_2), 5.98 (s, 1 H, pz- H^4), 7.02 (t, $^3J_{\text{H,H}} = 14.7$ Hz, 2 H, py- H^5), 7.35 (d, $^3J_{\text{H,H}} = 14.7$ Hz, 2 H, py- H^3), 7.49 (td, $^3J_{\text{H,H}} = 14.7$ Hz, $^4J_{\text{H,H}} = 7.35$ Hz, 2 H, py- H^4), 8.46 (d, $^3J_{\text{H,H}} = 14.71$ Hz, 2 H, py- H^6).

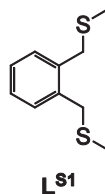
^{13}C $\{^1\text{H}\}$ NMR (125 MHz, CDCl_3): δ [ppm] = 27.2 ($^t\text{Bu-C}(\text{CH}_3)_3$), 46.7 (pz- CH_2), 55.4 (py- CH_2), 102 (pz- C^4), 121 (py- C^5), 123 (py- C^3), 136 (py- C^4), 148 (py- C^6). $^t\text{Bu-C}(\text{CH}_3)_3$, py- C^2 and pz- $\text{C}^{3,5}$ were not observed.

MS (ESI $^+$, MeOH) m/z (%): 863 (21 [$2\text{M}+\text{Na}$] $^+$), 443 (64 [$\text{M}+\text{Na}$] $^+$), 421 (100 [$\text{M}+\text{H}$] $^+$), 279 (36 [$-\text{SA}+\text{Na}$] $^+$), 257 (65, [$-\text{SA}$] $^+$), 201 (28).

IR (MeCN) $\tilde{\nu}$ [cm^{-1}]: 4432 (w), 4270 (w), 4035 (w), 3977 (w), 3163 (m), 3005 (m), 2943 (m), 2627 (w), 2414 (w), 2291 (m), 2252 (vs), 1442 (s), 1377 (s), 1037 (m), 918 (m), 748 (m).

Elemental analysis: Calcd. (%) for $\text{C}_{25}\text{H}_{36}\text{N}_6$: C 69.89, H 8.68, N 19.56. Found: C 69.89, H 8.78, N 19.46.

6.1.8. Synthesis of L^{S1}



L^{S1} was synthesized according to a modified literature procedure.^[188]

1,2-Benzenedimethanethiole (1.90 g, 11 mmol, 1.0 eq.) was dissolved in abs. THF and cooled to 0 °C. $^n\text{BuLi}$ (10 mL, 25.0 mmol, 2.5 M in hexane, 2.2 eq.) was added dropwise. After stirring for 1 h at 0 °C MeI (1.4 mL, 22 mmol, 2.0 eq.) was added. The reaction

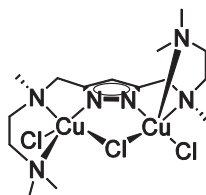
mixture was warmed to room temperature and stirred over night. For workup half-saturated NaCl solution (80 mL) was added and the THF was evaporated. The aqueous phase was extracted with DCM (2 x 100 mL). The combined organic phases were dried in vacuo to yield the product as a light-yellow oil that crystallizes on standing (1.45 g, 7.32 mmol, 66.6 %).

^1H NMR (300 MHz, CDCl_3): δ [ppm] = 2.06 (s, 6 H, 2 x CH_3), 3.88 (s, 4 H, 2 x CH_2), 7.24 (m, 4 H, ph).

MS (ESI^+ , MeCN) m/z (%): 237 (60, $[\text{M}+\text{K}]^+$), 151 (100, $[\text{M}-\text{SMe}]^+$).

6.2. Synthesis of complexes

6.2.1. Preparation of $\text{L}^2\text{Cu}_2\text{Cl}_3$ (**3**)



3

A solution of HL^2 (148 mg, 0.5 mmol, 1.0 eq.) in MeOH (20 mL) was treated with KO^tBu (56 mg, 0.5 mmol, 1.0 eq.) and stirred for 15 min. Then CuCl_2 (135 mg, 1.0 mmol, 2.0 eq) was added and the resulting green solution was stirred over night at room temperature. After removing all volatile compounds the remaining green solid was dissolved in MeCN (10 mL) and filtered. Slow diffusion of Et_2O into the filtrate led to the formation of green crystals (170 mg, 0.32 mmol, 63 %).

IR (KBr) $\tilde{\nu}$ [cm^{-1}]: 4398 (w), 3425 (m), 3000 (m), 2970 (s), 2877 (s), 2863 (s), 2823 (vs), 2788 (s), 1631 (w), 1517 (m), 1460 (vs), 1388 (m), 1335 (s), 1299 (m), 1285 (s), 1255 (m), 1244 (m), 1178 (m), 1162 (m), 1139 (w), 1100 (m), 1068 (m), 1039 (m), 1021 (m),

999 (s), 988 (m), 956 (s), 937 (m), 841 (m), 801 (s), 766 (s), 666 (w), 598 (w), 480 (w), 422 (m).

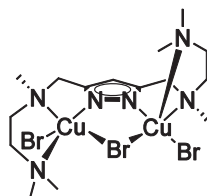
MS (ESI⁺, MeCN) *m/z* (%): 423 (40, [LCu₂+H]⁺), 257 (100, [LCu-CH₃N(CH₂)₂N(CH₃)₂]⁺).

UV/vis (MeCN) λ [nm] (ϵ [L·mol⁻¹·cm⁻¹]): 197 (11300), 218 (7760), 269 (8700), 304 (6490), 446 (512), 834 (157).

UV/vis (KBr) λ [nm]: 221, 264, 308, 463, 840.

Elemental analysis: Calcd. (%) for C₁₅H₂₁N₆Cu₂Cl₃: C 34.06, H 5.91, N 15.89. Found: C 34.01, H 6.18, N 16.36.

6.2.2. Preparation of L²Cu₂Br₃ (4)



4

A solution of **HL**² (148 mg, 0.5 mmol, 1.0 eq.) in MeOH (20 mL) was treated with KO^tBu (56 mg, 0.5 mmol, 1.0 eq.) and stirred for 15 min at room temperature. Then CuBr₂ (223 mg, 1.0 mmol, 2.0 eq.) was added and the resulting green solution was stirred over night at room temperature. After removing all volatile compounds the remaining green solid was dissolved in MeCN (10 mL) and filtered. Slow diffusion of Et₂O into the filtrate led to the formation of brown crystals (192 mg, 0.29 mmol, 58 %).

IR (KBr) $\tilde{\nu}$ [cm⁻¹]: 3410 (m), 2992 (m), 2966 (m), 2875 (s), 2860 (s), 2821 (vs), 2786 (m), 1629 (w), 1519 (w), 1459 (vs), 1388 (w), 1333 (m), 1282 (w), 1255 (w), 1237 (w), 1177 (w), 1182 (w), 1255 (w), 1237 (w), 1177 (w), 1162 (w), 1137 (w), 1098 (w), 1067 (w), 1048 (m), 1034 (m), 1020 (m), 998 (m), 984 (m), 956 (s), 934 (w), 841 (w), 801 (s), 764 (m), 665 (w), 597 (w), 479 (w), 429 (w).

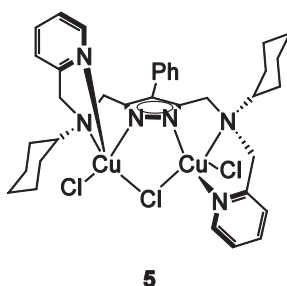
MS (ESI⁺, MeCN) *m/z* (%): 505 (88, [LCu₂Br]⁺), 421 (30, [LCu₂-H]⁺), 257 (100, [LCu-CH₃N(CH₂)₂N(CH₃)₂]⁺).

UV/vis (MeCN) λ [nm] (ε [L·mol⁻¹·cm⁻¹]): 202 (22100), 216 (20700), 294 (8480), 526 (474), 774 (239).

UV/vis (KBr) λ [nm]: 223, 334, 530, 797.

Elemental analysis: Calcd. (%) for C₁₅H₂₁N₆Cu₂Br₃: C 27.20, H 4.72, N 12.69. Found: C 27.36, H 4.78, N 12.78.

6.2.3. Preparation of L³Cu₂Cl₃ (**5**)



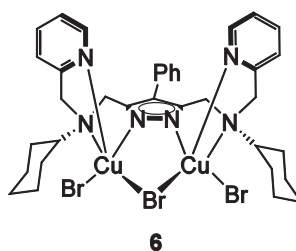
A solution of **HL**³ (275 mg, 0.5 mmol, 1.0 eq.) in MeOH (20 mL) was treated with KO^tBu (56 mg, 0.5 mmol, 1.0 eq.) and stirred for 15 min. Then CuCl₂ (135 mg, 1.0 mmol, 2.0 eq.) was added and the resulting green solution was stirred over night at room temperature. After removing all volatile compounds the remaining green solid was dissolved in MeCN (10 mL) and filtered. Slow diffusion of Et₂O into the filtrate led to the formation of brown crystals of **5** (207 mg, 0.27 mmol, 53 %).

IR (KBr) $\tilde{\nu}$ [cm⁻¹]: 3429 (w), 3065 (w), 2926 (vs), 2854 (s), 2360 (s), 2339 (m), 1602 (vs), 1528 (m), 1531 (m), 1481 (s), 1439 (vs), 1390 (m), 1369 (m), 1348 (m), 1298 (m), 1259 (s), 1153 (m), 1078 (s), 1047 (s), 1016 (s), 971 (s), 937 (m), 900 (m), 866 (m), 845 (m), 763 (vs), 687 (m), 667 (w), 639 (m), 523 (w), 506 (w), 412 (w).

MS (ESI⁺, MeCN) *m/z* (%): 752 (50), 673 (50, [LCu₂]⁺), 646 (72, [LCu + 2 H₂O]⁺), 421 (100, [LCu-cyNCH₂py]⁺).

Elemental analysis: Calcd. (%) for $C_{35}H_{43}N_6Cu_2Cl_3$: C 53.81, H 5.55, N 10.76. Found: C 53.48, H 5.56, N 10.74.

6.2.4. Preparation of $L^3Cu_2Br_3$ (**6**)



A solution of **HL**³ (275 mg, 0.5 mmol, 1.0 eq.) in MeOH (20 mL) was treated with KO^tBu (56 mg, 0.5 mmol, 1.0 eq.). The solution was stirred for 15 min. Then CuBr₂ (223 mg, 1 mmol, 2.0 eq.) was added and the resulting green solution was stirred over night at room temperature. After removing all volatile compounds the remaining green solid was dissolved in MeCN (10 mL) and filtered. Slow diffusion of Et₂O into the filtrate led to the formation of brown crystals of **6** (333 mg, 0.35 mmol, 70 %).

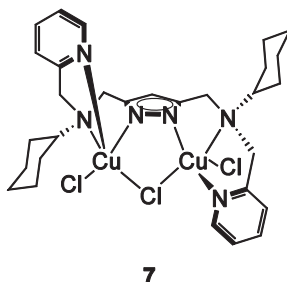
IR (KBr) $\tilde{\nu}$ [cm⁻¹]: 3432 (s), 3056 (m), 2930 (vs), 2855 (s), 1604 (s), 1573 (w), 1531 (w), 1480 (m), 1444 (s), 1386 (w), 1369 (w), 1349 (w), 1292 (m), 1260 (m), 1154 (m), 1075 (m), 1048 (m), 1016 (m), 972 (m), 937 (w), 890 (w), 867 (m), 844 (m), 765 (s), 695 (m), 639 (w), 580 (w), 525 (w), 508 (w).

MS (ESI⁺, MeCN) m/z (%): 833 (43, [LCu₂Br₂-H]⁺), 754 (36, [LCu₂Br-H]⁺), 675 (35, [LCu₂-H]⁺), 421 (100, [LCu-cyNCH₂py]⁺), 279 (45), 251 (63).

Elemental analysis: Calcd. (%) for $C_{35}H_{43}N_6Cu_2Br_3 \cdot 0.5 Et_2O \cdot 0.5 MeCN$: C 46.95, H 5.13, N 9.37. Found: C 46.41, H 5.08, N 9.31.



6.2.5. Preparation of $L^4Cu_2Br_3$ (**7**)

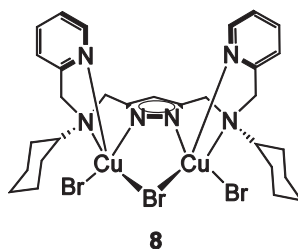


A solution of **HL**⁴ (241 mg, 0.5 mmol, 1.0 eq.) in MeOH (20 mL) was treated with one equivalent of KO^tBu (56 mg, 0.5 mmol, 1.0 eq.). The solution was stirred for 15 min. Then CuCl₂ (143 mg, 1 mmol, 2.0 eq.) was added and the resulting green solution was stirred over night at room temperature. After removing all volatile compounds the remaining green solid was dissolved in acetonitrile (10 mL) and filtered. The solvent was evaporated again. Slow diffusion of diethylether into the filtrate led to the formation of brown crystals of **7** (211 mg, 0.30 mmol, 59 %).

IR (KBr) $\tilde{\nu}$ [cm⁻¹]: 3433 (w), 3124 (w), 3073 (w), 3022 (w), 2924 (vs), 2852 (s), 1599 (s), 1571 (w), 1520 (w), 1481 (m), 1442 (s), 1388 (w), 1367 (w), 1347 (w), 1317 (m), 1294 (m), 1260 (w), 1152 (w), 1078 (m), 1049 (s), 1014 (m), 971 (w), 936 (m), 897 (w), 864 (w), 841 (w), 802 (w), 765 (s), 733 (w), 673 (w), 634 (w), 571 (w), 521(w).

MS (ESI, MeCN) m/z (%): 756 (32), 699 (47, [LCu₂Cl₂-H]⁺), 597 (39, [LCu₂-H]⁺), 513 (40, [LCu₂-cy-2]⁺), 345 (100, [LCu-cyNCH₂py]⁺), 317 (36), 251 (35, [(LCu-CH₂N(cy)CH₂py)⁺).

Elemental analysis: Calcd. (%) for C₃₉H₂₉N₆Cu₂Cl₃: C 49.40, H 5.57, N 11.92. Found: C 47.50, H 5.37, N 11.46.

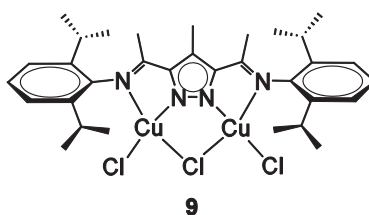
6.2.6. Preparation of $L^4Cu_2Br_3$ (**8**)

A solution of **HL**⁴ (241 mg, 0.5 mmol, 1.0 eq.) in MeOH (20 mL) was treated with KO^tBu (56 mg, 0.5 mmol, 1.0 eq.) and stirred for 15 min. Then CuBr₂ (223 mg, 1 mmol, 2.0 eq.) was added and the resulting green solution was stirred over night at room temperature. After removing all volatile compounds the remaining green solid was dissolved in MeCN (10 mL) and filtered. Slow diffusion of Et₂O into the filtrate led to the formation of brown crystals of **8** (285 mg, 0.34 mmol, 68 %).

IR (KBr) $\tilde{\nu}$ [cm⁻¹]: 3433 (w), 3124 (w), 3073 (w), 3022 (w), 2924 (vs), 2852 (s), 1599 (s), 1571(w), 1520 (w), 1481 (m), 1442 (s), 1388 (w), 1367 (w), 1347 (w), 1317 (m), 1294 (m), 1260 (w), 1152 (w), 1078 (m), 1049 (s), 1038 (m), 971 (w), 936 (m), 897 (w), 864 (w), 841 (w), 802(w), 765 (s), 733 (w), 674 (w), 634 (w), 571(w), 521 (w), 410 (w).

MS (ESI, MeCN) m/z (%): 597 (95, [LCu₂-H]⁺), 513 (37, [LCu₂-cy-2]⁺), 345 (100, [LCu-cyNCH₂py]⁺), 251 (45, [(LCu-CH₂N(cy)CH₂py)⁺).

Elemental analysis: Calcd. (%) for C₂₉H₃₉N₆Cu₂Br₃: C 41.54, H 4.69, N 10.02. Found: C 41.22, H 4.55, N 10.16.

6.2.7. Preparation of $L^9Cu_2Cl_3$ (**9**)

HL⁹ (242 mg, 0.5 mmol, 1.0 eq.) and KO^tBu (56 mg, 0.5 mmol, 1.0 eq.) were dissolved in abs. THF (20 mL). The solution was stirred for 15 minutes. Then CuCl₂ (139 mg, 1.0 mmol, 2.0 eq.) was added and the resulting brown solution was stirred over night at room temperature. After removing all volatile compounds the remaining brown solid was dissolved in DCM (10 mL) and filtered. Slow diffusion of pentane into this solution led to the formation of purple crystals of **9** (215 mg, 0.35 mmol, 70 %).

IR (KBr) $\tilde{\nu}$ [cm⁻¹]: 3440 (br), 3063 (w), 2963 (s), 2925 (w), 2871 (m), 1577 (s), 1495 (w), 1457 (w), 1440 (m), 1425 (m), 1384 (w), 1364 (m), 1342 (m), 1253 (m), 1183 (w), 1104 (vw), 1079 (vw), 1056 (vw), 981 (vw), 930 (vw), 846 (vw), 804 (m), 779 (m), 729 (w), 695 (vw), 594 (w), 452 (vw), 412 (vw).

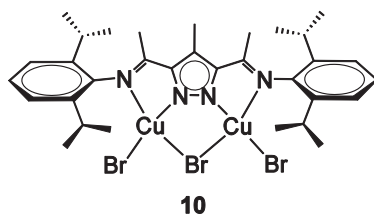
MS (ESI⁺, MeCN) m/z (%): 1032 (20), 699 (20), 486 (100, [L⁹]⁺), 351 (80).

UV/vis (CHCl₂) λ [nm] (ϵ [L·mol⁻¹·cm⁻¹]): 268.0 (6.02·10⁴), 430.0 (4.16·10³), 499.9 (4.49·10³), 736.0 (381).

UV/vis (KBr) λ [nm]: 272, 440, 510, 742.

Elemental analysis: Calcd. (%) for C₃₂H₄₃N₄Cu₂Cl₃: C 53.59, H 6.04, N 7.81. Found: C 53.00, H 6.0, N 7.75.

6.2.8. Preparation of L⁹Cu₂Br₃ (**10**)



HL⁹ (242 mg, 0.5 mmol, 1.0 eq.) and KO^tBu (56 mg, 0.5 mmol, 1.0 eq.) were dissolved in abs. THF (20 mL). The solution was stirred for 15 minutes. Then CuBr₂ (226 mg, 1.0 mmol, 2.0 eq.) was added and the resulting brown solution was stirred over night at room temperature. After removing all volatile compounds the remaining brown solid was

dissolved in DCM (10 mL) and filtered. Slow diffusion of pentane into this solution led to the formation of purple crystals of **10** (255 mg, 0.3 mmol, 60 %).

IR (KBr) $\tilde{\nu}$ [cm^{-1}]: 3422 (br), 3063 (w), 2962 (s), 2925 (w), 2867 (m), 2143 (w), 1640 (w), 1576 (s), 1460 (m), 1439 (m), 1425 (m), 1384 (w), 1364 (m), 1336 (m), 1250 (m), 1182 (w), 1103 (vw), 1074 (vw), 1056 (vw), 1017 (vw), 979 (vw), 935 (vw), 865 (vw), 846 (vw), 802 (m), 777 (m), 727 (w), 695 (vw), 592 (w), 563 (vw), 452 (vw).

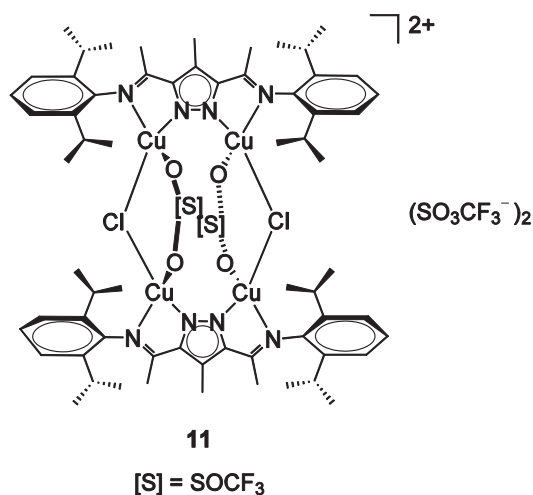
MS (ESI⁺, MeCN) m/z (%): 904 (20), 486 (100, [L⁹]⁺), 326 (68), 301 (95).

UV/vis (CH₂Cl₂) λ [nm] (ϵ [L·mol⁻¹·cm⁻¹]): 272.2 (3.51·10⁴), 451.9 (4.23·10³), 584.1 (2.16·10³).

UV/vis (KBr) λ [nm]: 272, 466, 599.

Elemental analysis: Calcd. (%) for C₃₂H₄₃N₆Cu₂Br₃: C 45.19, H 5.10, N 6.59. Found: C 44.81, H 5.00, N 6.58.

6.2.9. Preparation of L₂⁹Cu₄Cl₂(SO₃CF₃)₄ (**11**)



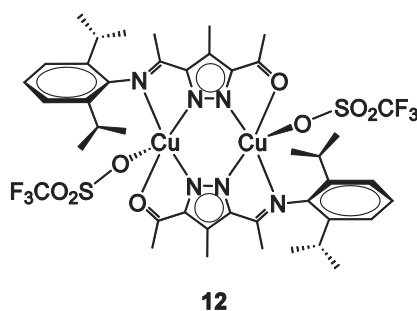
HL⁹ and KO^tBu were dissolved in abs. THF (20 mL). The solution was stirred for 15 minutes. Then CuCl₂ and Cu(SO₃CF₃)₂ were added and the resulting green solution was stirred over night at room temperature. After removing all volatile compounds the remaining brown solid was dissolved in acetone (10 mL) and filtered. Slow diffusion of

pentane into this solution led to the formation of red crystals of **11** (325 mg, 0.17 mmol, 68 %, experiment number 2).

experiment No	HL ⁹	Cu(SO ₃ CF ₃) ₂	CuCl ₂
1	241 mg, 0.5 mmol, 2eq.	270 mg, 0.75 mmol, 3 eq.	35 mg, 0.25 mmol, 1 eq.
2	241 mg, 0.5 mmol, 2eq.	215 mg, 0.63 mmol 2.5 eq.	50 mg, 0.38 mmol. 1.5 eq.
3	241 mg, 0.5 mmol, 2eq.	180 mg, 0.5 mmol, 2 eq.	69 mg, 0.50 mmol, 2 eq.

MS (ESI⁺, MeCN) m/z (%): 1306 (60, [L₂Cu₄Cl₃OTf-H]⁺), 1307 (100, [L₂Cu₃OTf-2H]⁺).

6.2.10. Preparation of L⁹Cu₂(SO₃CF₃)₂ (**12**)

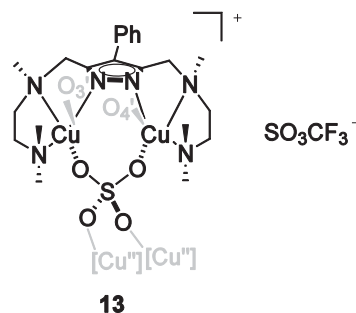


HL⁹ (242 mg, 0.5 mmol, 1.0 eq.) and KO^tBu (59 mg, 0.5 mmol, 1.0 eq.) were dissolved in abs. THF (20 mL) and the solution was stirred for 15 min. Then Cu(SO₃CF₃)₂ (362 mg, 1.0 mmol, 2.0 eq.) was added and the resulting brown solution was stirred over night at room temperature and filtered. Slow diffusion of pentane into this solution led to the formation of purple crystals of **12** (2.4 mg, 2.2 μmol, 0.44 %).

MS (ESI⁺, MeCN) m/z (%): 507 (20), 485 (100, [L]⁺), 351 (93).



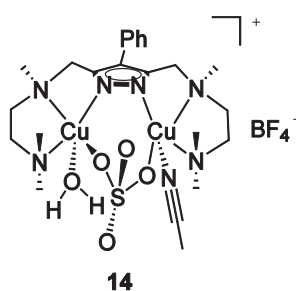
6.2.11. Preparation of $[\text{L}^1\text{Cu}_2(\text{SO}_4)](\text{SO}_3\text{CF}_3)$ (**13**)



Complex **1** (61 mg, 0.1 mmol, 1.0 eq.) was dissolved in abs. MeCN (20 mL) and Ag_2SO_4 (32 mg, 0.1 mmol, 1.0 eq.) and AgSO_3CF_3 (27 mg, 0.1 mmol, 1.0 eq.) were added. The solution turned blue immediately. After stirring at room temperature over night, the solution was filtered over celite. Slow diffusion of Et_2O into this solution led to the formation of blue crystals of **13** (10 mg, 13 μmol , 13 %).

MS (ESI^+ , MeCN) m/z (%): 593 (100, $[\text{LCu}_2\text{SO}_4]^+$).

6.2.12. Preparation of $[\text{L}^1\text{Cu}_2(\text{SO}_4)(\text{MeCN})(\text{H}_2\text{O})](\text{BF}_4)$ (**14**)

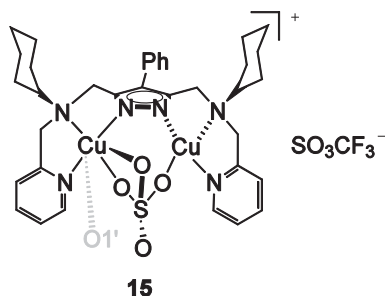


Complex **1** (60 mg, 0.1 mmol, 1.0 eq.) was dissolved in abs. MeCN (20 mL) and Ag_2SO_4 (32 mg, 0.1 mmol, 1.0 eq.) and AgBF_4 (20 mg, 0.1 mmol, 1.0 eq.) were added. The solution turned blue immediately. After stirring at room temperature over night, the solution was filtered over celite. Slow diffusion of Et_2O into this solution led to the formation of blue crystals of **14** (16 mg, 22 μmol , 22 %).

MS (ESI^+ , MeCN) m/z (%): 593 (100, $[\text{LCu}_2\text{SO}_4]^+$).



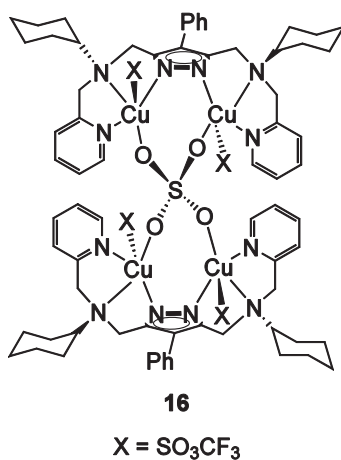
6.2.13. Preparation of $[L^3Cu_2(SO_4)](SO_3CF_3)$ (**15**)



Complex **6** (92 mg, 0.1 mmol, 1.0 eq.) was dissolved in abs. MeCN (20 mL) and Ag_2SO_4 (32 mg, 0.1 mmol, 1.0 eq.) and $AgSO_3CF_3$ (27 mg, 0.1 mmol, 1.0 eq.) were added. The solution turned blue immediately. After stirring at room temperature over night, the solution was filtered over celite. Slow diffusion of Et_2O into this solution led to the formation of blue crystals of **15** (6.6 mg, 7.2 μ mol, 7.2 %).

MS (ESI⁺, MeCN) m/z (%): 771 (100, $[LCu_2SO_4]^+$).

6.2.14. Preparation of $[L^3Cu_4(SO_4)](SO_3CF_3)_4$ (**16**)

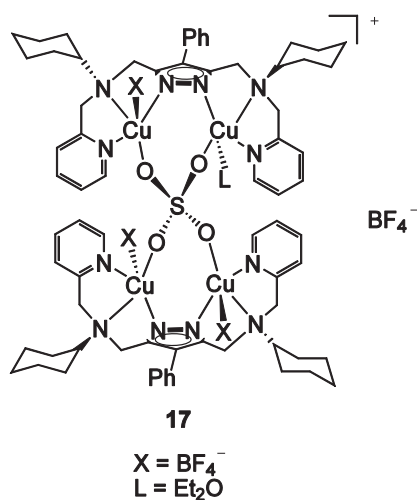


Complex **6** (92 mg, 0.1 mmol, 1.0 eq.) was dissolved in abs. MeCN (20 mL) and Ag_2SO_4 (17 mg, 50 μ mol, 0.50 eq.) as well as $AgSO_3CF_3$ (54 mg, 0.2 mmol, 1.0 eq.) were added.

The solution turned immediately blue. After stirring at room temperature over night, the solution was filtered over celite. Slow diffusion of Et₂O into this solution led to the formation of blue crystals of **16** (5.2 mg, 2.5 μmol, 5.1 %).

MS (ESI⁺, MeCN) m/z (%): 771 (100, [LCu₂SO₄]⁺).

6.2.15. Preparation of [(L³)₂Cu₄(SO₄)(Et₂O)(BF₄)₃](BF₄) (**17**)



Complex **6** (91 mg, 0.1 mmol, 1.0 eq.) was dissolved in abs. MeCN (20 mL) and Ag₂SO₄ (16 mg, 50 μmol, 0.50 eq.) as well as AgBF₄ (40 mg, 0.2 mmol, 2.0 eq.) were added. The solution turned blue immediately. After stirring at room temperature over night, the solution was filtered over celite. Slow diffusion of Et₂O into this solution led to the formation of blue crystals of **17** (8.5 mg, 4.6 μmol, 9.2 %).

MS (ESI⁺, MeCN) m/z (%): 771 (100, [LCu₂SO₄]⁺).

6.2.16. Preparation of $L^5_xCu_yBr_z$

HL⁵ (230 mg, 0.52 mmol, 1.0 eq.) and KO^tBu (58.0 mg, 0.52 mmol, 1.0 eq.) were dissolved in MeCN (15 mL). The solution was stirred for 15 minutes. Then CuBr (151 mg, 1.1 mmol, 2.0 eq.) was added. The reaction mixture was stirred over night. After removing all volatile compounds the remaining orange solid was dissolved in DCM (10 mL) and filtered. Until now no crystals suitable for X-ray analysis could be obtained. It is assumed that the product has a molecular structure similar to **18**.

¹H NMR (300 MHz, CD₃CN): δ [ppm] = 2.24 (s, 6 H, 2 x NCH₃), 2.70 – 2.80 (m, 4 H, -NCH₂CH₂), 2.90 – 3.05 (m, 4 H, py-CH₂), 3.61 (s, 4 H, pz-CH₂), 7.00 - 7.40 (m, 9 H, ph, py-*H*^{5,3}), 7.62 - 7.82 (m, 2 H, py-*H*⁴), 8.30 - 8.50 (m, 2 H, py-*H*⁶).

¹³C {¹H} NMR (75 MHz, CD₃CN): δ [ppm] = 36.6 (-NCH₂CH₂), 44.9 (-NCH₃), 54.9 (pz-CH₂), 58.2 (py-CH₂), 123 (py-C⁵), 126 (ph-C^{ortho}), 127 (py-C^{para}), 129 (py-C³), 130 (ph-C^{meta}), 135 (ph-C^{ipso}), 137 (pz-C^{3,5}), 138 (py-C⁴), 147 (pz-C⁴), 151 (py-C⁶), 161 (py-C²).

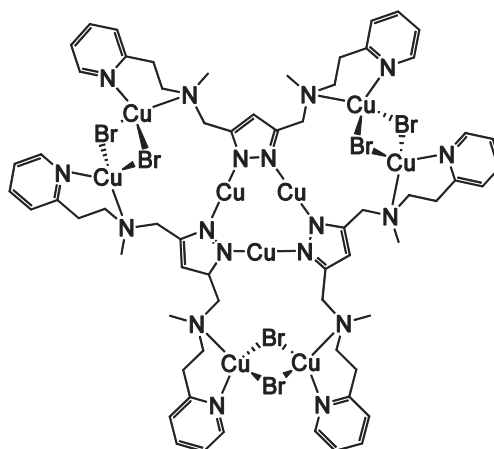
MS (ESI⁺, MeCN) *m/z* (%): 1213 (10, [L₂Cu₄Br]⁺), 1148 (18, [L₂Cu₃Br]⁺), 1069 (63, [L₂Cu₃]⁺), 565 (100, [LCu₂]⁺).

MS (ESI⁻, MeCN) *m/z* (%): 725 (47, [L₂Cu₂Br₂]⁻), 223 (100, [CuBr₂]⁻).

For comparison: Chemical shifts of [L⁵]⁻

For the reference spectrum **HL**⁵ was deprotonated with 1 eq. of KH at room temperature.

¹H NMR (300 MHz, CD₃CN): δ [ppm] = 2.19 (s, 6 H, NCH₃), 2.51 – 2.77 (m, 4 H, -NCH₂CH₂), 2.85 (dd, ³J_{H,H} = 8.4, 6.1 Hz, 4 H, py-CH₂), 3.47 (m, 4 H, pz-CH₂), 6.99 - 7.11 (m, 5 H, py-*H*³, ph-*H*^{ortho}), 7.18 (dd, ³J_{H,H} = 8.1 Hz, 7.1 Hz, ph-*H*^{meta}, ph-*H*^{para}), 7.41 (dd, ³J_{H,H} = 8.3 Hz, ⁴J_{H,H} = 1.3 Hz, 2 H, py-*H*⁵), 7.59 – 7.46 (m, 2 H, py-*H*⁴), 8.38 (ddd, ³J_{H,H} = 4.9 Hz, ⁴J_{H,H} = 1.9 Hz, ⁵J_{H,H} = 1.0 Hz, 2 H, py-*H*⁶).

6.2.17. Preparation of $L_3^6Cu_9Br_6$ (**18**)**18**

HL⁶ (182 mg, 0.50 mmol, 1.0 eq.) and KO^tBu (56.0 mg, 0.5 mmol, 1.0 eq.) were dissolved in MeCN (20 mL). The solution was stirred for 15 minutes. Subsequently CuBr (143 mg, 1.0 mmol, 2.0 eq.) was added. The reaction mixture was stirred over night. After removing all volatile compounds the remaining orange solid was dissolved in DCM (10 mL) and filtered. Layering the complex solution in DCM with pentane led to the formation of purple crystals of **18** (20.1 mg, 9.38 μ mol, 1.87 %).

¹H NMR (300 MHz, CD₃CN): δ [ppm] = 2.28 (s, 6 H, 2 x NCH₃), 2.59 – 2.84 (m, 4 H, -NCH₂CH₂), 2.86 – 3.11 (m, 4 H, py-CH₂), 3.59 (s, 4 H, pz-CH₂), 5.97 (s, 1 H, pz-H), 7.02 - 7.14 (m, 2 H, py-H⁵), 7.15 - 7.24 (m, 2 H, py-H³), 7.52 - 7.70 (m, 2 H, py-H⁴), 8.28 - 8.53 (m, 2 H, py-H⁶).

¹³C {¹H} NMR (75 MHz, CD₃CN): δ [ppm] = 36.6 (NCH₃), 44.5 (py-CH₂), 56.4 (NCH₂CH₂), 57.8 (pz-CH₂), 105 (pz-C⁴), 123 (py-C⁵), 125 (py-C³), 138 (py-C⁴), 150 (py-C⁶), 162 (py-C⁵), pz-C^{3,5} could not be observed.

MS (ESI⁺, MeCN) m/z (%): 1061 (23, [L₂Cu₄Br]⁺), 996 (25, [L₂Cu₃Br]⁺), 917 (100, [L₂Cu₃]⁺), 575 (25), 489 (48, [LCu₂]⁺, 459 (47, [L₂Cu₃]²⁺).

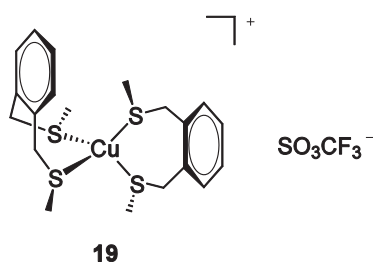
MS (ESI⁻, MeCN) m/z (%): 1077 (6, [L₂Cu₃Br₂]⁻), 651 (100 [LCu₂Br₂]⁻), 223 (96, [CuBr₂]⁻).

For comparison: Chemical shifts of $[L^6]^-$

For the reference spectrum HL^5 was deprotonated with 1 eq. of KH at room temperature.

1H NMR (200 MHz, CD_3CN): δ [ppm] = 2.15 (s, 6 H, 2 x CH_3), 2.63 (dd, $^3J_{H,H} = 8.8$ Hz, 5.8 Hz, 4 H, NCH_2CH_2), 2.85 (dd, $^3J_{H,H} = 8.9$ Hz, 5.8 Hz, 4 H, 2 x $pyCH_2$), 3.48 (s, 4 H, 2 x $pz-CH_2$), 5.75 (s, 1 H, $pz-H^4$), 7.06 (m, 4 H, 2 x $py-H^5$, 2 x $py-H^3$), 7.54 (td, $^3J_{H,H} = 7.7$ Hz, 1.9 Hz, 2 H, 2 x $py-H^4$), 8.36 (ddd, $^3J_{H,H} = 4.9$ Hz, $^4J_{H,H} = 1.8$ Hz, $^5J_{H,H} = 0.9$ Hz, 2 H, 2 x $py-H^6$).

6.2.18. Preparation of $[L^{S,1}Cu]^+SO_3CF_3^-$ (**19**)



$[Cu(MeCN)_4]SO_3CF_3$ (648 mg, 1.72 mmol, 1.0 eq.) was dissolved in MeOH (20 mL) and subsequently L^{S2} (12 mg, 0.9 mmol, 2.0 eq.) was added. The colourless reaction mixture was stirred over night. After removing all volatile compounds the remaining white solid was dissolved in MeCN (10 mL). Et_2O diffusion into the complex solution in MeCN led to the formation of colourless crystals of **19** (381 mg, 1.05 mmol, 61 %).

1H NMR (300 MHz, CD_3CN): δ [ppm] = 2.11 (s, 12 H, CH_3), 3.89 (s, 8 H, CH_2), 7.27 (s, 8 H, Ar-CH).

^{13}C $\{^1H\}$ NMR (75 MHz, CD_3CN): δ [ppm] = 17.7 (SCH_3), 37.1 ($ph-CH_2$), 129 ($ph-C^3$, $ph-C^4$), 131 ($ph-C^4$, $ph-C^5$), 136 ($ph-C^1$, $ph-C^6$).

IR (KBr) $\tilde{\nu}$ [cm^{-1}]: 4404 (w), 4304 (w), 3433 (w), 3068 (w), 2995 (w), 2951 (w), 2921 (m), 2852 (w), 2827 (w), 2288 (w), 1493 (m), 1449 (m), 1431 (m), 1323 (m),

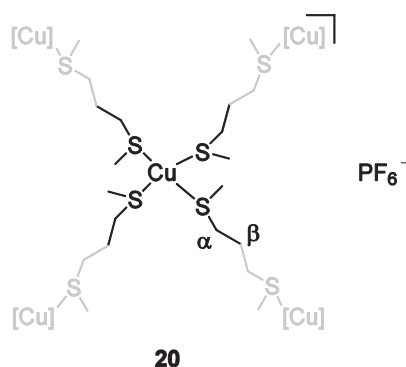
1270 (vs), 1223 (s), 1152 (s), 1138 (s), 1088 (w), 1030 (s), 982 (m), 964 (m), 838 (w), 778 (s), 756 (m), 712 (m), 667 (m), 637 (s), 602 (w), 571 (m), 517 (m), 469 (w).

MS (ESI⁺, MeCN) *m/z* (%): 459 (100 %, [ML₂]⁺).

UV/vis (KBr) [nm]: 224, 272 (sh).

Elemental analysis: Calcd. (%) for C₂₁H₂₈S₅CuO₃F₃: C 41.44, H 4.64, S 26.29. Found: C 41.35, H 4.69, S 26.43.

6.2.19. Preparation of [L^{S,2}Cu]⁺PF₆⁻ (**20**)



[Cu(MeCN)₄]PF₆ (169 mg, 0.45 mmol, 1.0 eq.) was dissolved in MeCN (10 mL) and subsequently L^{S1} (122 mg, 0.9 mmol, 2.0 eq.) was added. The colourless reaction mixture was stirred over night. After removing all volatile compounds the remaining white solid was dissolved in EtCN (6 mL). Et₂O diffusion into the complex solution in EtCN led to the formation of colourless crystals of **20** (120 mg, 0.25 mmol, 56 %).

¹H NMR (300 MHz, CD₃CN): δ [ppm] = 1.90 (quin, ³J_{H,H} = 6.83 Hz, 4 H, CH₂ (β)), 2.13 (s, 12 H, CH₃), 2.64 (t, ³J_{H,H} = 6.80 Hz, 8 H, CH₂ (α)).

¹³C {¹H} NMR (75 MHz, CD₃CN): δ [ppm] = 16.6 (CH₃), 27.7 (CH₂ (β)), 34.4 (CH₂ (α)).

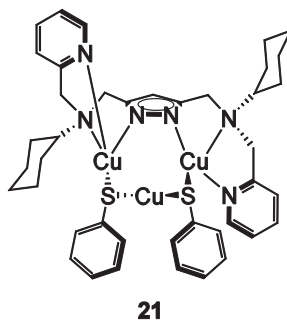
IR (KBr) $\tilde{\nu}$ [cm^{-1}]: 2979 (w), 2950 (w), 2932 (m), 2827 (w), 1443 (m), 1423 (m), 1348 (w), 1269 (w), 1130 (w), 1044 (m), 967 (m), 945 (w), 876 (sh), 839 (vs), 787 (sh), 729 (m), 694 (w), 665 (m), 558 (s), 482 (w), 449 (w).

MS (ESI⁺, MeCN) m/z (%): 335 (100, [M-PF₆]⁺), 199 (70, [L^{S1}Cu+H]⁺).

UV/vis (KBr) [nm]: 227, 250.

Elemental analysis: Calcd. (%) for C₁₀H₂₄S₄CuPF₆: C 24.97, H 5.03, S 26.66. Found: C 25.27, H 5.02, S 26.41.

6.2.20. Preparation of L⁴Cu₃(SPh)₂ (21)



HL⁴ (241 mg, 0.5 mmol, 1.0 eq.) and KO^tBu (56 mg, 0.5 mmol, 1.0 eq.) were dissolved in abs. MeCN (20 mL). After stirring at room temperature for a few minutes CuSPh (173 mg, 1.0 mmol, 2.0 eq.) and [Cu(MeCN)₄]BF₄ (159 mg, 0.5 mmol, 1.0 eq.) were added. The reaction mixture was stirred over night. The solvent was evaporated and the residue dried in vacuo. The resulting solid was dissolved in benzene (30 mL) and filtered. Overlaying this solution with hexane led to the formation of yellow crystals (330 mg, 0.38 mmol, 75 %).

¹H NMR (500 MHz, CD₂Cl₂, 273 K): δ [ppm] = 1.05 (dd, ³J_{H,H} = 25.3, 12.6 Hz, 2 H, cy-H⁴), 1.15 (dd, ³J_{H,H} = 25.5, 12.5 Hz, 4 H, cy-H³, cy-H⁵), 1.32 (dd, ³J_{H,H} = 22.7 Hz, 12.0 Hz, 4 H, cy-H², cy-H⁶), 1.57 (d, ³J_{H,H} = 12.1 Hz, 2 H, cy-H⁴), 1.75 (d, ³J_{H,H} = 12.7 Hz, 4 H, cy-H², cy-H⁶), 2.27 (d, ³J_{H,H} = 12.0 Hz, 4 H, cy-H³, cy-H⁵), 2.47 (t, ³J_{H,H} = 11.5 Hz, 2 H, cy-H¹), 3.69 (s, 4 H, py-CH₂), 3.78 (s, 4 H, pz-CH₂), 5.78 (s, 1 H,

pz- H^4), 6.94 – 6.84 (m, 8 H, py- H^5 , SPh- H^{meta} , SPh- H^{para}), 7.15 (d, $^3J_{H,H} = 7.8$ Hz, 2 H, py- H^3), 7.45 (d, $^3J_{H,H} = 7.0$ Hz, 4 H, SPh- H^{ortho}), 7.56 (td, $^3J_{H,H} = 7.7, 1.7$ Hz, 2 H, py- H^4), 7.98 (d, $^3J_{H,H} = 4.5$ Hz, 2 H, py- H^6).

^{13}C $\{^1\text{H}\}$ NMR (125 MHz, CD_2Cl_2 , 273 K): δ [ppm] = 26.3 (cy- C^2 , cy- C^3 , cy- C^5 , cy- C^6), 26.5 (cy- C^4), 48.8 (py- CH_2), 55.8 (pz- CH_2), 60.5 (cy- C^1), 98.3 (pz- C^4), 123 (py- C^5), 124 (py- C^3 , Sph- C^{para}), 128 (SPh- C^{meta}), 133 (SPh- C^{ortho}) 137 (py- C^4), 140 (SPh- C^{ipso}), 149 (py- C^2), 150 (py- C^6), 158 (pz- C^3 , pz- C^5).

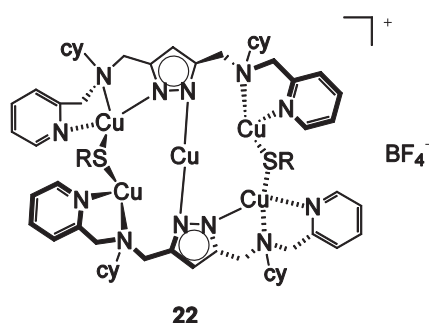
IR (KBr) $\tilde{\nu}$ [cm^{-1}]: 3456 (br), 3058 (w), 2926 (s), 2851 (m), 1649 (w, br), 1598 (m), 1576 (m), 1473 (s), 1436 (m), 1376 (vw), 1340 (vw), 1325 (vw), 1297 (vw), 1262 (m), 1152 (vw), 1084 (s), 1052 (vw), 1023 (s), 971 (vw), 959 (vw), 950 (vw), 894 (w), 870 (vw), 804 (m), 761 (w), 738 (m), 689 (s), 480 (w).

MS (FD, CH_2Cl_2) m/z (%): 1479 (100 [$\text{L}_2\text{Cu}_5(\text{SPh})_2$] $^+$), 880 (50 [M]).

UV/vis (KBr) [nm]: 238, 311(sh), 426 (sh).

Elemental analysis: Calcd. (%) for $\text{C}_{41}\text{H}_{49}\text{N}_6\text{S}_2\text{Cu}_3 \cdot \text{C}_6\text{H}_6$: C 58.98, H 5.79, N 8.79, S 6.69. Found: C 58.46, H 5.72, N 8.26, S 7.15.

6.2.21. Preparation of [$\text{L}^4_2\text{Cu}_5(\text{SPh})_2$] $^+\text{BF}_4^-$ (22)



HL^4 (241 mg, 0.5 mmol, 2.0 eq.) and KO^tBu (56 mg, 0.5 mmol, 2.0 eq.) were dissolved in abs. MeCN (20 mL). After stirring at room temperature for a few minutes CuSPh (87 mg, 0.5 mmol, 2.0 eq.) and $[\text{Cu}(\text{MeCN})_4]\text{BF}_4$ (236 mg, 0.75 mmol, 3.0 eq.) were added. The reaction mixture was stirred over night. The solvent was evaporated and the

residur dried in vacuo. The resulting solid was dissolved in DCM (10 mL) and filtered. Overlaying this solution with hexane led to the formation of yellow crystals (188 mg, 0.12 mmol, 48 %).

$^1\text{H-NMR}$ (500 MHz, CD_2Cl_2 , 233 K): δ [ppm] = 0.59 – 0.67 (m, 2 H, cy-*H*), 0.72 - 1.02 (m, 12 H, cy-*H*), 1.02 - 1.12 (m, 2H, cy-*H*), 1.12 - 1.32 (m, 6 H, cy-*H*), 1.32 - 1.46 (m, 6 H, cy-*H*), 1.46 - 1.60 (m, 4 H, cy-*H*), 1.95 (d, $^3J_{\text{H,H}} = 11.7$ Hz, 4 H, cy-*H*), 2.20 (m, 6H, cy-*H*^{1'}, cy-*H*), 2.62 (t, $^3J_{\text{H,H}} = 11.6$ Hz, 2 H, cy-*H*¹), 3.40 (d, $^2J_{\text{H,H}} = 15.0$ Hz, 2 H, py-*CH*₂') 3.44 (d, $^2J_{\text{H,H}} = 15.3$, 2 H, pz-*CH*₂'), 3.46 (d, $^2J_{\text{H,H}} = 15.3$ Hz, 2 H, pz-*CH*₂'), 3.65 (d, $^2J_{\text{H,H}} = 14.9$ Hz, 2 H, py-*CH*₂'), 3.82 (d, $^2J_{\text{H,H}} = 15.1$ Hz, 2 H, py-*CH*₂'), 3.93 (d, $^2J_{\text{H,H}} = 14.9$ Hz, 2 H, pz-*CH*₂'), 3.99 (d, $^2J_{\text{H,H}} = 15.4$ Hz, 2 H, pz-*CH*₂'), 4.11 (d, $^2J_{\text{H,H}} = 15.2$ Hz, 2 H, py-*CH*₂'), 5.91 (s, 2 H, 2 pz-*H*), 6.31 – 6.22 (m, 2 H, py-*H*^{5'}), 6.76 (t, $^3J_{\text{H,H}} = 7.6$ Hz, 4 H, Sph-*H*^{meta}), 6.79 (d, $^3J_{\text{H,H}} = 7.6$ Hz 2 H, py-*H*^{3'}) 6.87 (t, $^3J_{\text{H,H}} = 7.3$ Hz, 2 H, Sph-*H*^{para}), 6.90 (t, $^3J_{\text{H,H}} = 6.4$ Hz, 2 H, py-*H*⁵), 7.23 (t, $^3J_{\text{H,H}} = 7.5$ Hz, 2 H, py-*H*^{4'}), 7.30 (d, $^3J_{\text{H,H}} = 7.8$ Hz, 2 H, py-*H*³), 7.36 (d, $^3J_{\text{H,H}} = 7.4$ Hz, 4 H, Sph-*H*^{ortho}), 7.49 (d, $^3J_{\text{H,H}} = 4.6$ Hz, 2 H, py-*H*⁶), 7.67 (t, $^3J_{\text{H,H}} = 7.7$ Hz, 2 H, py-*H*⁴), 8.12 (d, $^3J_{\text{H,H}} = 4.2$ Hz, 2 H, py-*H*^{6'}).

^{13}C { ^1H } NMR (125 MHz, CD_2Cl_2 , 233 K): δ [ppm] = 14.01 (cy-*C*), 22.47 (cy-*C*), 25.23 (cy-*C*), 25.49 (cy-*C*), 25.72 (cy-*C*), 25.77 (cy-*C*), 27.79 (cy-*C*), 28.48 (cy-*C*), 29.44 (cy-*C*), 29.66 (cy-*C*), 31.64 (cy-*C*), 48.39 (pz-*CH*₂'), 48.77 (pz-*CH*₂), 54.80 (py-*CH*₂'), 56.35 (py-*CH*₂), 58.96 (cy-*C*^{1'}), 61.75 (cy-*C*¹), 97.78 (pz-*C*⁴), 121.86 (py-*C*^{5'}), 122.62 (py-*C*^{3'}), 123.31 (py-*C*⁵), 124.02 (py-*C*³), 124.50 (Sph-*C*^{para}), 128.02 (Sph-*C*^{meta}), 131.24 (Sph-*C*^{ortho}), 136.32 (py-*C*^{4'}), 136.87 (py-*C*⁴), 149.26 (pz-*C*⁵), 149.42 (py-*C*⁶), 150.22 (pz-*C*³), 151.38 (py-*C*^{6'}), 157.18 (py-*C*^{2'}), 157.70 (py-*C*²), Sph-*C*^{ipso} was not observed.

IR (KBr) $\tilde{\nu}$ [cm^{-1}]: 3545 (w), 3466 (w), 3378 (w), 3102 (w), 3059 (m), 2024 (vs), 2852 (vs), 2805 (s), 2670 (w), 2606 (w), 2189 (w), 1948 (w), 1868 (w), 1805 (w), 1632 (w), 1602 (s), 1574 (s), 1516 (m), 1471 (s), 1442 (s), 1387 (m), 1346 (m), 1324 (m), 1301 (m), 1267 (m), 1249 (m), 1156 (s), 1080 (sh), 1060 (vs), 1028 (sh), 976 (s), 945 (m), 895 (m), 869 (m), 838 (m), 821 (m), 760 (s), 745 (s), 693 (s), 652 (w), 641 (w), 520 (m), 483 (m), 462 (w), 421 (m).

MS (FD, CH_2Cl_2) m/z (%): 1479 (100, $[\text{M-BF}_4]^+$).

UV/vis (KBr) [nm]: 259, 317, 418.

Elemental analysis: Calcd. (%) for: $C_{70}H_{88}N_{12}S_2Cu_5BF_4$: C 53.77, H 5.67, N 10.73 S 4.09.

Found: C 52.83, H 5.81, N 10.91, S 4.10.



7. Crystallography

Table 7.1: Crystal data and refinement details for **3**, **4** and **5**.

	3	4	5
empirical formula	C ₁₅ H ₃₁ Cl ₃ Cu ₂ N ₆	C ₁₅ H ₃₁ Br ₃ Cu ₂ N ₆	C ₃₅ H ₄₃ Br ₃ Cu ₂ N ₆
formula weight [g·mol ⁻¹]	528.89	662.27	914.56
crystal size [mm ³]	0.33 × 0.3 × 0.27	0.22 × 0.12 × 0.11	0.50 × 0.10 × 0.08
crystal system	monoclinic	monoclinic	monoclinic
space group	<i>P2₁/c</i>	<i>P2₁/c</i>	<i>P2₁/c</i>
<i>a</i> [Å]	15.803(3)	15.866(3)	8.8938(2)
<i>b</i> [Å]	13.155(3)	13.607(3)	27.9983(8)
<i>c</i> [Å]	10.769(2)	10.890(2)	15.9176(4)
α [°]	90.00	90.00	90.00
β [°]	103.26(3)	103.19(3)	97.176(2)
γ [°]	90.00	90.00	90.00
<i>V</i> [Å ³]	2178.9(8)	2288.9(8)	3932.61(17)
ρ [g·cm ⁻³]	1.612	1.922	1.545
<i>Z</i>	4	4	4
<i>F</i> (000)	1088	1304	1832
μ [mm ⁻¹]	2.332	7.107	4.161
<i>T</i> _{min} / <i>T</i> _{max}	0.2926 / 0.6155	0.2867 / 0.5292	0.4295 / 0.7027
<i>hkl</i> range	±19, -15 - 16, -13 - 10	-18 - 20, ± 17, ±13	-9 - 11, ± 35, ± 20
θ range [°]	2.04 - 26.72	1.99 - 26.76	1.45 - 26.77
measured refl.	16712	19726	37590
unique refl. [<i>R</i> _{int} .]	4508 [0.1003]	4753 [0.0584]	8330 [0.0895]
observed refl. <i>I</i> > 2 σ (<i>I</i>)	3970	3760	8330
refined parameters	235	241	415
restraints	0	0	0
goodness-of-fit	1.003	1.047	1.019
<i>R</i> ₁ , ω <i>R</i> ₂ (<i>I</i> > 2 σ (<i>I</i>))	0.0433, 0.1088	0.0442, 0.0834	0.0390, 0.0847
<i>R</i> ₁ , ω <i>R</i> ₂ (all data)	0.0484, 0.1116	0.0670, 0.0895	0.0553, 0.0900
resid. el. dens. [e·Å ⁻³]	-1.257 / 0.875	-0.712 / 2.312	-0.770 / 0.613

Table 7.2: Crystal data and refinement details for 6, 7 and 8.

	6	7	8
empirical formula	C ₃₅ H ₄₂ Cl ₃ Cu ₂ N ₆	C ₂₉ H ₃₉ Cl ₃ Cu ₂ N ₆	C ₂₉ H ₃₉ Br ₃ Cu ₂ N ₆
formula weight [g·mol ⁻¹]	780.18	705.09	838.47
crystal size [mm ³]	0.21 × 0.18 × 0.05	0.22 × 0.18 × 0.07	0.09 × 0.08 × 0.07
crystal system	triclinic	triclinic	triclinic
space group	<i>P</i> $\bar{1}$	<i>P</i> $\bar{1}$	<i>P</i> $\bar{1}$
<i>a</i> [Å]	9.7372(19)	8.2867(13)	8.6776(17)
<i>b</i> [Å]	10.013(2)	11.3618(16)	8.9948(18)
<i>c</i> [Å]	18.441(4)	17.494(3)	20.305(4)
α [°]	88.96(3)	97.815(11)	95.97(3)
β [°]	85.95(3)	99.756(12)	95.08(3)
γ [°]	74.26(3)	110.130(11)	90.53(3)
<i>V</i> [Å ³]	1726.3(6)	1490.1(4)	1569.8(5)
ρ [g·cm ⁻³]	1.501	1.571	1.774
<i>Z</i>	2	2	2
<i>F</i> (000)	806	728	836
μ [mm ⁻¹]	1.499	1.727	5.203
<i>T</i> _{min} / <i>T</i> _{max}	0.6460 / 0.8163	0.7281 / 0.8802	0.3999 / 0.6419
<i>hkl</i> range	± 12, -12 – 11, -22 – 23	± 9, ± 13, ± 20	± 10, ± 11, -25 – 20
θ range [°]	2.11 – 26.83	1.21 – 25.03	2.28 – 26.83
measured refl.	10193	20125	13926
unique refl. [<i>R</i> _{int}]	6178 [0.0772]	20125 [0.0000]	6334 [0.1056]
observed refl. <i>I</i> > 2 σ (<i>I</i>)	3935	10018	3669
refined parameters	415	362	361
restraints	0	0	0
goodness-of-fit	1.022	0.965	0.925
<i>R</i> 1, ω <i>R</i> 2 (<i>I</i> > 2 σ (<i>I</i>))	0.0661, 0.1528	0.0967, 0.2333	0.0601, 0.1217
<i>R</i> 1, ω <i>R</i> 2 (all data)	0.1119, 0.1780	0.1709, 0.2788	0.1176, 0.1449
resid. el. dens. [e·Å ⁻³]	-1.414 / 0.710	-1.028 / 1.161	-1.036 / 0.691

Table 7.3: Crystal data and refinement details for 9, 10 and 12.

	9	10	12
empirical formula	C ₃₂ H ₄₃ Cl ₃ Cu ₂ N ₄	C ₃₂ H ₄₃ Br ₃ Cu ₂ N ₄	C ₄₂ H ₅₂ Cu ₂ F ₆ N ₆ O ₈ S ₂
formula weight [g·mol ⁻¹]	717.13	850.51	1074.10
crystal size [mm ³]	0.47 × 0.11 × 0.08	0.36 × 0.039 × 0.025	0.6 × 0.48 × 0.43
crystal system	orthorhombic	orthorhombic	orthorhombic
space group	<i>Pbca</i>	<i>Pbca</i>	<i>Pbca</i>
<i>a</i> [Å]	14.613(3)	15.118(3)	16.703(3)
<i>b</i> [Å]	14.684(3)	14.646(3)	14.908(3)
<i>c</i> [Å]	32.223(6)	32.230(6)	18.700(4)
α [°]	90.00	90.00	90.00
β [°]	90.00	90.00	90.00
γ [°]	90.00	90.00	90.00
<i>V</i> [Å ³]	6914(2)	7136(2)	4656.4(16)
ρ [g·cm ⁻³]	1.378	1.583	1.532
<i>Z</i>	8	8	4
<i>F</i> (000)	2976	3408	2216
μ [mm ⁻¹]	1.489	4.578	1.085
<i>T</i> _{min} / <i>T</i> _{max}	-	0.5802 / 0.9106	0.5577 / 0.6737
<i>hkl</i> range	±18, -18 – 16, ±40	±17, -17 - 15, ±38	-20 – 21, ±18, -21 – 23
θ range [°]	1.88 - 26.75	1.26 - 25.00	2.13 - 26.76
measured refl.	61285	53570	41217
unique refl. [<i>R</i> _{int} .]	7354 [0.1202]	5972 [0.1892]	4692 [0.0301]
observed refl. <i>I</i> > 2 σ (<i>I</i>)	5238	3574	4451
refined parameters	380	370	310
restraints	0	0	0
goodness-of-fit	0.958	0.987	1.159
<i>R</i> 1, ω <i>R</i> 2 (<i>I</i> > 2 σ (<i>I</i>))	0.0428, 0.0857	0.0692, 0.0950	0.0373, 0.0881
<i>R</i> 1, ω <i>R</i> 2 (all data)	0.0712, 0.0936	0.1332, 0.1113	0.0402, 0.0894
resid. el. dens. [e·Å ⁻³]	-0.547 / 0.368	-0.575 / 0.740	-0.453 / 0.561

Table 7.4: Crystal data and refinement details for **13**, **14** and **15**.

	13	14	15
empirical formula	C ₂₁ H ₃₅ Cu ₂ F ₃ N ₆ O ₇ S ₂ ·0.25 MeCN	C ₂₃ H ₄₀ BCu ₂ F ₄ N ₇ O ₅ S	C ₃₈ H ₄₆ Cu ₂ F ₃ N ₇ O ₇ S ₂
formula weight [g·mol ⁻¹]	742.02	740.57	961.02
crystal size [mm ³]	0.15 × 0.10 × 0.04	0.28 × 0.17 × 0.09	0.18 × 0.08 × 0.06
crystal system	tetragonal	monoclinic	triclinic
space group	<i>I</i> ₄	<i>P</i> ₂ ₁ / <i>c</i>	<i>P</i> $\bar{1}$
<i>a</i> [Å]	28.695(2)	15.706(3)	9.1594(18)
<i>b</i> [Å]	28.695(2)	18.789(4)	14.267(3)
<i>c</i> [Å]	16.348(3)	10.551(2)	17.249(3)
α [°]	90.00	90.00	100.96(3)
β [°]	90.00	90.70(3)	103.89(3)
γ [°]	90.00	90.00	106.96(3)
<i>V</i> [Å ³]	13461(3)	3113.6(11)	2009.2(7)
ρ [g·cm ⁻³]	1.488	1.580	1.589
<i>Z</i>	16	4	2
<i>F</i> (000)	6200	1528	992
μ [mm ⁻¹]	1.451	1.502	1.235
<i>T</i> _{min} / <i>T</i> _{max}	0.8403 / 0.9802	0.5215 / 0.8880	0.7567 / 0.9069
<i>hkl</i> range	0 – 25, 0 – 35, ± 20	±19, ±23, ±13	-11 - 10, ±18, ±21
θ range [°]	2.245-23.2	1.69 - 26.73	1.55 - 26.87
measured refl.	88116	28072	17402
unique refl. [<i>R</i> _{int}]	9877	6490 [0.0498]	8395 [0.0768]
observed refl. <i>I</i> > 2 σ (<i>I</i>)	7442	4933	5147
refined parameters	397	456	536
restraints	4	60	0
goodness-of-fit	1.147	1.039	0.976
<i>R</i> ₁ , ω <i>R</i> ₂ (<i>I</i> > 2 σ (<i>I</i>))	0.0504, 0.1362	0.0485, 0.1203	0.0657, 0.0935
<i>R</i> ₁ , ω <i>R</i> ₂ (all data)	0.0565, 0.1395	0.0690, 0.1285	0.1248, 0.1068
resid. el. dens. [e·Å ⁻³]	-0.636 / 0.928	-0.830 / 0.807	-0.462 / 0.844

Table 7.5: Crystal data and refinement details for **16**, **17** and **18**.

	16	17	18
empirical formula	C ₇₄ H ₈₆ Cu ₄ F ₁₂ N ₁₂ O ₁₆ S ₅	C ₇₄ H ₉₆ B ₄ Cu ₄ F ₁₆ N ₁₂ O ₅ S	C ₆₃ H ₈₁ Br ₆ Cu ₉ N ₁₈
formula weight [g·mol ⁻¹]	2042.01	1867.09	2141.78
crystal size [mm ³]	0.16 × 0.13 × 0.12	0.26 × 0.25 × 0.1	0.24 × 0.06 × 0.06
crystal system	monoclinic	orthorhombic	triclinic
space group	<i>Cc</i>	<i>Fdd2</i>	<i>P1̄</i>
<i>a</i> [Å]	14.856(3)	25.046(5)	12.695(3)
<i>b</i> [Å]	24.826(5)	77.382(16)	17.578(4)
<i>c</i> [Å]	25.615(5)	18.289(4)	20.951(4)
α [°]	90.00	90.00	65.37(3)
β [°]	91.70(3)	90.00	84.91(3)
γ [°]	90.00	90.00	87.23(3)
<i>V</i> [Å ³]	9443(3)	35447(12)	4232.8(15)
ρ [g·cm ⁻³]	1.436	1.399	1.680
<i>Z</i>	4	16	2
<i>F</i> (000)	4184	15360	2112
μ [mm ⁻¹]	1.087	1.057	5.091
<i>T</i> _{min} / <i>T</i> _{max}	0.5413 / 0.9108	0.7677 / 0.9100	0.4807 / 0.6882
<i>hkl</i> range	±17, ±28, -29 - 30	±29, ±90, -19 - 21	-15 - 13, ±21, ± 25
θ range [°]	1.59 - 24.71	1.40 - 24.63	1.27 - 25.85
measured refl.	35644	62573	47603
unique refl. [<i>R</i> _{int}]	15591 [0.1110]	14229 [0.1247]	16015 [0.1242]
observed refl. <i>I</i> > 2 σ (<i>I</i>)	10239	11506	7210
refined parameters	1108	1072	862
restraints	6	89	8
goodness-of-fit	0.942	0.998	0.873
<i>R</i> ₁ , ωR ₂ (<i>I</i> > 2 σ (<i>I</i>))	0.0710, 0.1470	0.0576, 0.1393	0.0685, 0.1287
<i>R</i> ₁ , ωR ₂ (all data)	0.1044, 0.1600	0.0739, 0.1477	0.1583, 0.1551
resid. el. dens. [e·Å ⁻³]	-0.429 / 0.706	-0.600 / 0.649	-0.579 / 0.900

Table 7.6: Crystal data and refinement details for **19** and **20**.

	19	20
empirical formula	C ₂₁ H ₂₈ CuF ₃ O ₃ S ₅	C ₁₀ H ₂₄ CuF ₆ PS ₄
formula weight [g·mol ⁻¹]	609.27	481.04
crystal size [mm ³]	0.28 × 0.11 × 0.08	0.22 × 0.15 × 0.15
crystal system	triclinic	monoclinic
space group	<i>P</i> $\bar{1}$	<i>C</i> 2/ <i>c</i>
<i>a</i> [Å]	8.0823(16)	12.604(3)
<i>b</i> [Å]	10.479(2)	23.420(5)
<i>c</i> [Å]	15.123(3)	9.1059(18)
α [°]	82.98(3)	90.00
β [°]	87.30(3)	133.79(3)
γ [°]	85.77(3)	90.00
<i>V</i> [Å ³]	1266.9(4)	1940.2(7)
ρ [g·cm ⁻³]	1.597	1.647
<i>Z</i>	2	4
<i>F</i> (000)	628	984
μ [mm ⁻¹]	1.318	1.682
<i>T</i> _{min} / <i>T</i> _{max}	0.7334 / 0.8873	0.6813 / 0.7990
<i>hkl</i> range	±10, ±13, ±19	±15, ±29, ±11
θ range [°]	1.96 - 26.97	2.40 - 26.92
measured refl.	12638	8143
unique refl. [<i>R</i> _{int.}]	5487 [0.0888]	2028 [0.0541]
observed refl. <i>I</i> > 2 σ (<i>I</i>)	4164	1611
refined parameters	298	147
restraints	0	0
goodness-of-fit	0.939	1.175
<i>R</i> 1, ω <i>R</i> 2 (<i>I</i> > 2 σ (<i>I</i>))	0.0453, 0.1049	0.0537, 0.0933
<i>R</i> 1, ω <i>R</i> 2 (all data)	0.0611, 0.1106	0.0772, 0.0991
resid. el. dens. [e·Å ⁻³]	-0.923 / 0.632	-0.466 / 0.735

Appendix A

Table A.1: Selected interatomic distances [Å] and angles [°] for **3**.

distances			
Cu1-N1	1.919(2)	Cu2-N2	1.922(2)
Cu1-N3	2.213(2)	Cu2-N5	2.175(2)
Cu1-N4	2.253(3)	Cu2-N6	2.307(2)
Cu1-Cl1	2.3912(9)	Cu2-Cl1	2.3817(9)
Cu1-Cl2	2.2206(8)	Cu2-Cl3	2.2246(8)
Cu1-Cu2	3.7927(13)		
angles			
N1-Cu1-N3	78.24(9)	N2-Cu2-N5	78.43(9)
N1-Cu1-N4	103.58(9)	N2-Cu2-N6	102.37(9)
N1-Cu1-Cl1	87.62(7)	N2-Cu2-Cl1	87.34(7)
N1-Cu1-Cl2	155.28(7)	N2-Cu2-Cl3	157.78(7)
N3-Cu1-N4	83.04(9)	N5-Cu2-N6	82.76(8)
N3-Cu1-Cl1	164.50(6)	N5-Cu2-Cl1	163.99(6)
N3-Cu1-Cl2	98.23(7)	N5-Cu2-Cl3	98.00(6)
N4-Cu1-Cl1	94.29(7)	N6-Cu2-Cl1	93.31(6)
N4-Cu1-Cl2	100.20(7)	N6-Cu2-Cl3	98.86(6)
Cl1-Cu1-Cl2	97.27(3)	Cl1-Cu2-Cl2	97.93(3)
Cu2-Cl2-Cu1	105.23(3)		

Table A.2: Selected interatomic distances [Å] and angles [°] for **4**.

distances			
Cu1-N1	1.936(4)	Cu2-N2	1.930(4)
Cu1-N3	2.170(4)	Cu2-N5	2.195(5)
Cu1-N4	2.329(4)	Cu2-N6	2.259(4)
Cu1-Br1	2.4996(9)	Cu2-Br1	2.5168(10)
Cu1-Br2	2.3671(9)	Cu2-Br3	2.3635(9)
Cu1-Cu2	3.8766(2)		
angles			
N1-Cu1-N3	79.15(16)	N2-Cu2-N5	79.10(17)
N1-Cu1-N4	101.60(16)	N2-Cu2-N6	104.49(17)
N1-Cu1-Br1	87.89(12)	N2-Cu2-Br1	88.10(13)
N1-Cu1-Br2	158.65(12)	N2-Cu2-Br3	153.64(12)
N3-Cu1-N4	82.68(14)	N5-Cu2-N6	83.20(16)
N3-Cu1-Br1	165.40(11)	N5-Cu2-Br1	166.03(12)
N3-Cu1-Br2	98.32(11)	N5-Cu2-Br3	98.57(13)
N4-Cu1-Br1	93.49(11)	N6-Cu2-Br1	94.75(12)
N4-Cu1-Br2	99.06(12)	N6-Cu2-Br3	101.25(12)
Br1-Cu1-Br2	96.19(3)	Br1-Cu2-Br3	95.38(3)
Cu1-Br1-Cu2	101.21(3)		

Table A.3: Selected interatomic distances [Å] and angles [°] for **5**.

distances			
Cu1-N1	1.905(6)	Cu2-N2	1.932(6)
Cu1-N3	2.185(5)	Cu2-N6	2.152(5)
Cu1-N4	2.246(5)	Cu2-N5	2.212(6)
Cu1-Cl2	2.2071(19)	Cu2-Cl1	2.3513(19)
Cu1-Cl1	2.3488(18)	Cu2-Cl3	2.254(2)
Cu1-Cu2	3.6894(6)		
angles			
N1-Cu1-N3	80.0(2)	N2-Cu2-N5	80.9(2)
N1-Cu1-N4	91.4(2)	N2-Cu2-N6	100.4(2)
N1-Cu1-Cl1	89.25(17)	N2-Cu2-Cl1	88.17(17)
N1-Cu1-Cl2	162.97(17)	N2-Cu2-Cl3	154.82(16)
N3-Cu1-N4	80.2(2)	N5-Cu2-N6	79.1(2)
N3-Cu1-Cl1	168.43(15)	N5-Cu2-Cl1	168.41(16)
N3-Cu1-Cl2	95.86(15)	N5-Cu2-Cl3	94.37(16)
N4-Cu1-Cl1	95.92(16)	N6-Cu2-Cl1	106.94(15)
Cl2-Cu1-N4	104.24(16)	N6-Cu2-Cl3	102.92(16)
Cl1-Cu1-Cl2	95.66(7)	Cl1-Cu2-Cl3	93.89(7)
Cu1-Cl1-Cu2	103.43(7)		

Table A.4: Selected interatomic distances [Å] and angles [°] for **6**.

distances			
Cu1-N1	1.934(3)	Cu2-N2	1.913(3)
Cu1-N3	2.153(3)	Cu2-N5	2.168(3)
Cu1-N4	2.185(3)	Cu2-N6	2.200(3)
Cu1-Br1	2.4652(5)	Cu2-Br1	2.4884(5)
Cu1-Br2	2.3962(5)	Cu2-Br3	2.3621(5)
Cu1-Cu2	3.8258(6)		
angles			
N1-Cu1-N3	80.18(11)	N2-Cu2-N5	80.74(11)
N1-Cu1-N4	99.58(12)	N2-Cu2-N6	100.17(12)
N3-Cu1-N4	79.22(11)	N5-Cu2-N6	77.87(11)
N1-Cu1-Br2	160.95(9)	N2-Cu2-Br3	157.43(9)
N3-Cu2-Br2	95.69(8)	N5-Cu2-Br3	95.45(8)
N4-Cu1-Br2	97.87(8)	N6-Cu2-Br3	100.74(8)
N1-Cu1-Br1	89.39(8)	N2-Cu2-Br1	89.07(8)
N3-Cu1-Br1	169.57(8)	N5-Cu2-Br1	169.78(8)
N4-Cu1-Br1	102.53(8)	N6-Cu2-Br1	103.34(8)
Br2-Cu1-Br1	94.259(19)	Br3-Cu2-Br1	94.288(19)
Cu1-Br1-Cu2	101.125(18)		

Table A.5: Selected interatomic distances [Å] and angles [°] for **7**.

distances			
Cu1-N1	1.897(6)	Cu2-N2	1.913(5)
Cu1-N3	2.236(6)	Cu2-N5	2.228(6)
Cu1-N4	2.184(6)	Cu2-N6	2.226(6)
Cu1-Cl1	2.3444(19)	Cu2-Cl1	2.330(2)
Cu1-Cl2	2.2253(19)	Cu2-Cl3	2.2265(19)
Cu1-Cu2	3.7734(14)		
angles			
N1-Cu1-N3	79.6(2)	N2-Cu2-N6	96.0(2)
N1-Cu1-N4	100.5(2)	N2-Cu2-N5	78.9(2)
N1-Cu1-Cl1	86.92(16)	N2-Cu2-Cl1	87.19(16)
N1-Cu1-Cl2	158.81(18)	N2-Cu2-Cl3	166.92(17)
N3-Cu1-Cl1	166.39(15)	N5-Cu2-N6	77.6(2)
N3-Cu1-N4	79.0(2)	N5-Cu2-Cl3	96.30(15)
N3-Cu1-Cl2	97.69(15)	N5-Cu2-Cl1	162.92(15)
N4-Cu1-Cl1	101.61(15)	N6-Cu2-Cl1	114.02(16)
N4-Cu1-Cl2	99.59(16)	N6-Cu2-Cl3	94.82(16)
Cl1-Cu1-Cl2	95.62(7)	Cl1-Cu2-Cl3	95.12(7)
Cu1-Cl1-Cu2	107.66(8)		

Table A.6: Selected interatomic distances [Å] and angles [°] for **8**.

Distances			
Cu1-N1	1.928(8)	Cu2-N2	1.930(8)
Cu1-N3	2.211(7)	Cu2-N5	2.243(7)
Cu1-N4	2.183(7)	Cu2-N6	2.177(7)
Cu1-Br1	2.4947(15)	Cu2-Br1	2.5319(15)
Cu1-Br2	2.3980(16)	Cu2-Br3	2.3729(15)
Cu1-Cu2	3.8718(18)		
Angles			
N1-Cu1-N3	79.3(3)	N2-Cu2-N5	79.7(3)
N1-Cu1-N4	95.0(3)	N2-Cu2-N6	99.3(3)
N1-Cu1-Br1	88.7(2)	N2-Cu2-Br1	88.4(2)
N1-Cu1-Br2	160.4(2)	N2-Cu2-Br3	158.2(2)
N3-Cu1-N4	76.1(3)	N5-Cu2-N6	77.7(3)
N3-Cu1-Br1	168.07(19)	N5-Cu2-Br1	168.18(19)
N3-Cu1-Br2	96.16(18)	N5-Cu2-Br3	95.95(18)
N4-Cu1-Br1	105.7(2)	N6-Cu2-Br1	104.3(2)
N4-Cu1-Br2	102.5(2)	N6-Cu2-Br3	100.7(2)
Br1-Cu1-Br2	94.94(5)	Br1-Cu2-Br3	95.15(5)
Cu1-Br1-Cu2	100.75(5)		

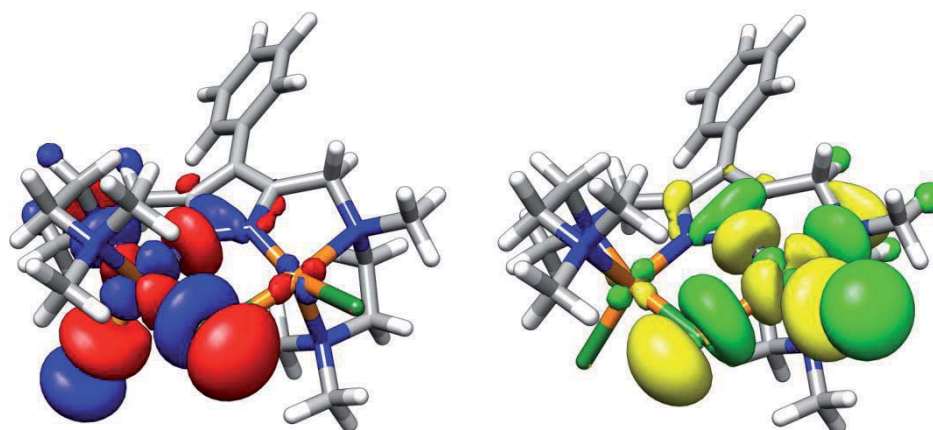


Figure A.1: SOMOs of complex 2 (0.02 a.u. level), left: spin up orbital (alpha), right: spin-down orbital (beta). The blue and green colored parts represent the positive part of the wave function, the red and yellow colored parts represent the negative part of the wave function.

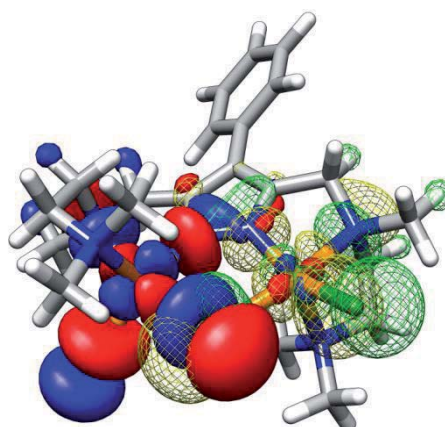


Figure A.2: Magnetic molecular orbitals of complex 2 (0.02 a.u. level). Solid: spin-up part, dashed, spin-down part.

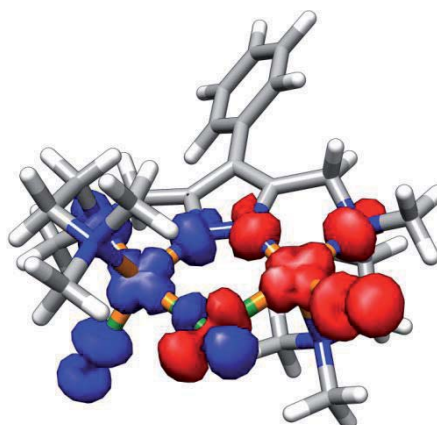


Figure A.3: Spin-density plot of 2 (0.002 a.u. level), spin-up part: blue, spin-down part: red.

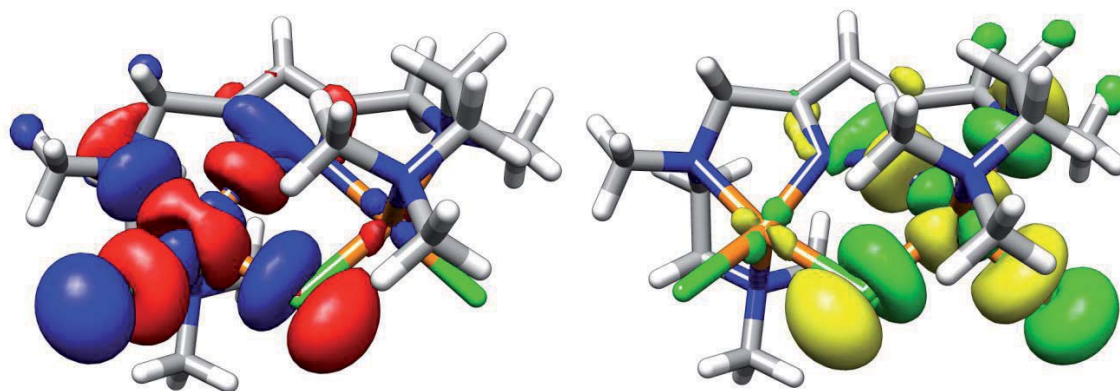


Figure A.4: SOMOs of complex **3** (0.02 a.u. level), left: spin-up orbital (alpha), right: spin-down orbital (beta). The blue and green colored parts represent the positive part of the wave function, the red and yellow colored parts represent the negative part of the wave function.

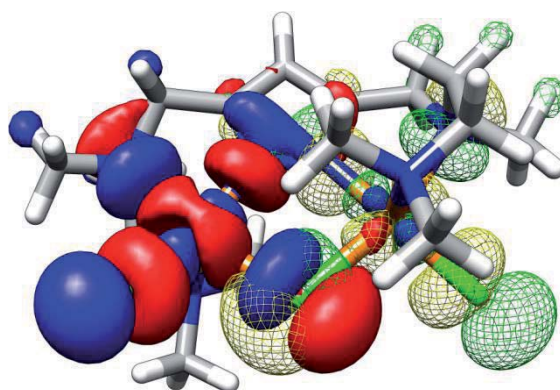


Figure A.5: Magnetic molecular orbitals of complex **3** (0.02 a.u. level). Solid: spin-up part, meshed, spin-down part.

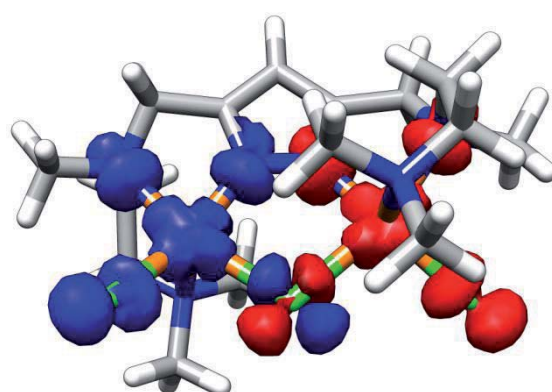


Figure A.6: Spin density plot of **3** (0.002 a.u. level), spin-up part: blue, spin-down part: red.

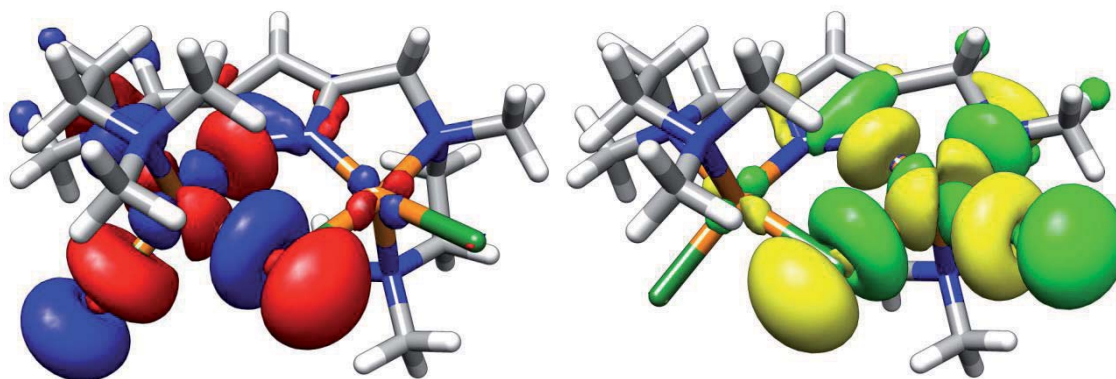


Figure A.7: SOMOs of complex 4 (0.02 a.u. level), left: spin-up orbital (alpha), right: spin-down orbital (beta). The blue and green colored parts represent the positive part of the wave function, the red and yellow colored parts represent the negative part of the wave function.

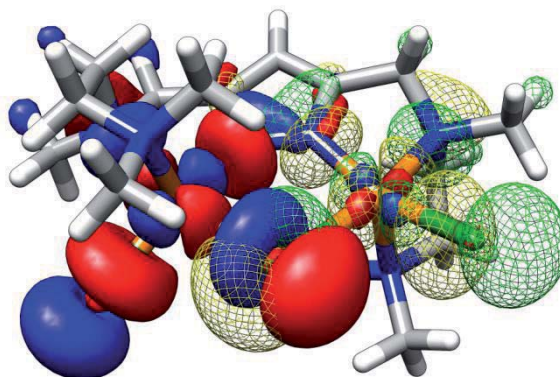


Figure A.8: Magnetic molecular orbitals of complex 4 (0.02 a.u. level). Solid: spin-up part, meshed, spin-down part.

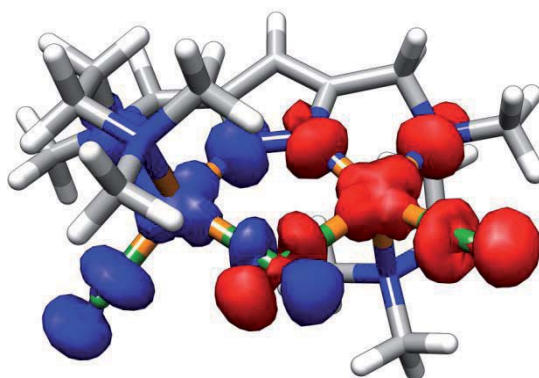


Figure A.9: Spin density plot of 4 (0.002 a.u. level), spin-up part: blue, spin-down part: red.

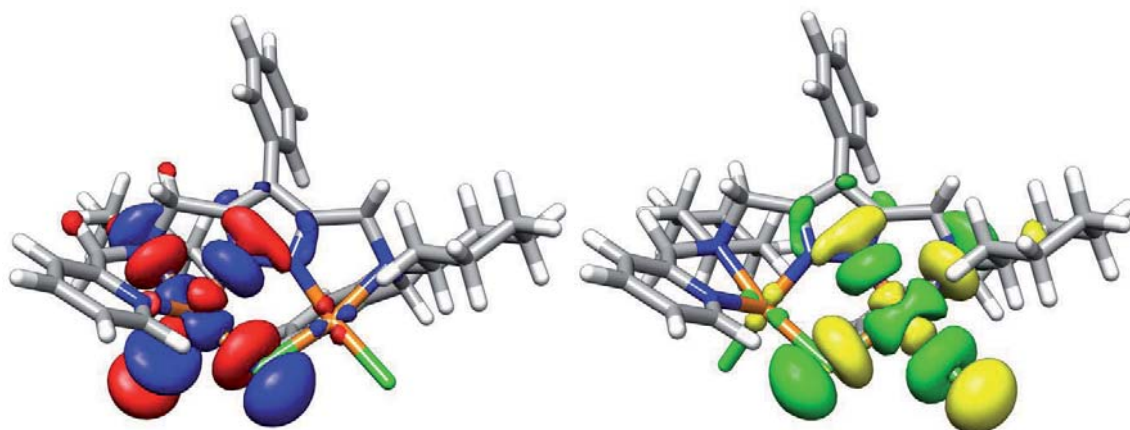


Figure A.10: SOMOs of complex **5** (0.02 a.u. level), left: spin-up orbital (alpha), right: spin-down orbital (beta). The blue and green colored parts represent the positive part of the wave function, the red and yellow colored parts represent the negative part of the wave function.

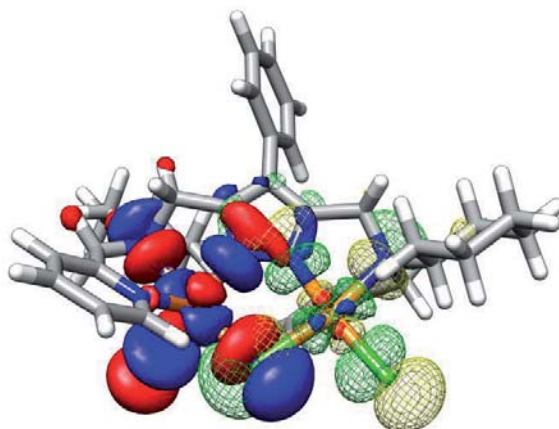


Figure A.11: Magnetic molecular orbitals of complex **5** (0.02 a.u. level). Solid: spin-up part, meshed, spin-down part.

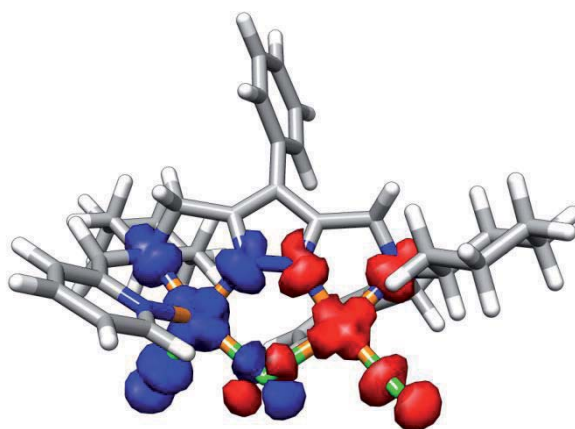


Figure A.12: Spin density plot of **5** (0.002 a.u. level), spin-up part: blue, spin-down part: red.

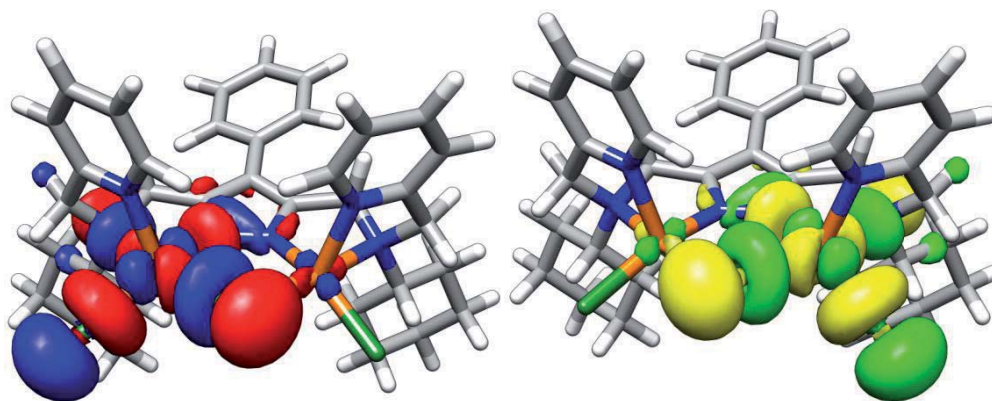


Figure A.13: SOMOs of complex **6** (0.02 a.u. level), left: spin-up orbital (alpha), right: spin-down orbital (beta). The blue and green colored parts represent the positive part of the wave function, the red and yellow colored parts represent the negative part of the wave function.

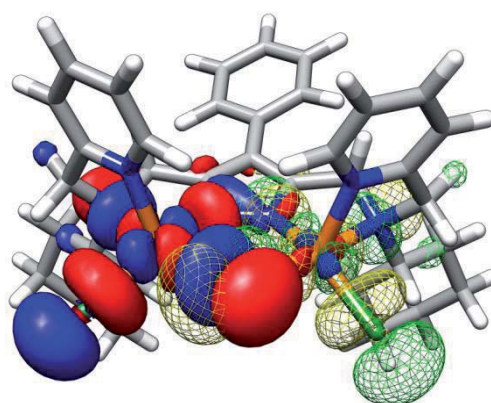


Figure A.14: Magnetic molecular orbitals of complex **6** (0.02 a.u. level). Solid: spin-up part, meshed, spin-down part.

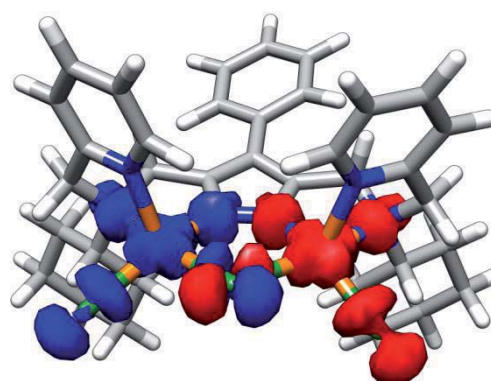


Figure A.15: Spin density plot of **6** (0.002 a.u. level), spin-up part: blue, spin-down part: red.

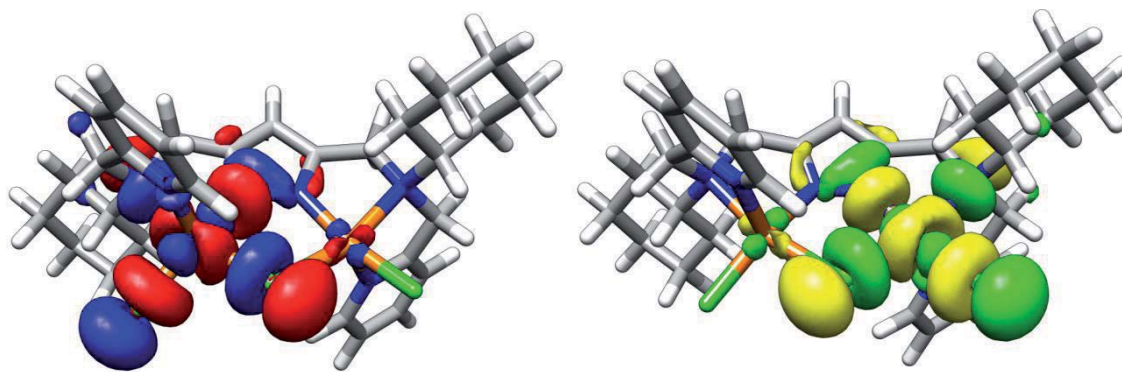


Figure A.16: SOMOs of complex 7 (0.02 a.u. level), left: spin-up orbital (alpha), right: spin-down orbital (beta). The blue and green colored parts represent the positive part of the wave function, the red and yellow colored parts represent the negative part of the wave function.

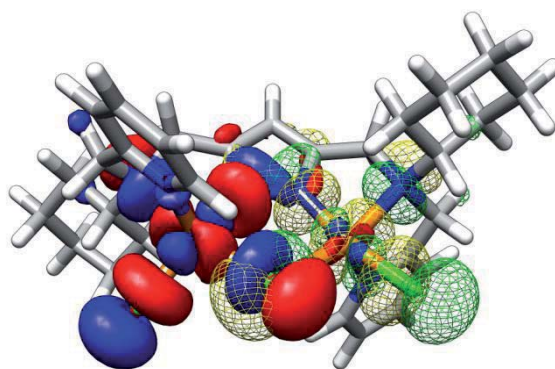


Figure A.17: Magnetic molecular orbitals of complex 7 (0.02 a.u. level). Solid: spin-up part, meshed, spin-down part.

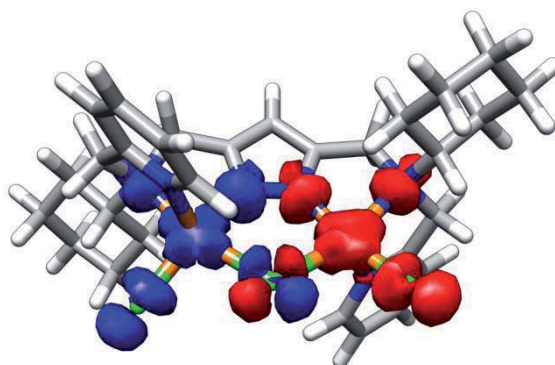


Figure A.18: Spin density plot of 7 (0.002 a.u. level), spin-up part: blue, spin-down part: red.

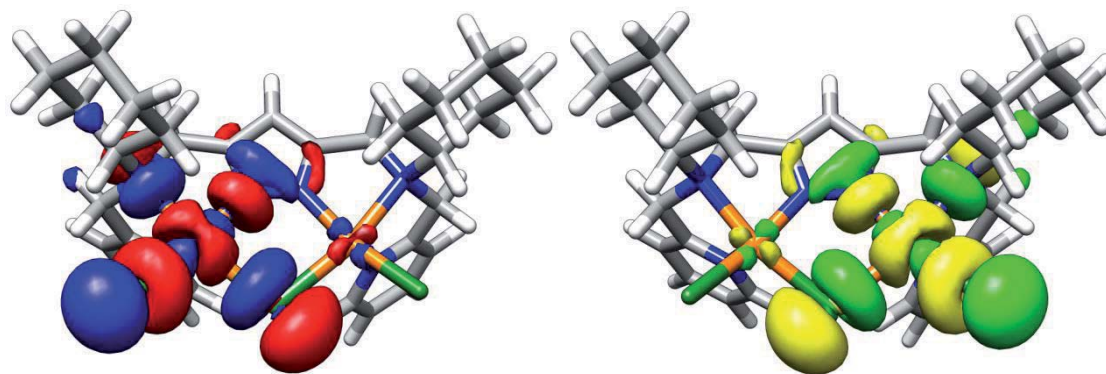


Figure A.19: SOMOs of complex **8** (0.02 a.u. level), left: spin-up orbital (alpha), right: spin-down orbital (beta). The blue and green colored parts represent the positive part of the wave function, the red and yellow colored parts represent the negative part of the wave function.

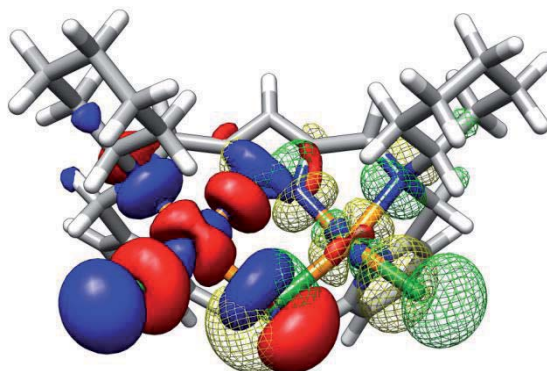


Figure A.20: Magnetic molecular orbitals of complex **8** (0.02 a.u. level). Solid: spin-up part, meshed, spin-down part.

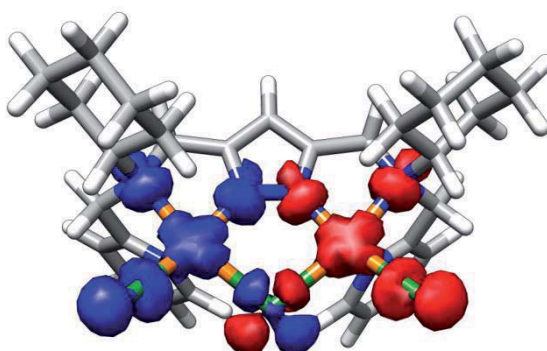
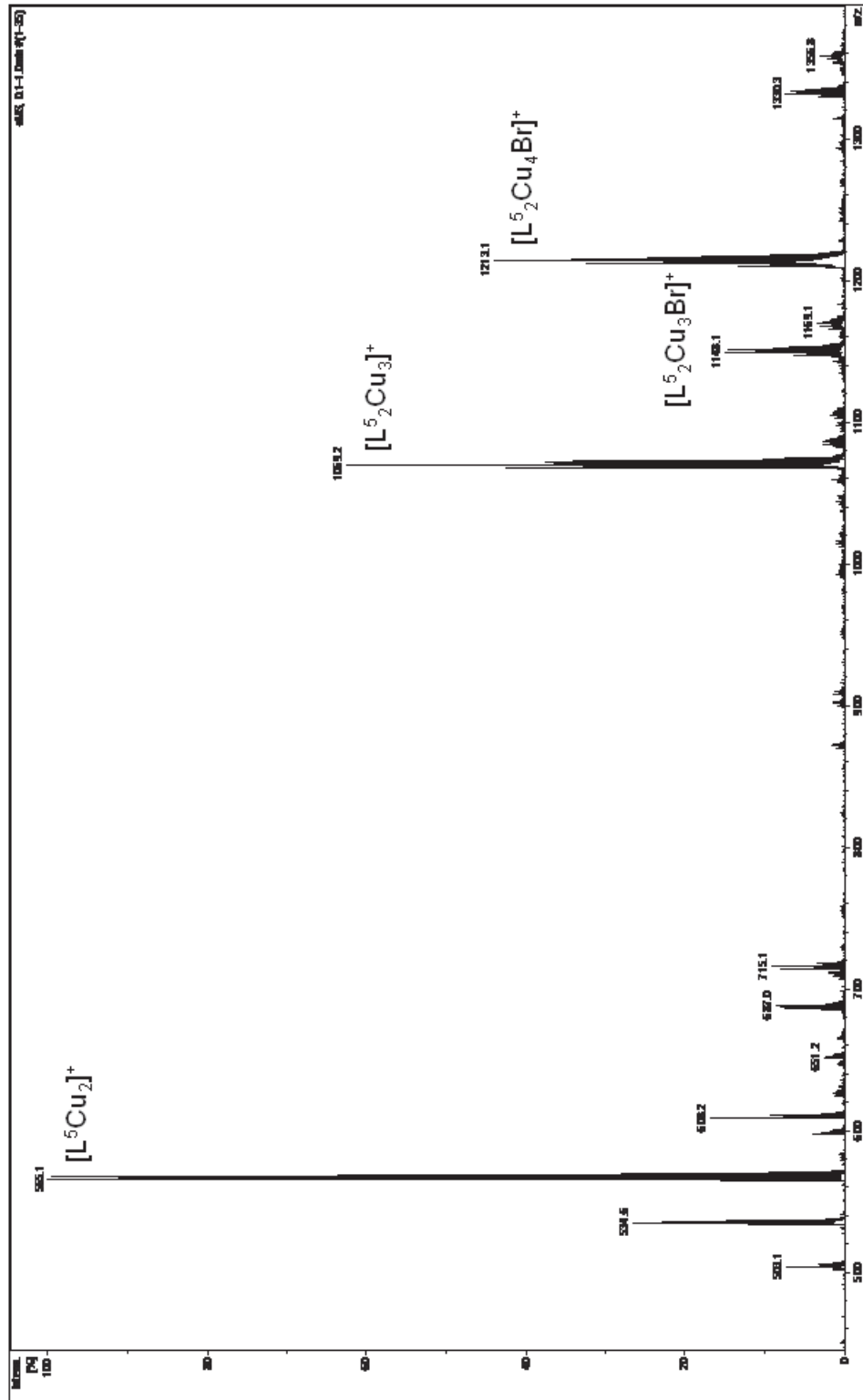
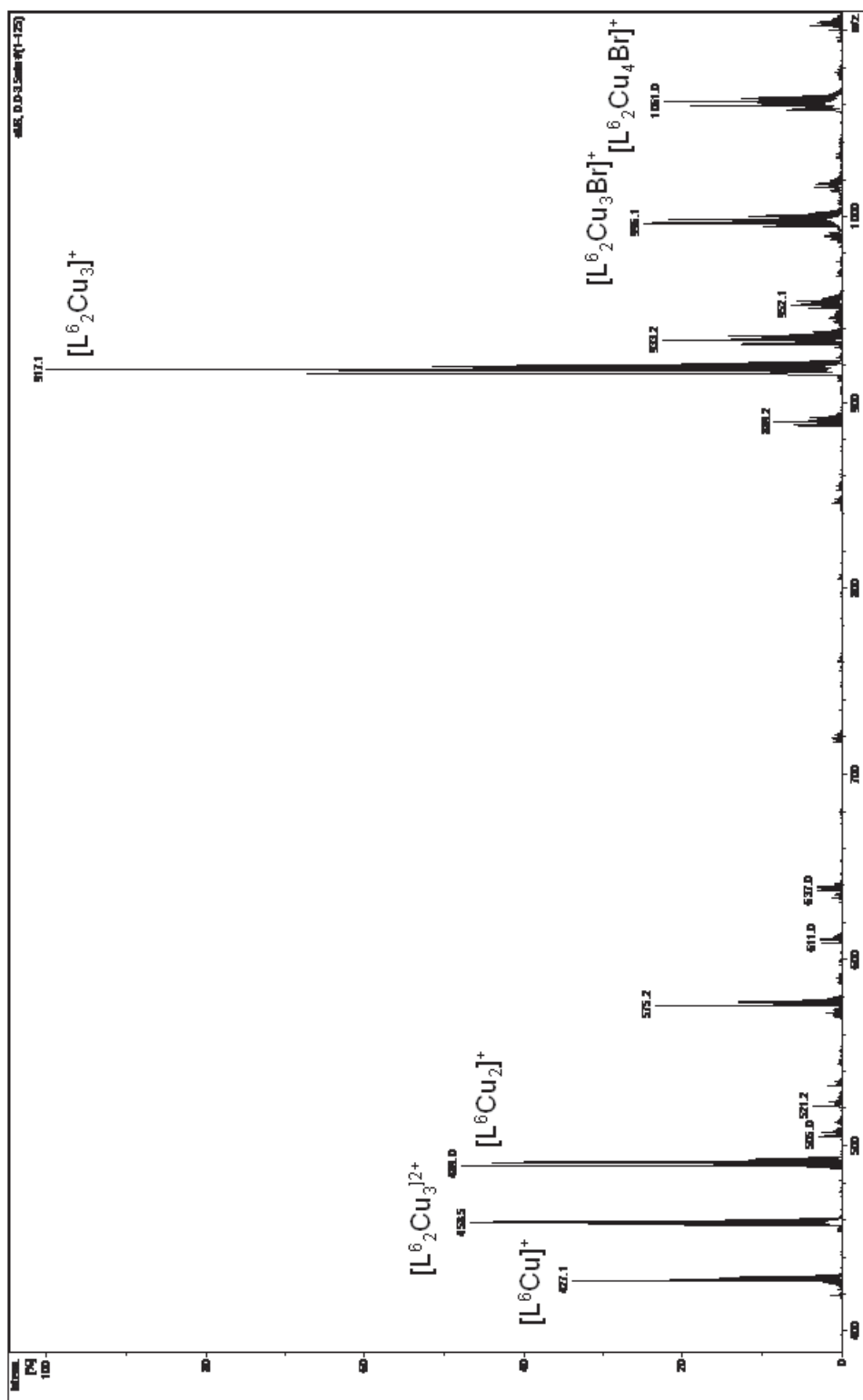


Figure A.21: Spin density plot of **8** (0.002 a.u. level), spin-up part: blue, spin-down part: red.



Appendix B

Figure B.1: ESI⁺ mass spectrum of L^5Cu_2Br in MeCN.

Figure B.2: ESI⁺ mass spectrum of **18** in MeCN.

8. Bibliography

- [1] H. B. Kraatz, N. Metzler-Nolte, *Concepts and models in bioinorganic chemistry*, Wiley-VCH, **2006**.
- [2] W. Kaim, B. Schwederski, *Bioanorganische Chemie*, B. G. Teubner Verlag, Wiesbaden, **2005**.
- [3] R. P. Csintalan, N. M. Senozan, *J. Chem. Educ.* **1991**, *68*, 365-367.
- [4] B. L. C. Vulpe, Susan Whitney, Seymour Packman, Jane Gitschier, *Nature Gen.* **1993**, *3*, 7-13.
- [5] K. Davies, *Nature* **1993**, *361*, 98-98.
- [6] D. H. Hamer, *Nature Gen.* **1993**, *3*, 3-4.
- [7] E. Wiberg, A. F. Holleman, N. Wiberg, *Lehrbuch der Anorganischen Chemie*, Walter de Gruyter, **2007**.
- [8] N. N. Greenwood, A. Earnshaw, *Chemie der Elemente, Vol. 1*, VCH, Weinheim, **1988**.
- [9] E. I. Solomon, M. J. Baldwin, M. D. Lowery, *Chem. Rev.* **1992**, *92*, 521-542.
- [10] E. I. Solomon, U. M. Sundaram, T. E. Machonkin, *Chem. Rev.* **1996**, *96*, 2563-2606.
- [11] G. N. George, J. Byrd, D. R. Winge, *J. Biol. Chem.* **1988**, *263*, 8199-8203.
- [12] C. Belle, W. Rammal, J.-L. Pierre, *J. Inorg. Biochem.* **2005**, *99*, 1929-1936.
- [13] A. Pomowski, W. G. Zumft, P. M. H. Kroneck, O. Einsle, *Nature* **2011**, *477*, 234-237.
- [14] W. G. Zumft, P. M. H. Kroneck, K. P. Robert, in *Advances in Microbial Physiology, Vol. Volume 52*, Academic Press, **2006**, pp. 107-227.
- [15] W. C. Trogler, *Coord. Chem. Rev.* **1999**, *187*, 303-327.
- [16] M. Dameris, *Angew. Chem. Int. Ed.* **2010**, *49*, 489-491.
- [17] A. R. Ravishankara, J. S. Daniel, R. W. Portmann, *Science* **2009**, *326*, 123-125.
- [18] W. G. Zumft, T. Matsubara, *FEBS Lett.* **1982**, *148*, 107-112.
- [19] J. A. Farrar, A. J. Thomson, M. R. Cheesman, D. M. Dooley, W. G. Zumft, *FEBS Lett.* **1991**, *294*, 11-15.
- [20] T. Rasmussen, B. C. Berks, J. N. Butt, A. J. Thomson, *Biochem. J.* **2002**, *364*, 807-815.
- [21] W. G. Zumft, *Microbiol. Mol. Biol. Rev.* **1997**, *61*, 533-616.

- [22] K. Brown, M. Tegoni, M. Prudencio, A. S. Pereira, S. Besson, J. J. Moura, I. Moura, C. Cambillau, *Nat. Struct. Mol. Biol.* **2000**, *7*, 191-195.
- [23] S. Iwata, C. Ostermeier, B. Ludwig, H. Michel, *Nature* **1995**, *376*, 660-669.
- [24] T. Tsukihara, H. Aoyama, E. Yamashita, T. Tomizaki, H. Yamaguchi, K. Shinzawa-Itoh, R. Nakashima, R. Yaono, S. Yoshikawa, *Science* **1995**, *269*, 1069-1074.
- [25] K. Brown, K. Djinovic-Carugo, T. Haltia, I. Cabrito, M. Saraste, J. J. G. Moura, I. Moura, M. Tegoni, C. Cambillau, *J. Biol. Chem.* **2000**, *275*, 41133-41136.
- [26] M. Savelieff, Y. Lu, *J. Biol. Inorg. Chem.* **2010**, *15*, 461-483.
- [27] N. J. Blackburn, M. E. Barr, W. H. Woodruff, J. van der Oost, S. de Vries, *Biochemistry* **1994**, *33*, 10401-10407.
- [28] G. Henkel, A. Müller, S. Weissgräber, G. Buse, T. Soulimane, G. C. M. Steffens, H.-F. Nolting, *Angew. Chem. Int. Ed.* **1995**, *34*, 1488-1492.
- [29] K. Paraskevopoulos, S. V. Antonyuk, R. G. Sawers, R. R. Eady, S. S. Hasnain, *J. Mol. Biol.* **2006**, *362*, 55-65.
- [30] T. Haltia, K. Brown, M. Tegoni, C. Cambillau, M. Saraste, K. Mattila, K. Djinovic-Carugo, *Biochem. J.* **2003**, *369*, 77-88.
- [31] P. Chen, S. I. Gorelsky, S. Ghosh, E. I. Solomon, *Angew. Chem. Int. Ed.* **2004**, *43*, 4132-4140.
- [32] S. Ghosh, S. I. Gorelsky, P. Chen, I. Cabrito, I. Moura, E. I. Solomon, *J. Am. Chem. Soc.* **2003**, *125*, 15708-15709.
- [33] S. I. Gorelsky, S. Ghosh, E. I. Solomon, *J. Am. Chem. Soc.* **2005**, *128*, 278-290.
- [34] S. Dell'Acqua, S. Pauleta, I. Moura, J. Moura, *J. Biol. Inorg. Chem.* **2011**, *16*, 183-194.
- [35] C. L. Coyle, W. G. Zumft, P. M. Kroneck, H. Körner, W. Jakob, *Eur. J. Biochem.* **1985**, *153*, 459-467.
- [36] J. Riestler, W. G. Zumft, P. M. Kroneck, *Eur. J. Biochem.* **1989**, *178*, 751-762.
- [37] S. Ferretti, J. G. Grossmann, S. S. Hasnain, R. R. Eady, B. E. Smith, *Eur. J. Biochem.* **1999**, *259*, 651-659.
- [38] E. Bouwman, J. Reedijk, *Coord. Chem. Rev.* **2005**, *249*, 1555-1581.
- [39] A. Müller, W. Jaegermann, J. H. Enemark, *Coord. Chem. Rev.* **1982**, *46*, 245-280.
- [40] K. Fujisawa, Y. Moro-Oka, N. Kitajima, *J. Chem. Soc., Chem. Commun.* **1994**, 623-624.

- [41] N. Kitajima, K. Fujisawa, M. Tanaka, Y. Morooka, *J. Am. Chem. Soc.* **1992**, *114*, 9232-9233.
- [42] E. C. Brown, N. W. Aboeella, A. M. Reynolds, G. Aullón, S. Alvarez, W. B. Tolman, *Inorg. Chem.* **2004**, *43*, 3335-3337.
- [43] E. C. Brown, I. Bar-Nahum, J. T. York, N. W. Aboeella, W. B. Tolman, *Inorg. Chem.* **2007**, *46*, 486-496.
- [44] M. Inosako, C. Shimokawa, H. Sugimoto, N. Kihara, T. Takata, S. Itoh, *Chem. Lett.* **2007**, *36*, 1306-1307.
- [45] I. Bar-Nahum, J. T. York, V. G. Young, W. B. Tolman, *Angew. Chem. Int. Ed.* **2008**, *47*, 533-536.
- [46] L. Yang, J. Tehranchi, W. B. Tolman, *Inorg. Chem.* **2011**, *50*, 2606-2612.
- [47] M. E. Helton, P. Chen, P. P. Paul, Z. Tyeklár, R. D. Sommer, L. N. Zakharov, A. L. Rheingold, E. I. Solomon, K. D. Karlin, *J. Am. Chem. Soc.* **2003**, *125*, 1160-1161.
- [48] J. T. York, E. C. Brown, W. B. Tolman, *Angew. Chem. Int. Ed.* **2005**, *44*, 7745-7748.
- [49] E. C. Brown, J. T. York, W. E. Antholine, E. Ruiz, S. Alvarez, W. B. Tolman, *J. Am. Chem. Soc.* **2005**, *127*, 13752-13753.
- [50] R. Sarangi, J. T. York, M. E. Helton, K. Fujisawa, K. D. Karlin, W. B. Tolman, K. O. Hodgson, B. Hedman, E. I. Solomon, *J. Am. Chem. Soc.* **2007**, *130*, 676-686.
- [51] J. T. York, I. Bar-Nahum, W. B. Tolman, *Inorg. Chem.* **2007**, *46*, 8105-8107.
- [52] P. Chen, K. Fujisawa, M. E. Helton, K. D. Karlin, E. I. Solomon, *J. Am. Chem. Soc.* **2003**, *125*, 6394-6408.
- [53] M. E. Helton, D. Maiti, L. N. Zakharov, A. L. Rheingold, J. A. Porco, K. D. Karlin, *Angew. Chem. Int. Ed.* **2006**, *45*, 1138-1141.
- [54] D. Maiti, J. S. Woertink, M. A. Vance, A. E. Milligan, A. A. Narducci Sarjeant, E. I. Solomon, K. D. Karlin, *J. Am. Chem. Soc.* **2007**, *129*, 8882-8892.
- [55] P. P. Paul, Z. Tyeklar, R. R. Jacobson, K. D. Karlin, *J. Am. Chem. Soc.* **1991**, *113*, 5322-5332.
- [56] L. Q. Hatcher, K. D. Karlin, *J. Biol. Inorg. Chem.* **2004**, *9*, 669 - 683.
- [57] I. Bar-Nahum, A. K. Gupta, S. M. Huber, M. Z. Ertem, C. J. Cramer, W. B. Tolman, *J. Am. Chem. Soc.* **2009**, *131*, 2812-2814.
- [58] I. G. Dance, *Polyhedron* **1986**, *5*, 1037-1104.
- [59] G. Henkel, B. Krebs, *Chem. Rev.* **2004**, *104*, 801-824.

- [60] B. Krebs, G. Henkel, *Angew. Chem. Int. Ed.* **1991**, *30*, 769-788.
- [61] K. Fujisawa, S. Imai, N. Kitajima, Y. Moro-oka, *Inorg. Chem.* **1998**, *37*, 168-169.
- [62] S. A. Koch, R. Fikar, M. Millar, T. O'Sullivan, *Inorg. Chem.* **1984**, *23*, 121-122.
- [63] C. D. Garner, J. R. Nicholson, W. Clegg, *Inorg. Chem.* **1984**, *23*, 2148-2150.
- [64] D. Coucouvanis, C. N. Murphy, S. K. Kanodia, *Inorg. Chem.* **1980**, *19*, 2993-2998.
- [65] T.-A. Okamura, N. Ueyama, A. Nakamura, E. W. Ainscough, A. M. Brodie, J. M. Waters, *J. Chem. Soc., Chem. Commun.* **1993**, 1658-1660.
- [66] I. G. Dance, P. J. Guernsey, A. D. Rae, M. L. Scudder, *Inorg. Chem.* **1983**, *22*, 2883-2887.
- [67] I. G. Dance, L. J. Fitzpatrick, M. L. Scudder, *J. Chem. Soc., Chem. Commun.* **1983**, 546-548.
- [68] E. Block, H. Kang, G. Ofori-Okai, J. Zubieta, *Inorg. Chim. Acta* **1990**, *167*, 147-148.
- [69] M. Baumgartner, W. Bensch, P. Hug, E. Dubler, *Inorg. Chim. Acta* **1987**, *136*, 139-147.
- [70] I. G. Dance, J. C. Calabrese, *Inorg. Chim. Acta* **1976**, *19*, L41-L42.
- [71] I. G. Dance, G. A. Bowmaker, G. R. Clark, J. K. Seadon, *Polyhedron* **1983**, *2*, 1031-1043.
- [72] M. Baumgartner, H. Schmalte, E. Dubler, *Polyhedron* **1990**, *9*, 1155-1164.
- [73] G. A. Bowmaker, G. R. Clark, J. K. Seadon, I. G. Dance, *Polyhedron* **1984**, *3*, 535-544.
- [74] I. G. Dance, *J. Chem. Soc., Chem. Commun.* **1976**, 68-69.
- [75] I. G. Dance, *Aust. J. Chem.* **1978**, *31*, 2195-2206.
- [76] E. Block, M. Gernon, H. Kang, G. Ofori-Okai, J. Zubieta, *Inorg. Chem.* **1989**, *28*, 1263-1271.
- [77] B. Becker, W. Wojnowski, K. Peters, E.-M. Peters, H. G. v. Schnering, *Polyhedron* **1992**, *11*, 613-616.
- [78] R. K. Chadha, R. Kumar, D. G. Tuck, *Can. J. Chem.* **1987**, *65*, 1336-1342.
- [79] A. F. Stange, W. Kaim, *Chem. Commun.* **1998**, 469-470.
- [80] D. Ohlmann, C. M. Marchand, H. Schönberg, H. Grützmacher, H. Pritzkow, *Z. Anorg. Allg. Chem.* **1996**, *622*, 1349-1357.
- [81] A. F. Stange, A. Klein, K.-W. Klinkhammer, W. Kaim, *Inorg. Chim. Acta* **2001**, *324*, 336-341.

- [82] J. Schneider, M. Köckerling, R. Kopitzky, G. Henkel, *Eur. J. Inorg. Chem.* **2003**, 2003, 1727-1734.
- [83] A. Stange, T. Schurr, A. Klein, W. Kaim, *Z. Anorg. Allg. Chem.* **2005**, 631, 663-671.
- [84] M. S. Ameerunisha Begum, O. Seewald, U. Flörke, G. Henkel, *Inorg. Chim. Acta* **2008**, 361, 1868-1874.
- [85] M. Gennari, M. Lanfranchi, R. Cammi, M. A. Pellinghelli, L. Marchiò, *Inorg. Chem.* **2007**, 46, 10143-10152.
- [86] Y. Lee, A. A. N. Sarjeant, K. D. Karlin, *Chem. Commun.* **2006**, 621-623.
- [87] B. Bosnich, *Inorg. Chem.* **1999**, 38, 2554-2562.
- [88] A. L. Gavrilova, B. Bosnich, *Chem. Rev.* **2004**, 104, 349-384.
- [89] A. M. Barrios, S. J. Lippard, *Inorg. Chem.* **2001**, 40, 1060-1064.
- [90] A. Bencini, D. Gatteschi, C. Zanchini, J. G. Haasnoot, R. Prins, J. Reedijk, *Inorg. Chem.* **1985**, 24, 2812-2815.
- [91] J.-L. Chou, D.-N. Horng, J.-P. Chyn, K.-M. Lee, F. L. Urbach, G.-H. Lee, H.-L. Tsai, *Inorg. Chem. Commun.* **1999**, 2, 392-395.
- [92] T. Gajda, R. Krämer, A. Jancsó, *Eur. J. Inorg. Chem.* **2000**, 2000, 1635-1644.
- [93] P. Gentschev, M. Lüken, N. Möller, A. Rompel, B. Krebs, *Inorg. Chem. Commun.* **2001**, 4, 753-756.
- [94] C. He, J. L. DuBois, B. Hedman, K. O. Hodgson, S. J. Lippard, *Angew. Chem. Int. Ed.* **2001**, 40, 1484-1487.
- [95] C. He, S. J. Lippard, *J. Am. Chem. Soc.* **2000**, 122, 184-185.
- [96] T. Kamiyuki, H. Okawa, N. Matsumoto, S. Kida, *J. Chem. Soc., Dalton Trans.* **1990**, 195-198.
- [97] R. Prins, P. J. M. W. L. Birker, J. G. Haasnoot, G. C. Verschoor, J. Reedijk, *Inorg. Chem.* **1985**, 24, 4128-4133.
- [98] J. Reim, B. Krebs, *J. Chem. Soc., Dalton Trans.* **1997**, 3793-3804.
- [99] T. N. Sorrell, C. O'Connor, O. P. Anderson, J. H. Reibenspies, *J. Am. Chem. Soc.* **1985**, 107, 4199-4206.
- [100] J. Ackermann, F. Meyer, E. Kaifer, H. Pritzkow, *Chem. Eur. J.* **2002**, 8, 247-258.
- [101] J. Ackermann, F. Meyer, H. Pritzkow, *Inorg. Chim. Acta* **2004**, 357, 3703-3711.
- [102] M. Konrad, F. Meyer, K. Heinze, L. Zsolnai, *J. Chem. Soc., Dalton Trans.* **1998**, 199-206.

- [103] A. Prokofieva, A. I. Prikhod'ko, E. A. Enyedy, E. Farkas, W. Maringgele, S. Demeshko, S. Dechert, F. Meyer, *Inorg. Chem.* **2007**, *46*, 4298-4307.
- [104] J. Klingele, S. Dechert, F. Meyer, *Coord. Chem. Rev.* **2009**, *253*, 2698-2741.
- [105] F. Meyer, K. Heinze, B. Nuber, L. Zsolnai, *J. Chem. Soc., Dalton Trans.* **1998**, 207-214.
- [106] F. Meyer, E. Kaifer, P. Kircher, K. Heinze, H. Pritzkow, *Chem. Eur. J.* **1999**, *5*, 1617-1630.
- [107] F. Meyer, P. Rutsch, *Chem. Commun.* **1998**, 1037-1038.
- [108] F. Meyer, S. Beyreuther, K. Heinze, L. Zsolnai, *Chem. Ber.* **1997**, *130*, 605-613.
- [109] J. C. Röder, F. Meyer, H. Pritzkow, *Organometallics* **2001**, *20*, 811-817.
- [110] B. Bauer-Siebenlist, F. Meyer, E. Farkas, D. Vidovic, J. A. Cuesta-Seijo, R. Herbst-Irmer, H. Pritzkow, *Inorg. Chem.* **2004**, *43*, 4189-4202.
- [111] F. Meyer, H. Pritzkow, *Angew. Chem. Int. Ed.* **2000**, *39*, 2112-2115.
- [112] A. Prokofieva, A. I. Prikhod'ko, S. Dechert, F. Meyer, *Chem. Commun.* **2008**, 1005-1007.
- [113] G. Noël, J. C. Röder, S. Dechert, H. Pritzkow, L. Bolk, S. Mecking, F. Meyer, *Adv. Synth. Cat.* **2006**, *348*, 887-897.
- [114] A. Kumar Singh, J. I. van der Vlugt, S. Demeshko, S. Dechert, F. Meyer, *Eur. J. Inorg. Chem.* **2009**, *2009*, 3431-3439.
- [115] B. Schneider, S. Demeshko, S. Dechert, F. Meyer, *Angew. Chem. Int. Ed.* **2010**, *49*, 9274-9277.
- [116] L. Penkova, S. Demeshko, M. Haukka, V. A. Pavlenko, F. Meyer, I. O. Fritsky, *Z. Anorg. Allg. Chem.* **2008**, *634*, 2428-2436.
- [117] J. Teichgräber, G. Leibelng, S. Dechert, F. Meyer, *Z. Anorg. Allg. Chem.* **2005**, *631*, 2613-2618.
- [118] V. Kruse, diploma thesis, Georg-August-Universität (Göttingen), **2007**.
- [119] A. Sachse, L. Penkova, G. Noël, S. Dechert, O. A. Varzatskii, I. O. Fritsky, F. Meyer, *Synthesis* **2008**, *5*, 800-806.
- [120] M. Stollenz, C. Große, F. Meyer, *Chem. Commun.* **2008**, 1744-1746.
- [121] A. F. Holleman, N. Wiberg, *Lehrbuch der Anorganischen Chemie, Vol. 102*, Walter de Gruyter, Berlin, **2007**.
- [122] T. G. Schenck, C. R. C. Milne, J. F. Sawyer, B. Bosnich, *Inorg. Chem.* **1985**, *24*, 2338-2344.

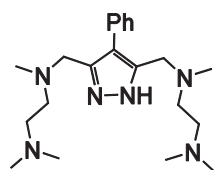
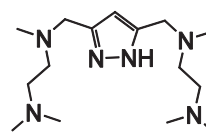
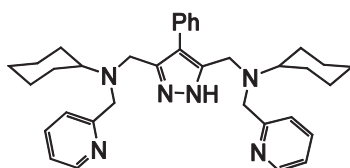
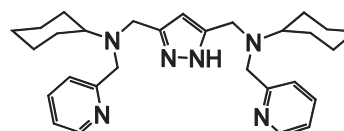
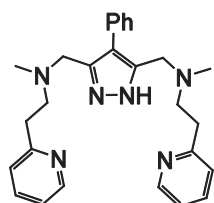
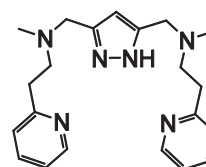
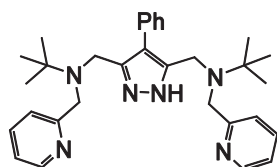
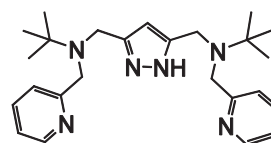
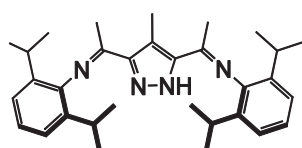
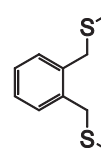
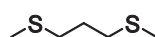
- [123] M. Stollenz, H. Gehring, V. Konstanzer, S. Fischer, S. Dechert, C. Grosse, F. Meyer, *Organometallics* **2011**, *30*, 3708-3725.
- [124] O. Kahn, *Molecular Magnetism*, VCH, **1993**.
- [125] A. W. Addison, T. N. Rao, J. Reedijk, J. van Rijn, G. C. Verschoor, *J. Chem. Soc., Dalton Trans.* **1984**, 1349-1356.
- [126] A. P. Gingsberg, *Inorg. Chim. Act. Rev.* **1971**, *5*, 45-68.
- [127] J. S. Miller, A. J. Epstein, *Angew. Chem. Int. Ed.* **1994**, *33*, 385-415.
- [128] W. Plass, *Chem. Unserer Zeit*, **1998**, *32*, 323-333.
- [129] S. Demeshko, G. Leibelng, S. Dechert, S. Fuchs, T. Pruschke, F. Meyer, *ChemPhysChem* **2007**, *8*, 405-417.
- [130] S. Demeshko, G. Leibelng, W. Maringgele, F. Meyer, C. Mennerich, H.-H. Klaus, H. Pritzkow, *Inorg. Chem.* **2005**, *44*, 519-528.
- [131] H. Matsushima, H. Hamada, K. Watanabe, M. Koikawa, T. Tokii, *J. Chem. Soc., Dalton Trans.* **1999**, 971-978.
- [132] V. H. Crawford, H. W. Richardson, J. R. Wasson, D. J. Hodgson, W. E. Hatfield, *Inorg. Chem.* **1976**, *15*, 2107-2110.
- [133] V. P. Hanot, T. D. Robert, J. Kolnaar, J. G. Haasnoot, J. Reedijk, H. Kooijman, A. L. Spek, *J. Chem. Soc., Dalton Trans.* **1996**, 4275-4281.
- [134] D. Ajo, A. Bencini, F. Mani, *Inorg. Chem.* **1988**, *27*, 2437-2444.
- [135] F. Neese, ORCA, Universität Bonn, Bonn, **2007**.
- [136] A. Schäfer, H. Horn, R. Ahlrichs, *J. Chem. Phys.* **1992**, *97*, 2571.
- [137] F. Weigend, *Physical Chemistry Chemical Physics* **2006**, *8*, 1057-1065.
- [138] C. Lee, W. Yang, R. G. Parr, *Physical Review B* **1988**, *37*, 785.
- [139] A. Becke, *J. Chem. Phys.* **1993**, *98*, 1372.
- [140] A. Schäfer, *J. Chem. Phys.* **1994**, *100*, 5829.
- [141] E. Ruiz, J. Cano, S. Alvarez, P. Alemany, *J. Comput. Chem.* **1999**, *20*, 1391-1400.
- [142] T. Soda, Y. Kitagawa, T. Onishi, Y. Takano, Y. Shigeta, H. Nagao, Y. Yoshioka, K. Yamaguchi, *Chem. Phys. Lett.* **2000**, *319*, 223-230.
- [143] A. Bencini, D. Gatteschi, *J. Am. Chem. Soc.* **1986**, *108*, 5763-5771.
- [144] A. Bencini, F. Totti, C. A. Daul, K. Doclo, P. Fantucci, V. Barone, *Inorg. Chem.* **1997**, *36*, 5022-5030.
- [145] A. Sachse, S. Demeshko, S. Dechert, V. Daebel, A. Lange, F. Meyer, *Dalton Trans.* **2010**, *39*, 3903-3914.
- [146] A. Sachse, S. Demeshko, F. Meyer, *Dalton Trans.* **2009**, 7756-7764.

- [147] A. Sachse, M. John, F. Meyer, *Angew. Chem. Int. Ed.* **2010**, *49*, 1986-1989.
- [148] J. C. Röder, F. Meyer, H. Pritzkow, *Chem. Commun.* **2001**, 2176-2177.
- [149] T.-L. Hu, J.-R. Li, C.-S. Liu, X.-S. Shi, J.-N. Zhou, X.-H. Bu, J. Ribas, *Inorg. Chem.* **2005**, *45*, 162-173.
- [150] A. Noble, J. Olguín, R. Clérac, S. Brooker, *Inorg. Chem.* **2010**, *49*, 4560-4569.
- [151] O. Kahn, *Comm. Inorg. Chem.* **1984**, *3*, 105-132.
- [152] O. Kahn, *Angew. Chem. Int. Ed.* **1985**, *24*, 834-850.
- [153] M. Kato, Y. Muto, *Coord. Chem. Rev.* **1988**, *92*, 45-83.
- [154] W. E. Hatfield, *Comm. Inorg. Chem.* **1981**, *1*, 105-121.
- [155] X. Liu, Y. Xing, K. Shao, G. Li, N. Xu, L. Ma, *Z. Anorg. Allg. Chem.* **2009**, *635*, 2627-2630.
- [156] T. S. Lobana, R. Sultana, G. Hundal, R. J. Butcher, *Dalton Trans.* **2010**, *39*, 7870-7872.
- [157] Y.-Q. Zheng, J.-L. Lin, *Z. Anorg. Allg. Chem.* **2003**, *629*, 1622-1626.
- [158] Y.-H. Wen, X.-L. Xie, L. Wang, *J. Coord. Chem.* **2011**, *64*, 459-472.
- [159] R. Ruiz, J. Sanz, F. Lloret, M. Julve, J. Faus, C. Bois, M. C. Munoz, *J. Chem. Soc., Dalton Trans.* **1993**, 3035-3039.
- [160] K. Fujisawa, S. Chiba, Y. Miyashita, K.-i. Okamoto, *Eur. J. Inorg. Chem.* **2009**, *2009*, 3921-3934.
- [161] S. Dhar, M. Nethaji, A. R. Chakravarty, *Dalton Trans.* **2004**, 4180-4184.
- [162] Simon P. Foxon, Gemma R. Torres, O. Walter, Jens Z. Pedersen, H. Toftlund, M. Hüber, K. Falk, W. Haase, J. Cano, F. Lloret, M. Julve, S. Schindler, *Eur. J. Inorg. Chem.* **2004**, *2004*, 335-343.
- [163] M. Stollenz, M. John, H. Gehring, S. Dechert, C. Grosse, F. Meyer, *Inorg. Chem.* **2009**, *48*, 10049-10059.
- [164] U. J. Scheele, M. Georgiou, M. John, S. Dechert, F. Meyer, *Organometallics* **2008**, *27*, 5146-5151.
- [165] M. A. Halcrow, *Dalton Trans.* **2009**, 2059-2073.
- [166] A. A. Mohamed, *Coord. Chem. Rev.* **2010**, *254*, 1918-1947.
- [167] M. Viciano-Chumillas, S. Tanase, L. J. de Jongh, J. Reedijk, *Eur. J. Inorg. Chem.* **2010**, *2010*, 3403-3418.
- [168] R. G. Pearson, *J. Chem. Educ.* **1968**, *45*, 581-587.
- [169] R. G. Pearson, *J. Am. Chem. Soc.* **1963**, *85*, 3533-3539.

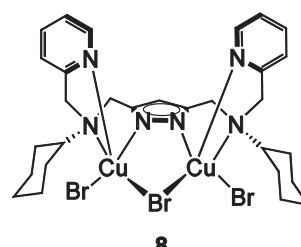
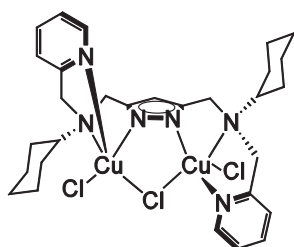
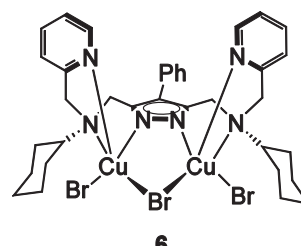
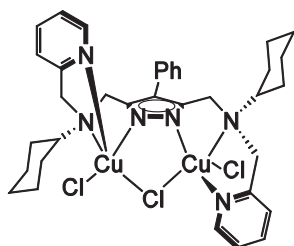
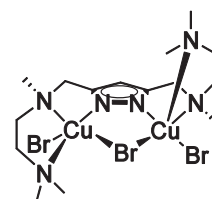
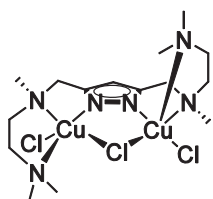
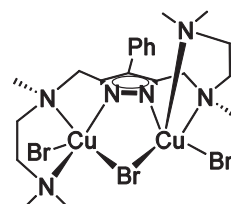
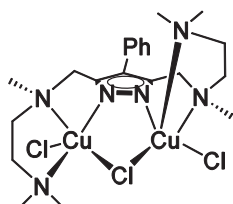
- [170] H. V. R. Dias, H. V. K. Diyabalanage, M. G. Eldabaja, O. Elbjeirami, M. A. Rawashdeh-Omary, M. A. Omary, *J. Am. Chem. Soc.* **2005**, *127*, 7489-7501.
- [171] H. V. R. Dias, H. V. K. Diyabalanage, M. A. Rawashdeh-Omary, M. A. Franzman, M. A. Omary, *J. Am. Chem. Soc.* **2003**, *125*, 12072-12073.
- [172] M. A. Omary, M. A. Rawashdeh-Omary, M. W. A. Gonser, O. Elbjeirami, T. Grimes, T. R. Cundari, H. V. K. Diyabalanage, C. S. P. Gamage, H. V. R. Dias, *Inorg. Chem.* **2005**, *44*, 8200-8210.
- [173] R. G. Raptis, J. P. Fackler, *Inorg. Chem.* **1988**, *27*, 4179-4182.
- [174] R. Bobka, J. N. Roedel, S. Wirth, I.-P. Lorenz, *Dalton Trans.* **2010**, *39*, 10142-10147.
- [175] I. Kinoshita, L. James Wright, S. Kubo, K. Kimura, A. Sakata, T. Yano, R. Miyamoto, T. Nishioka, K. Isobe, *Dalton Trans.* **2003**, 1993-2003.
- [176] H. Lang, A. del Villar, B. Walfort, G. Rheinwald, *J. Organomet. Chem.* **2004**, *689*, 1464-1471.
- [177] J.-H. Yu, Z.-L. Lu, J.-Q. Xu, H.-Y. Bie, J. Lu, X. Zhang, *New J. Chem.* **2004**, *28*, 940-945.
- [178] G. Yang, R. G. Raptis, *Inorg. Chem.* **2002**, *42*, 261-263.
- [179] H. V. R. Dias, C. S. P. Gamage, J. Keltner, H. V. K. Diyabalanage, I. Omari, Y. Eyobo, N. R. Dias, N. Roehr, L. McKinney, T. Poth, *Inorg. Chem.* **2007**, *46*, 2979-2987.
- [180] F. Meyer, A. Jacobi, L. Zsolnai, *Chem. Ber./Recueil* **1997**, *130*, 1441-1447.
- [181] A. A. Mohamed, L. M. Pérez, J. P. Fackler Jr., *Inorg. Chim. Acta* **2005**, *358*, 1657-1662.
- [182] K. Singh, J. R. Long, P. Stavropoulos, *J. Am. Chem. Soc.* **1997**, *119*, 2942-2943.
- [183] K. Singh, J. R. Long, P. Stavropoulos, *Inorg. Chem.* **1998**, *37*, 1073-1079.
- [184] A. Bondi, *J. Phys. Chem.* **1964**, *68*, 441-451.
- [185] K. Brandt, W. S. Sheldrick, *J. Chem. Soc., Dalton Trans.* **1996**, 1237-1243.
- [186] S. R. Cooper, *Acc. Chem. Res.* **1988**, *21*, 141-146.
- [187] H. Meliani, C. Viñas, F. Teixidor, R. Sillanpää, R. Kivekäs, *Polyhedron* **2001**, *20*, 2517-2522.
- [188] W. Levason, M. Nirwan, R. Ratnani, G. Reid, N. Tsoureas, M. Webster, *Dalton Trans.* **2007**, 439-448.
- [189] E. N. Baker, G. E. Norris, *J. Chem. Soc., Dalton Trans.* **1977**, 877-882.
- [190] J. R. Black, W. Levason, *J. Chem. Soc., Dalton Trans.* **1994**, 3225-3230.

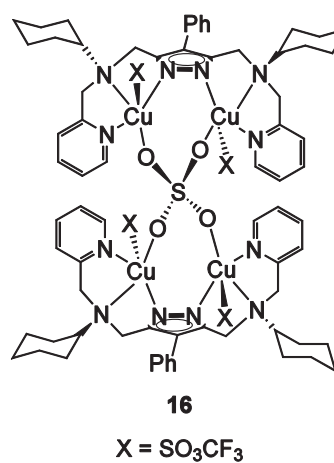
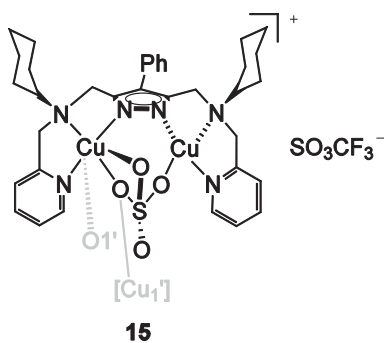
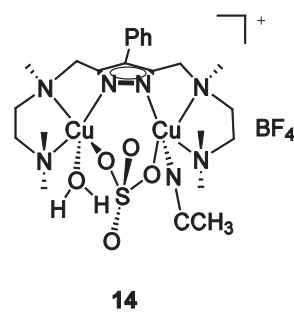
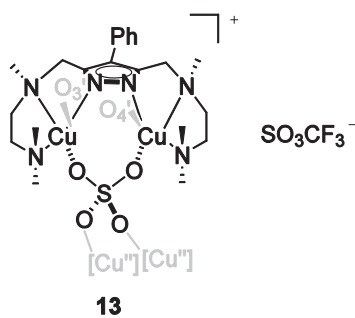
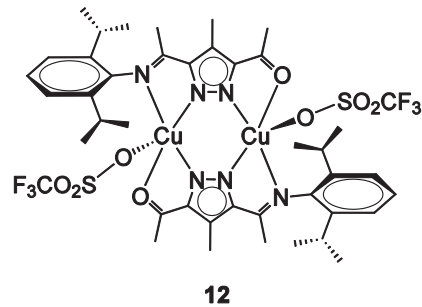
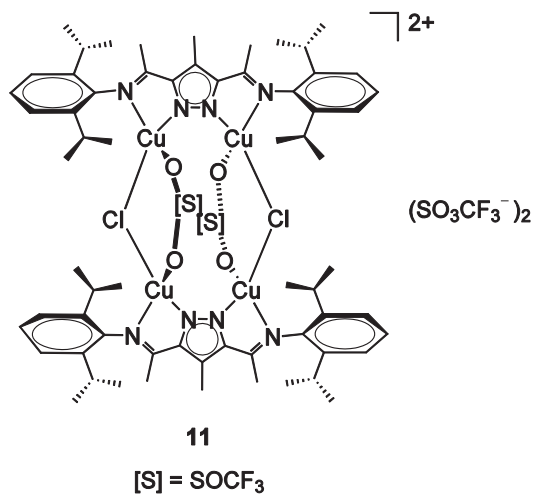
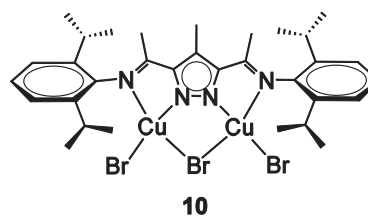
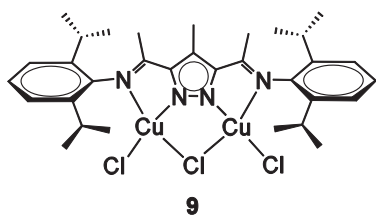
- [191] M. M. Olmstead, W. K. Musker, R. M. Kessler, *Inorg. Chem.* **1981**, *20*, 151-157.
- [192] S. G. Murray, F. R. Hartley, *Chem. Rev.* **1981**, *81*, 365-414.
- [193] J. J. Mayerle, R. B. Frankel, R. H. Holm, J. A. Ibers, W. D. Phillips, J. F. Weiher, *Proc. Nat. Ac. Sc.* **1973**, *70*, 2429-2433.
- [194] J. R. Black, N. R. Champness, W. Levason, G. Reid, *Inorg. Chem.* **1996**, *35*, 4432-4438.
- [195] Sanaullah, G. S. Wilson, R. S. Glass, *J. Inorg. Biochem.* **1994**, *55*, 87-99.
- [196] K. Taras-Goslinska, M. Jonsson, *J. Phys. Chem. A* **2006**, *110*, 9513-9517.
- [197] R. G. Pearson, *Inorg. Chim. Acta* **1995**, *240*, 93-98.
- [198] E. Bill, *JulX*, Max-Planck Institut für Bioanorganische Chemie, Mülheim/Ruhr.
- [199] STOE & CIE GmbH, X-Area, Darmstadt, **2002**.
- [200] STOE & CIE GmbH, X-RED, Darmstadt, **2002**.
- [201] G. M. Sheldrick, SADABS 2008/2, Göttingen, **2008**.
- [202] G. M. Sheldrick, SHELXS-97 Göttingen, **1997**.
- [203] G. M. Sheldrick, SHELXL-97, Göttingen, **1997**.
- [204] G. Sheldrick, *Acta Crystallographica Section A* **2008**, *64*, 112-122.
- [205] M. Granitzka, *private communication* Universität Göttingen, **2011**.
- [206] L. Banting, T. A. Crabb, *Magn. Reson. Chem.* **1987**, *25*, 696-706.

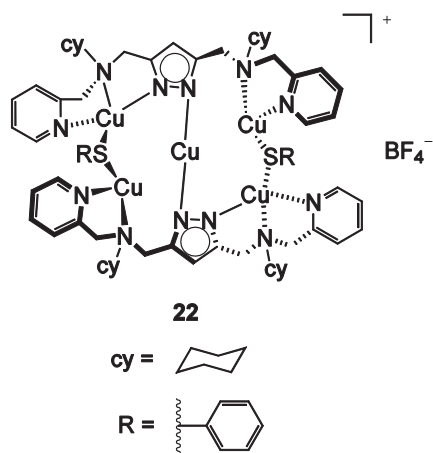
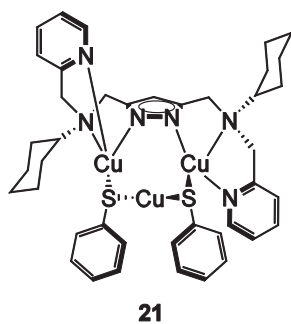
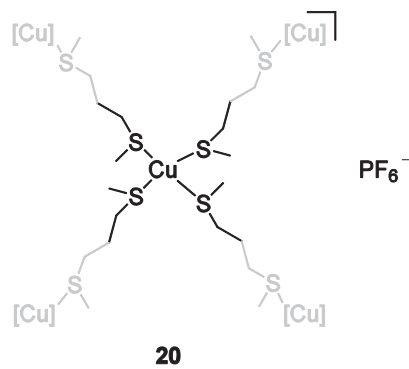
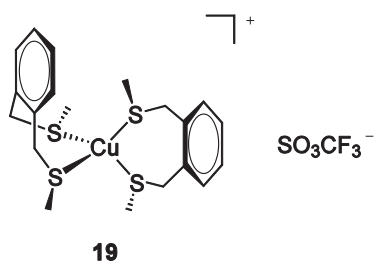
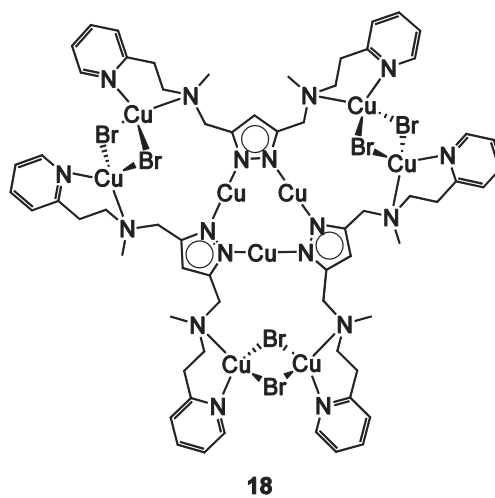
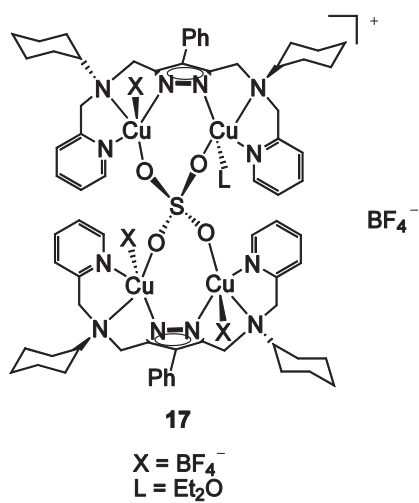
Structures of ligand precursors and ligands

HL¹HL²HL³HL⁴HL⁵HL⁶HL⁷HL⁸HL⁹L^{s1}L^{s,2}

Structures of complexes







**List of Abbreviations**

Å	Angström
ADP	anisotropic displacement parameter
B3LYP	hybrid functional (DFT calculation)
BP	functional (DFT calculation)
br	broad
cy	cyclohexyl
δ	chemical shift
<i>d</i>	distance
d	doublet
DCM	dichloromethane
DFT	density functional theory
ε	extinction coefficient
Et	ethyl
Et ₂ O	diethyl ether
EPR	electron paramagnetic resonance
eq	equivalents
ESI	electron spray ionization
EtCN	propionitrile
His	histidine
IR	infra red
<i>J</i>	magnetic or NMR coupling constant
λ	wavelength
M	molar
m	multiplet (NMR), medium (IR)

μ_{eff}	effective magnetic moment
Me	methyl
MeCN	acetonitrile
MeOH	methanol
MS	mass spectrometry
n Bu	<i>n</i> -butyl
NMR	nuclear magnetic resonance
ph	phenyl
PI	paramagnetic impurity
py	pyridine
pz	pyrazole
s	singulett (NMR), strong (IR)
sh	shoulder
SOMO	single occupied molecular orbital
Sph	thiophenolate
SQUID	superconducting quantum interference device
SVP	basis set (DFT calculation)
t	triplet
t Bu	<i>tert</i> -butyl
THF	tetrahydrofuran
TIP	temperature independent paramagnetism
TZVP	basis set (DFT calculation)
UV Vis	ultra-violet/visible
$\tilde{\nu}$	wave number
vs	very strong
vw	very weak
w	weak



Acknowledgements

At first, I want to thank my *Doktorvater* Prof. Dr. Franc Meyer for the supervision of this thesis, for the interesting topic and the scientific support. I am truly grateful for his continuous motivation during the last three years. Many thanks go also to my co-supervisor Prof. Dr. Ulf Diederichsen and my examination committee: Prof. Dr. Michael Mühlenberg, Dr. Heidrun Sowa, Prof. Dr. Dietmar Stalke and Prof. Dr. Dr. h.c. mult. Herbert W. Roesky for support and review of this work.

My special thanks go also to Prof. Dr. Ulf Ryde for giving me the opportunity to work in his group during my stay in Lund! Special thanks go also to Antonella – thank you for the nice time we had together there.

Many people contributed with their expertise to the completion of this work to whom I want to address my thanks: Dr. Sebastian Dechert for solving crystal structures and for teaching me how to do it myself, Kevin Pröpper for measuring and determining the solid state structure of compound **11** and Markus Granitzka for measuring and determining the solid state structures of compounds **21** and **22**; Dr. Serhiy Demeshko for measuring SQUID-data: Thank you very much for your patience to discuss the results and explain every detail to me; Jörg Teichgräber for measuring the cyclic voltammograms; Dr. Holm Frauendorf and the employees of the mass department for the measurement of the FD-MS spectra; the NMR and MS facilities of the Inorganic Chemistry department: especially Wolfgang Zollke for the recording of numerous NMR-spectra and Dr. Michael John for the help in interpreting these; Ricardo Mata for the help in interpreting my results of the DFT calculations.

Many thanks go to Petra Unger for her immense support in administrative matters. Jörg Teichgräber and Andreas Schwarz I want to thank for the supply of chemicals and laboratory equipment. I also want to acknowledge the work of the people of the electrical and craft machine shops, the caretakers and the glassblower craft shop.

I want to thank the whole working group for the good working atmosphere and the fun we had during our “Feierabendbier” and the group tours, especially Anni, Iris, Sven, Kai, Lina, Simone, Boris, Tine, Benni, “Morkas” and Inke. Special thanks go to my colleagues

from lab 230, Benni and “Morkas”: I want to thank you for the fun we had although you made me suffer with “Helge” sometimes.

I also acknowledge all students for their experimental work: Kai Kalz, Christoph Kornhaaß, Johannes Kaschel, Dennis Manz, Sven Neudeck, Iris Klawitter, Natascha Bruckner and Markus “Otto” Kinauer.

For correcting parts of this thesis I thank Dr. Inke Siewert, Lina Frensch, Boris Burger, Ann Christin Jahnke and Manuel Wittenberg.

Research fellowship and financial support of the DFG (IRTG 1422: “Metal Sites in Biomolecules: Structures, Regulation and Mechanisms”) and financial support of the sdw (Stiftung der deutschen Wirtschaft) is gratefully acknowledged.

I also want to thank all members of the IRTG 1422 for the good teamwork and the fun we had on our mutual mini-symposia, workshops and conferences, especially Simone, Boris, Toni, Kai, Anja und Peer.

Special thanks go to the Stipendiatengruppe Göttingen of the sdw for the great time I had with all of you, especially Lars, Urte, Gesa, Christina, Tina, Andreas, Henrike, Annika, Florian, Lope and Peter. I really enjoyed the mutual seminars and events and the organization of these with you.

Finally, I would like to thank my family and friends for their reliable backup. Ina, thank you very much for your friendship and support during the last weeks, no one understood me the way you did during this time. Manuel, Anni, Johannes and Olaf, thank you for such a great time here in Göttingen! Loving thanks go to Michael, thank you for being there for me during the last years!

**List of scientific contributions***PUBLICATIONS*

M. Stollenz, H. Gehring, V. Konstanzer, S. Fischer, S. Dechert, C. Große, F. Meyer, “From binuclear Copper(I)-Complexes with Pyrazolate-based Compartmental Ligands to octanuclear σ -Mesityl-bridged μ_4 -Oxo-Cuprocuprates: Versatile Tools for the Activation of Dioxygen and CC-Coupling Reactions”, *Organometallics* **2011**, 30, 3708 - 3725.

M. Georgiou, S. Wöckel, V. Konstanzer, S. Dechert, M. John, F. Meyer, “Structural Variations in Tetrasilber(I) Complexes of Pyrazolate-bridged Compartmental N-Heterocyclic Carbene Ligands”, *Z. Naturforsch.* **2009**, 64b, 1542 – 1552.

ORAL PRESENTATIONS

“News from bioinspired copper-sulfur chemistry”, 5th *Workshop of the International Research Training Group 1422 “Metal Sites in Biomolecules: Structures, Regulation and Mechanisms”*, Goslar, Germany, February **2010**.

Zweikernige Kupferkomplexe als Precursoren für ein Modell des Cu_Z -Zentrums der N_2O -Reduktase, *Norddeutsches Doktorandenkolloquium der Anorganischen Chemie*, Burg Warberg Braunschweig, Germany, September **2008**.

POSTERS AT CONFERENCES AND INTERNATIONAL WORKSHOPS

V. Konstanzer, N. Bruckner, K. F. Kalz, S. Demeshko, S. Dechert, U. Ryde, F. Meyer, "Pyrazolate-based dicopper complexes: Potential building blocks for emulating the Cu₂-site of N₂O-Reductase", *6th Workshop of the International Research Training Group 1422 "Metal Sites in Biomolecules: Structures, Regulation and Mechanisms"*, Lund, Sweden, February **2011**.

V. Konstanzer, S. Demeshko, S. Dechert, U. Ryde, F. Meyer, "New pyrazolate-based dicopper complexes: Potential building blocks for emulating multicopper enzyme active sites", *10th European Biological Inorganic Chemistry Conference (EuroBIC 10)*, Thessaloniki, Greece, June **2010**.

V. Konstanzer, S. Demeshko, S. Dechert, F. Meyer, "Novel multinuclear copper complexes", *12. JCF Frühjahrssymposium*, Göttingen, Germany, March **2010**.

V. Konstanzer, S. Dechert, F. Meyer, "En route to synthetic models for the Cu₂-site of N₂O-reductase", *Summer School "Computational Chemistry and Spectroscopy"*, Essen, Germany, September **2009**.

V. Kruse, K. F. Kalz, S. Dechert, F. Meyer, "Synthetic precursors for the Cu₂-site of N₂O-reductase", *4th Workshop of the International Research Training Group 1422 "Metal Sites in Biomolecules: Structures, Regulation and Mechanisms"*, Copenhagen, Denmark, February **2009**.



CURRICULUM VITAE

Personal data

Name: Vera Konstanzer, née Kruse
 Date of Birth: 05.09.1982
 Place of Birth: Lippstadt
 Nationality: German
 Marital Status: Married

Pre-Academic-Career:

08/1989 – 06/1993 Grundschule St. Margaretha, Sichtigvor
 08/1993 – 06/2002 Friedrich-Spee-Gymnasium, Rüthen
Abitur (cumulative grade 1.6)

Academic Career:

10/2002 – 12/2007 Undergraduate student, Georg-August-Universität Göttingen
 10/2004 *Diplomvorprüfung* (cumulative grade *gut*)
 04/2006 – 09/2006 Erasmus exchange student in the group of Prof. Dr. Anna-Karin Borg-Karlson, Kungliga Tekniska Högskolan, Stockholm, Sweden
 04/2007 – 09/2007 Diploma thesis in the group of Prof. Dr. Franc Meyer, Georg-August-Universität Göttingen, “*Synthese bioinspirierter Kupferkomplexe – auf dem Weg zu Modellkomplexen des Cu₂-Zentrums der N₂O-Reduktase*“
 12/2007 *Diplomprüfung* (cumulative grade *sehr gut*)
 Since 05/2008 Ph.D. student in the group of Prof. Dr. Franc Meyer, Georg-August-Universität Göttingen, Ph.D. thesis “*Multinuclear pyrazolate-based copper complexes inspired by the Cu₂-site of N₂O-reductase*”



